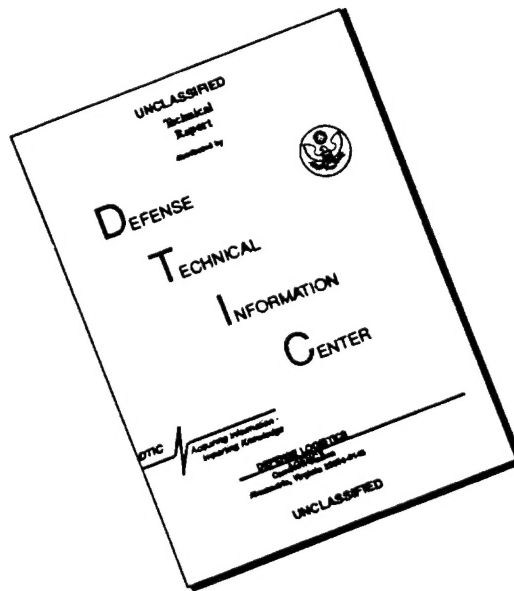


DISCLAIMER NOTICE



THIS DOCUMENT IS BEST QUALITY AVAILABLE. THE COPY FURNISHED TO DTIC CONTAINED A SIGNIFICANT NUMBER OF PAGES WHICH DO NOT REPRODUCE LEGIBLY.

GENERAL INSTRUCTIONS FOR COMPLETING SF 298

The Report Documentation Page (RDP) is used in announcing and cataloging reports. It is important that this information be consistent with the rest of the report, particularly the cover and title page. Instructions for filling in each block of the form follow. It is important to *stay within the lines* to meet *optical scanning requirements*.

Block 1. Agency Use Only (Leave blank).

Block 2. Report Date. Full publication date including day, month, and year, if available (e.g. 1 Jan 88). Must cite at least the year.

Block 3. Type of Report and Dates Covered. State whether report is interim, final, etc. If applicable, enter inclusive report dates (e.g. 10 Jun 87 - 30 Jun 88).

Block 4. Title and Subtitle. A title is taken from the part of the report that provides the most meaningful and complete information. When a report is prepared in more than one volume, repeat the primary title, add volume number, and include subtitle for the specific volume. On classified documents enter the title classification in parentheses.

Block 5. Funding Numbers. To include contract and grant numbers; may include program element number(s), project number(s), task number(s), and work unit number(s). Use the following labels:

C - Contract	PR - Project
G - Grant	TA - Task
PE - Program Element	WU - Work Unit Accession No.

Block 6. Author(s). Name(s) of person(s) responsible for writing the report, performing the research, or credited with the content of the report. If editor or compiler, this should follow the name(s).

Block 7. Performing Organization Name(s) and Address(es). Self-explanatory.

Block 8. Performing Organization Report Number. Enter the unique alphanumeric report number(s) assigned by the organization performing the report.

Block 9. Sponsoring/Monitoring Agency Name(s) and Address(es). Self-explanatory.

Block 10. Sponsoring/Monitoring Agency Report Number. (If known)

Block 11. Supplementary Notes. Enter information not included elsewhere such as: Prepared in cooperation with...; Trans. of...; To be published in.... When a report is revised, include a statement whether the new report supersedes or supplements the older report.

Block 12a. Distribution/Availability Statement. Denotes public availability or limitations. Cite any availability to the public. Enter additional limitations or special markings in all capitals (e.g. NOFORN, REL, ITAR).

DOD - See DoDD 5230.24, "Distribution Statements on Technical Documents."

DOE - See authorities.

NASA - See Handbook NHB 2200.2.

NTIS - Leave blank.

Block 12b. Distribution Code.

DOD - Leave blank.

DOE - Enter DOE distribution categories from the Standard Distribution for Unclassified Scientific and Technical Reports.

NASA - Leave blank.

NTIS - Leave blank.

Block 13. Abstract. Include a brief (*Maximum 200 words*) factual summary of the most significant information contained in the report.

Block 14. Subject Terms. Keywords or phrases identifying major subjects in the report.

Block 15. Number of Pages. Enter the total number of pages.

Block 16. Price Code. Enter appropriate price code (*NTIS only*).

Blocks 17. - 19. Security Classifications. Self-explanatory. Enter U.S. Security Classification in accordance with U.S. Security Regulations (i.e., UNCLASSIFIED). If form contains classified information, stamp classification on the top and bottom of the page.

Block 20. Limitation of Abstract. This block must be completed to assign a limitation to the abstract. Enter either UL (unlimited) or SAR (same as report). An entry in this block is necessary if the abstract is to be limited. If blank, the abstract is assumed to be unlimited.

DIRSIG
Digital Imaging and Remote Sensing Image Generation Model:
Infrared Airborne Validation
&
Input Parameter Analysis

Todd A. Kraska

Rochester Institute of Technology
Chester F. Carlson Center for Imaging Science

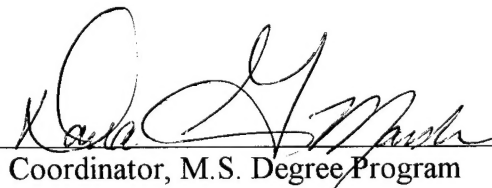
A thesis submitted in partial fulfillment of the
requirements for the degree of Master of Science
at the Chester F. Carlson Center for Imaging Science
in the College of Science
of the Rochester Institute of Technology

April 1996

Signature of the Author



Accepted by


Coordinator, M.S. Degree Program

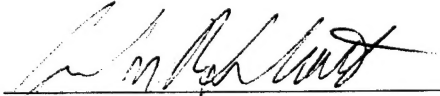
April 2, 1996

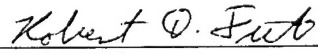
CHESTER F. CARLSON
CENTER FOR IMAGING SCIENCE
COLLEGE OF SCIENCE
ROCHESTER INSTITUTE OF TECHNOLOGY
ROCHESTER, NEW YORK

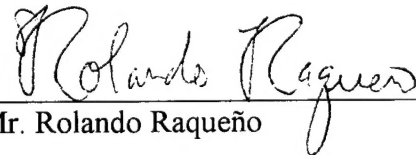
CERTIFICATE OF APPROVAL

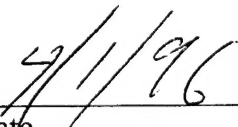
M.S. DEGREE THESIS

The M.S. Degree Thesis of Todd A. Kraska
has been examined and approved by the
thesis committee as satisfactory for the
thesis requirement for the
Master of Science degree


Dr. John Schott, Thesis Advisor


Dr. Robert Fiete


Mr. Rolando Raqueño


Date

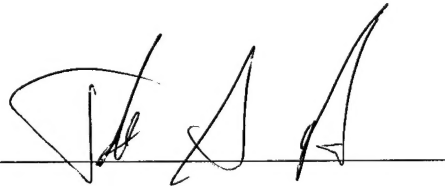
THESIS RELEASE PERMISSION FORM
ROCHESTER INSTITUTE OF TECHNOLOGY
COLLEGE OF SCIENCE
CHESTER F. CARLSON CENTER FOR IMAGING SCIENCE

DIRSIG
Digital Imaging and Remote Sensing Image Generation Model:

**Infrared Airborne Validation
&
Input Parameter Analysis**

I, Todd A. Kraska, hereby grant permission to the Wallace Memorial Library of R.I.T. to reproduce my thesis in whole or in part. Any reproduction will not be for commercial use of profit.

Signature: _____

A handwritten signature in black ink, appearing to read 'T. A. Kraska', written over a horizontal line.

Date: _____

1 April 96

DIRSIG
Digital Imaging and Remote Sensing Image Generation Model:

**Infrared Airborne Validation
&
Input Parameter Analysis**

by
Todd A. Kraska

Submitted to the Chester F. Carlson Center for Imaging Science
in partial fulfillment of the requirements
for the Master of Science Degree
at the Rochester Institute of Technology

Abstract

The civilian and military need for high resolution infrared imagery has dramatically increased in recent times. Regardless of the user or the need, infrared imagery can provide unique information that is not available in the visible region of the electromagnetic spectrum. Just as the need for real infrared imagery has increased, so has the need for computer generated infrared imagery, also known as synthetic imagery. Synthetic imagery is created by mathematically modeling the "real world" and the imaging chain, encompassing everything from the target to the sensor characteristics. The amount of faith that can be placed in a synthetic image depends on its accuracy in recreating the real world. The Digital Imaging and Remote Sensing Image Generation Model (DIRSIG) at the Rochester Institute of Technology (RIT) attempts to model the real world. It creates synthetic images through the integration of scene geometry, ray-tracer, thermal, radiometry, and sensor submodels. The focus of this project lies in evaluating the ability of DIRSIG to recreate the imaging chain and produce high resolution synthetic imagery. DIRSIG synthetic imagery of the Kodak Hawkeye plant and the surrounding area was compared to aerial infrared imagery of the same region using root mean square error and rank order correlation. This comparison helped to validate the output from DIRSIG and detect inadequacies in the image chain model. In addition to validating DIRSIG, a procedure for optimizing the input parameters, incorporating a sensitivity analysis, was developed. This reduces the time involved in creating a realistic and accurate synthetic image.

Table of Contents

Abstract.....	i
Table of Contents.....	ii
List of Figures & Tables.....	iv
1.0 Introduction.....	1
2.0 Objectives.....	4
2.1 DIRSIG Validation.....	4
2.2 Input Parameter Analysis & Optimization.....	6
3.0 Background.....	8
3.1 The Big Equation.....	8
3.2 Alternative SIG Models.....	11
3.3 DIRSIG Overview.....	17
3.3.1 Scene Geometry Submodel.....	17
3.3.2 Ray-Tracer Submodel.....	19
3.3.3 Thermal Submodel.....	23
3.3.4 Radiometry Submodel.....	24
3.3.5 Sensor Response and Modulation Transfer Functions.....	28
3.3.6 Final Image Generation Review.....	29
4.0 Technical Approach & Procedure.....	30
4.1 Validation of DIRSIG.....	30
4.1.1 Radiometric Validation.....	33
4.1.1.1 Rank Order Correlation.....	33
4.1.1.2 RMS Error.....	34
4.1.2 Geometric Validation.....	35
4.2 Input Parameter Analysis & Optimization.....	37
5.0 Experimental.....	41
5.1 Truth Imagery Collection	41
5.1.1 Aerial Image Collection - <i>Image 1</i>	41
5.1.2 Equipment Specifications- <i>Image 1</i>	43
5.1.3 Rooftop Image Collection - <i>Images 2-3</i>	44
5.1.4 Equipment Specifications- <i>Image 2-3</i>	45
5.1.5 Image Collection Summary.....	47
5.2 Scene Development & Synthetic Image Generation.....	50
5.2.1 Terrain Generation.....	51
5.2.2 Building Generation.....	52
5.2.3 Miscellaneous Object Creation.....	56
5.2.4 Meteorological Data -Weather & Atmosphere.....	57
5.2.5 Sensor Parameters & Profile.....	57
5.2.6 Image Creation Summary.....	58
5.3 DIRSIG Validation Results.....	61
5.3.1 Validation - Primary Truth Imagery (Bendix line scanner)	61
5.3.1.1 Material Radiometric Accuracy - RMS Error.....	67
5.3.1.2 Material Radiometric Accuracy - ROC.....	70

5.3.1.3 Radiometric Accuracy - Complex Phenomena.....	73
5.3.1.4 Geometric Accuracy.....	82
5.3.2 Validation - Alternate Truth Imagery (Inframetrics).....	85
5.3.3 Validation Summary.....	87
6.0 Input Parameter Sensitivity Analysis & Optimization.....	88
6.1 Input Parameter Sensitivity Analysis.....	88
6.1.1 Weather & Atmospheric Sensitivity.....	94
6.1.2 Material Parameter Sensitivity.....	102
6.1.3 Time History Material Parameter Sensitivity.....	110
6.2 Input Parameter Optimization.....	114
6.2.1 Meteorological Parameter Optimization.....	119
6.2.2 Material Parameter Optimization.....	120
6.5 Input Parameter Sensitivity Analysis & Optimization Summary.....	126
7.0 Recommendation & Conclusions.....	127
7.1 DIRSIG.....	127
7.2 Sensitivity Analysis & Input Parameter Optimization.....	129
7.3 Conclusion.....	130
8.0 References.....	131

APPENDIX A

Validation Analysis

APPENDIX B

DIRSIG Files

APPENDIX C

AutoCad Scene Construction

APPENDIX D

Material Files

Generic

Optimum

Angular Effects

APPENDIX E

Actual Weather Data

10 November 1991

12 October 1995

APPENDIX F

Sensitivity Analysis

Meteorological Data

Material Data

Time History Data

List of Figures & Tables

Figure 3.1 - Solar energy photon paths.....	8
Figure 3.2 - Self-emitted energy photon paths.....	9
Figure 3.3 - GTVISIT overview.....	11
Figure 3.4 - TI synthetic scene generation.....	13
Figure 3.5 - DIRSIG overview.....	17
Figure 3.6 - Facet material parameters.....	18
Figure 3.7 - DIRSIG data hierarchy.....	18
Figure 3.8 - Object & part bounding volumes.....	19
Figure 3.9 - Ray-tracer model.....	20
Figure 3.10 - Solar history.....	21
Figure 3.11 - Target Interactions.....	21
Figure 3.12 - Ray-tracer flow diagram.....	22
Figure 4.1 - Area of interest.....	32
Figure 4.2 - Relative minimum & maximum input values.....	37
Figure 5.1 - Piper Aztec aircraft.....	41
Figure 5.2 - Line scanner image acquisition.....	42
Figure 5.3 - Bendix line scanner.....	43
Figure 5.4 - Filtered Bendix responsivity.....	44
Figure 5.5 - Inframetrics video camera.....	45
Figure 5.6 - Filtered Inframetrics responsivity.....	46
Figure 5.7 - 2-D city template.....	50
Figure 5.8 - Contour map.....	51
Figure 5.9 - AutoCad terrain.....	52
Figure 5.10 - Church & YMCA buildings with reference object.....	53
Figure 5.11 - Scene layout.....	53
Figure 5.12 - AutoCad Buildings.....	54
Figure 5.13 - AutoCad Houses.....	55
Figure 5.14 - Miscellaneous object details.....	56
Figure 5.15 - Atmospheric profile.....	57
Figure 5.16 - Hawkeye scene construction.....	58
Figure 5.17 - Primary validation imagery.....	66
Figure 5.18 - Validation points.....	67
Figure 5.19 - Material evaluation - temperature comparison.....	69
Figure 5.20 - Material evaluation - ROC results.....	72
Figure 5.21 - Complex phenomena validation points.....	74
Figure 5.22 - Angular effect evaluation - <i>asphalt streets</i>	75
Figure 5.23 - Angular effect & shape factor evaluation - <i>asphalt shingles</i>	77
Figure 5.24 - Angular effect curves.....	78
Figure 5.25 - Angular, shape factor, & background effect evaluation - <i>grass</i>	79
Figure 5.26 - Angular, shape factor, & background effect evaluation - <i>r.g.</i>	80
Figure 5.27 - Geometric error.....	83

Figure 5.28 - Ground evaluation points.....	83
Figure 5.29 - Inframetrics rank order correlation imagery.....	85
Figure 5.30 - Inframetrics rank order correlation results.....	86
Figure 6.1 - THERM input parameters.....	89
Figure 6.2 - Shape factor.....	92
Figure 6.3 - Material orientations.....	96
Figure 6.4 - Meteorological parameter sensitivity analysis.....	97
Figure 6.5 - Material parameter sensitivity analysis flow chart.....	104
Figure 6.6 - Material parameter graph analysis.....	105
Figure 6.7 - Time history expected temperature error analysis graphs.....	111
Figure 6.8 - Time history sensitivity analysis - <i>Material comparison</i>	113
Figure 6.9 - DIRSIG radiance image.....	114
Figure 6.10 - DIRSIG debug images.....	114
Figure 6.11 - Angular emissivity curve.....	115
Figure 6.12 - Histogram comparison.....	116
Figure 6.13 - Scene analysis.....	118
Figure 6.14 - Histogram comparison summary.....	126
Table 3.1 - Radiance equation.....	26
Table 3.2 - Radiance equation variable definitions.....	27
Table 5.1 - Validation imagery - specification summary.....	47
Table 5.2 - Estimated geometric accuracy.....	60
Table 5.3 - DIRSIG input file summary.....	60
Table 5.4 - RMS error validation results - Bendix imagery.....	68
Table 5.5 - ROC validation results - Bendix imagery.....	72
Table 5.6 - Angular effect evaluation - <i>asphalt streets</i>	76
Table 5.7 - Angular effect & shape factor evaluation - <i>asphalt shingles</i>	77
Table 5.8 - Angular, SF, & background effect evaluation - <i>grass & r.g.</i>	81
Table 5.9 - Inframetrics ROC results.....	86
Table 6.1 - Meteorological sensitivity results.....	98
Table 6.2 - Material parameter sensitivity results.....	106
Table 6.3 - Object material parameter values.....	124
Table 6.4 - Input parameter effect summary.....	126

1.0 Introduction

A new tank with a low thermal signature has recently been designed by a foreign country. Will the tank be detectable by existing heat seeking missiles or does a new infrared (IR) sensor need to be designed for the missile? - Or can improvements be made to the computer algorithms of the existing missile to detect the new tank? While it would be difficult, if not impossible, to determine an answer to these questions without the actual use of the foreign tank, computer models, based on the first principles of physics, can actually be used to answer these questions before the military forces ever encounter the foreign tank in a real world situation when lives may be at risk.

With the increasing capabilities of computers in the last 20 years, the ability to model real world situations, such as this hypothetical scenario involving a low thermal signature tank, has dramatically increased. Specifically, this increase in computing speed and power has led to the development of artificial images that can be used in computer animation, flight simulation, and computer aided design and manufacturing. This process of developing artificial images is known as synthetic image generation (SIG). Synthetic images are useful in a vast array of imaging problems. They can be used to train analysts on the appearance of a target under different meteorological conditions, times of day, and look angles. In addition, SIG can be used to help designers evaluate various sensor systems before the actual hardware is fabricated. Synthetic images can also help determine the optimum acquisition parameters for a real imaging system by predicting the time at which the greatest contrast or resolution will be obtained for the desired targets. The result is a large savings in research and development cost as well as increased performance and operational capabilities.

While synthetic images can be created in virtually any region of the electromagnetic spectrum, images created in the long wave (8-14 μ m) and mid wave (3-5 μ m) infrared regions offer unique signatures compared to the visible region. Synthetic images in the LWIR and MWIR are primarily influenced by the thermal properties and emissivities of the objects in the scene. These infrared images prove useful in analyzing the thermal

characteristics and signatures of objects, viewing objects in simulated night conditions, and finding objects hidden or obscured by other visible features. While scale models of the real world are often created for analysis of sensor systems in the visible region, it is extremely difficult and often impossible to build miniature models with accurate thermal characteristics. Thus, synthetic images are one of the only ways to predict the performance of an infrared sensor system.

The usefulness of these synthetic images is negated if the output does not closely imitate the real world. As a result, the output from SIG must be evaluated and assessed according to criteria such as spectral and radiometric accuracy, geometric fidelity, robustness of application, and speed of image generation (Rankin 1992). Depending upon the application and use of the synthetic image, these criteria will have differing weights of importance. If the goal of the SIG process is to produce visually appealing pictures, radiometric fidelity will be of little importance while speed of image generation may be favored. However, in most technical applications, the speed of image generation is sacrificed for radiometric fidelity.

The focus of this project is validating the Digital Imaging and Remote Sensing Image Generation (DIRSIG) model by comparing DIRSIG imagery with real airborne imagery. While DIRSIG was validated in the IR region in 1992 by Rankin, several modifications have been incorporated into DIRSIG since this validation (Schott et. al., 1994). This validation will test some of these modifications as well as the robustness of DIRSIG as the synthetic images are compared to infrared imagery taken at different times, look angles, and locations. An algorithm for modifying and optimizing the object material parameters was also developed in an attempt to reduce the time required to develop accurate synthetic images.

In validating DIRSIG and analyzing the input parameters, the project was divided into smaller tasks. The first step was to define the exact goals and objectives of the project. The actual principles involved in the creation of a real image were then examined to provide a better understanding of the modeling process. Other synthetic image models

were researched to determine the weaknesses and strengths of DIRSIG. The process of generating a DIRSIG synthetic image was explained next. All this background knowledge led to a technical approach that could be used in achieving the defined objectives. The actual experimental validation of DIRSIG was then described in detail, followed by the sensitivity analysis and optimization of the input parameters. Recommendations for improvements and future work conclude the discussion of this project.

2.0 Objectives

2.1 DIRSIG Validation

While DIRSIG was validated using ground truth data in the IR region in 1992 by Rankin, synthetic images from DIRSIG have never been extensively compared or validated with actual aerial imagery; the primary validation prior to this work used roof-top imaging scenarios. As a result, the validations have not truly explored the limitations of DIRSIG and its ability to model real aerial imagery.

Rankin's validation focused on the DIRSIG submodels and the sensitivity of the output image to errors in various input parameters. Each of the DIRSIG subroutines were validated individually and recommendations were made to improve the synthetic images. These recommendations included adding fractional specularity and transmissivity, improving the shape factor computation, adding more materials to the material parameter database, modeling clouds in the scenes, and, finally, improving the thermal model. Based upon these recommendations, DIRSIG has been modified to include fractional specularity, transmissive objects, and clouds. However, some of the other options have not yet been implemented.

This validation concentrates on examining DIRSIG's current ability to recreate the entire imaging chain, from end to end (excluding optical and noise effects - DIRSIG has these capabilities but they were not complete at the time of validation), without the ability to examine each submodel that is used in the creation of the final synthetic image. However, it is still possible to modify the input parameters, such as the weather file and material file, to improve the radiometric accuracy of the final synthetic image. The testing also differs from the previous validation in that it further explores DIRSIG's ability to include atmospheric attenuation and sensor geometric effects in the final results. Following this goal of trying to evaluate the ability of DIRSIG to model the real world, several images taken with different imaging systems and parameters will be used in the validation. The primary comparison and validation will be accomplished with imagery from a Bendix line scanner. Once the synthetic image closely matches the primary truth

imagery and the individual material properties of all the facets have been determined, the same scene is compared to the secondary truth imagery. The secondary set of truth imagery from an Inframetrics camera greatly differs from the Bendix truth imagery. The Inframetrics imagery, which was acquired at a different time and under different atmospheric conditions, will help test the robustness of DIRSIG in modeling imaging conditions of the same target scene.

In conjunction with the validation of DIRSIG, a primary objective is to create a complex and realistic scene that can be used in future studies and testing. Synthetic imagery provides a useful tool to test image algorithms and analysis techniques, but it must closely resemble the real world. The scene that is developed for the validation will provide this capability. It will bridge the gap between the past validation of DIRSIG, where a simple scene with known test targets was used, and real imagery, where little actual information is known. In order to make the scene as realistic as possible, the scene must contain the complex interactions between objects, including buildings, houses, trees, and other structures that are found in the real world. This requires extensive research of the objects in the scene so that they can be recreated accurately. The research and effort in building the scene was shared with Russell White who will validate DIRSIG in the visible region of the electromagnetic spectrum. The validation of common targets in the two regions of the spectrum provides a quality check of the target parameters. The parallel validation also allowed the concentration on a single validation scene. This reduced the time required to build the scene, and allowed a more complex scene to be created.

2.2 Input Parameter Analysis & Optimization

In addition to validating DIRSIG, a procedure for optimizing the synthetic image input parameters was developed. Previously, a trial and error process was used to modify the input parameters until the synthetic image closely resembled the truth imagery. A better method for determining these input parameters is needed to reduce the time required to generate an accurate synthetic image. This is accomplished by first determining the bounds or limiting values for each of the input parameters, and then determining the effect of each input on the synthetic image. This step alone is an improvement over the trial and error guessing process that was previously used.

While bounding values are helpful in determining the range of values for the input parameters, the most effective way to fine tune the input parameters requires a sensitivity analysis of all the parameters. A sensitivity analysis shows which parameters create the largest changes, and therefore, most probable error in the synthetic output image. The parameter with the highest sensitivity can then be altered first to try and match the synthetic and real imagery, or a combination of the most sensitive parameters can be altered to create the desired output. In addition, a confidence interval in the estimation of the input parameters, i.e. an estimated error, should be developed for each input. Similar to the sensitivity analysis, this will indicate which parameters are most likely to cause error in the output image. The sensitivity analysis and the error estimation will provide tools for the input parameter optimization process. For example, a large error in the estimation of a material parameter can be tolerated if the output image is not sensitive to variations in that variable; however, it would be essential to alter a parameter with a large error in its predicted value if the image is highly sensitive to that parameter. This method of fine tuning the material parameters will likely reduce the time to generate synthetic images while also establishing guidelines for eventually automating the selection and modification of the material parameters.

Images of the same region of interest acquired under different imaging conditions, such as a nadir versus oblique look angle, or morning versus night acquisition, are also likely to aid in modifying the material parameters. It is unlikely that a material has the

exact same appearance under different imaging conditions. The multiple images of the same scene may provide insight into the reflectivity and emissivity of the objects in the scene. For example, the temperature of an aluminum-sided building and a wood-sided building that have been warmed by direct sunlight will be vastly different when compared to the respective temperatures on a cloudy day. On a sunny day, the temperature of the aluminum rises rapidly as the energy from the sun is absorbed, but on the cloudy day, the temperature of the aluminum will not rise as much. Similarly, the temperature of a wood-sided building will be greater on a sunny day than on a cloudy day. However, the wood-sided building will not have a large change in temperature between the cloudy day and the sunny day because wood has different thermal properties than aluminum. It is the difference in appearances of the objects that can help indicate some of the thermal material properties. The facet material parameters can then be adjusted to logically account for the images generated under the different acquisition parameters. The use of multiple images may be very useful in defining the proper material parameter values, but its use will be limited to scenes for which multiple images are available.

3.0 Background

3.1 The Big Equation

In order to understand the synthetic image generation process, it is first necessary to understand the physics and underlying principles that are involved in the capture of a real image. The first step is to visualize how the observed electromagnetic radiation ultimately reaches the sensor. The observed radiance at the front end of the sensor is comprised of nine different photon paths. The following diagrams show the different paths that electromagnetic radiation may travel before reaching the sensor. The first diagram shows the radiation originating from solar photons while the second diagram shows the radiation resulting from self-emission by the objects.

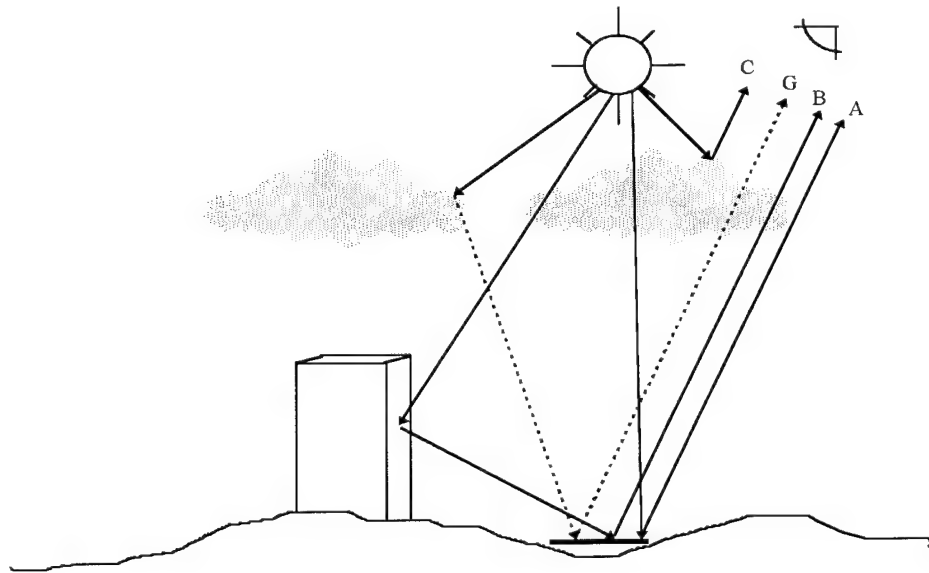


Figure 3.1 - Solar energy photon paths

Type A - Directly reflected solar photons attenuated by the atmosphere and clouds

Type B - Solar Photons reflected from the background onto the target

Type C - Solar photons scattered by the atmosphere

Type G - Solar photons scattered by the atmosphere onto the target

$$\begin{aligned}
 L_{solar} &= A_{photons} + C_{photons} + B_{photons} + G_{photons} \\
 &= E' \cos \sigma' \frac{r}{\pi} \tau_1 \tau_2 + F \cdot E_{ds\lambda} \frac{r}{\pi} \tau_2 + (1 - F) \cdot L_{bs\lambda} r_d \tau_2 + L_{us\lambda}
 \end{aligned}
 \tag{3.1}$$

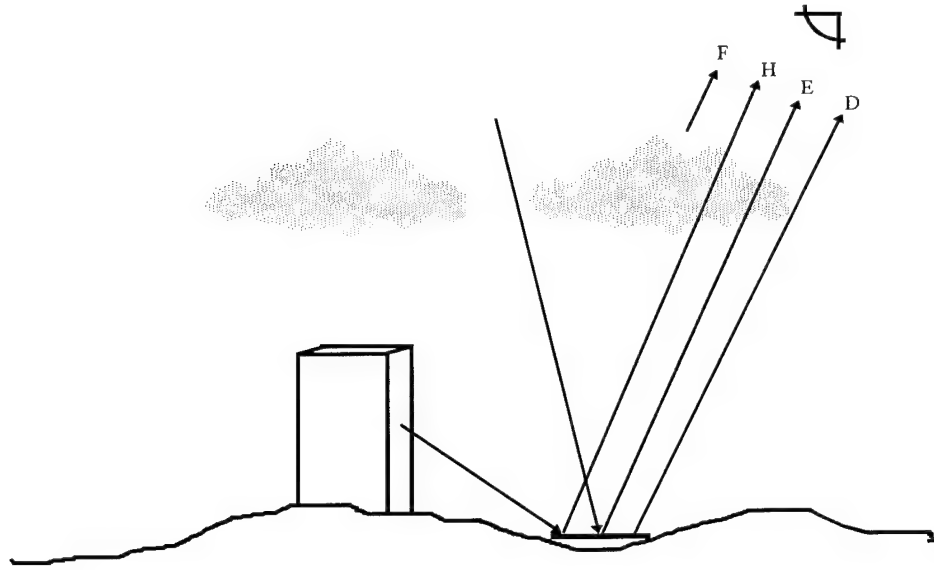


Figure 3.2 - Self-emitted energy photon paths

Type D - Self-emitted photons from the target attenuated by the atmosphere

Type E - Self-emitted photons from the sky reflected by the target to the sensor

Type F - Self-emitted photons from the atmosphere

Type H - Self-emitted photons from the background reflected by the target to the sensor

$$\begin{aligned}
 L_{self-emission} &= D_{photons} + E_{photons} + F_{photons} + H_{photons} \\
 &= \varepsilon L_{T\lambda} \tau_2 + F \cdot \frac{r_d}{\pi} E_{d\epsilon\lambda} \tau_2 + (1-F)r_d \cdot L_{b\epsilon\lambda} \tau_2 + L_{u\epsilon\lambda}
 \end{aligned} \tag{3.2}$$

After combining these two equations, $L_\lambda = L_{solar} + L_{self-emission}$, the total spectral radiance reaching the sensor can be described by the following “big equation”:

$$\begin{aligned}
 L_\lambda &= E'_s \cos \sigma' \frac{r(\lambda)}{\pi} \tau_1(\lambda) \tau_2(\lambda) + \varepsilon(\lambda) L_{T\lambda} \tau_2(\lambda) + F[E_{ds\lambda} + E_{d\epsilon\lambda}] \frac{r_d(\lambda)}{\pi} \tau_2(\lambda) + \\
 &\quad (1-F)[L_{bs\lambda} + L_{b\epsilon\lambda}] r_d(\lambda) \tau_2(\lambda) + L_{us\lambda} + L_{u\epsilon\lambda}
 \end{aligned} \tag{3.3}$$

E'_s - Exoatmospheric irradiance

$\cos \sigma'$ - the angle from the target normal to the sun

τ_1 - transmission of the atmosphere from the sun to the target

τ_2 - transmission of the atmosphere from the target to the sensor

$\varepsilon(\lambda)$ - target emissivity

$L_{T\lambda}$ - self-emitted radiance from target at temperature T

$E_{ds\lambda}$ - solar downwelled irradiance

$E_{d\epsilon\lambda}$ - self-emitted downwelled irradiance from the sky

F - shape factor (amount of sky hemisphere that the target can see)
 $1-F$ - the percentage of the atmosphere that is blocked by the background object
 $r_d(\lambda)$ - target reflectance
 $L_{bs\lambda}$ - background radiance from scattering
 $L_{be\lambda}$ - background radiance from self emission
 $L_{us\lambda}$ - upwelled radiance due to scattering of the atmosphere
 $L_{ue\lambda}$ - upwelled radiance due to the self emission of the atmosphere

This equation represents all the sources of radiation that are of significant importance in determining the radiance that reaches imaging systems sensitive to 0.3-14.5 μ m wavelengths. As noted, this equation is dependent upon the wavelength. Depending upon the spectral sensitivity of the imaging system, this equation may be simplified by neglecting certain terms since their effects are minimal at those wavelengths. While both solar photons and self-emissive photons must be accounted for in the MWIR, solar photons are of little importance for this validation and can be neglected in the 8-14 μ m LWIR region of the electromagnetic spectrum.

3.2 Alternative SIG Models

In order to generate any synthetic image, several inputs must be defined to produce the desired objects in a specified environment. For almost all computer models, these basic inputs include a geometrical representation of the object, an atmospheric transmission model, radiation sources and material characteristics. Some models also include texturing abilities and thermal submodels. The overall accuracy of the final synthetic image depends on the individual accuracy and integration of these submodels as well as the intended use of the synthetic images. Therefore, it is beneficial to examine other SIG models to learn where improvements might be made to the current DIRSIG program.

One of the leading computer models for the creation of accurate radiometric synthetic images was developed by the Electromagnetics Laboratory of the Georgia Tech Research Institute (Cathcart and Sheffer, 1988 a, 1988 b). This SIG program, the Georgia Tech Visible and Infrared Synthetic Imagery Testbed (GTVISIT), integrates the outputs from the submodels MAX, GTSIG, IRMA, and MODELIR to create a synthetic image. Each GTVISIT scene is comprised of two main aspects, a gridded terrain background and faceted objects located in that background. The gridded database consists of features (material types), elevations, radiance values, and thermal IR reflectances where the elevation and feature data may be real, synthetic, or a hybrid, and the radiance and infrared data are determined from the temperature and reflectivity of the object. The following diagram outlines the inputs and process in creating a GTVISIT synthetic scene.

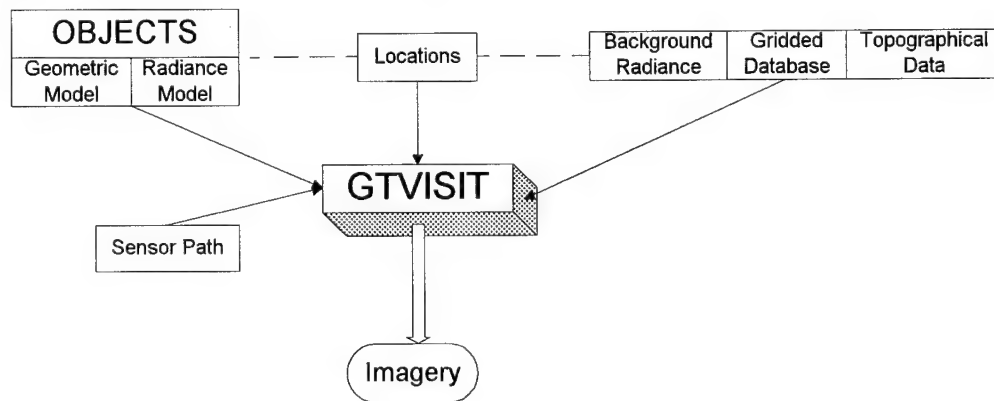


Figure 3.3 GTVISIT Overview (Cathcart and Sheffer, 1991)

Using all the various inputs into GTVISIT, it is then necessary to integrate these parts and determine the total radiance reaching the sensor. Different models propagate the radiance from the scene to the sensor through several techniques. While DIRSIG employs a ray-tracing method, GTVISIT uses a Z-buffer algorithm based on the principle of displaying or concealing surfaces using a visual line of sight to the sensor. GTVISIT also includes atmospheric attenuation for each object in the scene by pre-computing the radiance values in 12 orientations and then assigning an atmospheric radiance value to the facet. The thermal radiance values are then computed using first-principles techniques contained in the GTSIG submodel of GTVISIT.

By modeling all these real world phenomena, GTVISIT creates fairly realistic radiometric images. However, it falls short in that it does not account for angular emissivities or background effects on the radiance of the target. In addition, GTVISIT does not determine the solar history for the objects in the scene. Thus, while GTVISIT is one of the leading developers of radiometric synthetic images, there is still room for improvement.

The Physical Reasonable Infrared Signature Model, **PRISM**, is an extremely detailed model relying on highly sophisticated CAD drawings to create radiometrically accurate models of vehicles, primarily tanks (Gonda and Gerhart, 1989). This model relies on 3-D isothermal facets that interact with each other through conduction, convection, and radiation. PRISM models both the internal and external features of the tank. Using a Faceted Region Editor (FRED), BRL-CAD vehicle descriptions are translated into a format that PRISM can then use to predict the thermal signature. PRISM is also able to calculate the solar history and hence temperature of each facet for a diurnal time period. However, PRISM fails to calculate the interactions between the target and the background. Targets are "cut and pasted" into background scenes. PRISM creates very realistic images, but the difficulty in creating the detailed drawings and its failure to account for the interactions between the background and the target prevent its widespread use in other applications.

Texas Instruments (TI) has also developed a synthetic image generator for use with automatic target recognition (ATR) algorithms (Lindahl et al., 1990). This multi-sensor synthetic image generator is capable of producing IR, television (TV), and Laser Radar images. The following diagram illustrates the TI synthetic image generation process.

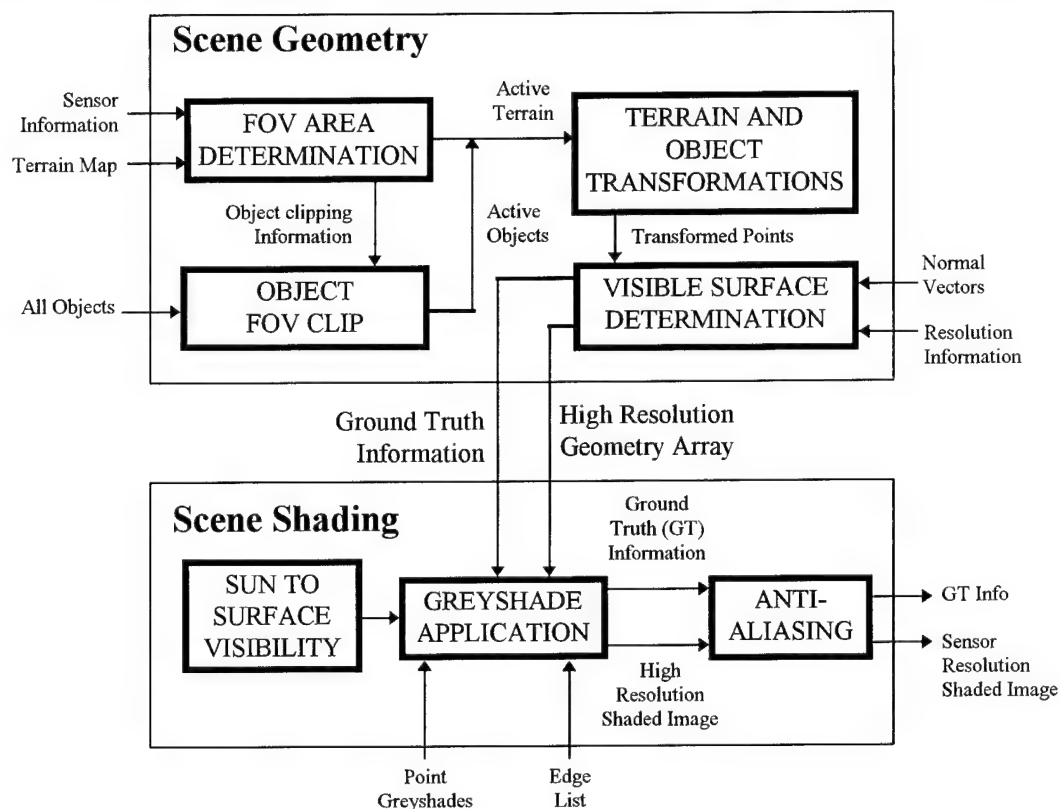


Figure 3.4 TI synthetic scene generation (Lindahl et al., 1990)

Similar to most SIG's, TI uses faceted objects placed in a fractal interpolated background environment derived from Defense Mapping Agency (DMA) Digital Terrain Elevation Data (DTED) and Digital Feature Analysis Data (DFAD). The objects, which are created using AutoCad 10, are initially placed onto the terrain scene using world coordinates and then both the terrain and the objects are translated to sensor coordinates. Trees may also be added to the scene using a fractal initiator/generator technique. Similar to GTVISIT, a Z-buffering algorithm is then used to determine which objects are hidden from the sensor by other surfaces. LOWTRAN 7 is also used to predict atmospheric transmission and attenuation. The Texas Instruments synthetic image generator also includes the ability to include sensor effects for each of the different sensor types; colored-noise that resembles the noise characteristics of the sensor is added to the synthetic image. Similarly, in order

to speed the generation of the synthetic image, "a two-dimensional Gaussian point-spread function is used to approximate the effects of optical diffraction and blur, detector and LED spatial response, and stabilization jitter for both the IR and TV sensors" (Lindahl et al., 1990).

TI's multisensor synthetic image generator sacrifices radiometric accuracy for computational speed. Its use of gray-shading and exclusion of solar or specular effects in the synthetic images reduce its abilities to model the real world. The results are realistic looking images, but have questionable radiometric fidelity. It provides useful synthetic images for automatic target recognition algorithms which rely more on relative image contrasts than absolute radiometric accuracy. Therefore, while this system can model many different sensors, it is of little benefit to those trying to assess the absolute radiometry.

Aerodyne Research, Inc., currently uses the **SPIRITS 2.0** (Spectral Infrared Imaging of Targets and Scenes) infrared SIG program for modeling aircraft targets and exhaust plumes (Stets et al., 1988). Relying on the LOWTRAN atmospheric model and IR Cloud Radiance Model (CLOUD) to recreate the atmosphere, SPIRITS integrates the results of cluttered background of terrain, sky and cloud with target images. While this program produces very detailed results of aircraft and vehicles with exhaust signatures, it has some limitations. It fails to create high resolution ground scenes and even treats the earth as a flat object with a uniform temperature and diffuse reflectivity. In addition, because the target and background are computed separately, it is not possible to include background effects in the calculations; however, this does not greatly detract from their model since most of their scenes involve high flying aircraft. This approach would not be possible for use by DIRSIG when high resolution ground scenes with radiometric accuracy are the primary goal. A new version of this program known as **AC-1** is scheduled for release next year. Some preliminary information about this new program will be available soon for analysis.

The Simulated Infrared Image (SIRIM) program created by the Environmental Research Institute of Michigan (ERIM) is vastly different from other thermal synthetic models. It calculates temperatures based on the 3-D volume of an object, versus traditional surface modeling. The volume modeling is achieved by subdividing the volume of an object into elements call voxels. "The voxels are simply cubic solids that fill the volume of the object" (Lyons 1991). This division of the object into voxels allows for complex thermal interactions and results in accurate temperature predictions. Thus, it could be useful in modeling thermal plumes and other volumetric shapes that have complex thermal gradients. Because of this unique modeling of object volumes, the geometric representation of an object is defined using constructive solid geometry (CSG) models in BRL-CAD. Boundary model representations, including wireframe and surface models, may be converted to CSG models using specialized translation programs. Similar to other high end thermal SIG models, a ray tracer is also used. The ray-tracer aids in creating the voxels, determining the solar loading of the voxels, and accounting for target-background interactions.

Four primary modules are used in the image generation process, in addition to the geometric modeling and ray-tracing. The information first travels into the VOXCRE module where the object volume is divided into voxels. The information is then directed to the VOXSUN, SVOXTMP, and RADCLC modules. The VOXSUN module, in conjunction with the ray-tracer, determines which voxels are exposed to solar heating and outputs the results to the temperature prediction module, SVOXTMP. SVOXTMP accounts for the conduction, convection, and radiation exchange between the voxels and surrounding object voxels as well as the environment. The output is a "three-dimensional temperature distribution of the object as a function of time but independent of sensor or viewing geometry." The temperature results are then used in the RADCLC module to determine the total radiance. The RADCLC module integrates the self emission of the object due to temperature and the reflected radiance from the environment. This is where the calculations end.

SIRIM does not propagate this radiance to a sensor or include any atmospheric transmission effects; it is not a complete end-to-end simulation package. This is a major limitation of SIRIM. In addition, the time required for the temperature calculations are extremely time consuming and computer resource intensive. If speed improvements could be made to the thermal calculations, SIRIM would be a valuable replacement to THERM, the DIRSIG thermal model. In its current form, the prolonged run times of SIRIM weighed against the added thermal accuracy do not warrant its integration into DIRSIG.

By examining other synthetic image generation programs, it is possible to determine the strengths and the weaknesses of these other SIG models. The ideal solution would be to create a synthetic image generation program that incorporated the strengths of all the various programs while minimizing the areas of weakness. DIRSIG is such an attempt at synthetic image generation. It was developed using the concepts of many different SIG models in order to create images that closely resemble real imagery.

3.3 DIRSIG Overview

In order for a synthetic image to accurately resemble the real world, it is necessary to develop a complete mathematical model of the entire imaging chain. This requires an understanding of the thermal radiance of the objects in the scene as well as the atmospheric effects on the radiance that ultimately reaches the IR sensor. The sensor effects must also be incorporated into the model to create realistic synthetic images. With all these inputs, it is then possible to try and develop a synthetic image. DIRSIG attempts to model the entire imaging chain using the inputs from various submodels. The following diagram, Figure 3.5, provides a brief overview of the submodels used in recreating the “real world” for a DIRSIG synthetic image. Each of these submodels will be described in detail.

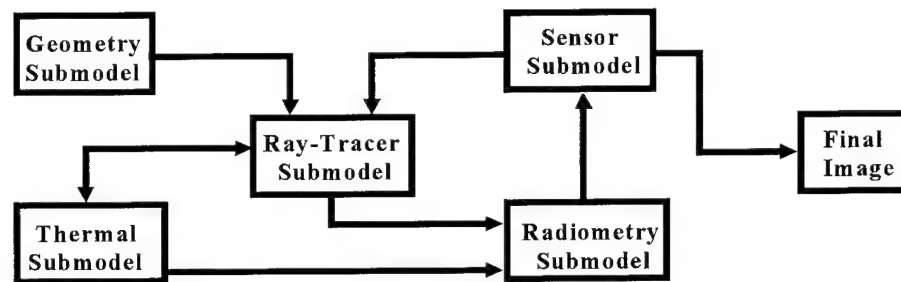


Figure 3.5 DIRSIG overview

3.3.1 Scene Geometry Submodel

In creating a synthetic image, one of the first steps is to build geometric models of the 3-Dimensional objects that will be in the output image. This is accomplished using computer aided design software known as AutoCad that has been enhanced with specialized DIRSIG related routines. In order to develop a scene that can be used by DIRSIG, it is necessary to create parts and objects that are made up of individual facets. A facet is a collection of points, usually triangular or rectangular, with a normal vector that describes the convex plane. These facets are the elementary building blocks to which various parameters or attributes are assigned and are then be used by the other DIRSIG submodels in creating the final synthetic image. The following diagram (Figure 3.6) illustrates the types of features that are assigned to each facet.

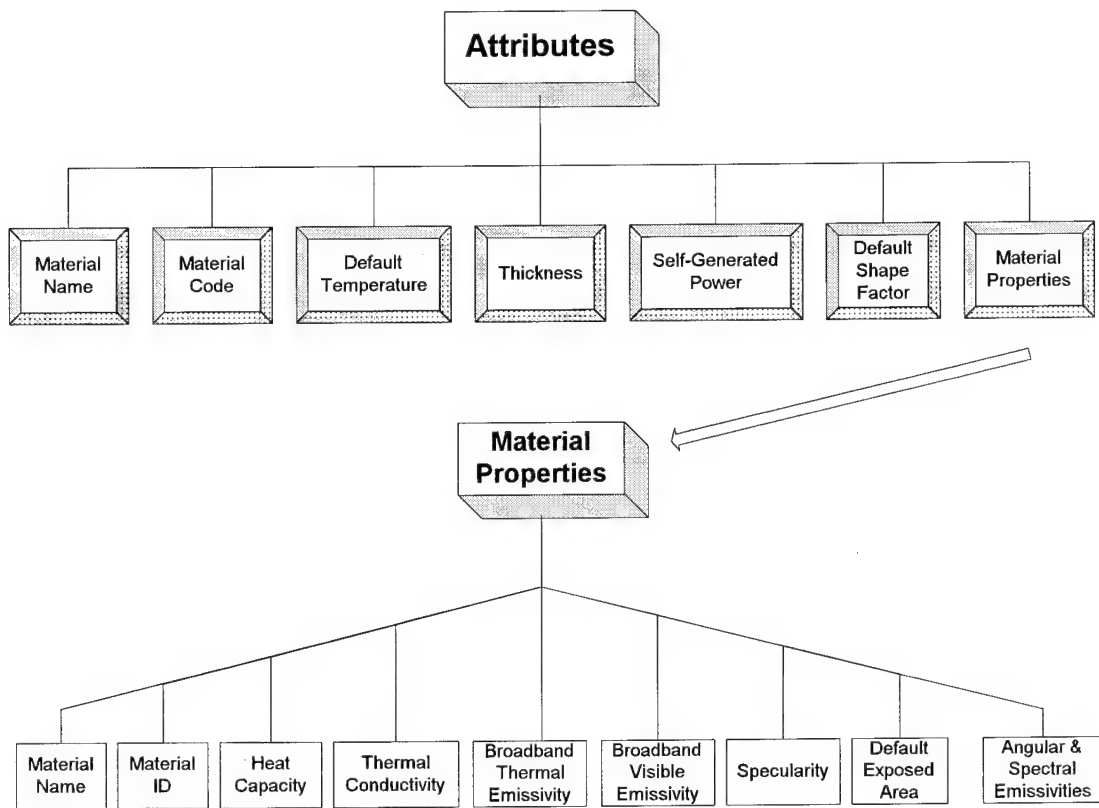


Figure 3.6 Facet material parameters

The faceted parts are then combined to form an object, and, finally, multiple objects may be integrated into one drawing to create the final 3-D scene, as depicted in Figure 3.7.

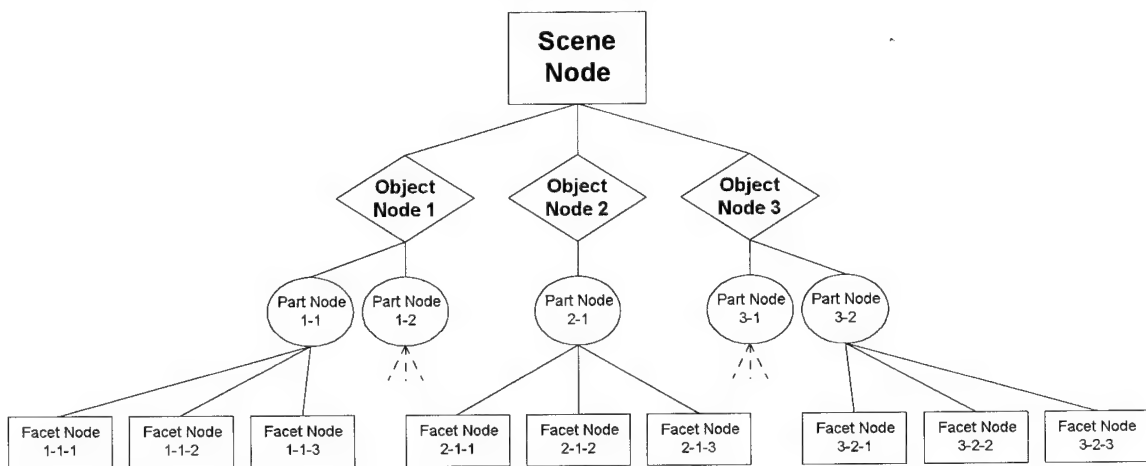


Figure 3.7 DIRSIG Data Hierarchy (Schott et al., 1993)

A certain data structure and hierarchy of information is assigned to the each object, part, and facet as the entire scene is created. The hierarchy of data assigned to each level was designed to minimize the amount of redundant information which can slow

computations and require more computer storage memory. Starting at the highest level, the scene node contains the name, date, geographical coordinates, and number of objects of the scene. The object node then contains the name, ID number, number of parts in that particular object with pointers to nodes describing each part, and the coordinates that define the edges of the bounding volume. The bounding volume of the object is used when the rays are cast into the scene (see Figure 3.8). If the ray does not hit the bounding region of the object, it is not necessary to cast the ray into the parts and facets of that object. This helps to reduce the computation time for the ray-tracer submodel. The part node data structure is the same as the object node, with bounding volumes to eliminate the need to check each facet within the part for a ray intersection. Finally, the facet node links the geometric location and orientation of the facet with the material properties.

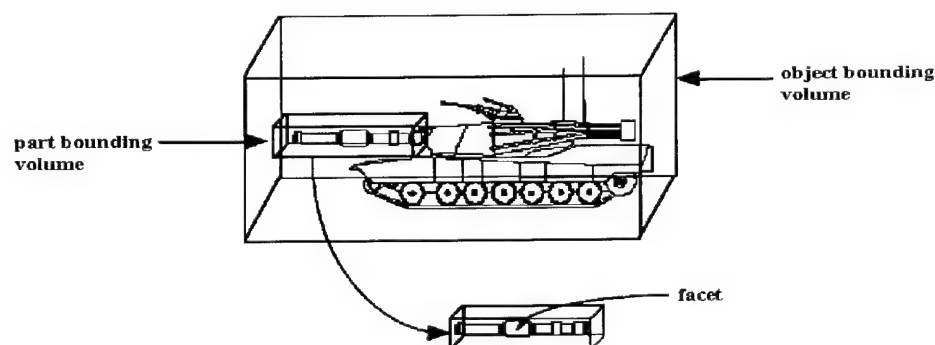


Figure 3.8 Object & part bounding volumes (Schott et al., 1993)

After all the DIRSIG hierarchy has been established and the scene is complete, the AutoCad scene is then 'translated' into real world geographical coordinates so that the other submodels of DIRSIG can recognize the inputs.

3.3.2 Ray-Tracer Submodel

The ray-tracer submodel is the vital connection and link to all the DIRSIG submodels. This submodel retraces the hypothetical path of a photon after it has reached the sensor. Beginning at an individual pixel in the synthetic image, a ray is cast into the scene (see Figure 3.9).

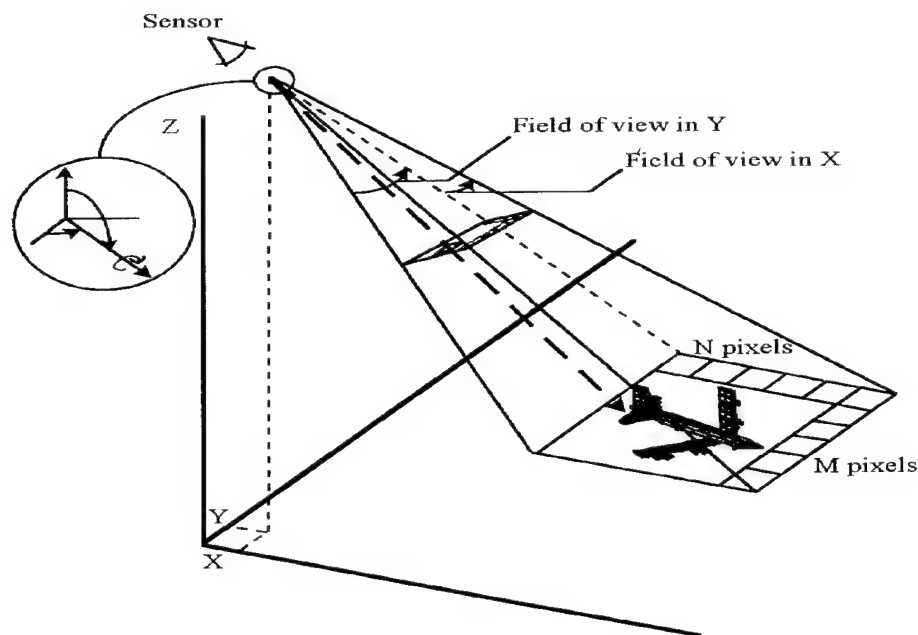


Figure 3.9 Ray-tracer (Schott et al., 1993)

An iterative process is used to determine the interaction of the ray with each object, part, and facet in the scene. From these interactions, the path of the radiance reaching the sensor can be determined. The energy losses and gains associated with the atmosphere are included in the process. This allows the proper radiance at each pixel to be computed by the radiometry submodel. The radiometry submodel is described in detail in Section 3.3.4.

Because each ray must be tested for intersection with every single object in the scene, bounding volumes for each object and part were developed to reduce the number of interactions that must be examined. This process reduces computation time because if an object is not hit by the ray, it is not necessary to determine the interaction of that ray with the sub-parts or facets. These bounding volumes may be parallelepipeds, cubes, or spheres. If a ray hits a particular object, it is then checked with the parts in that object, and finally, the interaction with the individual facets is determined. If it is found that a facet has been hit by a ray, the solar history of the facet is established so that a more accurate temperature can be predicted by THERM. THERM uses direct insolation, or direct sunlight values, from the weather file to more precisely predict the temperature of the object.

The solar history of the object is stored in an array as a function of time with values ranging from 0 to 1.

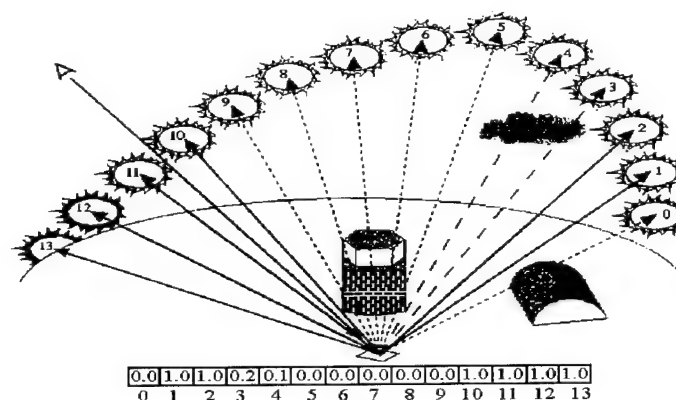


Figure 3.10 Solar history (Schott et al., 1993)

If the object was illuminated by the sun at a particular time, a value greater than 0 is placed in the array and the solar loading term in the weather file is weighted by this value. However, if the object has been in the shadow or not illuminated by the sun, a value of 0 is placed into the array. Therefore, when the solar loading value in the input weather file is multiplied by the solar history value of 0, the overall effect is a zero solar loading term when the target has been in shadow. After the solar history of the facet has been determined and the resulting direct insolation values have been calculated, the temperature of the facet may then be computed by THERM.

Once a ray hits a facet and the solar history has been calculated, the interaction between the ray and the facet depends on the specularity and shape factor of the target. A target may be specular, diffuse, a combination of the two, or even transmissive (see Figure 3.11). The shape factor of the facet is also calculated at this time as additional rays are cast from the facet to determine the amount of atmosphere that is blocked by surrounding objects.

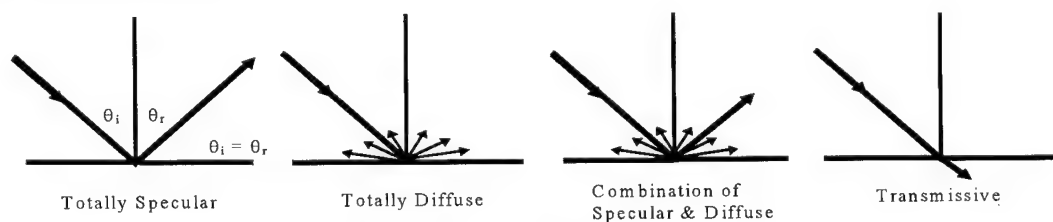


Figure 3.11 Target interactions

If the facet is reflective, then secondary rays must be cast out, similar to the original ray-tracing method. For completely specular targets, a single ray is cast out at an angle equal to the incidence angle. The properties of the background are determined and then used to calculate the radiance of the target facet. However, most targets are not completely specular. This requires a more rigorous method of determining the background effects. Therefore, 'diffuse' secondary rays are cast out over the hemisphere at 15° increments in the zenith and 30° increments in the azimuth. The procedure for determining the background hits is the same as for the specular case: test each object, part, and facet. Then, for each secondary ray that is cast, the temperature and properties of the object that is hit are recorded. The combined effects of these secondary hits are integrated to approximate the diffuse radiance value reaching the target. While this process of casting rays could continue indefinitely, a maximum of two bounces is usually sufficient to determine the appropriate radiance value in the IR region (Shor 1990). The following chart outlines the flow for determining the radiance if the object is reflective (specular, diffuse, or a combination).

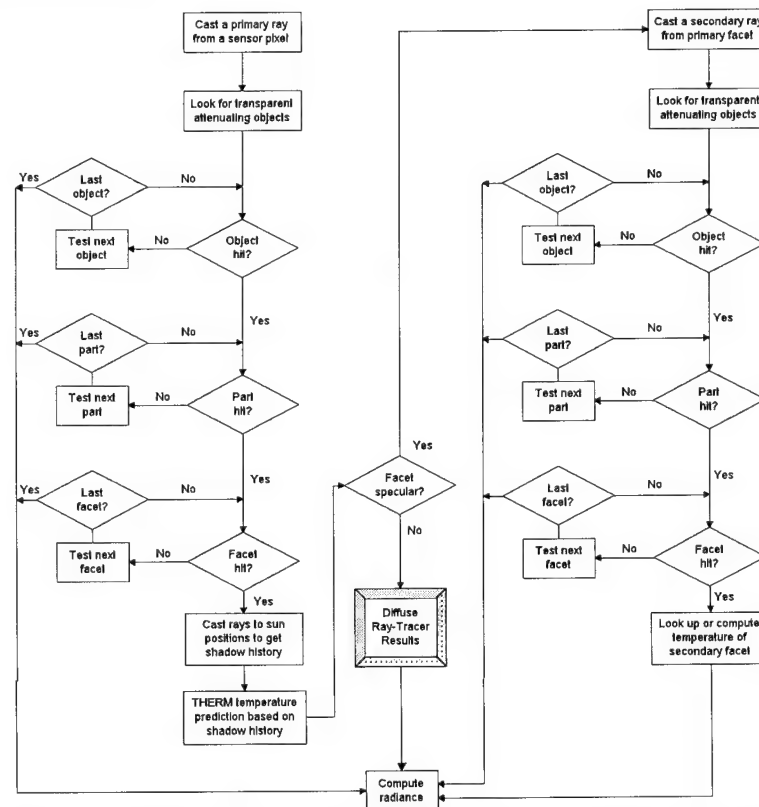


Figure 3.12 Ray-tracer flow diagram (Schott et al., 1993)

The result may actually be a transmissive facet in which the ray continues through the scene in a modified manner. Transmission is not discussed in detail because the validation of transmissive effects is beyond the scope of this project.

3.3.3 Thermal Submodel

The thermal submodel computes the temperature of each individual facet over a specified time history using the THERM model developed by the DCS Corporation. The output temperature of the facet from THERM is based on two main features: facet parameters and time dependent environmental parameters. In determining the output temperature, THERM uses a first principles model to evaluate the heat transfer between the target and the environment. THERM also treats each facet independently of the other facets and assumes that the facet has uniform characteristics.

This treatment of thermally independent facets leads to the one major limitation of THERM in that it does not determine the conduction between adjacent facets. However, THERM does allow the user to assign a self-generated power to each facet. This combined with the use of the solar history of the object helps to compensate for lack of thermal conduction, improving the temperature prediction and accuracy. This deficiency of DIRSIG could be eliminated by determining the conduction between the facets through a finite element analysis. This would improve the accuracy but would greatly add to the run time of DIRSIG images and is considered to be too detailed for most practical applications. However, in an attempt to reduce this deficiency, DIRSIG has recently been modified to allow indirect diffusion from internal heat sources. Internal heat sources may be used to simulate vehicle engines or other heat sources that are located inside other objects. This modeling helps to simulate actual thermal conditions without having to determine the conduction between facets (Sirianni 1994).

In determining the temperature of the facet, the most difficult errors to eliminate involve assigning proper values to the various material parameters. The errors in material parameter values arise from the limited database that is available for almost an infinite number of materials in the world. As a result, it is often necessary to try and vary some of

these material parameters to match the synthetic radiance values with those of the truth or real imagery.

There are several different material parameters of the facet that can be modified to produce more accurate results. The exposed area of the material is the fraction of the object's area that is exposed to the environmental conditions. The more an object is exposed to the environment, the more the atmosphere will affect the temperature of the object through convection. The thickness and heat capacity of the facet also influences the final temperature. Thicker objects with a higher heat capacity have more thermal inertia and hence, tend to resist changes in temperature. The thermal conductivity of the facet also influences the heat transfer between the facet and the surrounding environment. By varying these material parameters, more accurate final temperature results can be produced by THERM.

Time dependent environmental parameters are the other major input to THERM. Traditionally, real weather data is used as inputs to THERM. However, THERM can also be used to predict weather parameters and values when a complete set of weather information is not available.

These inputs to THERM will be the focus of the input parameter analysis and optimization. Estimating these inputs is critical in creating accurate synthetic images; the output from THERM is only as good as the inputs. Since the radiance reaching the sensor in LWIR images is dominated by the self-emission, *i.e. apparent temperature*, of objects, the output from THERM is the most likely source of error. Therefore, a complete understanding of the inputs to THERM will help produce better results. Treating THERM as a black box, the input parameter analysis will examine both the effects of changing the input parameters and the abilities of THERM to model the real world. Thus, the analysis will test both THERM itself, and the inputs to THERM.

3.3.4 Radiometry Submodel

In a real image, the number of photons emitted, absorbed, and reflected in a scene determine the resulting output image. To produce a synthetic image, a mathematical model of the photon paths must be used to account for all the different sources of radiation that might possibly reach a real sensor and create the image. Therefore, using inputs from THERM and the ray-tracer submodels, the radiometry submodel determines the spectral radiance reaching the sensor.

Because the radiance must travel through a non-uniform atmosphere before it reaches the sensor, different types of particles in the atmosphere may affect the radiance that eventually reaches the sensor. As a result, it is also necessary to have a model of the attenuating atmospheric conditions. DIRSIG currently uses an atmospheric model known as MODTRAN that can be completely controlled by inputs from the user. MODTRAN uses either an existing atmospheric database with the ozone density, water vapor density, temperature, and concentration of the gases H_2O , CO_2 , O_2 , O_3 , N_2O , CH_4 , NO , SO_2 , NO_2 , NH_3 , HNO_3 already defined depending on a mid-latitude summer, maritime, sub-arctic, or other conditions; or the atmosphere can be more accurately simulated by MODTRAN using time and location specific radiosonde data as inputs. While the upper atmosphere, including the troposphere and stratosphere, are fairly constant over time, the lower atmosphere near the surface can change very rapidly. Therefore, it is often beneficial to obtain hourly weather information from either in scene measurements or from local sources, such as an airport, that can then be input into the computer model.

From all these parameters, the final outputs of the Modtran model include the wavelength and angular dependent atmospheric transmission and upwelled/downwelled radiance values. These values are used in DIRSIG's model of the "big equation." As mentioned in the ray-tracer submodel description, facets may be transmissive, diffuse, specular, or a combination of specular and diffuse. Table 3.2 expressed the components of the "big equation" conceptually and mathematically.

$$L(\theta, \phi, \lambda) = \{[(\text{Solar scattering} + \text{Background}_{\text{specular}}) \cdot \text{Reflectivity}_{\text{specular}} \cdot \text{Specularity}] + [(\text{Solar scattering} + \text{Background}_{\text{diffuse}}) \cdot \text{Reflectivity}_{\text{diffuse}} \cdot (1 - \text{Specularity})] + [\text{Emissive component}]\} \cdot \text{total transmission} + \text{Upwelled Radiance} \quad (3.4)$$

Table 3.1 Radiance equation

Mathematical Expression	Conceptual Expression
$L(\theta, \phi, \lambda) =$	
$\frac{E_s(\lambda)}{\pi} \tau_1(\lambda) \tau_{1c}(\lambda) \cos(\theta_s) +$	Solar scattering
$L_{DE}(\theta_{SK}, \phi_{SK}, \lambda) + L_{DS}(\theta_{SK}, \phi_{SK}, \lambda) \cdot (1)$ or $\frac{E'_s(\lambda)}{\pi} \tau_1 \tau_{SB} \cos(\theta_B) (1 - \varepsilon_B(\theta_{BT}, \lambda) + L_{TB}(\lambda) \varepsilon_B(\theta_{BT}, \lambda)) \cdot (2)$	Specular Background Effects Sky (1) or Object (2)
$(1 - \varepsilon_T(\theta, \lambda)) \cdot$	Specular reflectivity
$S +$	Specular weighting factor
$\frac{E_s(\lambda)}{\pi} \tau_1(\lambda) \tau_{1c}(\lambda) \cos(\theta_s) +$	Solar scattering
$\int_0^{\frac{\pi}{2}} \int_0^{2\pi} \{ [L_{DE}(\theta_{SK}, \phi_{SK}, \lambda) + L_{DS}(\theta_{SK}, \phi_{SK}, \lambda)] \tau_{TB}(\lambda) + L_{TB}(\theta, \phi, \lambda) \} \cos(\theta) \sin(\theta) d\theta d\phi \cdot$	Diffuse Background Effects
$(1 - \varepsilon_T(\lambda)) \cdot$	Diffuse reflectivity (specular reflectivity at nadir)
$(1 - S) \cdot$	Diffuse weighting factor
$\varepsilon_T(\theta, \lambda) L_T(\lambda) \cdot$	Emissive Component
$\tau_2(\theta_E, p, \lambda) \tau_{2c}(\lambda) +$	Total transmission
$L_{uS}(\theta_E, p, \lambda) +$	Upwelled Radiance - Solar scattering
$L_{uE}(\theta_E, p, \lambda)$	Upwelled Radiance - Emissive

The results of these radiometry equations are then integrated using the spectral response function of the sensor in order to obtain the final radiance value at each pixel. The variables contained in the equations above are described in detail on the following page.

Table 3.2 Radiance equation variable definitions

Variable	Definition
$L(\theta, \phi, \lambda)$	spectral radiance reaching the front end of the sensor
$E_s(\lambda)$	the exoatmospheric solar spectral irradiance
$L_T(\lambda)$	the self-emitted spectral radiance from a blackbody at temperature T (target)
$L_{TB}(\lambda)$	the self-emitted spectral radiance from a blackbody at temperature T (background)
$L_{T(TBE)}(\lambda)$	the self-emitted spectral radiance from a blackbody at temperature T (extinction source between the target and the background)
$L_{T(STE)}(\lambda)$	the self-emitted spectral radiance from a blackbody at temperature T (extinction source between the sensor and the target)
$L_{DE}(\lambda)$	the downwelled spectral radiance due to self-emission of the atmosphere integrated over the skydome
$L_{DS}(\lambda)$	the downwelled spectral radiance due to scattering integrated over the sky-dome
$L_{DE}(\theta_{SK}, \phi_{SK}, \lambda)$	the directional downwelled spectral radiance due to self-emission of the atmosphere
$L_{DS}(\theta_{SK}, \phi_{SK}, \lambda)$	the directional downwelled spectral radiance due to scattering
$L_{uE}(\theta_E, \lambda)$	the upwelled spectral radiance due to self-emission of the atmosphere along the target-sensor path
$L_{uS}(\theta_E, \lambda)$	the upwelled spectral radiance due to scattering along the target-sensor path
$\tau_1(\lambda)$	the atmospheric spectral transmission along the source-target path
$\tau_2(\theta_E, \lambda)$	the atmospheric spectral transmission along the target-sensor path
$\tau_{1c}(\lambda)$	spectral transmission through all transparent objects along the sun-target path
$\tau_{2c}(\lambda)$	spectral transmission through all transparent objects along the target-sensor path
$\tau_{SB}(\lambda)$	spectral transmission through all transparent objects along the sun-background path
$\tau_{TB}(\lambda)$	spectral transmission through all transparent objects along target-background path
$\tau_{2c}(\lambda)$	spectral transmission through all transparent objects along the sensor-target path
$\varepsilon_T(\theta, \lambda)$	angular spectral emissivity for the target
$\varepsilon_B(\theta, \lambda)$	angular spectral emissivity for the background
θ	the angle between the normal to the surface and the sensor-target path
θ_s	the angle between the normal to the surface and the sun-target path
θ_B	the angle between the normal to the background and the sun-background path
θ_E	the angle between the normal to the earth at the target and the sensor-target path
θ_{SK}	the angle between the normal to the earth and the specularly reflected ray from the sensor to target area
θ_{BT}	the angle between the normal to the background and the target hit point
ϕ	the azimuth angle between the projection of the ray cast to the sky on the ground and the scene's reference direction
ϕ_{SK}	the azimuth angle between the projection of the ray cast to the sky on the ground and the scene's reference direction
p	the range between the target and the sensor

3.3.5 Sensor Response and Modulation Transfer Functions

The sensor submodel is the final submodel that affects the synthetic output image. The sensor submodel converts the radiance values from the radiometry submodel to digital count values, employing the spectral response of the sensor in the calculations. The spectral response of the sensor describes the responsivity of the sensor at different wavelengths, scaled by the maximum sensitivity of the sensor in the specified region so that the output ranges from 0 to 1. For example, a thermal imaging sensor will not be very responsive in the visible region while it should have a responsivity near one in the infrared region of the electromagnetic spectrum. The following equation is used to calculate the radiance after it has passes through the sensor.

$$L_w(\theta) = \sum_{\lambda=\lambda_{\min}}^{\lambda_{\max}} L(\theta, \lambda) \mathcal{R}(\lambda) \Delta\lambda \quad (3.5)$$

$L_w(\theta)$ - radiance at zenith angle θ integrated over λ_{\min} to λ_{\max}

$L(\theta, \lambda)$ - radiance at zenith angle θ and wavelength λ

$\mathcal{R}(\lambda)$ - Spectral Responsivity at wavelength λ

This radiance is then converted to a digital count value using the following equation.

$$DC = \text{gain} \cdot L_w(\theta) + \text{offset} \quad (3.6)$$

DC - final digital count value

$L_w(\theta)$ - radiance at zenith angle θ integrated over λ_{\min} to λ_{\max}

gain - gain of the sensor

offset - offset of the sensor in digital counts

While the sensor is one of the last submodels to affect the synthetic image, its location in the scene must be established using one the first submodels, AutoCad. Using the CAMERA function from AutoCad, the user can view the scene as it would appear from various sensor look angles, positions, and magnifications. The optimum or desired position of the sensor is then set and the geometric information is then recorded from AutoCad. After this information is recorded, it is saved in a file so that the ray-tracer and radiometry submodels can access this information for their calculations.

The sensor submodel can also be used to incorporate other effects into the final synthetic output image. Motion, optical, electronic, and sampling effects may be added to

the sensor model to make the synthetic image appear more realistic. Random and periodic noise can also be added to degrade the quality of the image. Various sensor configurations including frame cameras, pushbroom scanners, and line scanners may be selected in the sensor submodel to create the geometric distortions commonly found in real imagery obtained using these sensor configurations. While line scanner effects were included in the validation, optical and noise effects were just being finished at the time of validation. All these effects add to the realism of the synthetic image.

3.3.6 Final Image Generation Review

The final generation of a DIRSIG synthetic image requires the integration of all these submodels. Some of the submodels perform multiple tasks at various stages in the synthetic image generation process. Beginning with the scene geometry submodel, the user creates a scene of objects with defined locations, dimensions, and material parameters. The facet attributes which are assigned to the objects are then referenced by the ray-tracer. Using a time of day specified by the user, a solar history at 15 minute intervals is also created for each facet by the THERM submodel, and then this is input to the ray-tracer. The ray-tracer then casts out a ray from each pixel in the scene in order to determine the background interactions. With the solar history and attributes of each pixel known, the temperatures are then computed using THERM. The temperature and ray-tracer results may then be used by the radiometry submodel to solve the spectral radiance equations. The radiance reaching the front of the sensor at each wavelength may then be passed to the sensor submodel so that the spectral response of the sensor may be incorporated into the final results. Finally, the sensor submodel integrates the radiance results over the appropriate wavelengths and converts the output to digital count values for the final output synthetic image.

DIRSIG and its submodels are designed so that continual improvements can be made to the synthetic image generation process. While DIRSIG could not function without each submodel, examining the submodels can point to areas of possible improvements. In addition, the compartmentalization of DIRSIG allows for possible replacements of the submodels if improvements or better models become available.

4.0 Technical Approach & Procedure

4.1 Validation of DIRSIG

The process of validating DIRSIG in the infrared region consists of three main steps. These steps include procuring aerial images of the region of interest, creating a synthetic image of this same region using DIRSIG, and, finally, evaluating the synthetic imagery using the truth imagery. Each of these three main tasks can then be subdivided into smaller tasks.

The first step is to obtain aerial images of a region in which certain parameters and information are known. This includes extensive knowledge of the sensor and its characteristics. If a model of the sensor is not available, DIRSIG will not be able to produce reasonable results. The exact location of the aircraft at the imaging time is also needed so that the sensor can be properly positioned in the synthetic image. Weather information and radiosonde data from the imaging time and location that the image was taken must also be obtained to accurately model the atmosphere using MODTRAN. Finally, either access to the region of interest or the combination of maps and plans should be available so that the geometry of the various objects in the scene can be recreated using AutoCad.

The next major step and task in the validation of DIRSIG is to reproduce and create the synthetic image of a particular region of interest from the aerial image. In order to validate the geometry of DIRSIG, care must be taken to ensure that each object is reproduced as accurately as possible with the proper dimensions. The dimensions of the buildings can be obtained from maps, surveys, or owners of the various structures. If either of these methods is not possible, it is possible to estimate the size, location, and dimensions of the objects through the use of visible imagery and photogrammetry. However, the results from photogrammetry will probably not be as accurate as the results from plans or blueprints. In addition, photogrammetry is extremely time consuming. On-sight inspection of the scene would also help to determine some of the material properties

of the targets in the scene. Finally, terrain and elevation profiles of the region can be recreated from USGS maps.

The creation of a realistic synthetic image is a major task that has its own procedure or approach that one should follow. This validation will help determine the procedure for generating a realistic scene in the DIRSIG environment. This will be accomplished largely through a trial and error process because of the limited scenes that are available for reference. It will also explore the limitations of the DIRSIG environment in handling the complexity of a realistic scene. As discussed earlier, this task will be shared with Russell White as he validates DIRSIG in the visible region. This scene will then be available for future use and testing of DIRSIG as well as image analysis programs.

After the region of interest has been assembled using AutoCad and the appropriate material parameters have been assigned to the facets, the scene can then be processed using DIRSIG to create the synthetic image. This will provide an initial synthetic image with which a comparison can be made to the actual imagery. However, there are often errors in the synthetic image that arise from differences in the material parameters, weather information, and thermal predictions. As a result, these input parameters are modified through an iterative process until the synthetic image closely resembles the aerial imagery.

Once the two images have been closely matched, or at least to the best abilities of the operator, it is necessary to complete the final stage of the validation by comparing the two images. Several different methods of comparing images are available, including root mean square (RMS) error and rank order correlation. These methods are discussed in more detail in the following subsection. Once the synthetic image is in its final form, the images can be compared in terms of digital count, radiance, or temperature values.

After this initial validation has been completed and all the material parameters have been firmly established, the synthetic scene will be compared to alternate imagery of the same region of interest. However, this imagery will have different imaging conditions and parameters. As a result, the objects in the scene will appear different. For example, an

aluminum sided building may be sunlit in one image but in the shade in the other image. DIRSIG must be able to accurately model both conditions based on the material parameters that were established for the first image; the material parameters will not be modified when comparing the synthetic image with the second real image. This will help to test the robustness of DIRSIG. Ideally, the same errors should be found when the synthetic image is compared to the alternate truth imagery, different errors indicating deficiencies in the robustness of DIRSIG.

Using these criteria, a scene incorporating the Kodak Hawkeye plant and the surrounding area of NW Rochester, NY, has been selected to validate DIRSIG. One of the major reasons for selecting this area was the availability of both visible and LWIR

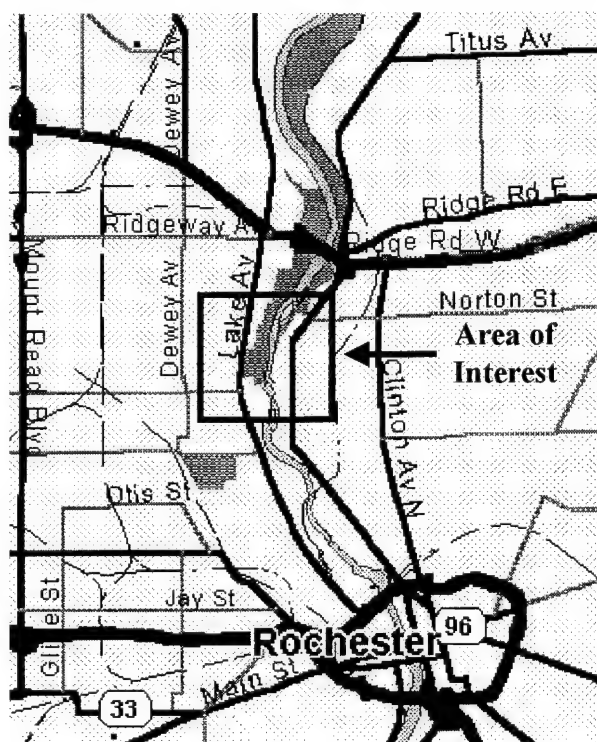


Figure 4.1 Area of interest

imagery. This allowed the sharing of the workload in building a realistic scene of these proportions. The area of interest, a 1km \times 1km region, is shown relative to the city of Rochester, NY, in Figure 4.1. Aerial images are available in the visible and thermal regions of the spectrum, permitting the use of the same scene for both the visible and thermal validations of DIRSIG. In addition, this area is readily accessible to obtain geographic measurements and information. Additional images of this region were also taken from the roof-tops of neighboring buildings using RIT infrared

cameras. One other primary reason for selecting this region was based on the fact that synthetic imagery of the Kodak Hawkeye plant has already been created (Salacain 1995). While extensive additions and modifications will be required, it provides a starting point from which expansions and improvements can be made.

4.1.1 Radiometric Validation Methods

In order to determine the accuracy of the synthetic image, a comparison between the synthetic image and the truth imagery is necessary. These methods of comparison include the rank order correlation and the root mean square error of specified targets. Each method offers a unique comparison that provides different results and insight into the resulting accuracy of the synthetic imagery. The results from these methods can then be used in assessing problems and deficiencies in the synthetic image generation process.

4.1.1.1 Rank Order Correlation

Rank order correlation is used to “evaluate the relative contrast produced in a synthetic image as compared to truth” (Schott et al., 1993). Relative contrast in an image is important for both human and computer based classifiers in evaluating an image and detecting specified objects within a scene. Each object or a specified number of objects in the scene are given a ranking in terms of the brightness of the object. This brightness ranking can then be used to compare a synthetic image with a real or truth image. If the contrast rankings in the synthetic image do not closely resemble the rankings of the truth image, a problem has been detected in the synthetic image generation process that will then result in an error when computer or human assessment of the synthetic image is performed.

Once the objects in both the synthetic and the real image have been ranked according to their brightness, or digital count values, the comparison and, hence, assessment of the synthetic image can be accomplished. An initial evaluation can be seen by graphing the rank order in the truth image versus the rank order in the synthetic image. Ideally, this would be a perfectly linear graph with a one-to-one target correlation. “Any difference in ranking between the DIRSIG image and the truth image is indicative of a contrast reversal for that object in the DIRSIG scene” (Schott et al., 1993). Because the thermal properties of objects will vary at different times, the rank order in the synthetic image will also vary. By comparing images at different times of the day using the rank order correlation

method, a good overall assessment of the synthetic image generation process can be found.

By examining the rank order of each corresponding object in the two scenes, an overall rank order correlation coefficient can be assigned to the image. The Spearman rank order correlation is defined as:

$$\rho_{TOD} = 1 - \frac{6 \sum (R_i - R'_i)^2}{n^3 - n} \quad (4.1)$$

ρ_{TOD} - correlation coefficient for each image pair at a particular time of day (TOD)

n - number of samples

R_i - rank in the truth image for the i^{th} object

R'_i - rank in the synthetic image for the i^{th} object

This overall rank order correlation can then be used in comparing the overall accuracy of the synthetic images. However, the one major problem with rank order correlation comparisons is that it is insensitive to overall radiometric gain or bias errors. To detect these gains and biases in the radiometry, the root mean square error method of comparison is needed.

4.1.1.2 RMS Error

While the rank order correlation can help detect radiometric problems in individual objects, the root mean square (RMS) error method is useful in detecting overall problems in the synthetic image generation process. The root mean square error method helps to detect overall gain or bias problems in the radiometry of the synthetic image caused by errors in the atmospheric parameters or sensor characteristics. The actual RMS error is found by comparing the mean radiance values of objects in the synthetic image with the same objects in the truth or real image.

$$RMS = \sqrt{\frac{1}{n} \sum (L_i - L'_i)^2} \quad (4.2)$$

n - number of objects

L_i - radiance in the truth image for the i^{th} object

L'_i - radiance in the synthetic image for the i^{th} object

While this equation shows the RMS calculation using radiance values from the real imagery and the synthetic imagery, temperatures are often used when dealing with thermal imagery. The radiance at the sensor can be converted to an apparent temperature very easily using known temperatures, Planck's equation, and the sensor responsivity. The spectral radiance values for temperatures that span the range of expected values in the scene are found from the Planck equation.

$$L(\lambda) = \frac{2hc^2}{\lambda^5 (e^{\frac{hc}{\lambda kT}} - 1)} \quad (4.3)$$

$L(\lambda)$ - spectral radiance
 T - absolute kinetic temperature of the target
 c - speed of light (2.99792458×10^8 m sec⁻¹)
 h - Planck's constant (6.626176×10^{-34} Jsec⁻¹)
 k - Boltzmann constant (1.380662×10^{-23} J K⁻¹)

These spectral radiance values are then multiplied by the sensor responsivity and integrated in the appropriate bandpass.

$$L = \int_{\lambda_{min}}^{\lambda_{max}} L_{\lambda \text{ Planck}} \cdot \mathcal{R} d\lambda \quad (4.4)$$

The radiance values are plotted against the reference temperatures to determine a piecewise linear equation that can be used to calculate the apparent temperatures.

4.1.2 Geometric Validation

The validation of DIRSIG will also include a geometric validation and comparison between the line scanner imagery and the synthetic imagery from DIRSIG. This geometric comparison will help to validate the modeling of a line scanner in DIRSIG. Any geometric bias in the synthetic image will be removed prior to assessing the geometric accuracy. A geometric bias would likely result from uncertainty in the location of the plane. This geometric bias will be removed through a first order registration, *rotation and scaling*, to match the synthetic image and the truth image.

Similar to the radiometric validation, the geometric validation will be accomplished using RMS error. The overall RMS error in the scene is found by selecting several objects

throughout the scene. The coordinates of the these objects in the truth and synthetic imagery are recorded. The error in the x and y directions for each object is then used in determining the geometric error:

$$RMS_{\text{geometry}} = \sqrt{\sum Error(x)_i^2 + Error(y)_i^2} \quad (4.5)$$

$Error(x)_i$ - Error in x value for the i^{th} object location

$Error(y)_i$ - Error in y value for the i^{th} object location

4.2 Input Parameter Analysis & Optimization

Knowing that the generic input parameters to DIRSIG would not provide the necessary accuracy for the validation, it was necessary to develop a method to optimize the input parameters. An ad hoc approach could be used to modify the input parameters, but it would be impractical to modify each of the input parameters and rerun DIRSIG in a scene this complex. A more structured and calculated approach was needed. This led to a sensitivity analysis of each of the input parameters. The sensitivity analysis provides insight into the amount of change in a input parameter that is necessary to optimize the input parameter and obtain the desired output value.

One of the first steps in a sensitivity analysis is to determine the expected range of values and standard deviation for the input parameters. The range of values and standard deviation can be found from published databases, measured values, or a combination of these two resources. Because of the limited data, sometimes only two values are available for each parameter from the published resources. When this occurs, the values are not representative of an absolute minimum or maximum. They are more likely representative of a relative minimum and maximum that have a distribution of values that intersect with each other. These relative minimum and maximum values can be used as the range of values for the sensitivity analysis, $\Delta_{parameter}$, but the standard deviation, $\sigma_{parameter}$, is still needed for the optimization of the input parameters. The standard deviation is derived from the relative minimum and maximum by assuming that the available values are separated by two standard deviations. (see Figure 4.2 below)

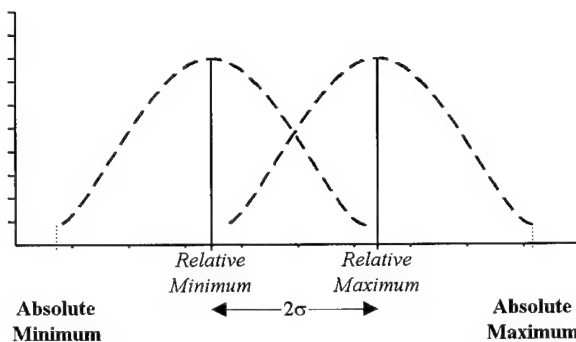


Figure 4.2 Relative minimum & maximum input values

$$\sigma_{parameter} = \frac{max_{relative} - min_{relative}}{2} \quad (4.6)$$

With the range of values and standard deviation of each input parameter, the sensitivity analysis can be conducted.

In order to determine the sensitivity of an input parameter, the parameter is varied over the specified range of values, $\Delta parameter$. The resulting output is recorded for each variation of the input. The output is then graphed against the changing input parameter. As long as the graphs are approximately linear, a first order linear regression can be used to determine the overall output sensitivity to the input parameter, $\Delta output / \Delta parameter$. The units of the output depend on the output of the object being studied. Unfortunately, the output sensitivity value may not always be in the desired units for the analysis. A mathematical conversion is then needed.

This was the case for the input parameter analysis involving THERM. Because a sensor ultimately detects radiance, the ‘big equation’ was used to convert the output sensitivity from THERM, $\Delta T_{ground} / \Delta parameter$, into a radiance sensitivity at the sensor, $\Delta L_{sensor} / \Delta parameter$ (the actual inputs to THERM and the ‘big equation’ conversions are discussed in detail in **Section 6.0**).

$$\Delta parameter \Rightarrow \text{THERM} \Rightarrow \frac{\Delta T_{ground}}{\Delta parameter} \Rightarrow \text{Big Equation} \Rightarrow \frac{\Delta L_{sensor}}{\Delta parameter}$$

It is often difficult to analyze errors and differences in radiance units; most thermal analysis is conducted using apparent temperature. Therefore, radiance sensitivity values are converted into apparent temperatures using a reference blackbody. First, the radiance for a blackbody at 300 & 301°K is calculated using the Planck equation (Eq 4.3). These two radiance values are then propagated to radiance values at the sensor where the sensor responsivity can also be included. The difference between these values provides the change in radiance per unit change in temperature, $\Delta L_{BB} / \Delta T_{BB}$. The inverse is then

multiplied by the radiance sensitivity to obtain the final input parameter sensitivity expressed as an apparent temperature, $\Delta T_{\text{apparent}}/\Delta \text{parameter}$.

$$\frac{\Delta L_{\text{sensor}}}{\Delta \text{parameter}} \cdot \frac{\Delta T_{\text{BB}}}{\Delta L_{\text{BB}}} \Rightarrow \frac{\Delta T_{\text{apparent}}}{\Delta \text{parameter}} \quad \textbf{Input Parameter Sensitivity}$$

The input parameter sensitivity reveals the change in apparent temperature for any amount of change in the input parameter, but the sensitivity value is of little benefit in comparing different input parameters. The sensitivity value is dependent upon the units of the input parameter. As a result, a metric for comparing different input parameters is needed to optimize the input parameters. The standard deviation is representative of the expected error in the input parameter. Multiplying the input parameter sensitivity by the standard deviation of the input parameter then provides an expected temperature error.

$$\frac{\Delta T_{\text{apparent}}}{\Delta \text{parameter}} \cdot \sigma_{\text{parameter}} \Rightarrow \Delta T_{\text{expected}} \quad \textbf{Expected Temperature Error}$$

This results in a common unit, *temperature*, among all the input parameters and allows them to be compared with each other. These expected temperature errors can then be ranked in decreasing order when optimizing the input parameters. The parameter with the highest expected temperature error can be optimized first, followed by the remaining input parameters. A review of all the terms involved in the input parameter sensitivity analysis and optimization is shown below.

- $\Delta \text{parameter}$ - Change in the input parameter
(based on relative minimum & maximum range of values)
- $\Delta T_{\text{ground}}/\Delta \text{parameter}$ - Temperature sensitivity @ ground
(output from THERM)
- $\Delta L_{\text{sensor}}/\Delta \text{parameter}$ - Radiance sensitivity @ sensor
(output from big equation)
- $\Delta L_{\text{BB}}/\Delta T_{\text{BB}}$ - Radiance-to-apparent temperature conversion
(output from radiance conversion)

$\Delta T_{\text{apparent}} / \Delta \text{parameter}$ - Apparent temperature sensitivity @ sensor
(mathematical conversion)

$\sigma_{\text{parameter}}$ - Input parameter standard deviation
(based on the relative minimum & maximum values)

$\Delta T_{\text{expected}}$ - Expected temperature error
(based on 1 standard deviation of the input parameter)

After several input parameters of objects in the scene have been altered, the synthetic image should be reproduced using DIRSIG. The difference between the synthetic image and the real image should then be reexamined. This is necessary to ensure that modifying the input parameters has not greatly altered the interactive relationships between objects in the scene. Background objects sometimes have a large influence on the observed radiance or temperature of a target, and the wrong interactions may result from too much modification of an input parameter. As long as the interactions and phenomena remain the same, differences can be reduced by additional modification of the input parameters.

5.0 DIRSIG Validation

The theoretical approach to the validation of DIRSIG that was outlined in the previous section was used as a reference to obtain the experimental data and results. This section describes the actual experimental data, from obtaining the primary and secondary truth imagery, creating the synthetic scene and imagery, to ultimately comparing the truth and synthetic imagery.

5.1 Truth Imagery Collection

The acquisition of the truth imagery was one of the first steps in the validation of DIRSIG. The general image collection process is described along with the equipment specifications. The primary truth imagery from a Bendix line scanner is discussed first, followed by the secondary truth imagery from an Inframetrics video camera.

5.1.1 Aerial Image Collection - *Image 1*

The infrared truth imagery used in the validation of DIRSIG was originally acquired on 10 November 1991 as part of the New York State Energy Research and Development Authority (NYSERDA) and Rochester Gas and Electric Company (RG&E) survey to improve the study of infrared heat loss in structures (Snyder 1994). This imagery was selected because it was readily available in digital form, and extensive documentation of the imagery existed. As discussed earlier, documentation of the imagery, the collection, and the equipment specifications is essential in trying to recreate imagery using DIRSIG.

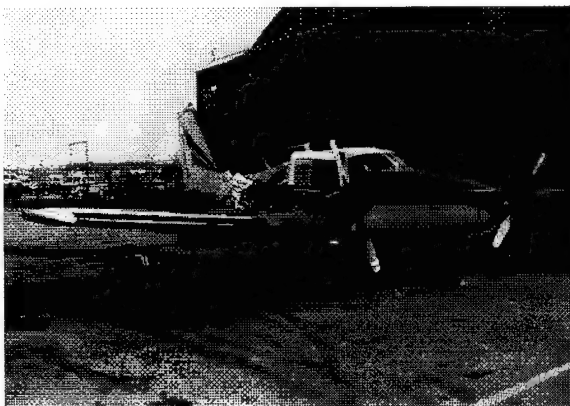


Figure 5.1 Piper Aztec aircraft

Near ideal thermal imaging conditions existed on the cold, fall morning - the sky was clear with a visibility of 15 miles and the wind was less than 5 mph. As the plane, a Piper Aztec twin engine aircraft that had been modified with a 28 inch camera hole in the bottom of the

fuselage, flew over the city, a Bendix LN3 line scanner detected the radiation reaching the sensor in the 8 - 14 μm region of the electromagnetic spectrum. A simple line scanner, such as the Bendix, “employs a spinning mirror to project the image of the detector along a line on the ground perpendicular to the aircraft. By sampling the signal from the detector, the across-track image lines can be formed. During the rotation of the scan mirror, the sensor platform advances slightly and consecutive rotations of the mirror sweep out consecutive lines on the ground which are sampled to form the across-track lines that make up the image” (Schott 1996). (see Figure 5.2)

Line scanners are one of the simplest methods of acquiring imagery, but this simplicity leads to some problems. One of the major problems associated with line scanners is distortion. Because the line of sight of the scanner is redirected mechanically by the scan mirror and not optically, the effective focal plane is a curved surface. This results in a compressive distortion in the across track direction. This phenomena is known as tangential distortion (Lillesand & Kieffer, 1987). Post processing can reduce this tangential distortion, but it cannot restore the lost resolution. The flight path of the Kodak area consisted of several racetrack flight lines as depicted in the figure below to ensure complete coverage of the region and also allow for post processing of the image to reduce the areas with serious tangential distortion.

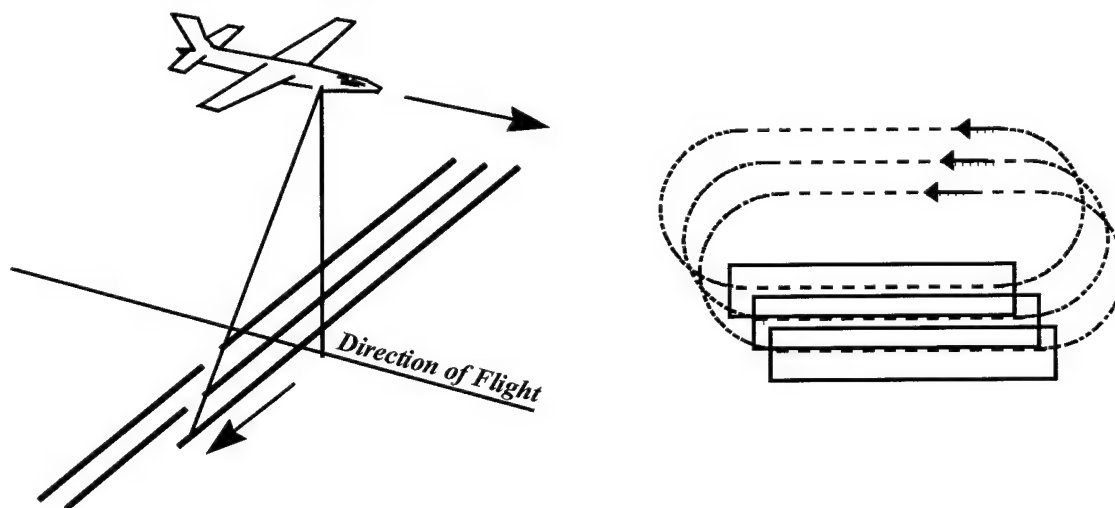


Figure 5.2 Line scanner image acquisition

5.1.2 Equipment Specifications - *Image 1*

In order to accurately recreate imagery using DIRSIG, it is not only necessary to know details about the image collection but also the equipment specifications. The Bendix LN3 line scanner imaging system consists of several integrated components (see Figure 5.3). The heart of the system is the scanner, which contains the scan mirror, detector, and blackbody reference. The detectors are maintained at 77°K using liquid nitrogen. The liquid nitrogen improves the performance of the system by reducing the noise at the detector. Another aspect of the system that improves the imagery is the roll autopilot. A roll autopilot is used to determine the attitude of the aircraft throughout each scan line so that the effects of an unstable platform can be removed in post processing. This attitude information along with the data from the detector are recorded by a tape deck for eventual conversion on the ground into the actual digital image.

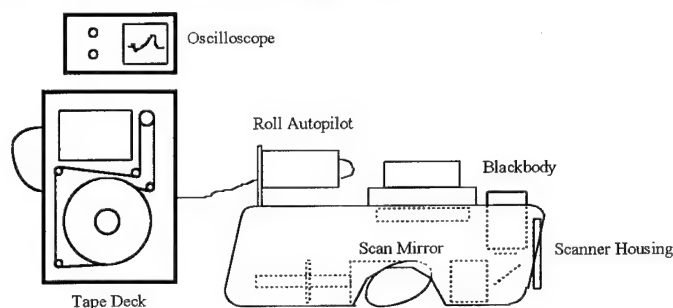
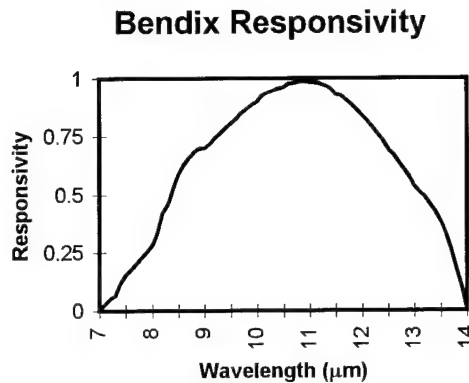


Figure 5.3 Bendix line scanner

With a basic understanding of the components and operation of the Bendix Line Scanner, it is now possible to discuss the exact equipment specifications that provide the high resolution thermal imagery. As explained earlier, the scan mirror rotates in the across track direction, recording a raster image in the process. The Bendix LN3 utilizes a 3-inch scan mirror spinning at 110 rev/sec, providing a 120° scan angle in the across track direction. With 10° at the edge of the scan used to reference a constant black body, the resulting ground swath at a flying altitude of 1000 ft. is -1443 ft. to +1732 ft. With an instantaneous field of view (IFOV) of 1.0 milliradians, the resulting resolution of the imaging system at nadir is one foot at the 1000 ft. imaging altitude.



The spinning scan mirror reflects the radiation to a Mercury-Cadmium-Telluride (HgCdTe) detector. The filtered detector responsivity is shown in the graph to the left. The 8-13.5 μm region of the spectrum, where the detector responsivity is greatest, will be modeled in DIRSIG.

Figure 5.4 Filtered Bendix responsivity

5.1.3 Rooftop Image Collection - *Images 2-3*

The second set of imagery of the Kodak Hawkeye plant and the surrounding area was obtained using RIT's Inframetrics Model 600 LWIR camera. Preliminary aerial images were acquired as part of a multi-purpose DIRS flyover in the Fall of 1995. In order to obtain the images using a conventional aircraft, the window of a Cessna 172 was held open so that an unobstructed radiation path existed from the ground to the Inframetrics camera. Unfortunately, this flyover failed to provide any useful imagery because of improper camera settings. As a result, rooftop imagery had to be used in the validation.

The rooftop imagery was taken from two locations: the roof of the Kodak Hawkeye plant & the roof of the YMCA building. These two locations provided additional and unique perspectives of the region of interest. Imaging from the roof of the Kodak Hawkeye plant, the church was the primary target while the Hawkeye plant was the focal point from the YMCA building. Unlike the Bendix image, these images were taken at approximately 1400 on 9 October 1995 in sunny conditions. The sky was clear and the wind was relatively calm. At both locations, the Inframetrics camera was mounted on a tripod for stability. The camera was focused on the desired target, using the monitor to display the thermal video, and a VCR to record the imagery. (Figure 5.5 depicts the camera setup & the components of the Inframetrics imaging system.) Different temperature ranges were selected on the Inframetrics controller to ensure complete

coverage of the temperature ranges in the scene and eliminate saturation in the output image, a problem that plagued the flyover imagery. Once the rooftop imaging was complete, the temperature of the river was measured. The temperature of the river provided a reference temperature that could later be used for in-scene calibration of the imagery. Selected frames from the video were then converted into digital imagery using IMLAB and RIT facilities. This digitization revealed a large amount of noise in the imagery. Post processing was used to average multiple frames of the video in an attempt to reduce the noise. These post processed images were used in the validation. However, the amount of noise in the imagery combined with the fact that the camera's calibration was not updated in the lab prior to acquisition, the validation analysis was limited to rank order correlation techniques.

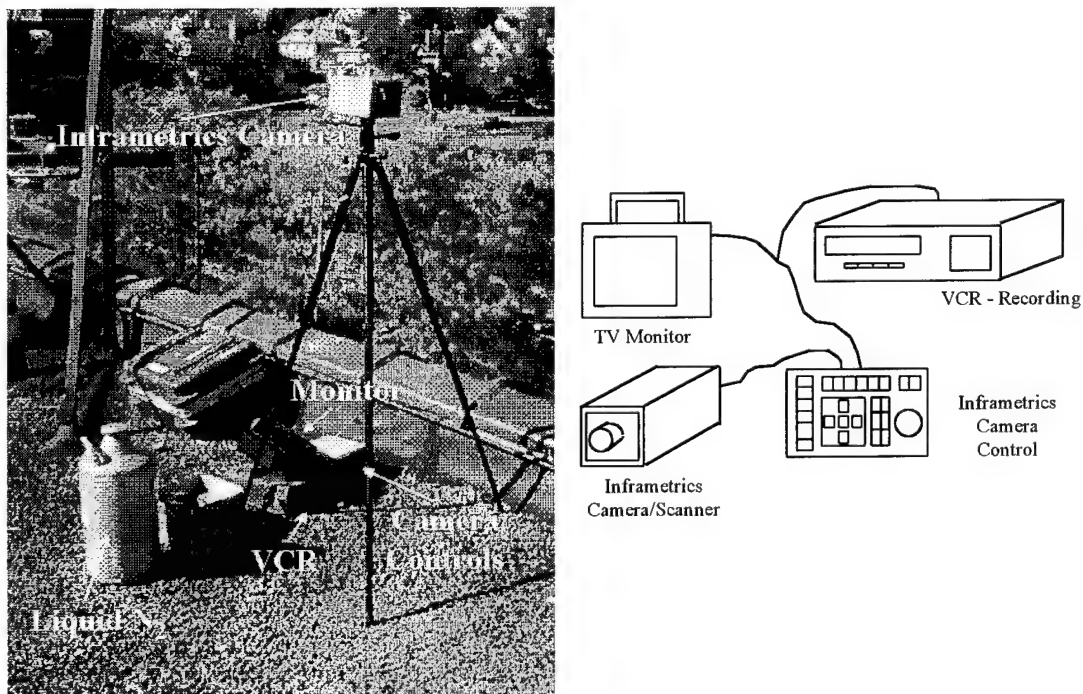


Figure 5.5 Inframetrics video camera system

5.1.4 Equipment Specifications - Images 2-3

The Inframetrics Model 600 IR Imaging Radiometer resembles a normal VCR camcorder; a camera body is used to acquire the image, a small monitor is used to display real time video output, and a video recorder is used for permanent storage. Similar to traditional cameras, the Inframetrics uses lenses and mirrors to direct the photons to the

detector, but the lenses are fabricated of materials that transmit longer wavelengths of energy. This is where the similarities end with a traditional camera, and the Inframetrics more closely resembles the Bendix line scanner. Instead of using a traditional photosensitive medium such as film to detect the photons, the Inframetrics camera has a single Mercury-Cadmium-Telluride (HgCdTe) detector that is scanned mechanically across the scene. Also like the Bendix line scanner, a blackbody reference source maintained at 77 °K using liquid nitrogen is used for calibration of the detector while ensuring maximum thermal contrast, resolution, and noise reduction of the imaging system. (Figure 5.6 shows the responsivity of the Inframetrics system.)

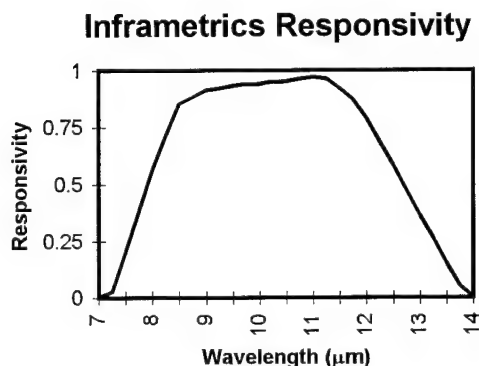


Figure 5.6 Filtered Inframetrics Responsivity

In order to acquire an image, the operator of the camera must first set the desired imaging parameters on the control unit. This includes limiting the electromagnetic spectrum to the 8-12μm region using pre-set filters. The desired center reference temperature and the appropriate temperature span are also entered by the operator. The viewing area is then brought into focus, and the infrared system is ready to record video imagery.

The acquisition of high quality video imagery depends on both the frame rate and the scan speed of the system. The frame rate refers to the rate at which images are updated on the monitor, and the scan speed is the rate at which complete thermal imagers are acquired by the mechanical scanner. The actual video imagery is updated at a frame rate of 60Hz to prevent flicker in the monitor display, and the scan rate of 4 kHz provides a balance between resolution and distortion. So what does all this mean in the end -- the Inframetrics is capable of acquiring rapidly moving targets without distortion.

Like any imaging system, the final ground resolution is defined by the imaging system parameters. The field of view for the Inframetrics is 15 degrees in the vertical by 20 degrees in the horizontal. With a 2mrad resolution in both the horizontal and vertical directions, this field of view results in 200 lines per frame with 256 pixels per line. The output video imagery is displayed as 128 shades of gray, a 7 *bit* dynamic range. These 128 shades of gray are used to display either a 5, 10, 20, 50, 100, or 200 degree temperature range, as selected by the operator. The final parameter that affects the resolution and is also used to describe the quality of a thermal imaging system is the Noise Equivalent Temperature Difference (NE Δ T). While the Inframetrics camera has an advertised NE Δ T of 0.2°C, actual imagery places the NE Δ T closer to 0.5°C.

5.1.5 Image Collection Summary

The image collection and equipment specifications are summarized in the following table. The resulting imagery can also be seen below. Visible imagery is also shown in conjunction with the thermal imagery as a reference.

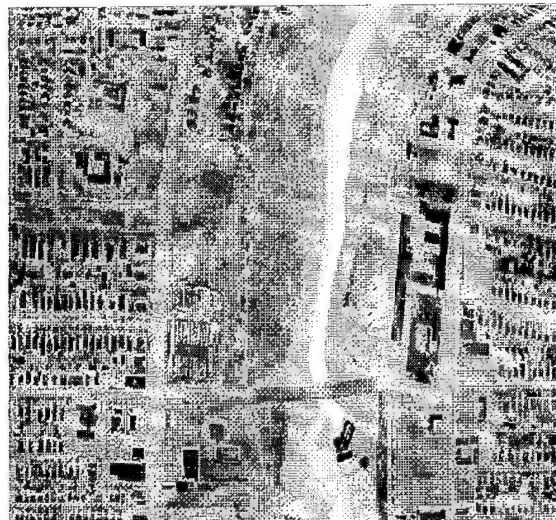
Table 5.1 Validation imagery - specification summary

Imaging System Parameter	Image 1	Image 2	Image 3
Date	10 Nov 91	12 Oct 95	12 Oct 95
Time of Day(EST)	0230	1300	1500
Platform	Piper Aztec	Kodak Roof	YMCA Roof
Altitude	1000 ft (AGL)	585 ft (MSL)	497 ft (MSL)
Perspective	Nadir	Oblique	Oblique
Camera	Bendix LN3 Line Scanner	Inframetrics Video Camera	Inframetrics Video Camera
Bandpass	8-14 μ m	8-12 μ m	8-12 μ m
Recording Device	Tape Deck	Video Tape	Video Tape
IFOV	1 mRad	2 mRad	2 mRad
NEΔT	0.2 °C	0.5 °C	0.5 °C
Resolution	1 ft	2.5 ft	2 ft

Image 1 - Bendix (Nadir)

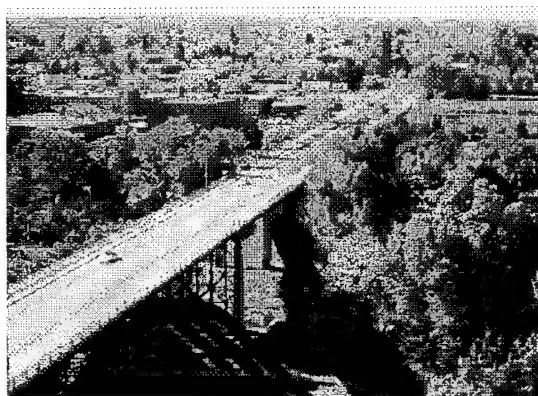


Visible



LWIR

Image 2 - Inframetrics (Oblique Church)

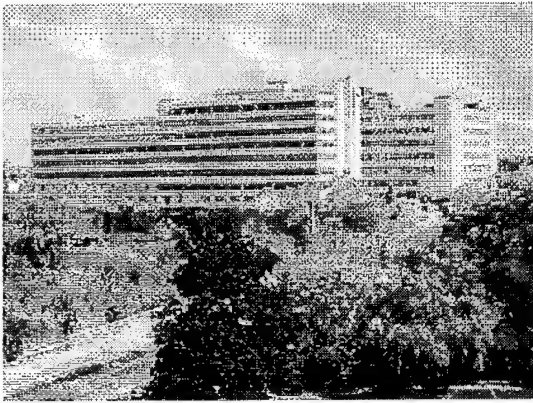


Visible

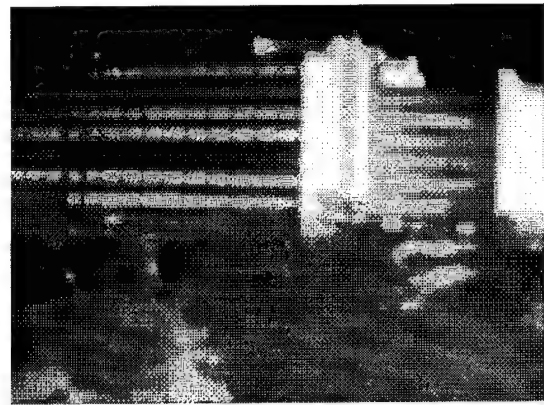


LWIR

Image 3 - Inframetrics (Oblique Hawkeye)



Visible



LWIR

5.2 Scene Development & Synthetic Image Generation

Once the area of interest was defined from the available imagery, the creation of the synthetic image began. However, before any facets could be drawn on AutoCad, the dimensions, sizes, and locations of all objects in the scene needed to be estimated. Initial thoughts involved using a GPS to approximate positions, measuring buildings with a tape measure, estimating distances from imagery, and using actual blueprints to recreate the objects in the scene. In the end, a combination of all these methods would have to be used to model the area near the Kodak Hawkeye plant.

A major breakthrough in the development of the scene occurred when it was discovered that the city of Rochester had digital drawings of the city, depicting all roads, sidewalks, property boundaries, and buildings. While the drawings were only in two dimensions, it provided a plan view, or outline, for all objects in the scene. This would permit highly accurate drawings in two dimensions, x and y . The following picture shows the plan view of the region of interest that was obtained from the **City of Rochester - Department of Environmental Services (Mr. Jeff Tiede)**.

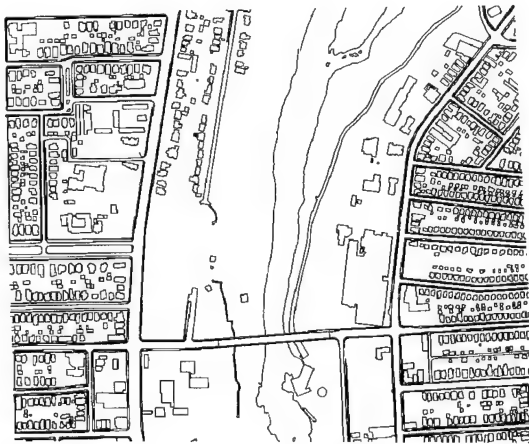


Figure 5.7 2-D city template

However, the elevation of the ground and the heights of structures were still needed. This information would ultimately be provided by a combination of USGS elevation maps and the methods previously discussed. With the dimensions of all the objects in the scene, the drawing of each facet could begin.

5.2.1 Terrain Generation

The drawing of the terrain proved to be one of the most difficult tasks in the development of the scene because of the lack of information available. Defense Mapping Agency (DMA) Digital Elevation Models (DEM) of the area were considered, but these maps have a resolution of only 30 meters, or 100 feet. Because a higher resolution was desired, USGS maps from 1972 were used to provide elevation information. These maps have a resolution ranging from 5 feet to 25 feet, depending on the rate of change of the elevation. However, this information still needed to be converted into a digital form so that it could be used in drawing the terrain facets in AutoCad.

The USGS maps were first photocopied and then enlarged to provide better detail of the contour lines. These enlarged maps were digitized using a digitizing tablet connected to a personal computer. A first order registration, *rotation* and *scaling*, was

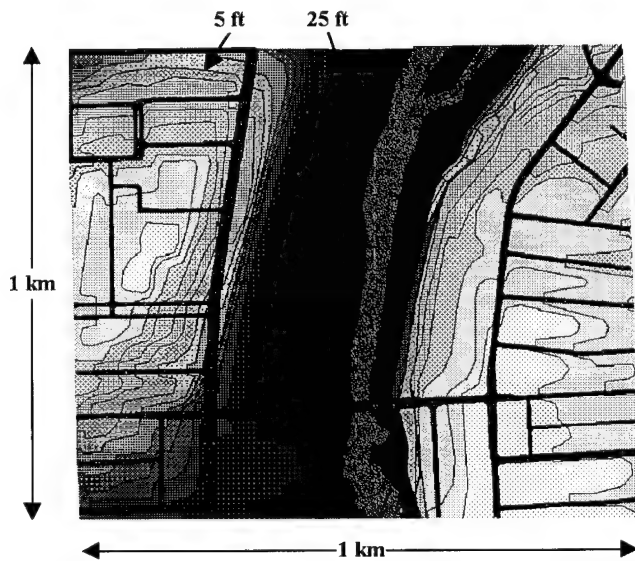


Figure 5.8 Contour map

then performed to match the elevation information with the digital template of the city. The results can be seen in the contour map (Figure 5.8), where the overall scene is approximately 3000ft×3000ft (1km×1km). Also shown is the decrease in resolution of the contour map from 5 ft to 25 ft. The contour map provided precise latitude, longitude, and elevation data for the terrain. The terrain facets, to include the roads and river, could then be drawn.

The resulting terrain can be seen in the following pictures. The terrain included a maximum elevation of 525 feet and a minimum elevation of 245 feet. In addition to the

undulating grassy terrain, a 200 foot gorge made of rock, clay, and grass bisects the region. A 100 foot waterfall can also be found near the southern edge of the region. Asphalt roads and concrete sidewalks complete the essential components in the layout of the terrain. More detail on the actual construction of the terrain can be found in Appendix C - AutoCad Scene Construction.

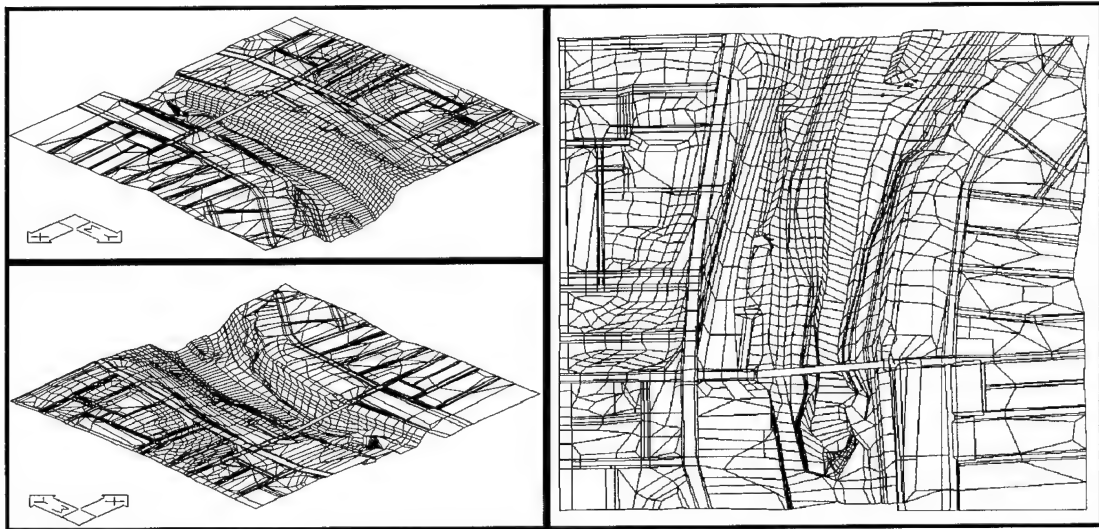


Figure 5.9 AutoCad terrain

5.2.2 Building Generation

With the terrain completed, the next stage in the development of the scene involved adding houses and buildings. The city template provided a starting point as it showed the outlines of all structures, but it didn't provide any information about heights of buildings or roof shapes. While USGS maps were used to provide the elevation of the terrain, an alternative method of determining the heights and shapes of the buildings was needed. This is where the visible imagery of the scene and site measurements were used to provide the remaining pieces of information.

On-site measurements were taken of several buildings near the Kodak Hawkeye plant. These measurements were obtained using two methods, depending on the accessibility of the object being measured. For objects that were relatively small and that could be reached easily, such as windows, a tape measure was used. Unfortunately, this method could not be used to measure the heights of buildings. So, a picture of the

building was taken with a reference object placed into the imagery. Knowing the size of the reference object, a 6' board, a scale for each picture could then be developed to estimate the heights of the buildings. This method provided fairly accurate geometric information for several buildings. Figure 5.10 shows the reference object that was used to estimate the size of the buildings.



Figure 5.10 Church & YMCA buildings with reference object

These buildings, including the Kodak Hawkeye plant, the RG&E electrical plant, and a strip mall were the focal points for the geometric and radiometric validation. The locations of these key buildings in the scene are shown below, along with the AutoCad drawings (Figure 5.12) and resulting DIRSIG imagery (Figure 5.11).

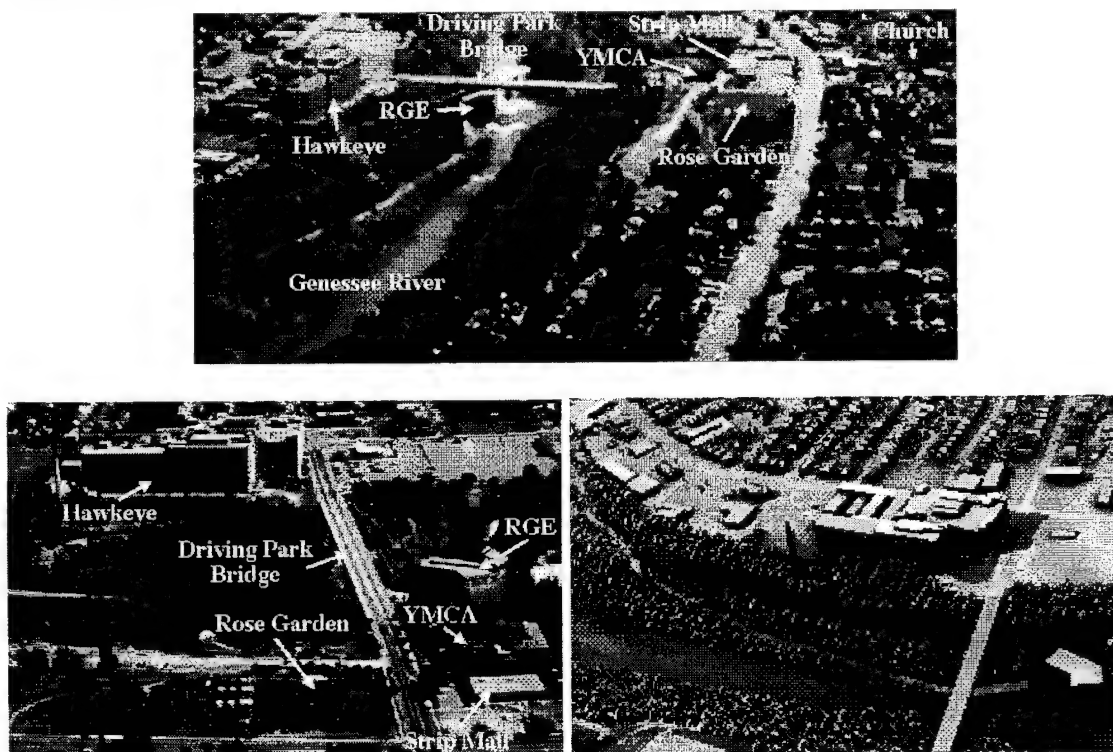


Figure 5.11 Scene layout

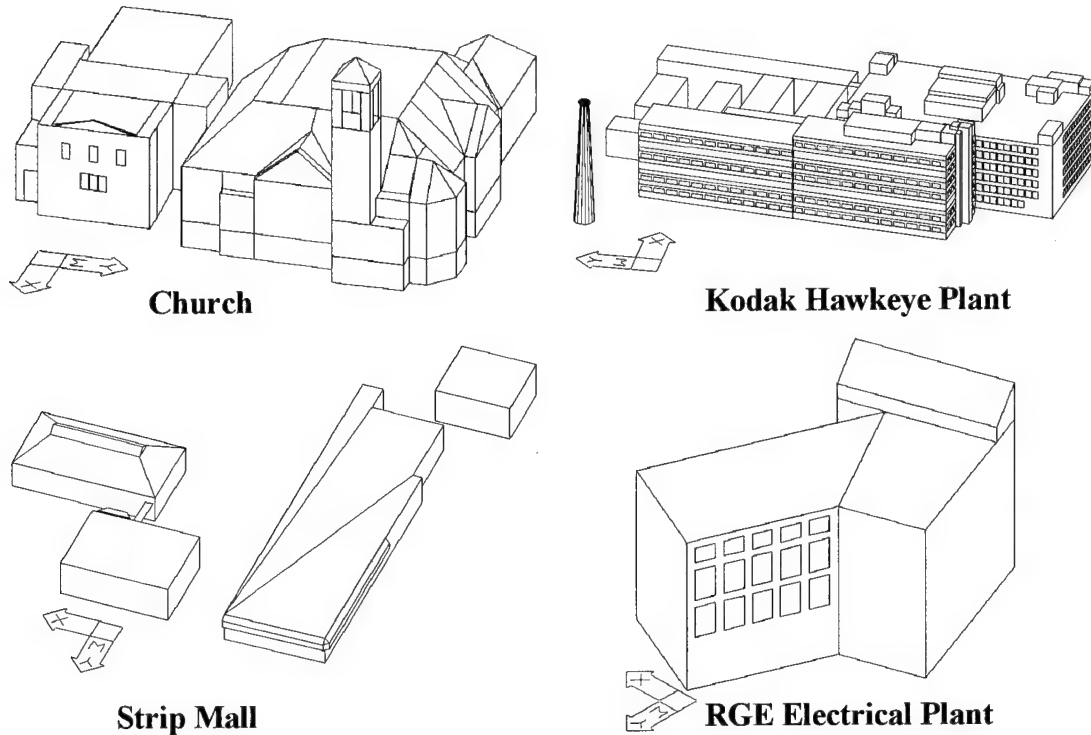


Figure 5.12 AutoCad Buildings

This method of information gathering was very time consuming, even for two students, and with over 800 houses and buildings in the scene, an alternative method was desperately needed. So, an inspection and characterization of the objects in the scene was performed. This inspection revealed the houses in the scene could be categorized into four main types: roof perpendicular to the street, roof parallel to the street, hipped roof, & garage. Because the houses were so similar, it was possible to create just four generic houses. Using the 2-D template from the city, these 'generic' houses were scaled to fit the appropriate dimensions of the houses in the scene. The x & y scaling was based on the outline of the houses as provided by the city template and the z scale factor was set to the height of the house. For two story houses, a scale factor of approximately 35 was used, resulting in a building height of 35 feet. Similarly, garages were given a z scale factor of 10-15 to provide roof heights of about 12 feet. These generic houses were inserted at the elevations of the terrain, sinking them in the ground slightly to ensure that they were not floating in the air. As seen in the following drawings, the detail of the houses was limited

to reduce the number of facets in the scene. With over 800 houses in the scene, the addition of just two windows per house adds almost 2000 facets to the scene, greatly increasing the computational time required to generate the synthetic image.

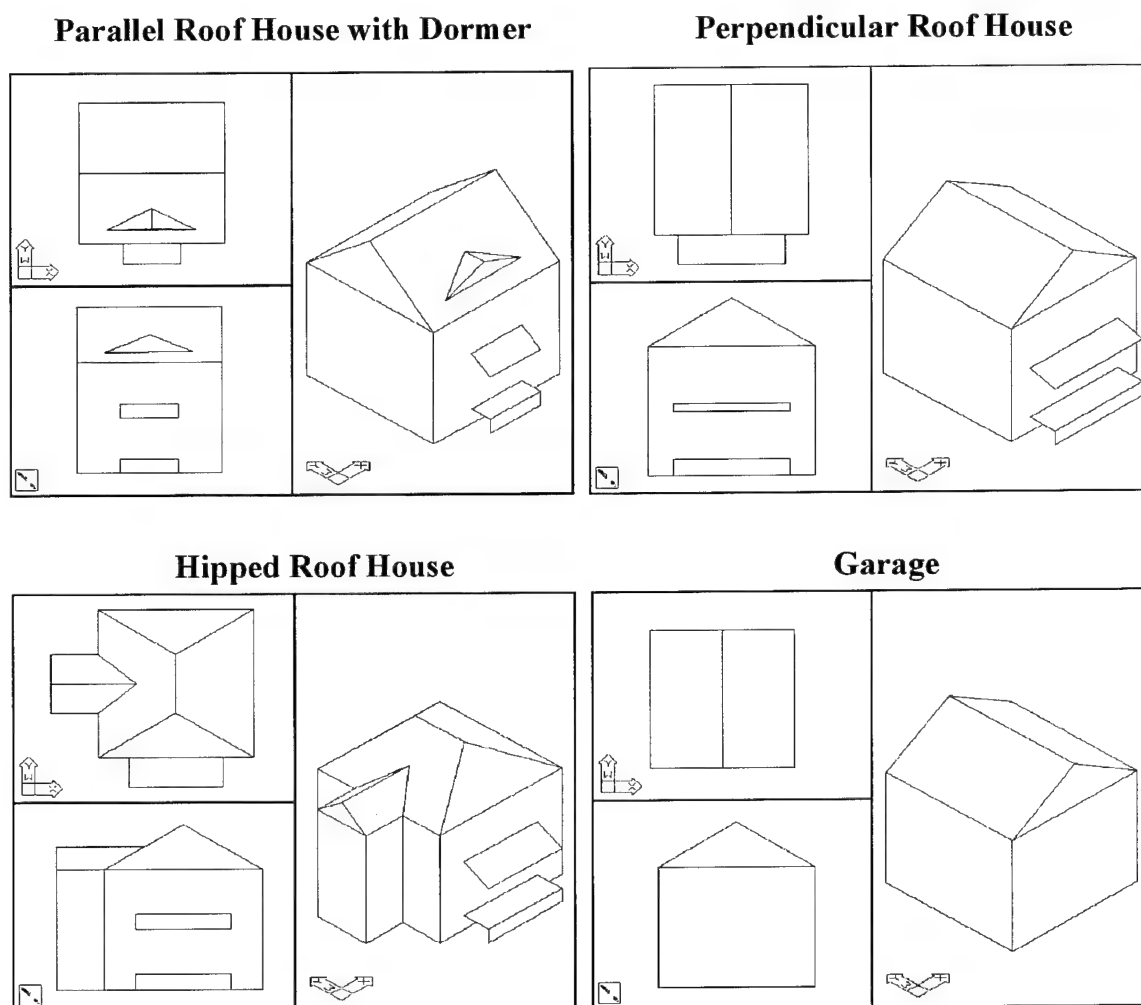


Figure 5.13 AutoCad Houses

About 100 buildings and houses did not fit into these four main categories. In these cases, actual imagery was used to estimate the size and shape of the buildings. Aerial imagery in the visible region was available at both a nadir perspective and an oblique perspective. The size and shape of the remaining buildings were estimated based upon the size of the surrounding objects. While not as accurate as measuring the building, it provided a close approximation of the roof structure and height of the building (the plan view of the building being used to 'frame' the walls).

5.2.3 Miscellaneous Object Creation

While it was impossible to recreate every object in the city, it was necessary to try and recreate the important features that were prominent in the truth imagery. The final additions to the scene consisted of various objects to make the scene appear more realistic. This meant that trees would need to be included in the scene, but they would not have to reveal individual leaves or intricate structures. Because of a memory limitation that was related to the number of facets in the scene, the trees in the gorge were very basic, created using only 20 facets per tree without a tree trunk. The trees in the residential areas were still primitive but contained over 75 facets, including a tree trunk and basic branch structure. In the end, over one thousand of these trees were 'planted' throughout the gorge and the residential areas. While all the trees were deciduous and not coniferous, the trees provided the thermal shading and variation in the scene that was typical of a real image. Additional objects included the rose garden near the strip mall on the western side of the gorge. The Driving Park Bridge, created by Jim Salacain, was also included in the scene to add realism to the scene (Salacain 1995). Some of the special buildings and objects are shown in the following visible imagery and thermal DIRSIG imagery.

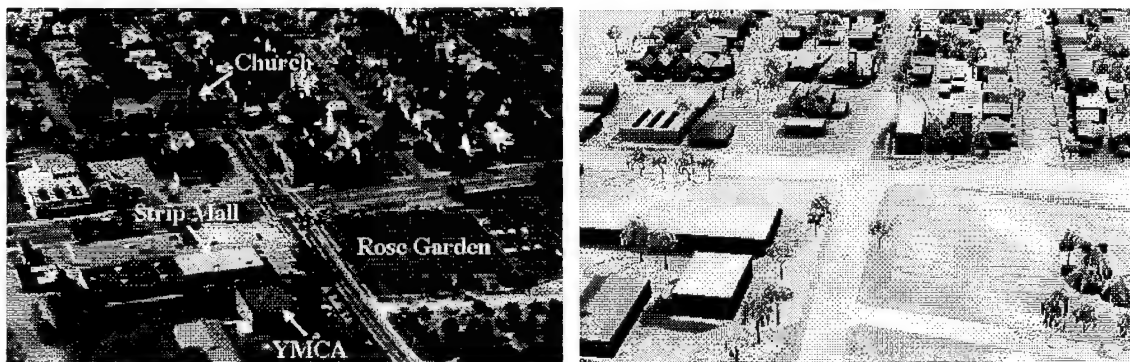


Figure 5.14 Miscellaneous object details

5.2.4 Meteorological Data - Weather & Atmosphere

Meteorological data used in modeling the truth imagery was obtained from the U.S. National Climactic Center. The weather data for the local Rochester area included all necessary information for the DIRSIG weather file, except for the direct & diffuse insolation values. These solar loading values were estimated using THERM's ability to forecast the weather. By describing the preceding 48 hours of weather to THERM, it can predict the remaining weather parameters that are needed for DIRSIG. The atmospheric profile was created by Modtran using a combination of radiosonde data from Buffalo, NY from 0700, corrected for local surface temperature, and Modtran specified inputs. These specified inputs included the atmospheric model type, aerosol extinction type, and cloud models (The Modtran card deck and meteorological information can be found in Appendix B). An example of a Modtran estimated atmospheric profile can be seen in the following graphs for the 10 November 1991 imaging data. The use of the measured meteorological data, weather data, and computer model results provided all necessary information for the DIRSIG synthetic imagery.

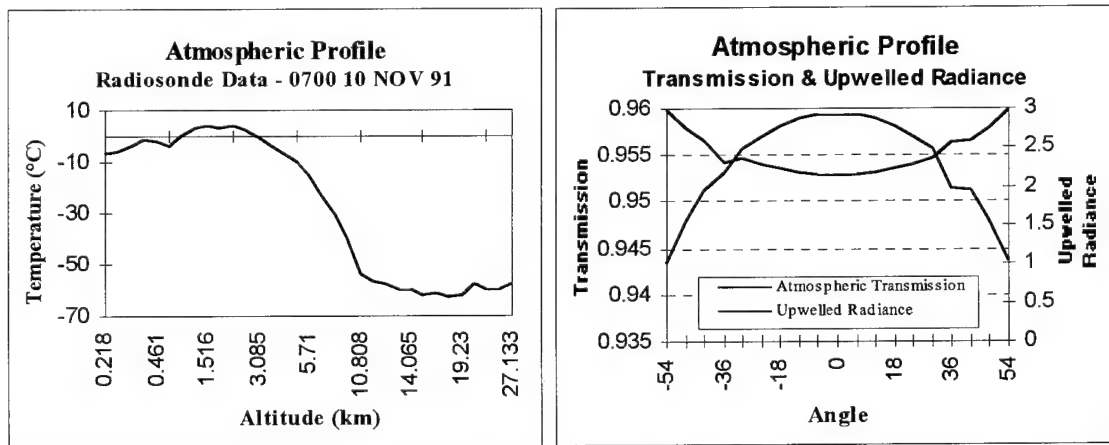


Figure 5.15 Atmospheric profile

5.2.5 Sensor Parameters & Profile

The completion of the synthetic image relied on the image collection parameters and equipment specifications. These were extracted from the collection parameters discussed earlier. The sensor responsivity was specified in the *.sen file and the image

collection parameters were included in the *.adv and *.snd files. The motion profile of the plane was specified for the Bendix line scanner - *Image 1*. This information was taken from the recordings of the autopilot on the image collection date and is listed in the *.prf and *.psf files. The exact format and data in these files can be found in Appendix B.

5.2.6 Image Creation Summary

The large variety of items and the size of the area resulted in a very complex scene. This complexity was reduced by dividing the scene into 20 different 'regions', 16 land regions and 4 water regions. While each of the land regions was a DIRSIG object, consisting of the terrain, street, sidewalk, house, and building parts, the water regions

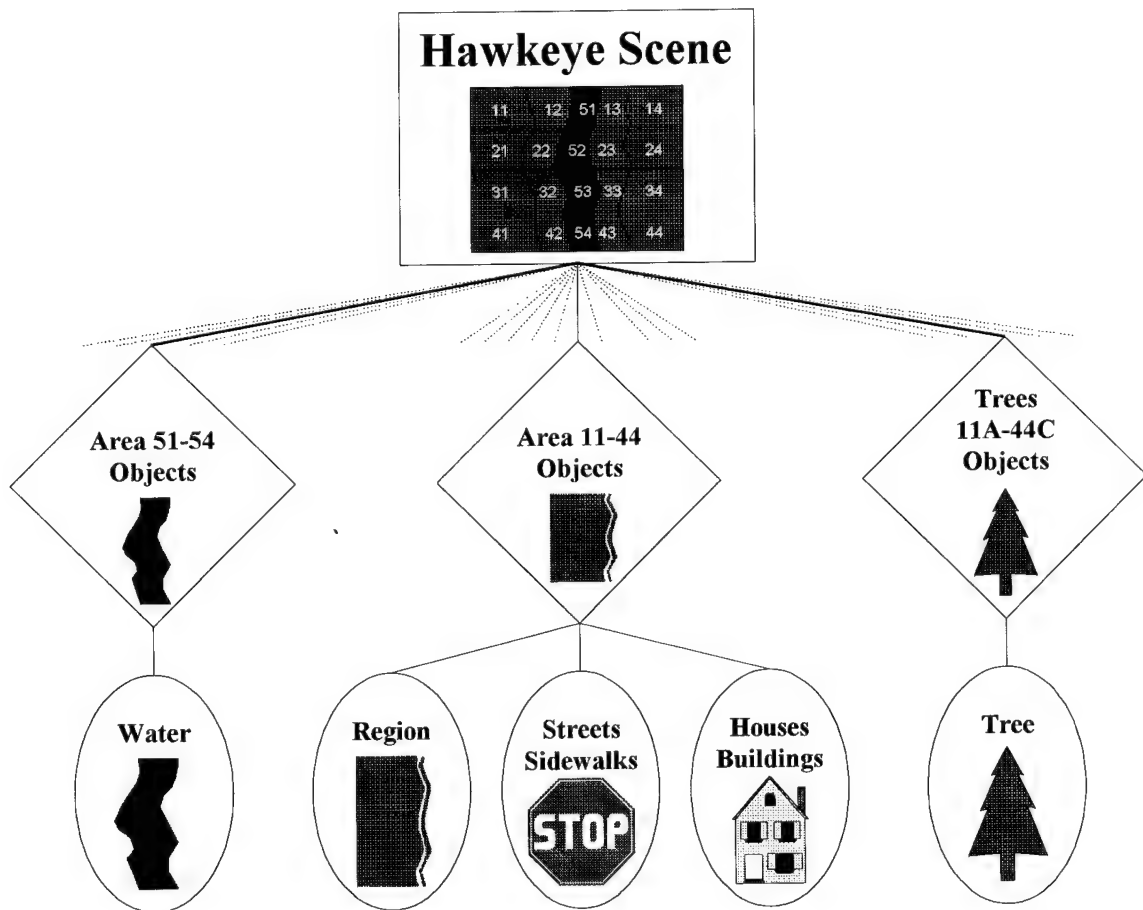


Figure 5.16 Hawkeye scene construction

consisted only of water. The tree objects were similar to the water regions, comprised of only individual trees. These divisions helped when making modifications to the scene and

also allowed the scene to be tested quickly. In a scene this complex that often requires modifications, it can be extremely difficult and time consuming to make any changes at the facet level. This problem was alleviated through the division of the scene and the use of AutoCad script files. Script files were used to rebuild all the objects and the overall scene. This reduced the effort and time required to rebuild a scene after a modification was made.

In the end, about 50 materials from a database of over 250 materials were assigned to facets in the scene. Generic material parameter values were initially used in the scene but were later optimized to reduce the radiometric error. The optimization of the material parameters is described in detail in the following section. A listing of the materials that were assigned to the various faceted objects in the scene is shown below.

<i>Building Construction Materials (BCM)</i>	<i>Soils/Water</i>	<i>Surface Construction Materials (SCM)</i>	<i>Vegetation</i>
Roof - aluminum	Soil - clay - gray	Asphalt - parking lot - dark/new	Grass
Roof - asphalt shingles - colored *	Soil - clay - red	Asphalt - parking lot - old/weathered	Tree - deciduous
Roof - gravel	Soil - dirt - brown	Asphalt - street	Tree - trunk
Roof - steel	Soil - gravel - light brown	Concrete - street/sidewalk	
Wall - brick - colored *	Water - Genesee River		
Wall - concrete			
Wall - wood - colored *			
Window - glass			

* - 10 colors were available for each of these materials

The goal of this validation is to determine how well DIRSIG models the real world, but the error in the synthetic image depends on the accuracy of its creation. While error in the synthetic image was reduced through the optimization of the input parameters, including the material and meteorological parameters, some errors are still unavoidable and inevitable. These errors may only be eliminated through countless hours of research and work. As a result, some error is often accepted to reduce the time involved in researching and creating a scene. The following table summarizes the expected geometric accuracy/error that was tolerated when creating the buildings for the synthetic image. While this geometric error could have been reduced, these errors represented an acceptable balance between time and accuracy.

Table 5.2 Estimated geometric accuracy

Object	Estimated Geometric Accuracy		
	X	Y	Z
Undulating Terrain	± 10 ft	± 10 ft	± 5 ft
Gorge	± 10 ft	± 10 ft	± 15 ft
River Bed	± 10 ft	± 10 ft	± 5 ft
Streets/Sidewalks	± 3 ft	± 3 ft	± 5 ft
Houses	± 5 ft	± 5 ft	± 5 ft
Detailed Buildings	± 2 ft	± 2 ft	± 2 ft
Estimated Buildings	± 5 ft	± 5 ft	± 10 ft

All these different components that have been discussed are required to generate a single DIRSIG image. The best results are achieved when measured or actual data is available, but the DIRSIG environment provides the tools to estimate all the input parameters if measured data is not available. The following table summarizes the input files and the sources that were used in recreating the Bendix line scanner imagery and the Inframetrics video imagery (the files can be found in Appendix B)

Table 5.3 DIRSIG input file summary

Inputs	Description	Source
<i>*.adv</i>	AutoCad view file containing the scene and imaging parameter coordinates in AutoCad units	DVIEW & user specified
<i>*.cdk</i>	Modtran card deck used to create the radiance file	CONTROL 7 & user specified
<i>*.ems</i>	Material emissivities that are a function of the wavelength and look angle	DCS Corporation & NEF Database
<i>*.gdb</i>	Geometric Database containing each facet's location, normal, and material	DIRSIGFMT & AutoCad output
<i>*.mat</i>	Material file containing the physical properties of each material	DCS Corporation & NEF Database
<i>*.prf</i>	platform motion profile containing the flight profile of the plane	Actual sensor data
<i>*.psf</i>	platform specification file containing the imaging system parameters	Actual sensor data
<i>*.rad</i>	radiance file containing the bandpass atmospheric parameters used in DIRSIG	Modtran
<i>*.rsd</i>	radiosonde data from Buffalo NY that is used by Modtran to predict the atmospheric profile	Measured data Buffalo, NY
<i>*.sen</i>	Sensor responsivity file containing the spectral response of the sensor	Actual sensor data
<i>*.snd</i>	Scene node file containing the bandpass spectral ranges and the data that relates the scene position to the earth and sun	DVIEW & user specified
<i>*.wth</i>	weather file containing 48 hours of weather prior to the imaging time	THERM or measured data - Rochester, NY
<i>model</i>	line scanner file containing synthetic image parameters	Actual sensor data

5.3 DIRSIG Validation Results

Once all the DIRSIG input files were completed, a synthetic image was generated. The resulting image was acceptable, but some differences were apparent between the synthetic and primary truth imagery. This was understandable since only a limited amount of actual measured data was available for the creation of the synthetic image. Since a synthetic image is only as good as the inputs, it was evident that some of the input parameters needed improvement. This is where the analysis of the meteorological and material input parameters was used to optimize the inputs and reduce the differences between the synthetic and truth imagery. The input parameter analysis and optimization is discussed in detail in the following section, **Section 6.0 - Input Parameter Analysis & Optimization**. These optimized input parameters were then used for the final validation with the truth imagery.

With the input parameters to DIRSIG optimized, the process of validating the synthetic imagery could begin. A quick assessment of the imagery could be made visually, but the goal of the validation was to assess the imagery mathematically using root mean square error and rank order correlation. The RMS error of the Bendix line scanner imagery was found first, followed by the rank order correlation. The Inframetrics imagery was then analyzed using only rank order correlation.

5.3.1 Validation - Primary Truth Imagery (Bendix line scanner)

The imagery shown on the following pages was used to validate DIRSIG. The Bendix and DIRSIG line scanner imagery of the entire region is presented first. This imagery is followed by additional imagery of selected regions of interest, to include the church, gorge, garden, strip mall, and Hawkeye plant. The imagery has been contrast enhanced, where the entire temperature span in the imagery is less than 10 degrees. The fact that the temperature range was so limited reveals the difficulty in simulating nighttime LWIR imagery. During the day, solar effects add to the temperature range and thermal contrast in a scene as the visible characteristics of the objects affect the temperatures. At night, these visible characteristics have limited effects on the temperature of objects. As a result, objects

tend to look similar at night, and the overall temperature range in a scene is much less than the day.

Visually examining the imagery on the following pages, several differences and discrepancies must be explained. In the imagery of the overall scene, the river is noticeably wider in the synthetic image than in the truth image. This difference results from the water level variation of the Genesee river. The 2-D city template was used to set the boundaries of the river, but evidently the water level of the river was higher when the city template was developed. Another difference that must be mentioned involved the trees in the synthetic image. The trees in the synthetic image were provided to enhance the visual appearance of the image. These trees provided the shading and variation visible in the truth imagery. However, these trees have the characteristics of deciduous trees during the summer, not coniferous trees in the winter that are present in the truth imagery.

There are also some visual differences that must be pointed out in the imagery of the selected regions. Most importantly is the geometric difference between the truth and synthetic imagery. The synthetic imagery of these selected regions was generated using a frame camera model to reduce DIRSIG run times while the actual imagery shows the line scanner distortions. An additional geometric difference is evident in the mall imagery. After the truth imagery was acquired in 1991, the gas pumps at the top left of the image were removed and replaced with the strip mall shown in the synthetic image. In addition, none of the houses in the synthetic imagery had chimneys. As a result, the white hot chimneys seen in the truth imagery are not seen in the synthetic imagery. The final visual difference that must be explained is the dark shadows evident around the bases of the buildings in the synthetic imagery. These dark shadows were caused by a coding error in DIRSIG. The coding error has since been fixed and these effects are no longer evident in the synthetic imagery.

The imagery shows that DIRSIG was able to closely model the real world, despite the relatively low contrast typical of the night imaging conditions. After visually assessing the synthetic image, it was necessary to quantify the radiometric accuracy of the synthetic

imagery. With over 800 houses, buildings, and objects in the scene, it would be impossible to evaluate each individual object. Therefore, key structures were identified to test the radiometric accuracy of DIRSIG. Once the validation points were identified, it was necessary to establish a common unit for comparison of the imagery. The output imagery from DIRSIG was in radiance units while the Bendix imagery was in digital counts. The Bendix imagery was first converted from digital counts into radiance values using the gain and bias of the sensor (Snyder 1994).

$$L = 0.06825 \cdot \Delta DC + 27.8 \quad (5.1)$$

where $\Delta DC = DC_{object} - DC_{blackbody}$
 $DC_{blackbody} = 164.79$

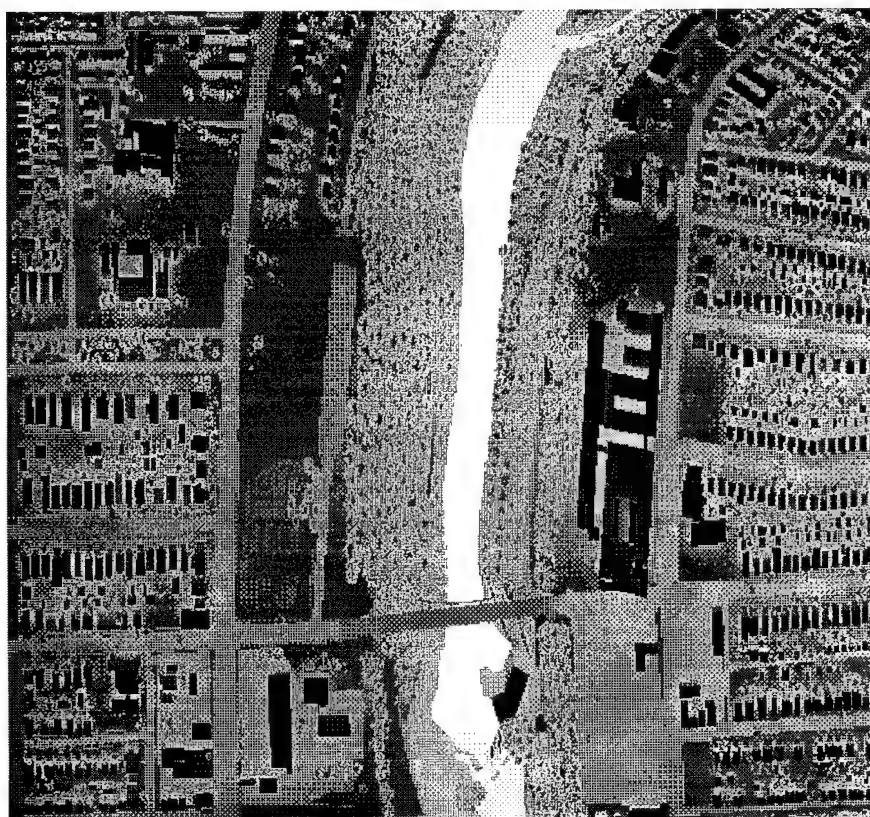
This established a common unit of radiance between the synthetic and truth imagery. To make the analysis more informative, the radiance values were converted to apparent temperatures. Reference temperatures ranging from 260 to 305°K were used to develop a linear conversion as described in Section 4.0. This linear conversion was applied to both the Bendix and DIRSIG imagery.

$$T_{apparent} = Radiance_{input} \cdot 1.922 + 223.426 \quad (5.2)$$

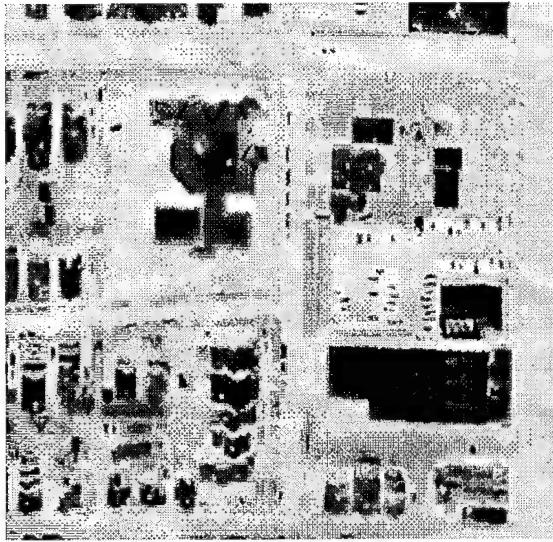
The apparent temperatures of the specified structures in the synthetic image could then be compared to the apparent temperatures of the same structures in the truth imagery.



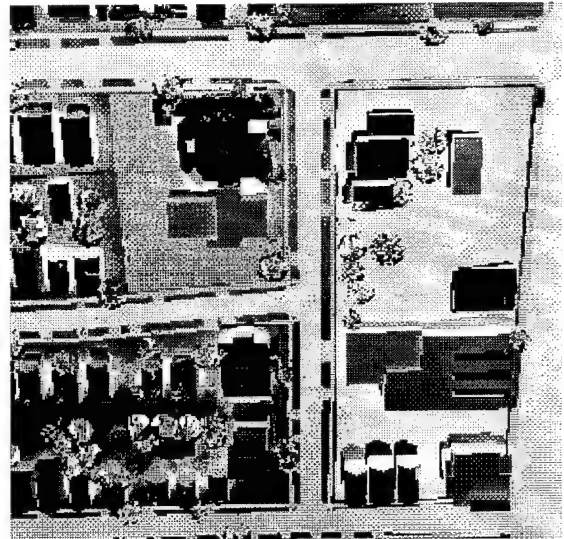
Bendix Imagery



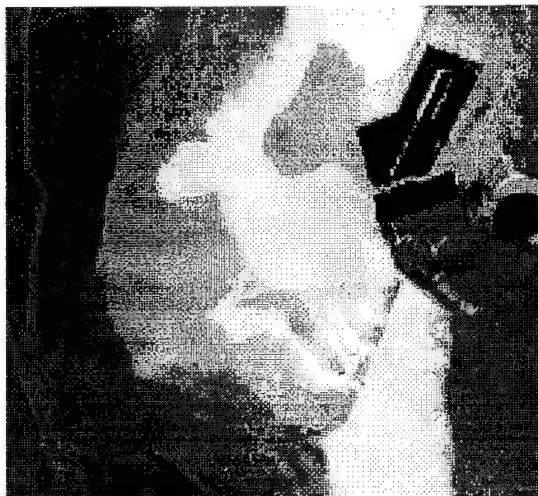
DIRSIG Imagery



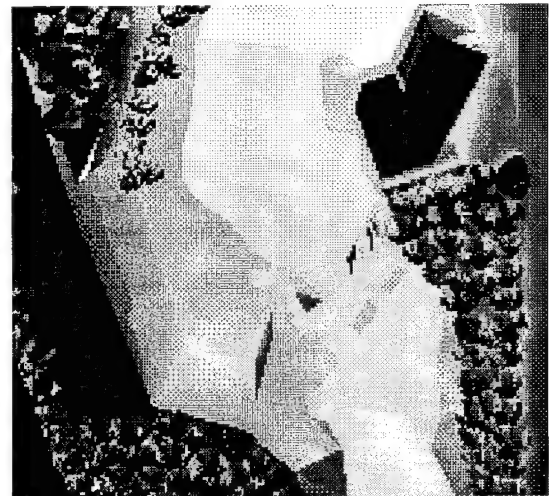
Bendix church imagery



DIRSIG church imagery



Bendix gorge imagery



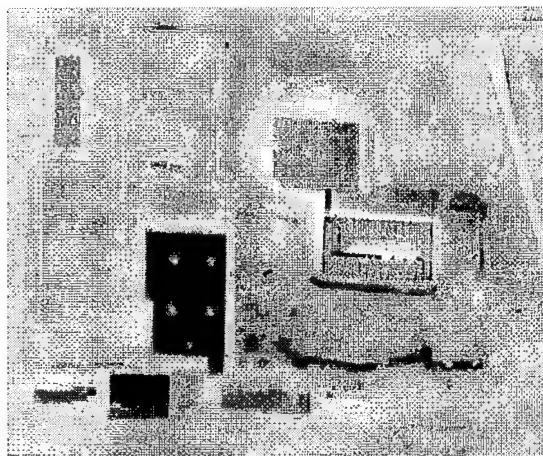
DIRSIG gorge imagery



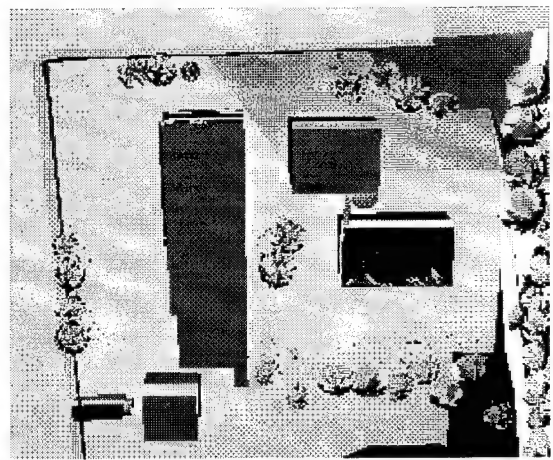
Bendix garden imagery



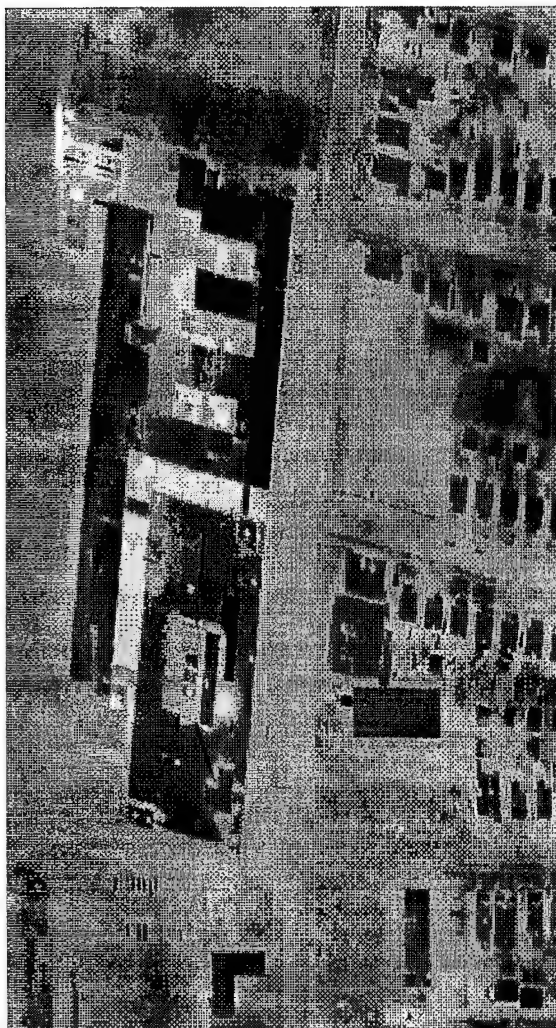
DIRSIG garden imagery



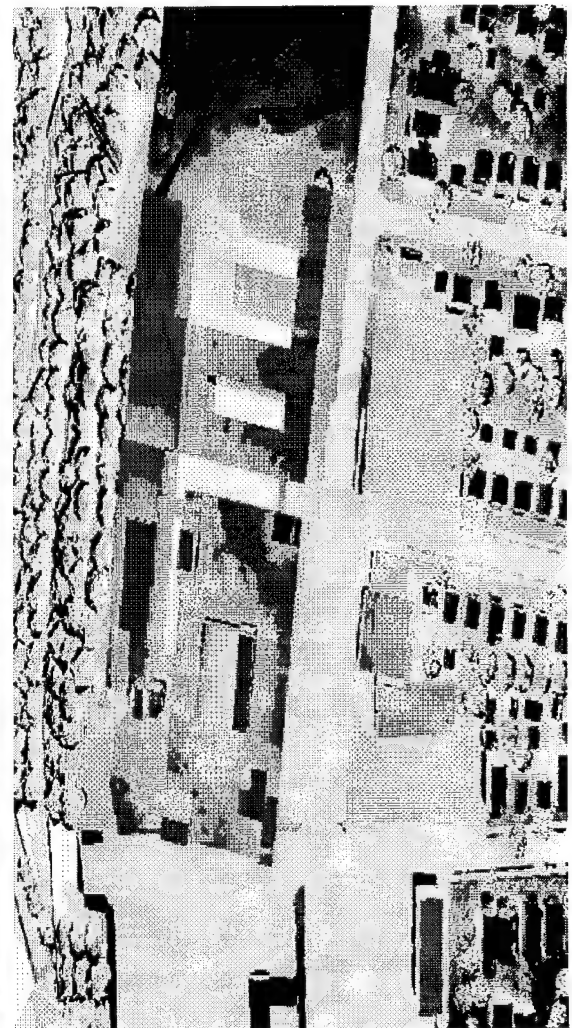
Bendix mall imagery



DIRSIG mall imagery



Bendix Hawkeye imagery



DIRSIG Hawkeye imagery

Figure 5.17 Primary validation imagery

5.3.1.1 Material Radiometric Accuracy - Root Mean Square Error

The major task of the validation involved assessing the radiometric accuracy of the synthetic imagery. The average apparent temperature from several pixels in the synthetic image were compared to the average apparent temperature from the same object in the truth imagery. The root mean square error detected global errors as well as individual errors. The truth values were compared to two sets of DIRSIG imagery; one created from the generic inputs and the other created from the optimized inputs. This showed the improvement of the DIRSIG imagery after optimizing the input parameters. The imagery below shows the material validation points that were used to assess the imagery.

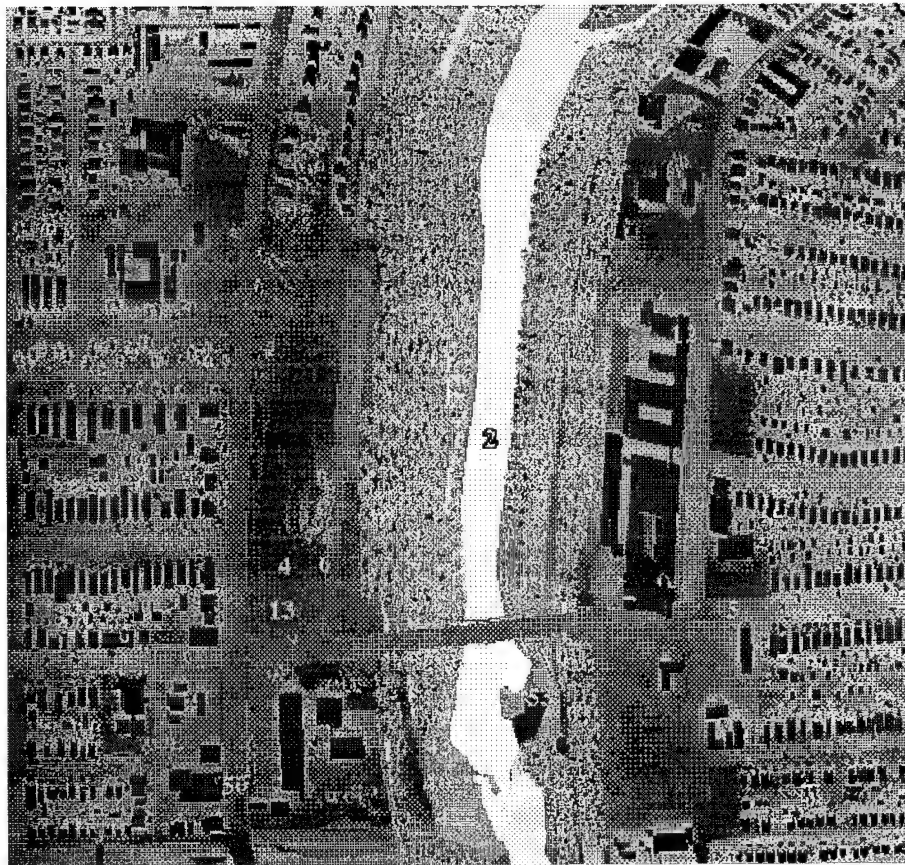
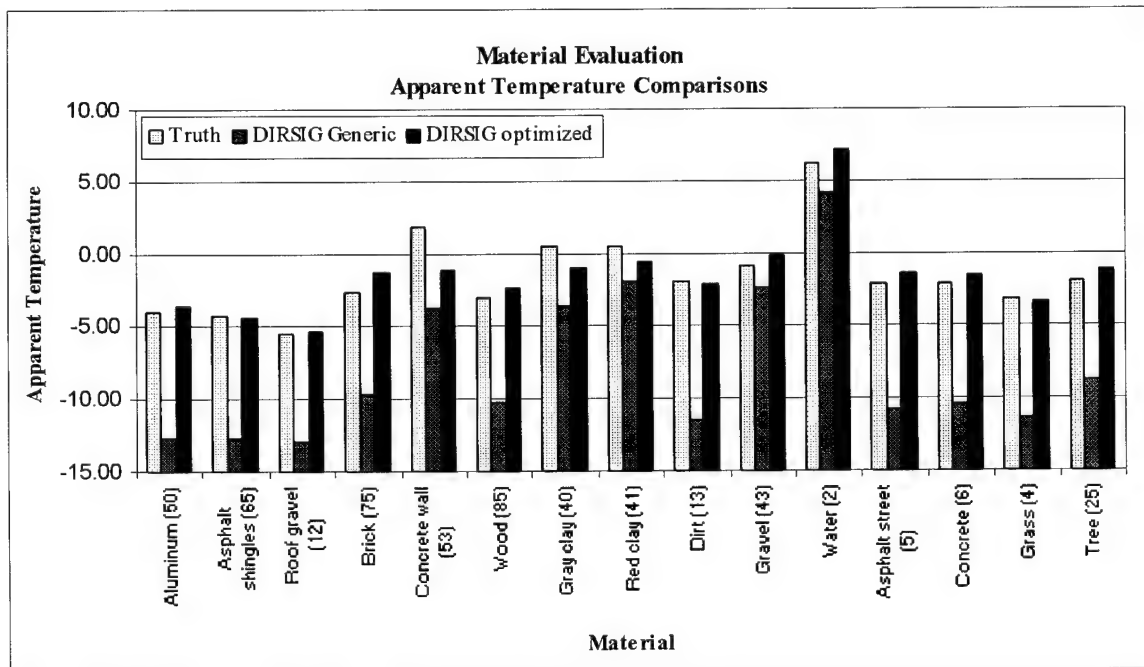


Figure 5.18 Validation points

Table 5.4 RMS error validation results - Bendix imagery

Object (Mat ID number)	RMS Apparent Temperatures				
	Truth	SIG		Error	
		Gen	Opt	Gen	Opt
Building Construction					
Materials					
aluminum #50	-3.96	-12.67	-3.56	-8.71	0.40
asphalt shingle #65	-4.29	-12.71	-4.35	-8.42	-0.06
roof gravel #12	-5.50	-12.90	-5.29	-7.40	0.21
brick #75	-2.58	-9.73	-1.29	-7.15	1.29
wall concrete #53	1.83	-3.70	-1.20	-5.53	-3.03
wall wood #85	-3.10	-10.21	-2.39	-7.11	0.72
Soils/Water					
gray clay #40	0.43	-3.56	-0.99	-3.99	-1.41
red clay #41	0.44	-1.99	-0.64	-2.43	-1.08
brown dirt #13	-1.99	-11.50	-2.16	-9.51	-0.17
lt brown gravel #43	-0.85	-2.33	-0.24	-1.48	0.62
water - Genesee River #2	6.23	4.11	7.11	-2.13	0.87
Surface Construction					
Materials					
asphalt street #5	-2.10	-10.77	-1.43	-8.67	0.67
concrete #6	-2.11	-10.33	-1.49	-8.22	0.62
Vegetation					
grass #4	-3.19	-11.33	-3.33	-8.13	-0.14
tree deciduous #25	-1.97	-8.79	-1.14	-6.82	0.83

RMS Error
Generic - 6.8707
Optimum - 1.0782



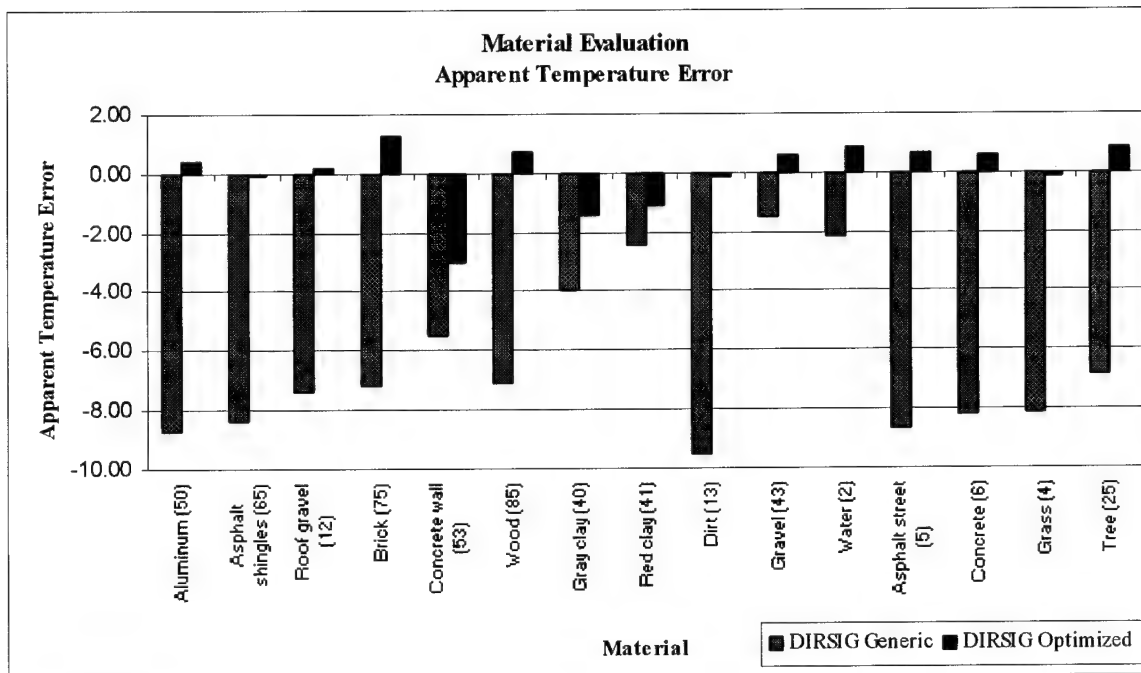


Figure 5.19 Material evaluation results

The dramatic improvement in the synthetic image after optimizing the input parameters was evident in these results. The large bias seen in the generic input parameters was eliminated by increasing the surface air temperature by 4 degrees. The input parameter analysis also showed which material parameters to alter to further reduce the error in the synthetic image (see Section 6.1.2). The overall optimization reduced the apparent temperature error from nearly seven degrees to approximately one degree. In addition, there were no materials with exceptionally large errors in the final synthetic imagery. It was possible to closely model the specified points with the optimized materials database. The only trends that manifested themselves in the results were for materials with vertical orientations. The nadir perspective of the Bendix imagery made it difficult to find large consistent areas of these materials for optimizing the input parameters.

These same validation points were then assessed using rank order correlation. Similar to the RMS analysis, both the generic and optimized DIRSIG imagery was analyzed to determine the improvement or degradation after the input parameter optimization. The ROC analysis removed the global errors in the results caused by the surface air and determined the relative improvement after the optimization of the material parameters.

5.3.1.2 Material Radiometric Accuracy - Rank Order Correlation

Understanding the RMS error and bias in the results, the rank order correlation showed how accurately DIRSIG created the relative differences in the apparent temperatures of the materials. It removed the large bias seen in the generic input parameters and revealed the relative improvement in the results after the optimization of the material parameters. It is the relative temperature differences that automated target recognition system rely on to distinguish objects. The rank order correlation results are shown in the imagery, table, and graphs on the following pages. The hottest object was ranked number 1 and the coldest object was ranked number 15. A ROC coefficient of 1.0 is perfect.

The ROC analysis yielded very strong validation results for both the generic and optimized DIRSIG imagery. The ROC coefficient increased from 0.8892 to 0.9214 after the optimization of the input parameters. The removal of the global error in the generic results showed the accuracy of the generic materials in representing the actual materials in the scene. Seven materials in the generic DIRSIG imagery had the exact same rank as the truth imagery in comparison to 10 exact rankings in the optimized DIRSIG imagery. In addition, the largest ranking error was 5 for the generic and 4 for the optimized imagery. DIRSIG was able to closely model the real world, despite the low contrast typical of the night imaging conditions.

The main area of error was centered on the soils and the building construction materials. Large rank errors were seen for the dirt and gravel and the brick and concrete walls. This is understandable because of the similarity in these materials. The material parameters, i.e. thermal conductivity, heat capacity, and emissivities, for the soils were all closely related. As for the brick and concrete walls, the apparent temperature of these materials is strongly affected by the internal heat. Not accounting for the internal heat may have contributed to the error. Despite these ranking errors, the overall results showed that DIRSIG can model the very difficult nighttime LWIR imaging conditions present in the truth imagery quite well.



Bendix rank order correlation



DIRSIG rank order correlation

Table 5.5 ROC validation results - Bendix imagery

Object (Mat ID number)	Truth	ROC results			
		SIG		Error	
		Gen	Opt	Gen	Opt
water - Genessee River #2	1	1	1	-	-
wall concrete #53	2	5	6	3	4
red clay #41	3	2	3	1	-
gray clay #40	4	4	4	-	-
light brown gravel #43	5	3	2	2	3
tree deciduous #25	6	6	5	-	1
brown dirt #13	7	12	10	5	3
asphalt street #5	8	10	8	2	-
concrete #6	9	9	9	-	-
brick #75	10	7	7	3	3
wall wood #85	11	8	11	3	-
grass #4	12	11	12	1	-
aluminum #50	13	13	13	-	-
asphalt shingle #65	14	14	14	-	-
roof gravel #12	15	15	15	-	-

ROC Coefficient

Generic - 0.8892

Optimum - 0.9214

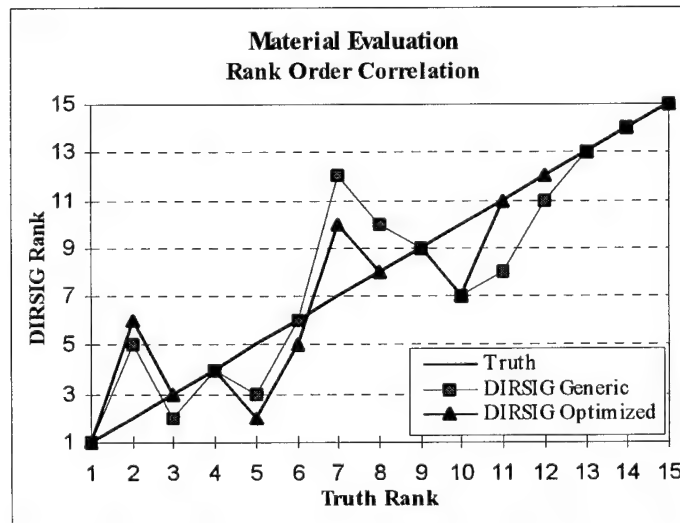


Figure 5.20 Rank order correlation results

5.3.1.3 Radiometric Accuracy - Complex Radiometric Phenomena

While the material comparison tested the accuracy of specific materials, the validation should also test the entire SIG process and not just one aspect. Therefore, to test the ability of DIRSIG to include shape factor effects, angular effects, background effects, and other complex radiometric phenomena, additional validation points were needed.

In testing the limits of a system, the input variables should be strictly controlled; isolate the input variables and then change them one at a time. This validation was no exception. Since asphalt roads and shingles were known to a high degree of accuracy, these materials along with roof gravel and grass would be used to test the ability of DIRSIG to model the real world. Using materials that are known to a high degree of accuracy reduces the material parameter error and limits the control variables, allowing the focus to be placed on testing the model and its ability to include complex radiometric effects. The asphalt streets tested the angular effects of the sensor as they are found throughout the scene at different orientations and distances to the sensor. In following this philosophy of changing only one variable at a time, asphalt shingles were examined next. They provided excellent angular effects as well as some limited background and shape factor effects. A key structure located in the parking lot south of the Hawkeye plant was examined for these effects. The grass between houses and the gravel roof of Hawkeye finally tested the robustness of DIRSIG in modeling complex radiometric phenomena. The angular effects, shape factor effects, and background effects could all be analyzed from these materials. For the roof gravel, complex thermal exchanges existed between the roof gravel, the atmosphere, and the surrounding walls. Similar phenomena were evident for grass as the apparent temperature rose dramatically between the houses. Because this analysis required high resolution DIRSIG imagery to approximate the one foot resolution of the Bendix imagery, the sub-images shown earlier were used in the analysis. The following imagery shows the actual analysis points that were used to examine the phenomenology effects.



Figure 5.21 Complex phenomenology validation points

Similar to the validation of the scene materials, the analysis of the complex radiometric phenomena was accomplished using both root mean square error and rank order correlation. The temperature error in the material that was found from the material validation was removed prior to the analysis of the complex radiometric phenomena. This was done to try and remove any temperature bias caused by an error in the material so that the resulting errors would be from the phenomenology.

The ability to include angular effects was the first phenomenological indicator that was analyzed. As the sensor-target angle increases from 0 to 90 degrees, the emissivity decreases for most materials. Therefore, the apparent temperature should change as the

sensor-target angle varies. The results of the angular effects in the asphalt streets can be seen in the following graphs where points 2, 3, 4, & 6 are near nadir while 1, 5, & 7 are more towards oblique angles (see Figure 5.21 for the location of the validation points).

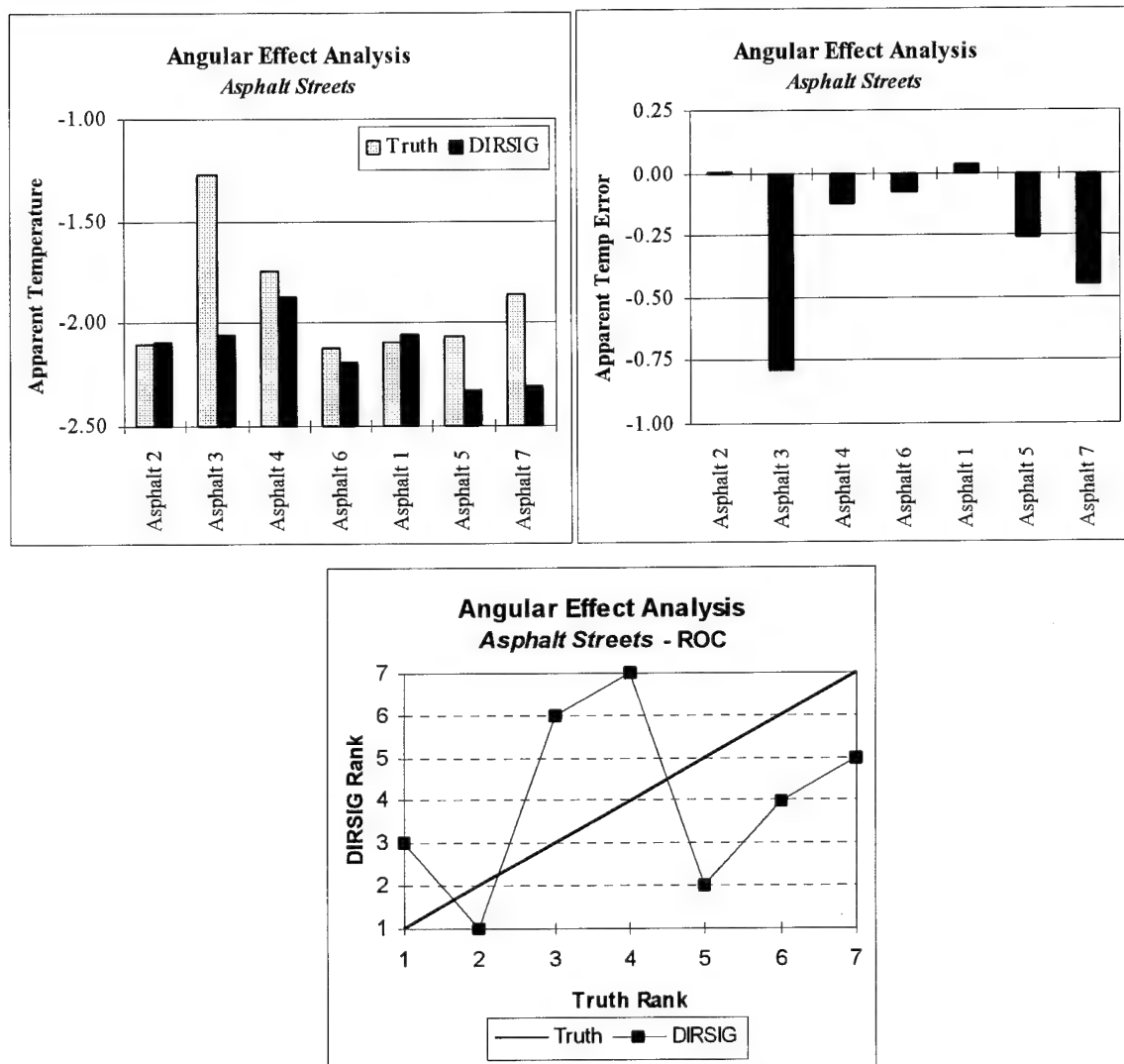


Figure 5.22 Angular effect evaluation

No real conclusive angular effect patterns could be seen in these validation points. The variation in the apparent temperatures was most likely caused by shape factor effects, not angular effects. The shape factor was near one in the synthetic image for all these points, but the actual imagery may have had different surroundings objects as it was difficult to model every tree in the scene. The phenomenology control of these validation points was not great enough to make any conclusive decisions regarding the angular effects. These

points were a bad selection for the examination of angular effects. The actual numeric values for the angular effect evaluation of the asphalt streets are shown in Table 5.6.

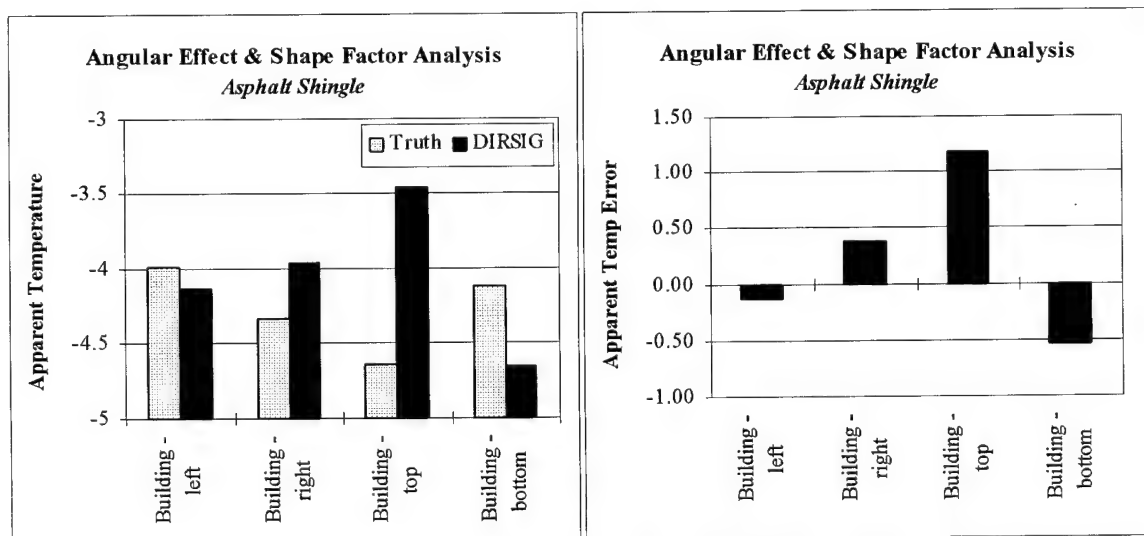
Table 5.6 Angular effect evaluation - *asphalt street*

Object - structure number (orientation)	Apparent Temperature			ROC		
	Truth Error	SIG		Truth	SIG	Error
Asphalt Street 1	-2.097	-2.06	0.04	5	2	3
Asphalt Street 2	-2.099	-2.10	0.00	6	4	2
Asphalt Street 3	-1.270	-2.06	-0.79	1	3	2
Asphalt Street 4	-1.746	-1.87	-0.12	2	1	1
Asphalt Street 5	-2.069	-2.33	-0.26	4	7	3
Asphalt Street 6	-2.120	-2.19	-0.07	7	5	2
Asphalt Street 7	-1.863	-2.31	-0.45	3	6	3

RMS Error - 0.3607

ROC Coefficient - 0.2857

The second phenomenological evaluation was conducted using an asphalt shingled roof to the south of the Hawkeye plant (see Figure 5.21 for the location of the validation points). The sloped roof provided indications on the inclusion of shape factor effects but primarily it showed angular effects. The selected roof was chosen because it offered four distinct orientations. Each side of the roof is exposed to different backgrounds, and each side has a different sensor-target angle. The results are shown in the graphs below.



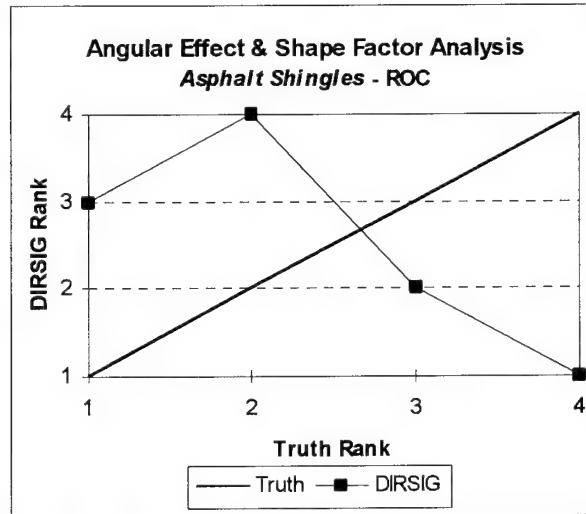


Figure 5.23 Angular effect & shape factor evaluation - *asphalt shingles*

While it was difficult to determine the accuracy from the RMS error, the failure of DIRSIG to correctly model the angular and shape factor effects was very evident in the rank order correlation. The exact opposite phenomenology was seen in the DIRSIG imagery. This revealed a serious problem with the synthetic imagery.

Table 5.7 Angular effect & shape factor evaluation - *asphalt shingles*

Object - structure number (orientation)	Apparent Temperature			ROC		
	Truth Error	SIG		Truth	SIG	Error
Asphalt Shingle 1- left	-3.997	-4.14	-0.14	1	3	2
Asphalt Shingle 2 - right	-4.337	-3.96	0.38	3	2	1
Asphalt Shingle 3 - top	-4.647	-3.46	1.18	4	1	3
Asphalt Shingle 4 - bottom	-4.122	-4.65	-0.53	2	4	2

RMS Error - 0.6793

ROC Coefficient - -0.8

The problem was not an error in the DIRSIG modeling approach, but in the input files to DIRSIG. The output is only as good as the input. DIRSIG requires the user to specify an angular emissivity falloff curve as part of the emissivity file. Initially, measured data from the 1992 validation was used for the angular curves. However, preliminary synthetic imagery showed that these curves decreased too dramatically after 60 degrees as contrast reversals were seen in the imagery (see Section 6.2). A polynomial approximation

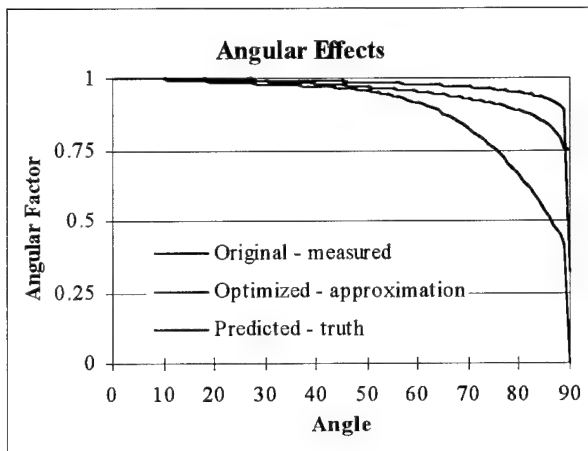
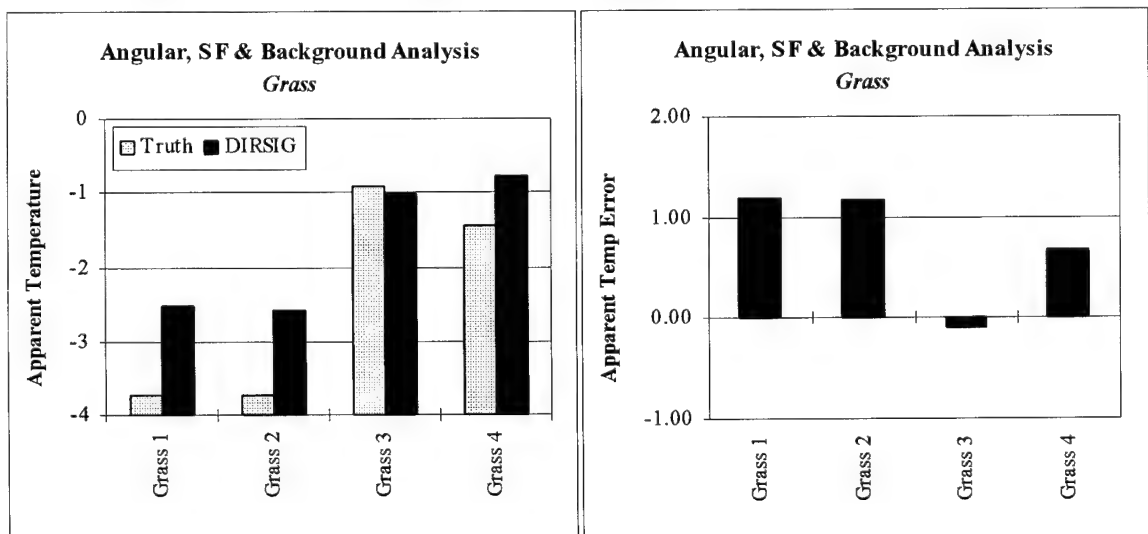


Figure 5.24 Angular effect curves

was then used for the angular effect curves. The resulting imagery used in the validation showed that the curves were still not appropriate and that new angular curves are needed. The angular curves should be more lambertian, near 1.0 and then decrease sharply near 90 degrees. Figure 5.24 shows the original measured curve for brick, the polynomial approximation that was used in the validation, and, finally, the predicted curve that most likely resembles the actual angular falloff of the material.

Knowing that DIRSIG had difficulty in modeling the angular effects, the final phenomenological evaluation was conducted using materials that placed more emphasis on background and shape factor effects. In the truth imagery, the grass in the front of the houses was much colder in comparison to the grass between the houses. The apparent temperature of the grass was higher between the houses because the shape factor was less and the surrounding walls of the houses provide a warmer background temperature than the sky. Grass 1 & 2 are in the front of the houses while Grass 3 & 4 are near the sides of houses (see Figure 5.21 for the location of the validation points).



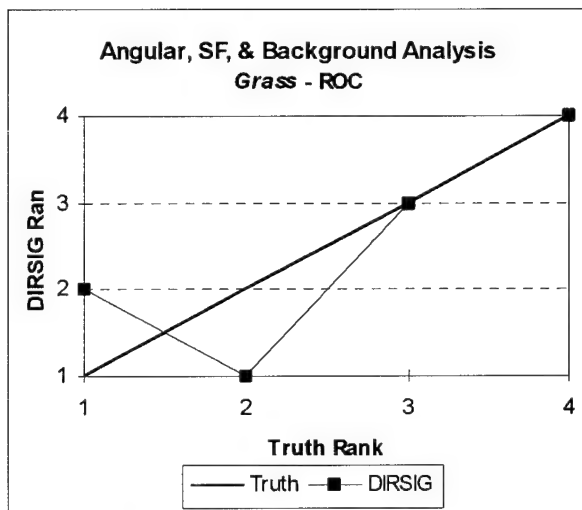
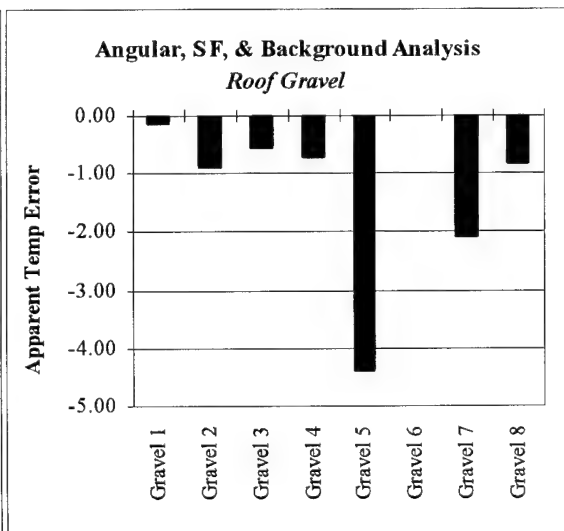
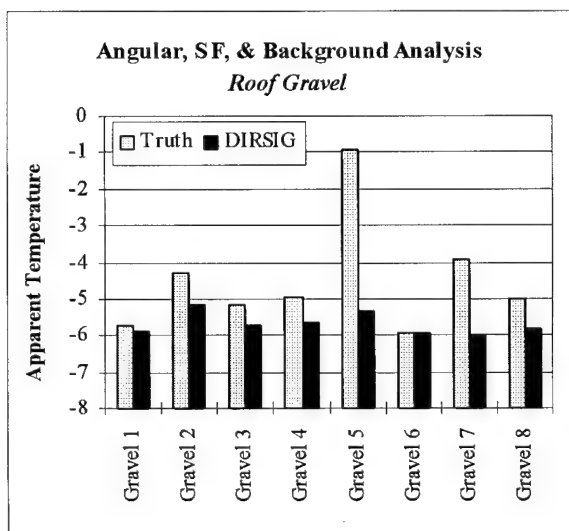


Figure 5.25 Angular, shape factor, & background effect evaluation - *grass*

The ability of DIRSIG to include shape factor and background effects was supported by these evaluation points. While the first two points were reversed in the rank order correlation, the apparent temperature comparison showed that the temperatures of these two points were very close. The DIRSIG error was minimal in modeling the complex phenomenology seen in these points. (see Table 5.8 for the numerical values)

The background and shape factor effects were examined in more detail with the roof gravel of the Hawkeye building. Complex thermal interactions were evident between the various structures in the Hawkeye building complex. Some roof gravel was fully exposed to the sky while other areas saw less than half of the sky. Points 1, 6, & 7 were fully exposed to the sky; points 3, 4, & 8 were partially exposed to the sky, and points 2 and 5 were close to walls. (see Figure 5.21 for the location of the validation points)



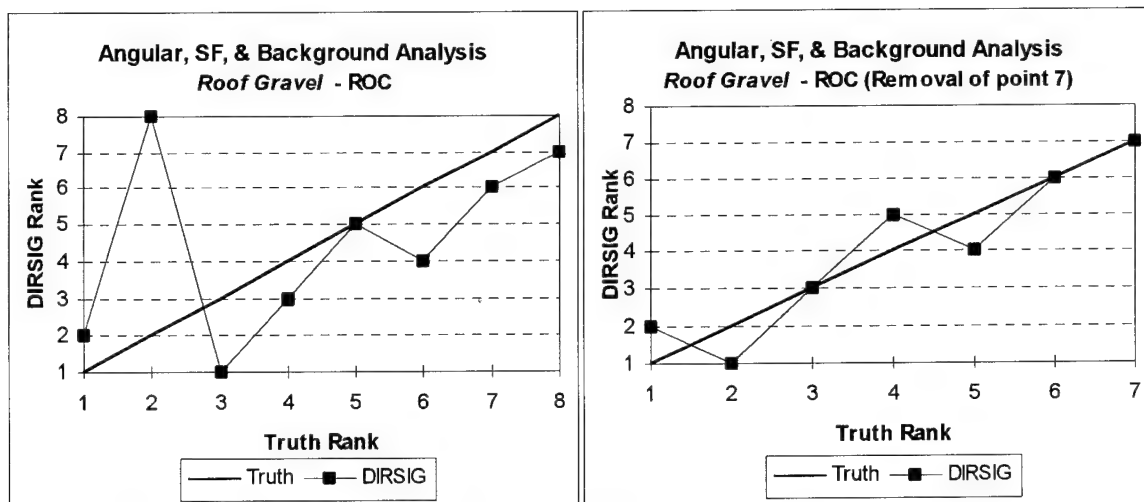


Figure 5.26 Angular, shape factor, & background effect evaluation - *roof gravel*

DIRSIG also recreated the phenomenology seen in these evaluation points with a relatively high degree of accuracy. The apparent temperature errors were large, but the appropriate phenomenology was seen. The RMS error analysis showed that all the validation points were too cold. DIRSIG includes the background effects, but the background objects should have a larger effect on the temperature of the target. This was most likely caused by internal heating of the building. The internal temperature of the Hawkeye building is around 20°C. This internal heat increases the external temperature of the wall that is in radiational exchange with the roof gravel. THERM has no information regarding this high internal temperature; it only knows about the external surface temperature. This is where self-generated power might be needed to increase the temperature of these building walls that provide the background effects for the roof gravel. However, no materials in the scene were given self-generated power. This could explain some of the problems with the phenomenology, in particular validation point 7. Validation point 7, the second warmest/brightest object in the truth imagery, was removed from the rank order correlation because it was suspected that the error was caused by internal heat underneath the roof gravel. After removing point 7, the rank order correlation results improved dramatically, from 0.429 to 0.928, as shown in Figure 5.26.

Table 5.8 Angular, shape factor, & background effect evaluation

Object - structure number (orientation)	Apparent Temperature			ROC		
	Truth Error	SIG		Truth	SIG	Error
Grass 1 - front house	-3.728	-2.53	1.20	3	3	-
Grass 2 - front house	-3.73	-2.57	1.17	4	4	-
Grass 3 - side house	-0.909	-1.01	-0.10	1	2	-
Grass 4 - side house	-1.449	-0.78	0.67	2	1	-
Hawkeye Roof Gravel						
Roof Gravel 1 - full exposure	-5.719	-5.86	-0.14	7	6	1
Roof Gravel 2 - near wall	-4.282	-5.17	-0.88	3	1	2
Roof Gravel 3 - partial exposure	-5.190	-5.72	-0.53	6	4	2
Roof Gravel 4 - partial exposure	-4.929	-5.65	-0.72	4	3	1
Roof Gravel 5 - near wall	-0.942	-5.34	-4.40	1	2	1
Roof Gravel 6 - full exposure	-5.953	-5.95	0.00	8	7	1
Roof Gravel 7 - full exposure	-3.898	-5.97	-2.07	2	8	6
Roof Gravel 8 - partial exposure	-5.002	-5.84	-0.84	5	5	-

Summary of Complex Phenomenology Results - RMS & ROC

Angular Effects	Angular & SF Effects	Angular, SF & Bkg Eff	Angular, SF & Bkg Eff
<i>Asphalt Streets</i>	<i>Asphalt Shingles</i>	<i>Grass</i>	<i>Roof Gravel</i>
RMS - 0.361	RMS - 0.679	RMS - 1.799	RMS - 0.904
ROC - 0.286	ROC - -0.80	ROC - 0.80	ROC (1) - 0.429
			ROC (2) - 0.928

While an attempt was made to control the phenomenology analysis, adding one new variable each time, the points that were used revealed that it is difficult to isolate phenomenology validation points in a scene this complex. Therefore, for future work, more effort should be placed in selected better phenomenology validation points that isolate the control variables being analyzed.

Unfortunately, the line scanner imagery could not be used to examine all phenomena present in the real world. Shadows and solar effects are a major area of study in synthetic image generation, but the 0200 imaging time virtually eliminated the effects of the sun/shadow history during the day. The Inframetrics imagery would provide the medium for examining solar effects.

5.3.1.4 Geometric Accuracy

Before the Inframetrics imagery was analyzed, the geometric accuracy of the Bendix line scanner was assessed. The geometric accuracy of the synthetic image relies heavily on the accuracy with which the synthetic image is created. The geometric accuracy of the scene creation varied, but in general, the scene was created to within a tolerance of ± 10 feet. Any error larger than this could likely be attributed to a DIRSIG geometry error. While the geometry was validated when the DIRSIG code was updated to include the sensor geometric effects, the field of view was limited. The expanded field of view in the current scene further tested and validated the geometry of DIRSIG.

The geometric validation was accomplished using **ENVI 2.0**. 27 evaluation points were identified in both images. These points were used to do a first order rotation and scaling of the imagery. The output RMS error in pixels was then recorded. The RMS error of 2.28 pixels in the synthetic image or 8.75 pixels in the truth image corresponds to a geometric error of about 10 feet based on the resolution of the imagery. (see Figure 5.28 for the location of the analysis points)

GCP ID #	BASE(X,Y)		WARP(X,Y)		PREDICT(X,Y)		ERROR(X,Y)		RMS
12	1818	208	424	39	425.36	35.13	1.36	-3.87	4.1
21	1609	1024	379	251	378.19	254.62	-0.81	3.62	3.71
2	1632	746	383	177	382.63	180.39	-0.37	3.39	3.41
15	454	270	95	64	96.37	67.07	1.37	3.07	3.36
16	864	520	194	127	196.34	128.95	2.34	1.95	3.04
25	1210	554	283	403	284.01	400.16	1.01	-2.84	3.02
3	1540	810	362	196	360.68	198.46	-1.32	2.46	2.79
13	1885	302	442	62	441.91	59.38	-0.09	-2.62	2.62
5	1527	1483	296	283	295.07	380.73	-0.93	-2.27	2.45
24	1664	418	390	95	389.03	92.75	-0.97	-2.25	2.45
20	1555	1524	368	386	367.16	388.27	-0.84	2.27	2.42
11	285	1504	62	399	60.53	397.33	-1.47	-1.67	2.23
7	1211	1521	282	392	284.12	391.37	2.12	-0.63	2.21
6	1295	1482	305	378	304.24	380.04	-0.76	2.04	2.18
23	1524	470	355	110	355.45	108.17	0.45	-1.83	1.88
10	351	1518	77	402	76.52	400.31	-0.48	-1.69	1.76
26	793	1577	182	412	183.45	411.00	1.45	-1.0	1.76
22	1498	1023	352	254	351.39	255.61	-0.61	1.61	1.72
18	293	580	60	152	58.75	151.38	-1.25	-0.62	1.39
17	402	524	85	134	84.84	135.24	-0.16	1.24	1.26
19	285	595	58	156	56.88	155.46	-1.12	-0.54	1.24
9	722	1704	166	445	166.82	445.60	0.82	0.60	1.01
27	573	790	127	205	127.18	204.09	0.18	-0.91	0.93
8	759	1496	174	390	174.91	389.83	0.91	-0.17	0.93
1	1473	1341	347	340	346.64	340.51	-0.36	0.51	0.62
14	432	379	92	96	91.50	96.32	-0.5	0.32	0.60
4	1297	1316	304	336	304.05	335.85	0.05	-0.15	0.16

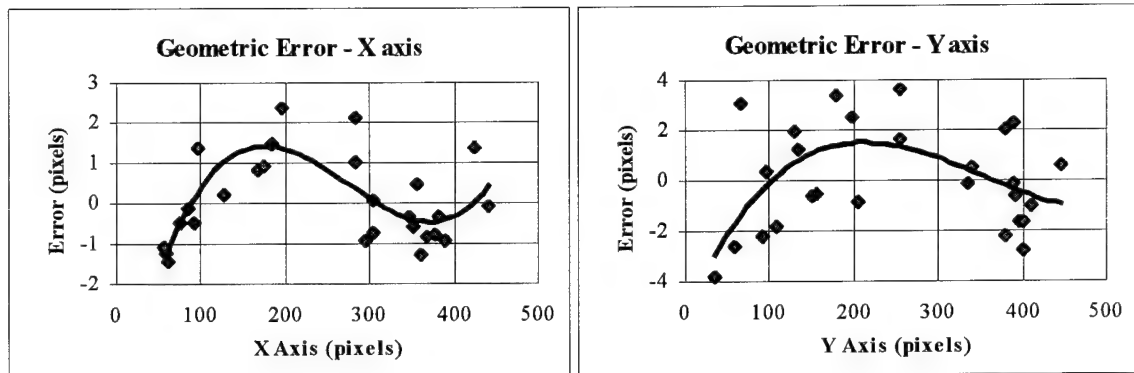


Figure 5.27 Geometric error



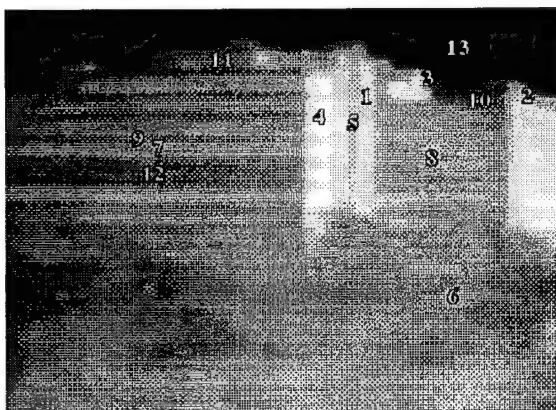
Figure 5.28 Ground evaluation points

This error was dominated by the error in the scene creation. It was impossible to remove the scene creation error by rotating and scaling the imagery. It can only be eliminated by recreating the scene with greater detail. It was difficult to attribute any of this

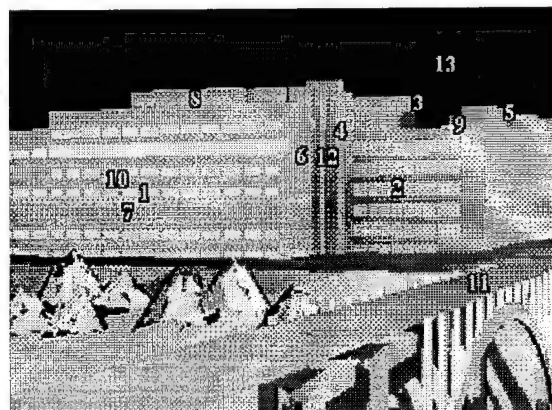
error to actual error in the geometry of the line scanner. In order to verify that the geometric error was dominated by the error in the scene creation, the RMS error was plotted as a function of the pixel location in the x and y directions (see Figure 5.27). The results showed the error was random. This was further supported by the fact that a third order polynomial curve fit resulted in a R^2 error of 0.544 in the *x direction* and 0.273 in the *y direction*. These R^2 errors must be closer to 1.0 to make any statistical conclusions regarding the geometric error. In conclusion, the imagery looks good and the appropriate distortions are evident in the scene so it is safe to assume the line scanner effects are being reproduced properly at this resolution.

5.3.2 Validation - Alternate Truth Imagery (Inframetrics video camera)

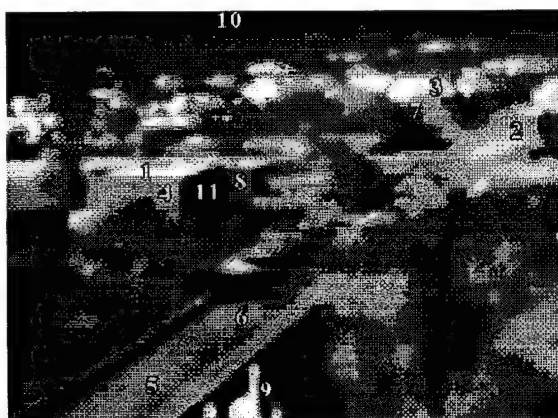
Following the validation of the synthetic imagery using the Bendix truth imagery, the synthetic imagery with the same optimum material parameters was compared to the Inframetrics truth imagery. As discussed earlier, this tested the robustness of DIRSIG. It also revealed how well the material parameters were optimized; it did not test any of the meteorological inputs since entirely new weather and atmospheric inputs were required. Ideally, similar rank order correlation results would be found when comparing the synthetic imagery with the alternate roof-top imagery. Large differences in the validation results between the aerial and roof-top imagery would indicate a deficiency in the synthetic image generation process. The rank order correlation results for the imagery of Hawkeye and the church can be seen below.



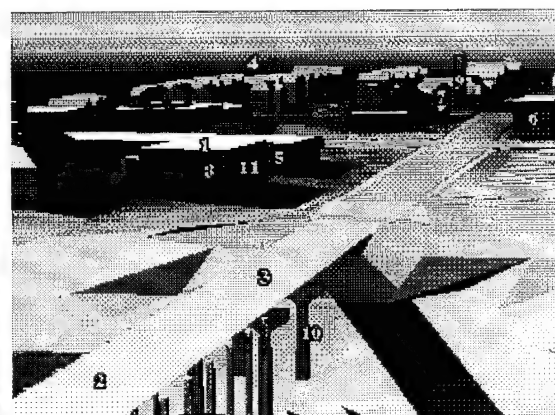
Truth Hawkeye imagery



DIRSIG Hawkeye imagery



Truth church imagery



DIRSIG church imagery

5.29 Inframetrics rank order correlation imagery

Table 5.9 Inframetrics rank order correlation results

Validation point (orientation)	ROC		
	Truth Error	SIG	
Brick wall 1 (south)	1	4	3
Brick wall 1 (south)	2	5	3
Brick wall 1 (south)	3	3	-
Brick wall 1 (south)	4	6	2
Brick wall 1 (south-west)	5	12	7
Bridge street	6	11	5
Window (west)	7	1	6
Window (west)	8	2	6
Brick wall 1 (west)	9	10	1
Brick wall 1 (west)	10	9	1
Brick wall 1 (west)	11	8	3
Brick wall 2(west)	12	7	5
Sky	13	13	-

Validation point (orientation)	ROC		
	Truth	SIG	Error
YMCA roof	1	1	-
Building (east)	2	6	4
Church tower (east)	3	9	6
YMCA side (east)	4	8	4
Bridge street	5	2	3
Bridge street	6	3	3
Church side (east)	7	7	-
Strip mall (east)	8	5	3
Bridge support	9	10	1
Sky	10	4	6
YMCA side (north)	11	11	-

ROC Coefficient - Hawkeye imagery
0.4395

ROC Coefficient - Church imagery
0.400

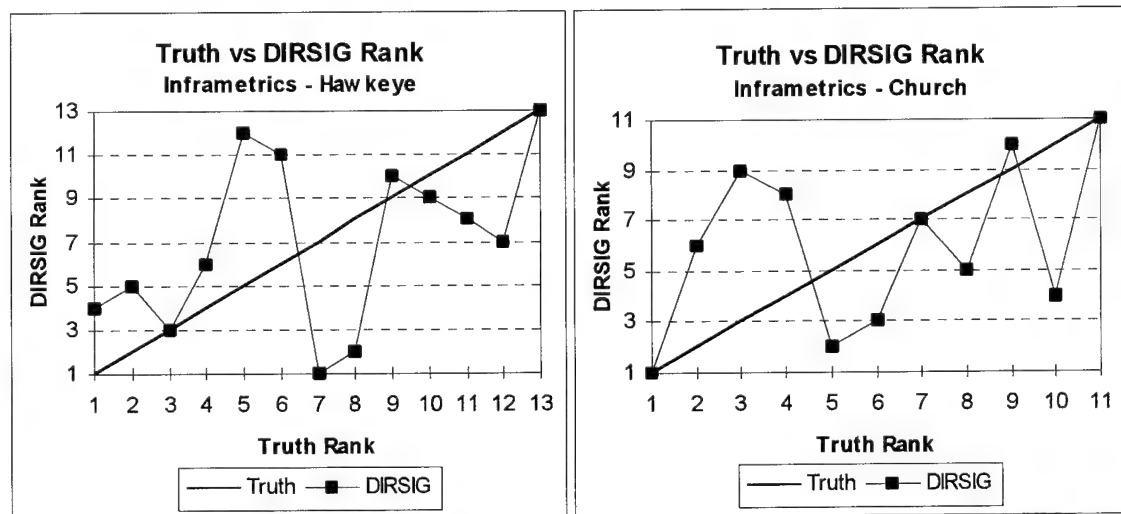


Figure 5.30 Inframetrics rank order correlation results

The poor results seen in the Inframetrics imagery can be attributed to a variety of problems. The quality of the Inframetrics imagery was very low. The angular effect problem seen in the Bendix imagery probably also caused errors in the Inframetrics imagery. Most

importantly, this is where the true robustness of the material file that was created for the Bendix imagery failed. Because of the low thermal contrast at night, all the variations that one normally sees in a material are reduced. A dark colored brick looks the same at night as a light colored brick. In addition, the sensitivity analysis showed that the visible characteristics of an object have virtually no effect on the temperature of an object at night (see Section 6.1.2). As a result, little effort was spent in optimizing the visible characteristics of the materials. However, when these optimized material parameters were used on the daytime imagery, the visible characteristics of the object played a major role in determining the temperature. Therefore, these errors in the daytime imagery are understandable.

In order to fix this problem, the primary imagery should be daytime imagery. During the day, the visible characteristics of an object become more important. In addition, the other material parameters also become more sensitive when solar influences are present. This is supported by the time history sensitivity analysis that was conducted in Section 6.1.3. The optimized material parameters of the daytime imagery can then be used to simulate nighttime imagery.

5.3.3 Validation Summary

DIRSIG is fully capable of modeling LWIR systems. It accurately creates the radiometry seen in thermal imagery acquired in the low contrast conditions that prevail at night. The optimization of the input parameters greatly reduced the RMS error while only slightly helping the already high ROC coefficient in the Bendix truth imagery. However, this material file failed when it was used in the Inframetrics validation. The validation also revealed some limitations and problems with the inputs to the DIRSIG synthetic image generation process. Problems existed with angular and background effects. The background effects are linked to THERM while the angular effects are linked to the material emissivity file. THERM has already been identified as a weak link in the image generation process but more research is needed in the area of angular emissivities if DIRSIG is used to model imaging systems.

6.0 Input Parameter Sensitivity Analysis & Optimization

The first DIRSIG rendering of the scene had some errors. This was expected as generic input parameters were used throughout the scene. While many object temperatures in the synthetic image were relatively close to those in the truth image, the generic input parameters did not provide enough accuracy for the validation. So, in order to make the synthetic image closely resemble the truth imagery, the input parameters were analyzed and optimized.

6.1 Input Parameter Sensitivity Analysis

Before any changes were made to the input parameters, a sensitivity analysis of the input parameters was conducted. The sensitivity analysis would help to optimize the input parameters by showing the amount of change needed in an input parameter to improve the radiometric accuracy of the synthetic imagery. However, the prolonged run times of DIRSIG make it difficult to do a sensitivity analysis using DIRSIG, recording the change in radiance for every change in all the input parameters. This led to running an off-line version of THERM, the DIRSIG thermal model, where THERM would be treated as a 'black box.' The changes in the output temperatures as a function of the changes in the input parameters could quickly be calculated without having to run DIRSIG multiple times.

Reviewing the major input parameters to THERM, material, weather, and geographic parameters are all needed to determine the temperature of a material. Changing just one of the inputs in these three major areas will affect the temperature. Figure 6.1 shows all the input parameters to THERM that were potential variables for the sensitivity analysis. Although all these parameters affect the temperature of a material, some of the variables, such as the geographic parameters, are known to a high degree of precision and can therefore be eliminated from the sensitivity analysis. In the end, a sensitivity analysis would be performed on all the material parameters and the weather parameters of wind speed, air temperature, and direct & diffuse insolation. These

THERM inputs are the only parameters that have a significant affect on the temperature and resulting self emission of the object.

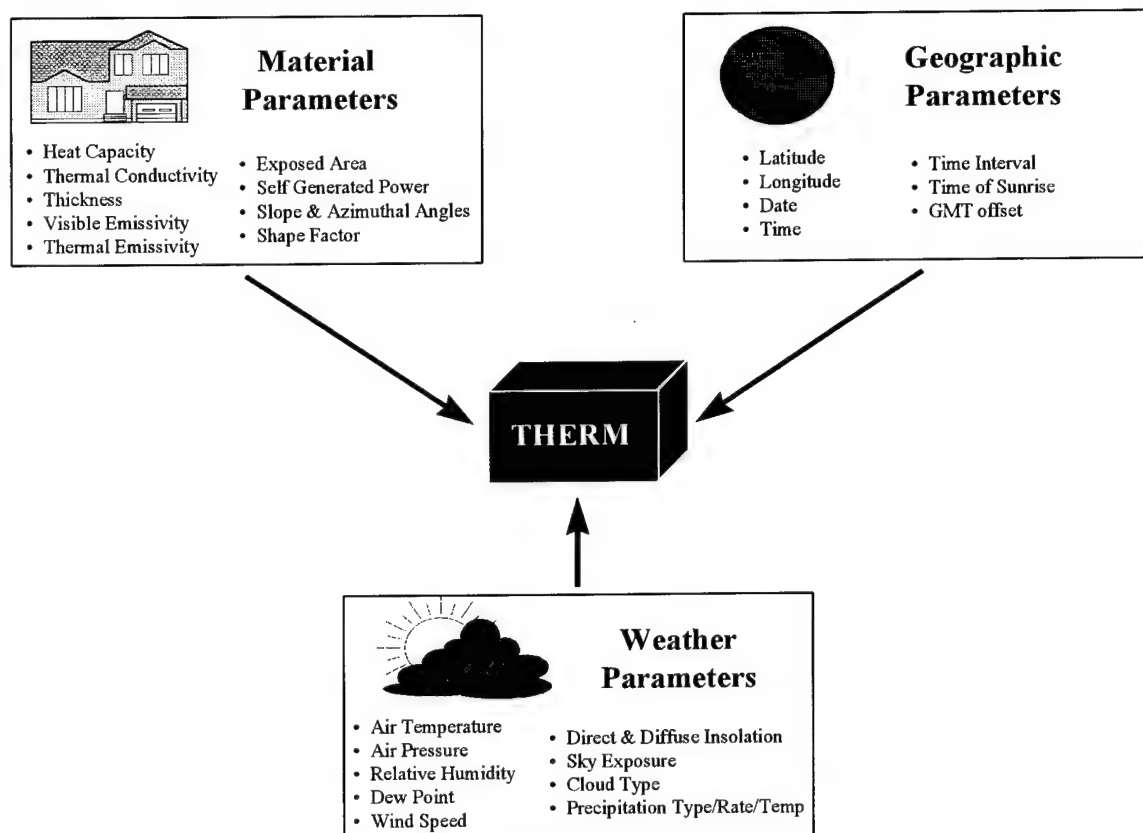


Figure 6.1 THERM input parameters

Since a sensor ultimately detects radiance, the other major factors that affect the radiance at the sensor also had to be examined. The major inputs from the 'big equation' that were considered for the sensitivity analysis were shape factor, background radiance, upwelled radiance, and downwelled radiance. Since shape factor and the background effects are estimated using the ray-tracer submodel, their error was assumed to be negligible. The other factors, transmission and upwelled & downwelled radiance, did need to be examined since they were estimated using Modtran. Their sensitivity values would be found by iterating through the 'big equation'. These three atmospheric parameters and the three weather parameters are all collectively referred to as meteorological parameters in the sensitivity analysis.

A sensitivity analysis requires some knowledge of the input parameters, including a minimum and maximum range of values, $\Delta parameter$, and an estimate of the standard error, $\sigma_{parameter}$. The range of values for the DIRSIG input parameters came from a variety of sources. For the meteorological parameters, which were partially based on actual measured data, the range of values was found by estimating the error in the measured data. These error estimates were obtained from Rankin's thesis which analyzed the error in each of the DIRSIG submodels. This method worked well for the meteorological parameters, but there was no measured material parameter data for the objects in the scene. This absence of measured data led to the use of the DCS Corporation database and the Nonconventional Exploitation Factors (NEF) modeling database compiled by the National Image Resource Library. Both databases were used to estimate a relative minimum, maximum, and standard deviation for all the material parameter values. The range for the material parameters such as thickness and thermal conductivity were as much as $\pm 50\%$ of the generic mean value. In contrast, for the meteorological input parameters where the inputs are known fairly accurately, such as air temperature and downwelled radiance, the range of values was only about $\pm 15\%$ of the measured value. The minimum and maximum range of values for the meteorological and material parameters were then used to estimate the standard error. All input parameter sensitivity values are expressed as apparent temperature errors at the sensor resulting from one standard deviation error in the input parameter $\Delta T_{apparent} / \Delta parameter \cdot \sigma_{parameter} \Rightarrow \Delta T_{expected}$. The parameter with the highest expected error would be changed first in the optimization of the input parameters.

There was still one major problem in conducting a sensitivity analysis using THERM. THERM only outputs temperatures at the ground, not radiance or apparent temperature values at the sensor. Because a sensitivity analysis showing the change in the apparent temperature of an object at the sensor was desired, a method of converting the output temperatures on the ground to apparent temperatures at the sensor was needed. In other words, a simplified version of the 'big equation' was needed. This led to the development of a MathCad spreadsheet that could read in the changes of the input parameters along with the corresponding changes in output temperature values (see

Appendix F for MathCad spreadsheet). This data would then be converted into a final output sensitivity.

The first step in calculating the input parameter sensitivity was to convert the THERM output temperatures to spectral radiance values using the Planck equation. This spectral radiance information was calculated at wavelength intervals that corresponded to the wavelengths of the sensor responsivity data. For the Bendix line scanner, the radiance was calculated at 0.1 μm increments. The spectral radiance was multiplied by the spectral sensor responsivity and integrated across the bandpass of interest.

$$L_T = \sum_{\lambda=8\mu\text{m}}^{\lambda=14\mu\text{m}} \text{Responsivity}_{\lambda} \cdot L_{\text{material } \lambda} \quad (6.1)$$

While the sensor responsivity is normally incorporated after the radiance has reached the sensor, integrating the sensor responsivity at the ground allowed the Modtran bandpass averages for the atmospheric parameters to be used. These bandpass values are acceptable because the benefits of a full spectral radiance calculation are minimal for this analysis. The result from this calculation was a single radiance value of the material at the ground that could be propagated to a LWIR radiance at the sensor using the 'big equation'.

In the LWIR region, the effects of solar photons are negligible and may be eliminated from the calculations. This assumption is further supported by the fact that neither the Bendix or the Inframetrics imaging systems are responsive outside the 7-14 μm region of the electromagnetic spectrum. These assumptions led to the implementation of the following equation to determine the radiance at the sensor.

$$L_{\text{sensor}} = \{\varepsilon \cdot L_T + [F \cdot L_{d\varepsilon} + (1 - F) \cdot L_{b\varepsilon}] r_d\} \tau_2 + L_{u\varepsilon} \quad (6.2)$$

The output from THERM provides only the radiance at the ground due to the temperature of the object, L_T . Values for the remaining seven terms were still needed to approximate the radiance reaching the sensor.

The remaining terms were obtained from a combination of Modtran results and scene estimation. Starting from left to right, the emissivity, ε , was taken from the material

parameters list. This is normally a spectral emissivity, but the integration of the radiance in the bandpass of interest allowed the use of the average thermal emissivity value found in the materials file. Shape factor, F , is the amount of sky that an object can see and is thus dependent upon the location of the material in the scene. For materials such as roads, grass, and water that have unobstructed views of the sky, it is possible to assume the shape factor is 1.0, but for materials such as roof shingles and wood siding, an estimation of the shape factor is needed. As a result, an estimation based on Figure 6.2 and Equation 6.3 was used in determining a shape factor value, where β is the pitch angle of the roof and α is the angle to the horizon for a flat surface and a flat horizon.

$$F = 1 - \frac{\beta}{\pi} \quad (6.3)$$

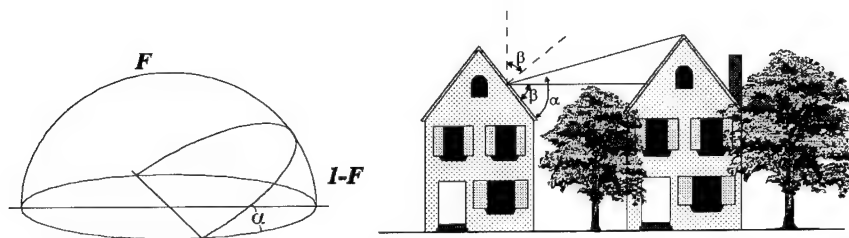


Figure 6.2 Shape factor

The small angle difference between β and α can be neglected because this is merely an estimation of shape factor and the difference in the final radiance is minimal (Snyder 1994). The resulting estimation of shape factor determines the amount of influence the background radiance has on the radiance reaching the sensor for that particular object/material. The background radiance, $L_{b\epsilon}$, affecting the material is actually comprised of the radiance from grass, asphalt roads, trees, roofs, walls, and other objects surrounding the material. As a result, the radiance from these objects was averaged to approximate the background radiance reaching any material. A final background radiance value of $20.41 \text{ watts}/(\text{m}^2 \text{sr})$ was used as an estimate of the actual background radiance (Snyder 1994). The amount of background radiance and sky radiance that ultimately reaches the sensor depends not only on the shape factor but also on the reflectivity of the material. Because photons can only be reflected, emitted, or transmitted by an object, $r + \epsilon + \tau = 1$, the reflectivity term in the equation is merely $1 - \epsilon$ for non-transmissive, or *opaque*, materials.

The remaining terms, τ_2 , L_{ue} , and E_{de} were all estimated using the Modtran outputs. The bandpass sky radiance of $4.289 \text{ watts}/(m^2 sr)$, atmospheric transmission of 0.91, and upwelled radiance value of $2.51 \text{ watts}/(m^2 sr)$ were used for the estimation of the radiance reaching the sensor in the LWIR (Snyder 1994).

Once the radiance was propagated to the sensor, the change in radiance was expressed as a function of the change in the input parameter. This change in radiance was converted into an apparent temperature, and the sensitivity of the input parameter was graphed. Graphing the sensitivity verified linearity for the range of input parameter values. This general procedure for determining the input parameter sensitivity was followed for all the input parameters and is described in more detail in the following sections for the meteorological and material input parameters.

6.1.1 Weather & Atmospheric Sensitivity

While there was a high degree of confidence in the meteorological values, including both the weather parameters & the atmospheric parameters, they were still a potential source of error. The main error in these parameters arises from the fact that the weather and atmospheric readings were not taken at the exact imaging site. The weather data was measured at the Rochester airport, only 5 miles from the imaging site, but the radiosonde data was taken 60 miles away in Buffalo, NY. The error in the meteorological data is small as long as similar conditions exist at the recording area and the imaging area. The error also increases greatly if the weather is changing at the time of imaging.

The weather was relatively stable around the 10th of November when the imagery was acquired. This increased the confidence in the meteorological values. The meteorological parameters that were analyzed in the sensitivity analysis included:

<i>Weather Parameters</i>	<i>Atmospheric Parameters</i>
Temperature	Transmission
Wind Speed	Upwelled Radiance
Direct & Diffuse Insolation	Downwelled Radiance

While each of these input parameters has a slightly different effect on the temperature of a material, in general, the effects of meteorological parameters are global since the meteorological inputs influence the temperature of all materials in the scene. The parameters are described in more detail below, along with the expected error and the probable relationship between a change in the input parameter and the change in the output temperature.

Air Temperature (°C) - The air temperature affects the temperature of the material as the material is in constant thermal exchange, *convection and radiation*, with the surrounding air. Because the air is usually colder than any material in the scene, it tends to reduce the temperature of the objects. Therefore, a colder temperature will generally cause all the materials in the scene to have a colder temperature. The sky temperature is traditionally the coldest object in the scene.

$\pm 2^{\circ}\text{C}$

Positive Relationship

Wind Speed (m/s) - Wind speed affects the temperature of a material because it changes the convection rate between the material and the air. In general, wind tends to reduce the thermal contrast in the scene as it carries heat away from warm materials and warms cold materials.

± 2.5 m/s

Material Dependent Relationship

Direct & Diffuse Insolation (L/hr) - The amount of solar heating that a material receives during the day directly affects its temperature. On a cloudy day, the amount of sunlight that reaches the material is reduced, and hence, it will have a lower temperature. The affect of the insolation depends on the visible emissivity and reflectivity of the material.

$\pm 15\%$ Variation

Positive Relationship

Transmission (%) - The transmission of the atmosphere directly affects the radiance reaching the sensor. As the atmospheric transmission decreases, so does the radiance reaching the sensor. The transmission of the atmosphere tends to affect all materials equally.

$\pm 2-3\%$ Variation (Absolute Min: 0.0; Absolute Max: 1.0) *Positive Relationship*

Upwelled Radiance (w/m^2sr) - The upwelled radiance from the atmosphere that reaches the sensor alters the radiance that actually leaves the materials at the ground. The upwelled radiance is affected by the type and amount of atmosphere between the target and the sensor.

$\pm 10\%$ Variation

Positive Relationship

Downwelled Radiance (w/m^2sr) - The downwelled sky radiance is the radiance from the atmosphere that strikes a target. Similar to upwelled radiance, it is affected by the type and amount of atmosphere between the target and the sensor. The emissivity of the material determines the effect that downwelled radiance has on the material.

$\pm 15\%$ Variation

Positive Relationship

In order to reduce the time involved in calculating the meteorological sensitivity values, a batch file was created. This batch file automated the process of typing the inputs into THERM, but several inputs had to be specified to run the batch file. These inputs included the material ID number and the orientation of the material. Based on the material ID number, the program would extract the required material parameter values from the DIRSIG material database. The orientation value then provided a reference to several orientation files that contained information on the zenith, azimuth, and shape factor of a facet. Figure 6.3 shows the typical facet orientations that were used for the materials. These orientations were all estimated based on typical uses for the material. For example, most of the asphalt roads were assumed to have a 0.0° zenith and azimuth with a shape

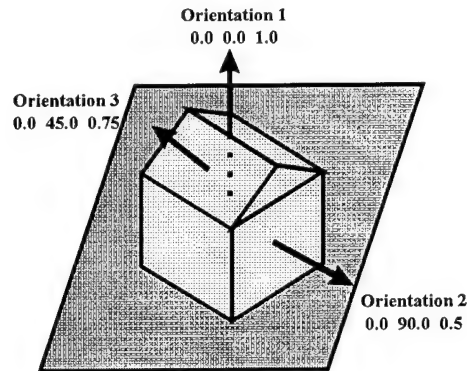


Figure 6.3 Material orientations

factor of 1.0, while a wood sided building would have a zenith of 0.0° , an azimuth of 90.0° , and a shape factor of 0.5.

The batch file was then used to run THERM multiple times, using a different weather file each time and recording the output temperature values for each material. The different weather files contained the variation in the input parameters, *temperature*, *wind speed*, and *direct & diffuse insolation*, for the sensitivity analysis. The resulting temperature values were then read into MathCad and converted to radiance values at the sensor. At this time, the transmission, upwelled, and downwelled radiance sensitivity values were found by iterating through the LWIR equation in MathCad. This provided the sensitivity values for all the meteorological parameters: temperature, wind speed, direct & diffuse insolation, transmission, upwelled, and downwelled radiance. This entire process is described visually in Figure 6.4 on the following page.

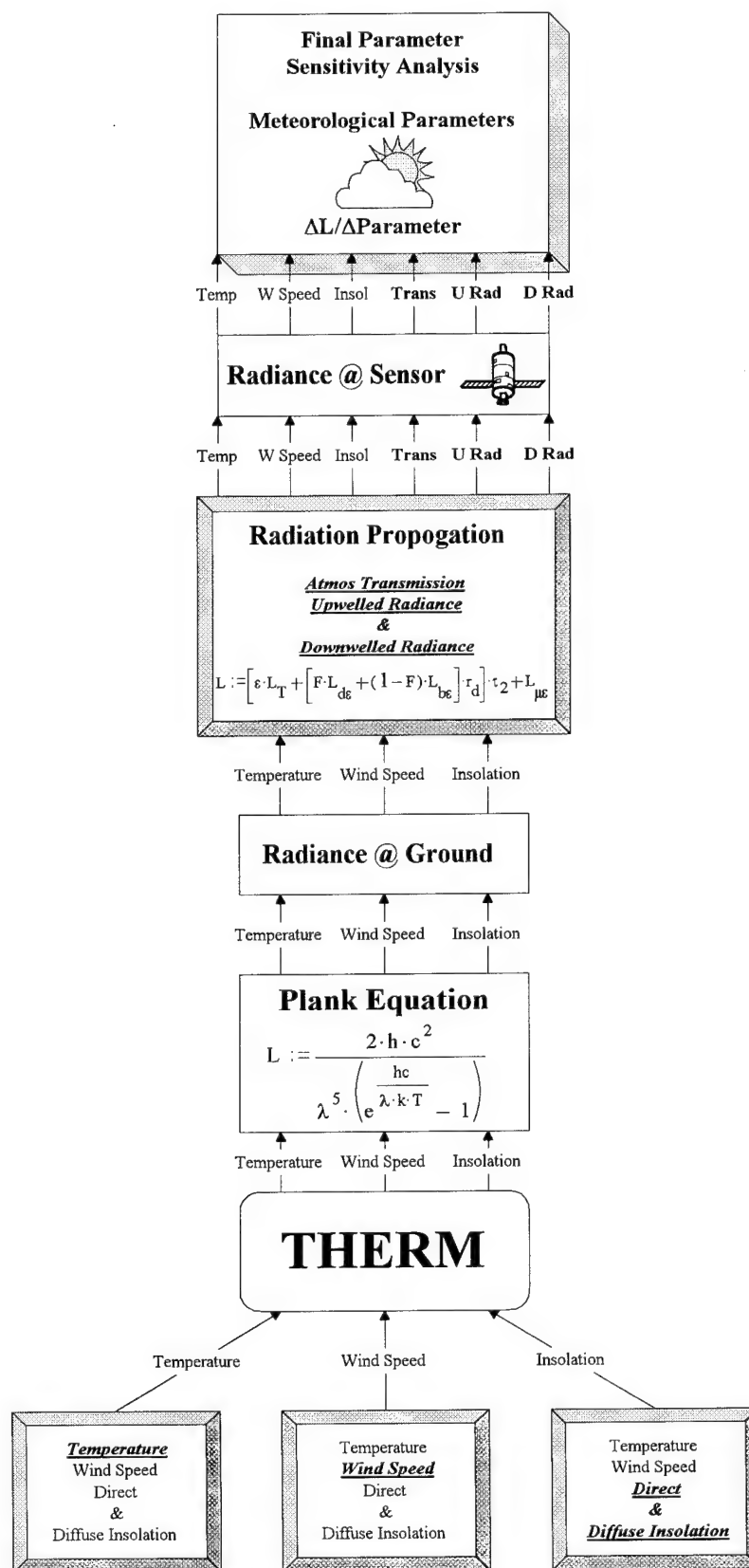


Figure 6.4 Meteorological parameter sensitivity analysis flow chart

Once the sensitivities of all the materials to the meteorological parameters were calculated, the results were converted into expected temperature errors. This allowed the different input parameters to be compared with each other, despite differing units, and also provided an average scene temperature error to each of the meteorological parameters. The average scene error would be used later to optimize the meteorological parameters. Optimizing the meteorological parameters would help remove global errors in the synthetic image and make it more closely resemble the truth imagery. The resulting meteorological temperature errors based on the sensitivity results are summarized in the following table.

Table 6.1 Meteorological sensitivity results
expressed as apparent temperature errors

Material Name (number)	Air Temp	Wind Speed	Direct & Diffuse Insolation	Atmos Trans (τ)	Upwelled Radiance (L_{ue})	Downwelled Radiance (L_{de})
Building Construction Mats						
Roof-aluminum (50)	0.378	-0.212	0.000	0.422	0.250	0.066
Roof-asphalt shingles-color (65)	0.803	-0.487	0.000	0.421	0.250	0.037
Roof-gravel (12)	1.067	-0.538	0.164	0.375	0.250	0.059
Roof-steel (52)	0.958	-0.607	0.000	0.349	0.250	0.124
Wall-brick-color (75)	1.136	-0.522	0.061	0.403	0.250	0.041
Wall-concrete (53)	0.484	-0.214	0.010	0.461	0.250	0.018
Wall-wood-color (85)	0.453	-0.245	0.000	0.448	0.250	0.032
Window-glass (54)	0.456	-0.254	0.000	0.451	0.250	0.031
Soils/Water						
Soil-clay-gray (40)	1.161	-0.639	0.010	0.404	0.250	0.021
Soil-clay-red (41)	1.150	-0.606	0.012	0.404	0.250	0.029
Soil-dirt-brown (13)	1.122	-0.556	0.047	0.397	0.250	0.044
Soil-gravel-light brown(43)	1.113	-0.475	0.507	0.399	0.250	0.050
Water-Genesee River (2)	1.150	-0.566	0.498	0.396	0.250	0.015
Surface Construction Materials						
Asphalt-street (5)	1.160	-0.527	0.239	0.410	0.250	0.026
Concrete-sidewalk (6)	1.139	-0.497	0.242	0.405	0.250	0.038
Vegetation						
Grass (4)	1.136	-0.522	0.061	0.403	0.250	0.041
Tree-deciduous (25)	0.844	-0.403	0.003	0.438	0.250	0.021
Tree-trunk (18)	0.499	-0.294	0.000	0.465	0.250	0.011
AVERAGE	0.900	-0.453	0.103	0.414	0.250	0.039

Clearly, the most sensitive parameter is air temperature. The average expected error for air temperature, 0.900, is almost twice as great as the next closest parameter, wind speed, -0.453. This relationship is understandable since a material is in direct

thermal exchange with the environment, but the magnitude is a little surprising. The changing of the air temperature by just one degree results in a 0.5 degree change in the apparent temperature of most materials. Thus, the air temperature will be the major meteorological factor influencing the apparent temperature of the materials. Similar to the effects of changing the air temperature, the wind speed also strongly affects the apparent temperature. The change in wind speed directly affects the thermal exchange between a material and the environment. However, it was surprising that the increased wind speed reduced the temperature of all materials. It was initially thought that the wind speed would increase the temperature of some materials while decreasing the temperature of others. All objects will tend to approach the reference temperature of the surrounding air. Therefore, the air should warm some objects and cool others. This shows an inadequacy of THERM in modeling the environment.

In analyzing the other parameters, the relatively high error/sensitivity of the atmospheric transmission and upwelled radiance results from the fact that these parameters directly affect the radiance and apparent temperature at the sensor.

$$L_{sensor} = L_{ground} \cdot \tau_2 + L_u \quad (6.4)$$

The direct relationship between these two input parameters and the apparent temperatures suggests that any error in these two parameters will cause large errors in the synthetic image. The only real difference between the effects of these two input parameters is that upwelled radiance affects all materials equally. It is independent of the material type because the upwelled radiance is additive. In contrast, atmospheric transmission is material dependent because it is multiplicative with the radiance at the ground, and not all materials have the same radiance at the ground. However, transmission (τ_2) and upwelled radiance (L_u) are highly negatively correlated so an error in one parameter tends to be offset or negated by the other. As a result, errors in either of these two parameters will have reduced or minimal effects on the apparent temperature at the sensor.

While the effects of the remaining two parameters do not directly affect the radiance at the sensor, they do affect the self-emission of the object on the ground. The resulting temperature errors of the downwelled radiance and the direct & diffuse insolation

were minimal when compared to the other parameters. This was somewhat surprising. For many materials, the direct & diffuse insolation error was 0.0, with an average of 0.103 for all materials. Apparently, most materials have reached a state of equilibrium with respect to the solar influences and the effects of the solar heating during the day are non-existent. While the increased intensity of the sun may have caused an elevated temperature of the material during the day, the temperature change that occurred during the day is not apparent as most materials have already lost the majority of their internal heat caused by the sun. The minimal importance of downwelled radiance was also somewhat unexpected. The cold temperature of the sky apparently reduced the downwelled radiance reaching the material on the ground. In addition, the reflectance of most materials is around 0.1 in the LWIR. Therefore, only 10% of the downwelled radiance that a target sees is propagated to the sensor. Thus, the effects of downwelled radiance are minimal when compared to the other radiance paths.

While a single meteorological input parameter has an effect on all materials in the scene, the effect varies from material to material. The primary differences result from shape factor. It is evident that materials that are not exposed to 100% of the sky are not as greatly influenced by it. The background seems to provide some 'protection' from the sky. The obscuring of the sky by surrounding objects results in warmer material temperatures and reduced sensitivity values. This is illustrated by the difference in the expected temperature errors for the concrete wall and concrete sidewalk. The temperature error due to a change in the air temperature for the concrete wall, 0.484, is about half the error of the concrete sidewalk, 1.139. In general, the error, or sensitivity, of the construction materials for walls is about $\frac{1}{2}$ the value of most materials in the scene. This effect is also seen in the wind speed results. Just as the materials are protected from the temperature of the sky, they seem to be protected from the wind. Thus, THERM seems to account for the fact that surrounding objects will not only block the sky temperature but also the wind.

The meteorological sensitivity results provided the information necessary to improve the results of the synthetic image. While these input parameters affect each

material differently, the effects are global. The change in just one of these input parameters will affect the apparent temperature of all materials in the scene. This must be considered when optimizing the input parameters.

6.1.2 Material Parameter Sensitivity

The generic material parameters that were used in the sensitivity analysis were developed from a combination of both the DCS Corporation and the NEF materials database. A total of over 250 materials were available for selection and assignment to the facets in the scene. Unfortunately, 250 materials does not even begin to describe the infinite number of materials in the world. However, these materials provided a starting point and reference from which 'new materials' could be developed.

The database from the DCS corporation contained valuable information on the thermal characteristics of materials but contained no detailed spectral information. The NEF database on the other hand had detailed spectral emissivity curves and little information on the thermal characteristics. This led to an integration of the DCS material parameter values with the spectral information from the NEF database to create a spectral material database.

Once this was accomplished, a detailed sensitivity analysis began on the material parameters for the over 50 scene materials (only 18 were actually analyzed because some materials had the exact same parameters except for the visible emissivities - 10 colored bricks, 10 colored woods, 10 colored shingles & 3 asphalt types). Similar to the meteorological parameters, each of the material parameters has a slightly different effect on the temperature of the material; but unlike the meteorological parameters, the changing of a single material parameter does not affect the entire scene. The material parameters are described in more detail below, along with the absolute minimum and maximum allowable values for any material, and the expected relationship between a change in the material parameter and the change in the output temperature.

Heat Capacity ($L/cm \cdot ^\circ C$) - Heat capacity is the amount of thermal storage that is capable by an object, where heat capacity is determined by multiplying the mass density and the specific heat.

Min: 0.0

Positive Relationship

Thermal Conductivity ($L\cdot cm/hr\cdot ^\circ C$) - The thermal conductivity provides an indication as to the rate at which energy is transferred by the diffusion process (Incropera 1990). The greater the thermal conductivity, the greater the rate of heat transfer between the material and the surrounding environment.

Min: 0.0

Positive Relationship

Thickness (cm) - The thickness of a material affects the thermal inertia, the resistance of a material to changes in the thermal environment. Increased thickness results in a material that is not as affected by the air temperature.

Min: 0.0

Positive Relationship

Visible Emissivity (%) - The visible emissivity is 'the fraction of visible insolation that is absorbed by a material.' It is the average emissivity of a material in the .4 to 2.0 μm region of the electromagnetic spectrum.

Min: 0.0; Max: 1.0

Positive Relationship

Thermal Emissivity (%) - The thermal emissivity is the fraction of thermal energy that is absorbed by a material. It is the average emissivity of a material in the 8 to 14 μm of the electromagnetic spectrum. The temperature of a material increases as the thermal emissivity approaches 1.0.

Min: 0.0; Max: 1.0

Positive Relationship

Exposed Area (%) - An adjustment term or 'fudge factor' that is used to describe the percentage of the facet that is exposed to the environment. When the surface is exposed to the environment on both sides, a positive shape factor is used. In contrast, a negative shape factor is used when one side of the surface is not exposed to the surrounding environment; it is exposed to stagnant air or another material. Recent improvements have been made to the exposed area within DIRSIG to reduce some of the guesswork associated with this parameter. If (shape factor < 0.5):

$$\text{Exposed Area} = \text{Exposed Area} \cdot \text{Shape Factor} \cdot 2.0$$

Min: -1.0; Max: 1.0

Positive/Negative Relationship

Self Generated Power SGP (L/hr) - This is also a 'fudge factor' that is used to compensate for facets that are actively generating power. This might include the hood of a car that is heated by the engine, or even the side of a heated house in the winter time.

Min: 0.0; Max: 10.0

Positive Relationship

Shape Factor SF (%)^{*} - The shape factor is the amount of sky that the material can 'see.' The raytracer program that is implemented by DIRSIG calculates this parameter within 5-10% of the exact value.

Min: 0.0; Max: 1.0

Positive Relationship

$$^* L - \text{Langley where } 1 \frac{W}{m^2} = 0.086 \frac{L}{hr} \text{ and } 1L = 1 \frac{cal}{cm^2}$$

Also like the meteorological sensitivity study, the sensitivity of each material parameter was accomplished using a batch file. The MathCad analysis for the material parameters was similar to the meteorological parameter analysis. The following flow chart describes the material parameter sensitivity analysis in detail.

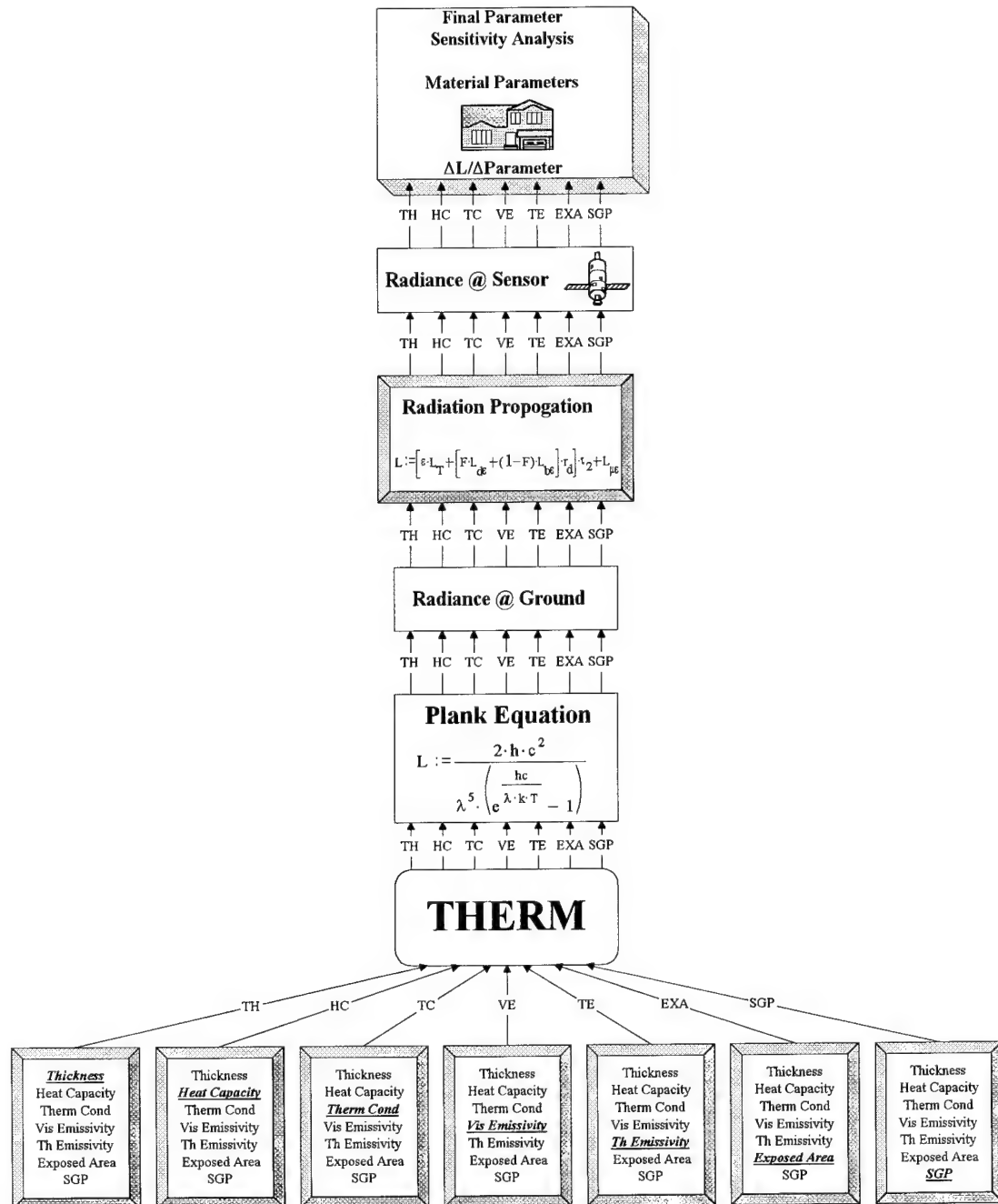
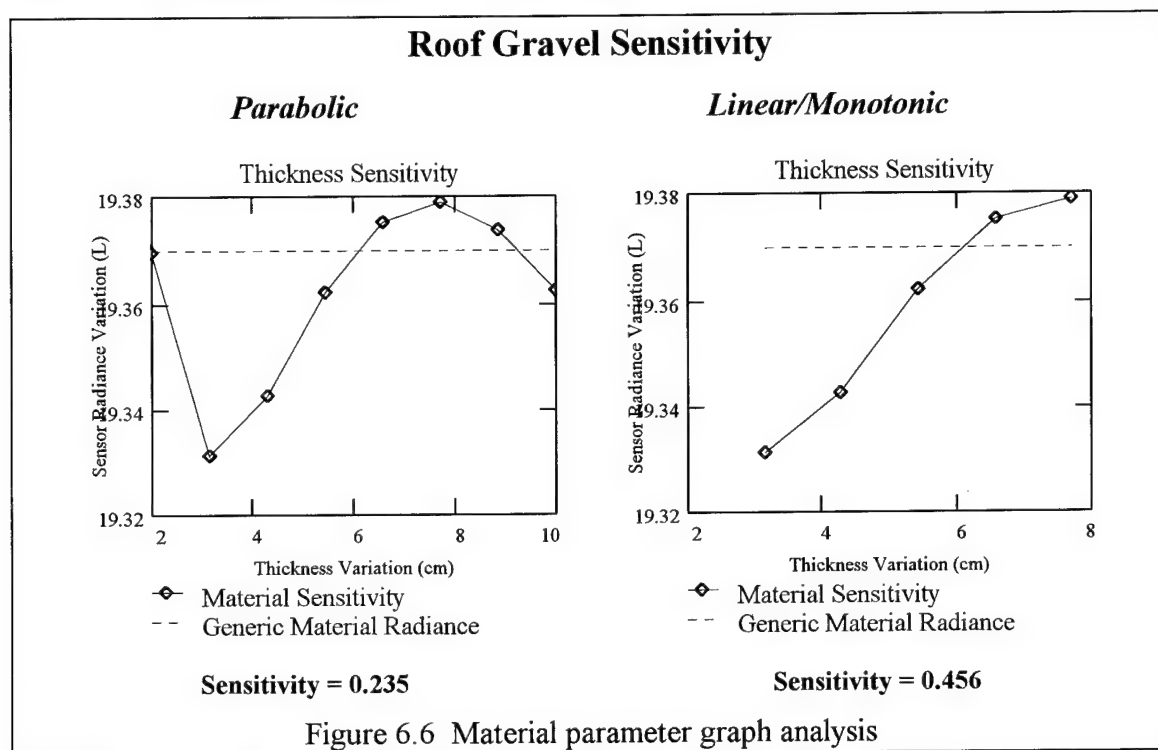


Figure 6.5 Material parameter sensitivity analysis flow chart

As discussed earlier, the change in the material temperature was then graphed as a function of the change in the input parameter, $\Delta parameter$. This was done to ensure linearity so that a first order approximation of the slope of the line provided an acceptable value for $\Delta L_{sensor} / \Delta parameter$. Unfortunately, not all graphs were monotonic and linear; some were parabolic in shape as can be seen below.



These graphs showed that changing the material parameter over the specified range was not linear for all values. In order to use the first order approximation, the range had to be confined to limit the analysis to a range of values where the curve was monotonic and linear. The most common non-linearities occurred in the thickness and heat capacity values. Typically, if the curve was not linear, only 2 data points near the minimum or maximum needed to be eliminated to make the curve linear. Once the range was reduced, a new sensitivity value was calculated for the material parameter. The following table summarizes the expected temperature errors resulting from the sensitivity analysis of the material parameters (the sensitivity units are provided as a reference).

Table 6.2 Material parameter sensitivity results
expressed as apparent temperature errors

Material Name	Heat Capacity $\frac{^{\circ}\text{C}}{\sigma (L/\text{cm} \cdot ^{\circ}\text{C})}$	Thermal Conductivity $\frac{^{\circ}\text{C}}{\sigma (L \cdot \text{cm}/\text{hr} \cdot ^{\circ}\text{C})}$	Thickness $\frac{^{\circ}\text{C}}{\sigma (\text{cm})}$	Visible Emissivity $\frac{^{\circ}\text{C}}{\sigma (\text{unitless})}$	Thermal Emissivity $\frac{^{\circ}\text{C}}{\sigma (\text{unitless})}$	Exposed Area $\frac{^{\circ}\text{C}}{\sigma (\text{unitless})}$		SGP $\frac{^{\circ}\text{C}}{\sigma (L/\text{hr})}$
						+	-	
BCM								
aluminum	-0.0031	0.0000	-0.0131	0.0000	-0.0182	-0.132	0.184	3.845
asphalt shingle	-0.0334	0.0013	-0.1240	0.0000	-0.0109	-0.593	0.765	3.805
roof gravel	0.0618	0.1357	0.0724	0.0016	-0.0446	-2.461	1.441	3.564
steel	-0.0117	0.0000	-0.0810	0.0000	-0.1213	-0.645	0.903	3.448
brick	0.0277	0.0447	-0.0500	0.0000	-0.0152	-0.350	0.378	3.855
wall concrete	0.0405	0.0079	0.0628	0.0002	-0.0377	-0.285	0.331	4.366
wall wood	0.0026	0.0036	-0.0170	0.0000	-0.0377	-0.326	0.341	3.281
window glass	-0.0101	0.0020	-0.0113	0.0000	-0.0191	-0.189	0.252	4.188
Soils/Water								
gray clay	0.0172	0.0276	-0.1012	0.0001	-0.0230	-1.625	1.738	3.433
red clay	0.0244	0.0308	-0.0817	0.0001	-0.0191	-1.528	1.636	3.401
brown dirt	0.0209	0.0821	-0.0801	0.0004	-0.0335	-1.445	1.579	3.541
lt brown gravel	0.1283	0.3795	-0.0993	0.0024	-0.0403	-1.387	1.543	3.797
water - river	0.0066	0.0283	-0.0124	0.0008	-0.0380	-1.565	1.721	3.442
SCM								
asphalt street	0.1008	0.1833	-0.0980	0.0002	-0.0373	-1.490	1.656	3.809
concrete	0.1108	0.0233	0.2131	0.0034	-0.0787	-1.288	1.518	4.122
Vegetation								
grass	0.1038	0.0512	0.4710	0.0008	-0.0575	-1.125	1.456	4.560
tree deciduous	0.0457	0.0228	0.2062	0.0000	-0.0063	-0.699	0.918	4.683
tree trunk	-0.0026	0.0047	-0.0457	0.0000	-0.0066	-0.293	0.336	3.654
AVERAGE	0.0350	0.0572	0.0117	0.0006	-0.0358	-0.968	1.039	3.822

The results of the material parameter sensitivity analysis contained some peculiarities that warranted further analysis. One of the most noticeable irregularities was the minimal effect of visible emissivity on many of the materials. While the temperatures of materials are traditionally very responsive to changes in the visible emissivity, the 0200 imaging time negated the effects of the materials' visible characteristics. The materials had already released all their stored energy that was generated during the day when the sun and visible emissivity influence the temperature. This phenomena was supported by the insensitivity of most materials to changes in the direct & diffuse insolation. The materials had reached a state of equilibrium with respect to solar influences. As a result, it was difficult to optimize the visible emissivity of the materials. This caused a serious problem

when the optimized material parameters were used for validation with the daytime Inframetrics imagery. The optimized material parameters were not robust enough because of the inability to optimize the visible characteristics of the materials.

The extreme sensitivity of all materials to self generated power and exposed area was not unexpected. It is difficult to estimate the effects of the internal side of a facet. When THERM calculates a material temperature, it assumes the material is only affected by the surrounding environment; it knows nothing about what is on the other side of the material. Self generated power and exposed area can be used to balance the influence between the external and internal environments of a facet. All materials were fairly equally sensitive to changes in the self generated power. The main differences in the sensitivities resulted from different material thermal emissivities and orientations. Since adding power is virtually independent of the other input parameters, this parameter could be used on an individual facet to change its temperature while not changing the temperature of the same material at a different location in the scene. This might be important for increasing the temperature of active materials, such as buildings, where internal heat sources raise the temperature of the external surface

However, no facets in the scene were initially given self generated power; therefore, exposed area had the highest sensitivity/apparent temperature error in the scene. As a result, it should be the first material parameter to be optimized to reduce large errors in the apparent temperatures of materials. It was also evident that the apparent temperature error of exposed area was strongly influenced by the actual shape factor of an object. Soils and vegetation with shape factors near 1.0 are almost 5 times more sensitive to changes in the exposed area than wall construction materials such as wood or brick that have shape factors near 0.5. Shape factor seemed to magnify the effects of the exposed area.

The apparent temperature error of exposed area was magnitudes greater than any other parameter. All other parameters were relatively insensitive to input errors when compared to exposed area. Ignoring the exposed area, the relatively high sensitivity of

most materials to changes in the thermal conductivity was surprising. Because the visible factors had virtually no effect on the apparent temperature of the materials, it seemed that the materials might have reached a state of equilibrium with the surrounding environment. The high sensitivity of the thermal conductivity contradicted this. Apparently, the materials had not reached a state of equilibrium with respect to the background, only the solar inputs. In examining the meteorological conditions, the surface temperature and atmosphere are in a constant state of fluctuation. As the temperature of the background continually changes, the time to reach equilibrium is based on the thermal conductivity. For example, the metallic materials, steel and aluminum, had no change in temperature as $\Delta parameter_{thermal\ conductivity}$ was varied. The high thermal conductivity of these materials causes them to lose their heat more quickly and, hence, reach equilibrium with a fluctuating environment faster than other materials. Most other materials have some lag time in responding to the environment. Therefore, the thermal conductivity has a relatively large influence on their apparent temperature. If the imaging time had been closer to sunset, around 1700 hours when the environment is changing more rapidly, the thermal conductivity may have had a more pronounced influence on the temperatures of the materials, and the sensitivity values would have been even larger. Overall, these effects were minor; the sensitivity of thermal conductivity was only high in relation to the other material parameters, excluding exposed area and self generated power.

Thermal emissivity also had a relatively high temperature error/sensitivity when exposed area and self generated power were ignored. This is explained by the fact that the radiance reaching the sensor is in the thermal region of the electromagnetic spectrum. The thermal emissivity of the material regulates how much energy from the material actually reaches the sensor. In addition, the thermal emission dominates the radiation exchange at night. A material that has a temperature of 10°C and thermal emissivity of 0.9 might appear the same as a different material at 11°C with a thermal emissivity of 0.85. Similar to all the other material input parameters, the thermal emissivity sensitivity decreases as the shape factor decreases.

concrete wall (0.5): -0.0377

concrete sidewalk (1.0): -0.0787

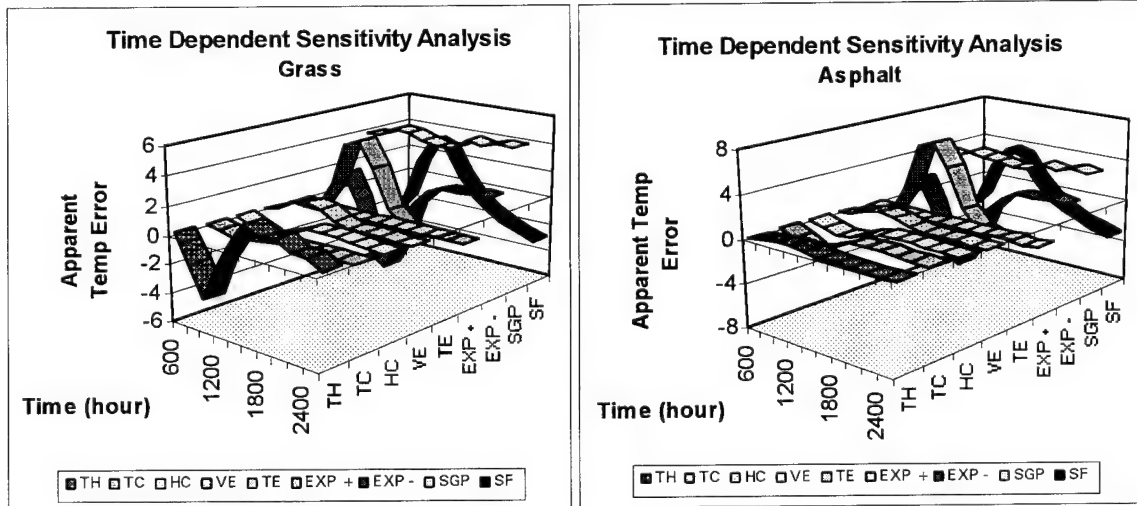
Thus, thermal emissivity is one of the input parameters that must be optimized to reduce the error in the synthetic image.

The final input parameters, thickness and heat capacity, act as one parameter within THERM. The integration of these two parameters resulted in some confusing sensitivity values. Both positive and negative sensitivities/errors were found within the heat capacity and thickness parameter categories. Unlike the other parameters where shape factor can be used to describe anomalies, no clear factor presented itself. Initial thoughts lead one to believe that a very small thermal inertia or very large thermal inertia in the presence of a very cold sky caused the unique results. Thickness affects the thermal inertia and thermal exchange between the material and the surrounding environment. As discussed earlier, the environment is in a constant state of fluctuation and minor changes in the air temperature have large effects on the temperatures of materials. The thermal inertia can result in prolonged response times to the environment and might cause these results. Regardless of the cause, care should be taken when optimizing these input parameters because of their unpredictable sensitivities.

6.1.3 Time History Material Parameter Sensitivity Analysis

As discussed earlier, the temperature of a material is dependent upon the input parameters, including time. Therefore, a time history sensitivity analysis was also conducted to see how the sensitivity values for the material parameters change over time. Understanding how the sensitivity values change over time provides information on the responsivity of a material to the solar region of the electromagnetic spectrum, 0.4 to 2.0 μm . This information is useful when optimizing the material parameters and provides insight on how the material will respond under different viewing conditions and parameters.

The time history sensitivity analysis was conducted on two of the most prominent and well defined materials in the scene, *asphalt* and *grass*. These two materials should provide the general characteristic responsivity of any material over time, from 0600 in the morning until the 0200 imaging time on the next day, where sunrise was @ 0655 and sunset was @ 1655. The resulting sensitivity values, converted to apparent temperature errors at the sensor, can be seen in the following graphs.



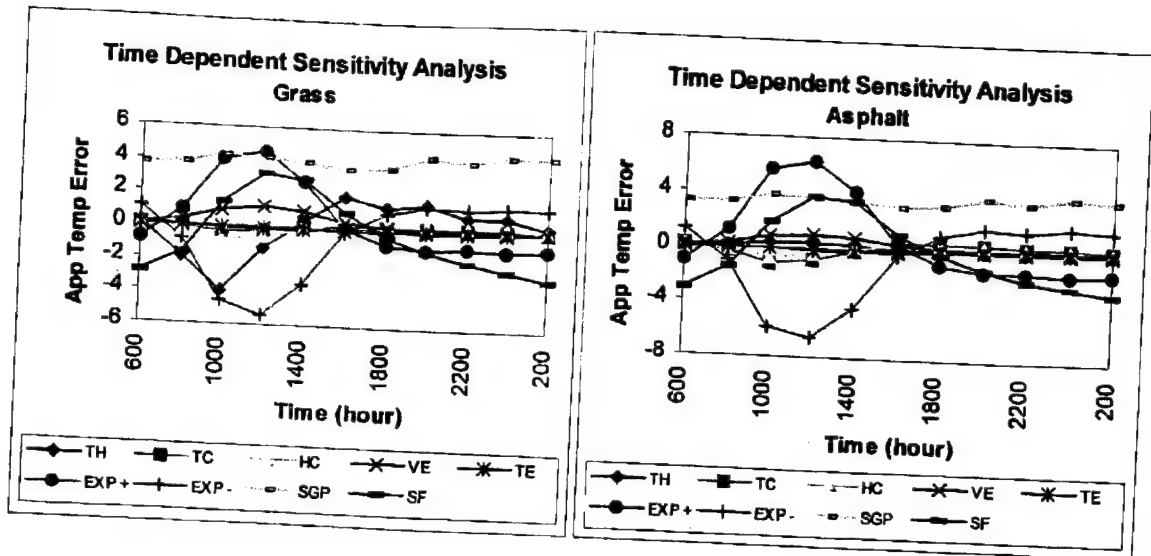
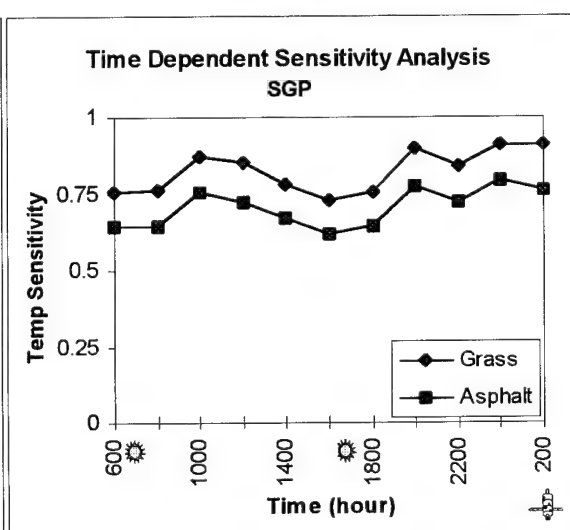
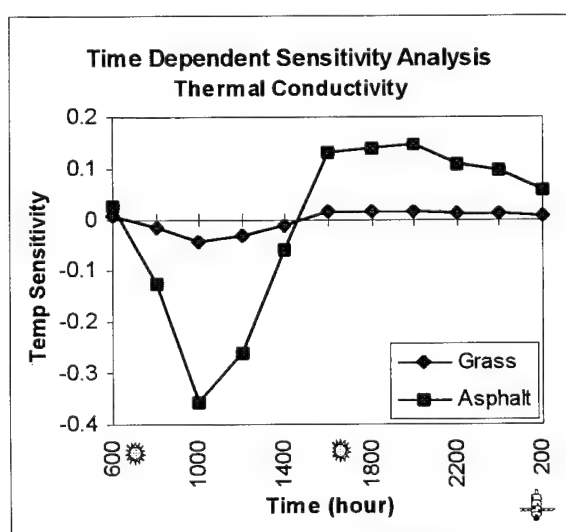
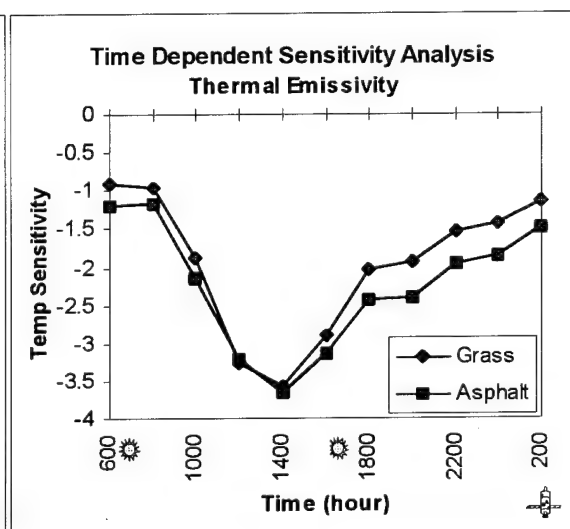
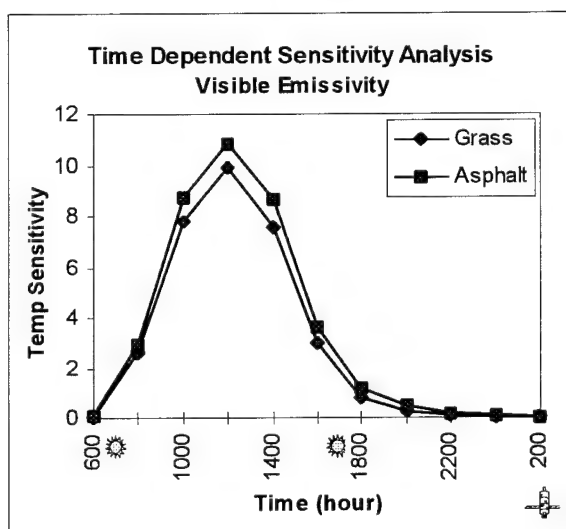
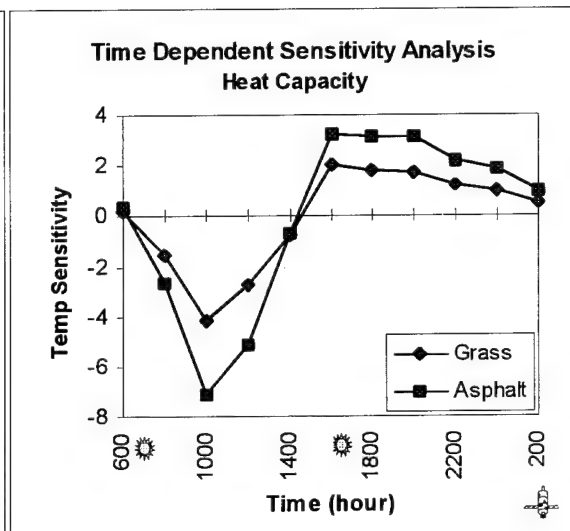
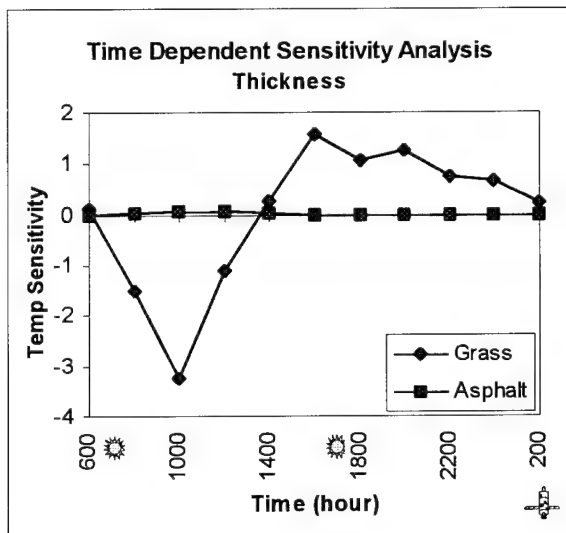


Figure 6.7 Time history expected temperature error analysis graphs
Parameter comparison

From these graphs, it is evident that the exposed area parameter has the highest expected temperature error changes as the solar influence varies from sunrise to sunset. The expected temperature error of visible emissivity and shape factor also increase dramatically after the sun rises. This is expected as the temperature of a material is highly influenced by its visible characteristics. A black car gets much hotter on a sunny day than a white car. Similarly, if the car is in the shade and the effective shape factor of the object is reduced, it will not be as responsive to solar effects.

In the graphs below, a comparison is made between the various grass and asphalt material parameters. Unlike the previous graphs, the actual sensitivity values, $\Delta T_{\text{apparent}} / \Delta \text{parameter}$, are plotted, not the expected or apparent temperature errors. This was done to determine the relative differences in the time history sensitivity values for differing materials. In general, the shape of both curves is the same, as might be expected, only the magnitudes are different. The failure of the asphalt thickness to closely mimic the grass might be caused by the large thickness of asphalt and its high thermal inertia when compared to the small thickness of grass and its low thermal inertia.



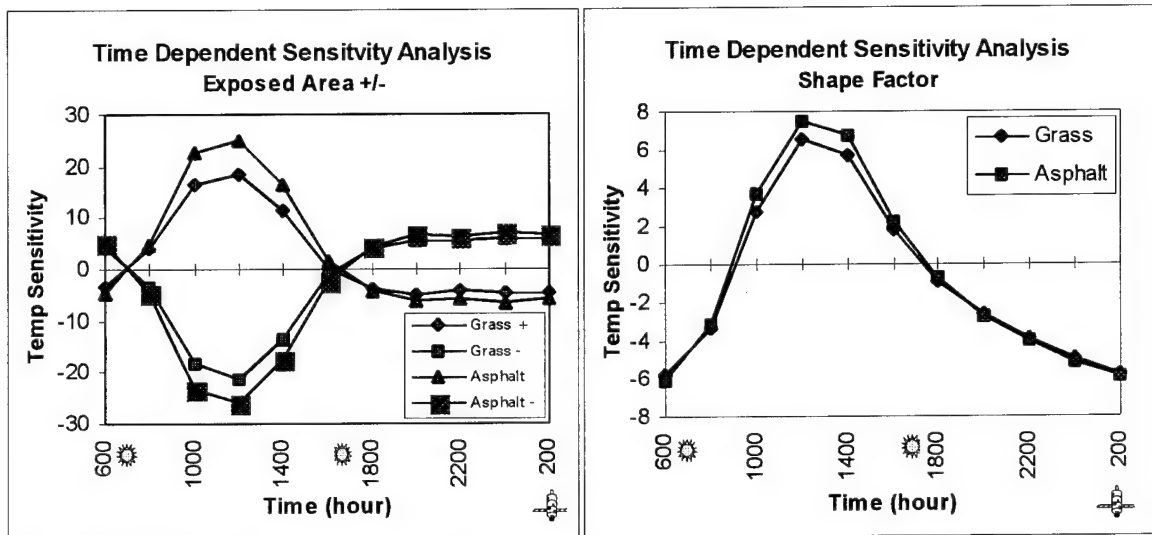


Figure 6.8 Time history sensitivity analysis - *Material comparison*

From these graphs, it is evident that the sensitivity of the materials increases dramatically in the presence of solar loading. The materials are much less sensitive to input error and are much less responsive in the absence of solar loading. The only material parameter for which this does not seem to hold true is self generated power, SGP. This is understandable since the active heating of a facet does not depend much on the sun; the heating of the facet by the SGP term is the driving force behind the temperature of the facet.

The time history sensitivity analysis was useful in showing the characteristic behavior of a material over time. It showed the large effects of solar loading during the day and how these effects diminish over time. It also supported the earlier conclusion that the materials have reached an equilibrium with respect to the solar loading. Thus, the temperatures of the objects at imaging time are dominated by the material properties and the background, both sky and other objects.

6.2 Input Parameter Optimization

With the results of the sensitivity analysis, the material parameters could be

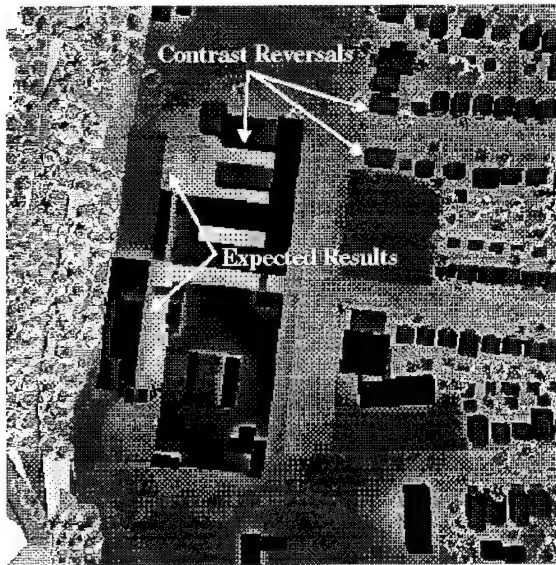
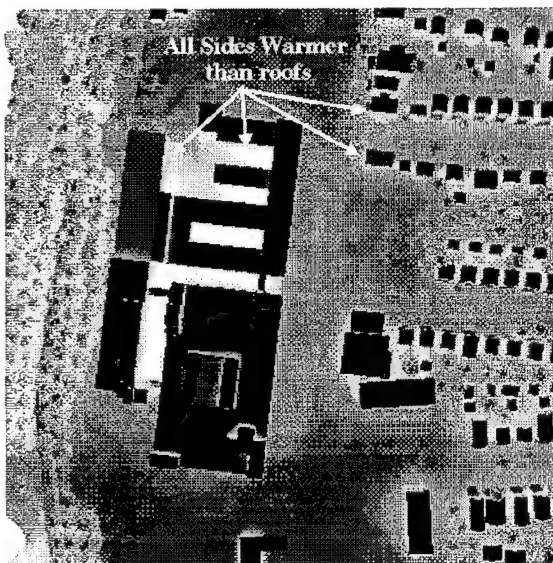


Figure 6.9 DIRSIG radiance image

optimized. A visual assessment was first made of the DIRSIG imagery. This revealed a problem in the radiance image. The sides of the buildings in the truth imagery had higher apparent temperatures than the roofs of the buildings, but the opposite was true in the synthetic imagery. These contrast reversals were evident for some of the structures in the scene, but not all. So, it was then necessary to determine the cause of this contrast reversal in the synthetic image.

The DIRSIG debug images provided the tools to detect the problem. The temperature debug image revealed that the sides of the houses were in fact warmer than the roofs. The shape factor debug image also confirmed that the structures were modeled

Temperature Image



Shape Factor Image

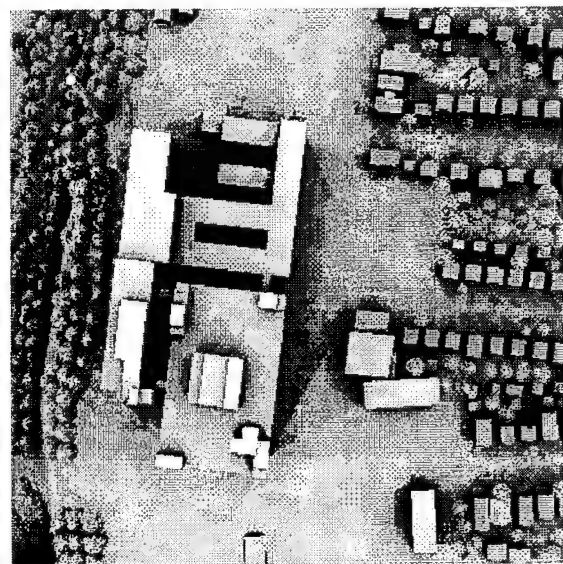


Figure 6.10 DIRSIG debug images

correctly. The problem was with the radiance values and not the actual temperatures of the objects. Because the radiance values were near the expected values for so many objects in the scene, the key was to detect the radiance term that was vastly different. This inspection revealed low emissivity values for the sides of some structures. The grazing angles of the sensor resulted in a large reduction of the spectral emissivity value by the angular emissivity factor. Evidently, the angular emissivity factors that were obtained from the 1992 validation by Rankin were too small and needed to be modified. Fortunately, Snyder's evaluation of houses as part of the NYSERDA project involved estimating angular emissivities using the following equation.

$$\varepsilon_{\theta} = \varepsilon_{\perp} \cdot [0.9 \cos(\theta)]^{0.07} [1.0 / (0.9^{0.07})] \quad (6.5)$$

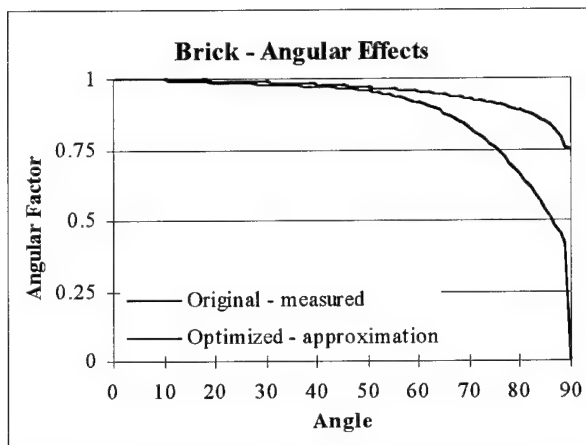


Figure 6.11 Angular emissivity curve

This equation was then used to modify materials with angular emissivities less than 0.75. The scene was then reprocessed and everything was visually acceptable. With acceptable visual results, it was possible to proceed with the task of optimizing the input parameters.

Before any actual modifications could be made to the input parameters, it was necessary to do a mathematical comparison of the truth and synthetic imagery. This was accomplished by calculating the histogram of both images. The mean values and standard deviations of the histograms could be compared to determine the difference between the images. This comparison shows potential global errors in the radiance values of the synthetic image, i.e. an erroneous gain affecting the standard deviation and bias affecting the mean value. The following conceptual diagram shows the histogram of the truth imagery and the synthetic imagery

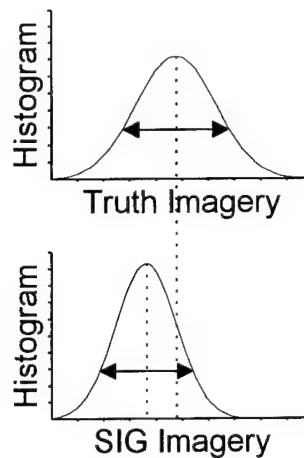


Figure 6.12 Histogram comparison

These graphs show both a mean level radiance error and a standard deviation error of the synthetic image. In analyzing the synthetic image, the only variables that affect all the radiance values reaching the sensor are the atmosphere, weather, and the sensor gain and bias. An individual error in a particular material parameter would not likely cause a dramatic shift in the overall mean and standard deviation of the synthetic radiance values, unless there was an extremely large percentage of one material in the scene. Therefore, the efforts to reduce the global error in the synthetic image would begin by examining the atmospheric and weather parameters and then proceed to optimizing the material parameters in the scene.

Like the sensitivity analysis, the process of optimizing the input parameters was accomplished using an off-line version of THERM followed by a MathCad program. The flow diagram on the following page illustrates the procedure used to optimize the input parameters. A batch file was once again used to determine the output temperature for each material that was assigned to a facet in the scene. The output temperature is converted into a radiance at the sensor using the 'big equation'. The radiance at the sensor is multiplied by a weight factor which corresponds to the percentage of the material in the scene. The mean level radiance and standard deviation can then be calculated from the following equations.

$$\bar{L} = \sum_i w_i \cdot L_i$$

$$\sigma = \sqrt{\sum_i w_i \cdot (L_i - \bar{L})^2}$$

i - for all materials in the scene (6.6)

The DIRSIG primary material debug image shows the material for each pixel in the scene. A histogram of the debug image provides the appropriate weighting factors for each material. This allows the average scene radiance and standard deviation to be estimated as the input parameters are changed without having to rerun DIRSIG. This process greatly reduced the time required to determine the overall scene effects when changing the input parameters. Without it, it would take several days using DIRSIG to determine the effects of a single input change on the output image. With all the analysis tools in hand, the actual meteorological and material parameters could finally be optimized to reduce the error in the synthetic image.

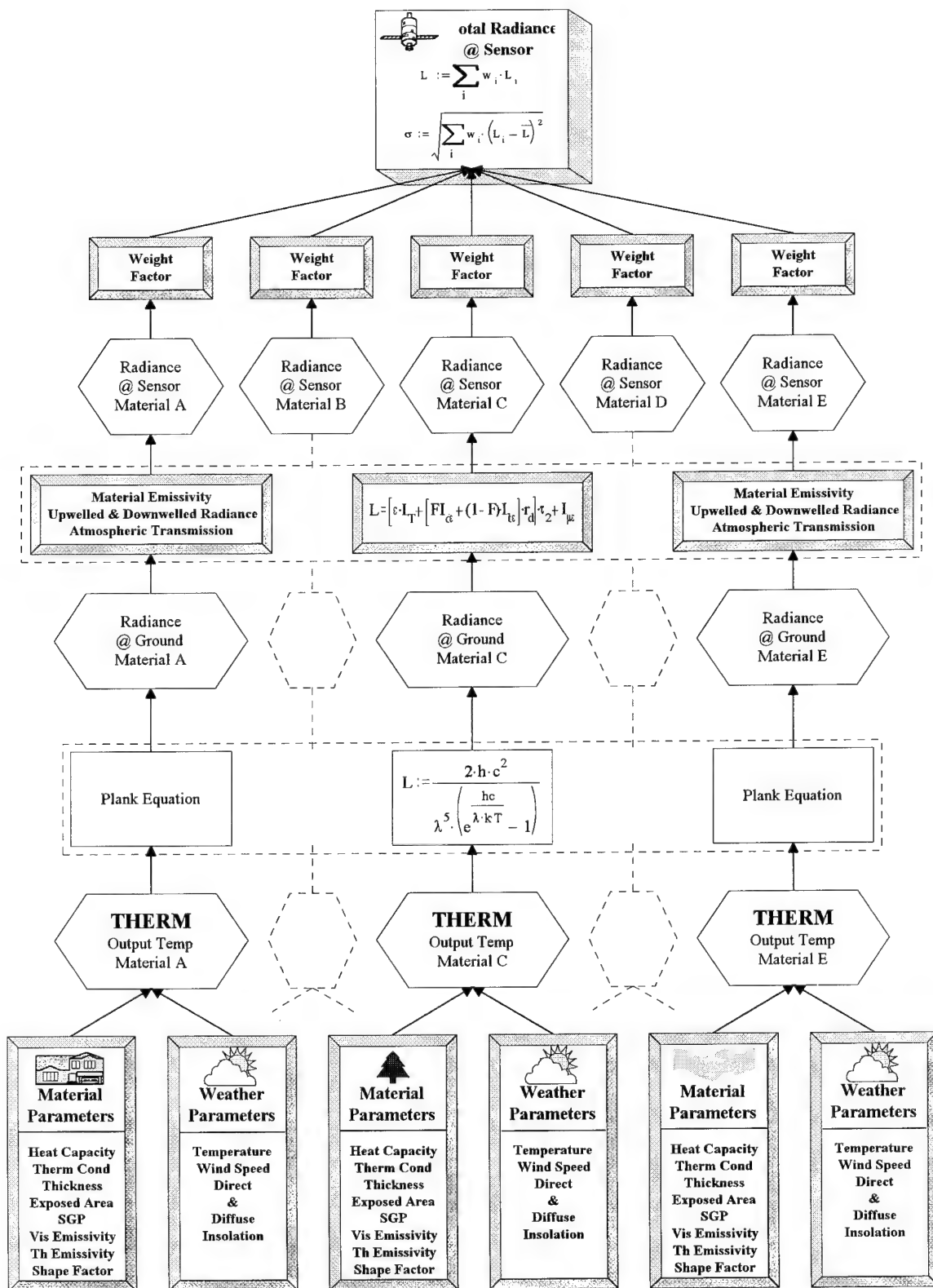


Figure 6.13 Scene analysis

When optimizing the input parameters, the expected temperature errors at the sensor provide the means to reduce the error in the synthetic image. While it might be possible to remove all the error by changing a single parameter, a better approach involves modifying multiple parameters by a small amount to achieve the desired change. For example, all error might be reduced by a 1σ change in the thermal conductivity. A 0.2σ change in thermal conductivity, 0.3σ change in the thermal emissivity, and a 0.3σ change in the heat capacity provide the same reduction in error. It is more likely that multiple parameters have a small error versus one parameter having a large error. This also applies to the meteorological parameters, not just the material parameters.

6.2.1 Meteorological Parameter Optimization

When the synthetic image was analyzed, the apparent temperatures at the sensor were about six degrees too low. The only parameters that affect the entire scene are the meteorological parameters and the sensor gain and bias. With a large bias error in the synthetic image, the sensitivity analysis showed that it would most likely be caused by an error in one of the weather parameters. This is where actual measured data provided a clue into the actual error. The temperature of the asphalt shingle roofs was known from ground collection data that was acquired at the time of the imagery. This placed the actual temperature of asphalt shingles around -7.25°C , but THERM showed the temperature to be -11.27°C . A scene wide bias of $3\text{-}4^{\circ}\text{C}$ in the temperatures at the ground could only be caused by the weather file, specifically the air temperature. While the wind speed was also considered, the wind was less than 5 mph throughout the day and calm at the imaging time. Based on the temperature error at the ground, the air temperature was increased by 2σ , 4°C , to reduce the error.

It was initially thought that this large bias in the synthetic image was caused by an inadequacy of THERM. THERM uses the surface air temperature to predict an upper air temperature. It is this upper air temperature that the objects are in radiational exchange with, not the surface air temperature. This required changing the surface air temperature to increase the upper air temperature profile generated by THERM. While this may have

been the source of error, the air temperature near the Kodak Hawkeye plant may have actually been several degrees warmer than the at the airport where the surface air temperature was recorded. The airport is to the south of the city in a suburban area whereas the Hawkeye plant is in the middle of the city. It is possible that the city air temperature was several degrees warmer than the airport and this is what caused the error.

The atmospheric transmission & upwelled radiance could be modified to improve the radiance values. However, little additional information was known on the atmosphere that could be used to alter the radiance values. This led to a trail and error approach of modifying the Modtran card deck. Several atmospheres were created by modifying the atmospheric profile of the constituents, but modifying these parameters had little influence on the radiance reaching the sensor. The only way to obtain a noticeable change in the radiance values was to actually modify the output radiance file from Modtran that is used in DIRSIG. This was not acceptable. The validation needed to be accomplished using the output from the DIRSIG submodels.

The following table summarizes the results of the optimization of the meteorological parameters.

<i>Meteorological Parameter</i>	<i>Optimized</i>
Temperature	2σ
Wind Speed	--
Direct & Diffuse Insolation	--
Atmospheric Transmission	--
Downwelled Radiance	--
Upwelled Radiance	--

6.2.2 Material Parameter Optimization

With the global errors in the synthetic image removed, it was time to remove the individual errors in the materials. The optimization of the material parameters would further reduce the error in the synthetic image. Reviewing the results of the sensitivity analysis, the exposed area and the thermal conductivity had the highest average expected temperature errors, followed by thermal emissivity, heat capacity, and thickness. The

most sensitive parameters would be changed first, followed by the remaining material parameters.

It was first necessary to know the difference between the synthetic image created with the optimum weather file and the truth imagery. This difference showed how much change was actually needed in the apparent temperature for each material. The expected temperature errors from the sensitivity study revealed the amount of temperature change that was possible by varying the material parameters. The goal was to alter the parameters and combine their respective temperatures errors in a way that reduced the overall apparent temperature error. This required using the generic values and standard deviations to provide reference points for optimizing each material parameter value. For example, the changing of a material parameter value by half a standard deviation would reduce the apparent temperature error by $\frac{1}{2}$ of that parameter's expected temperature error.

$$\text{Apparent Temp Error} - 0.5(\Delta T_{exp})_{exposed\ area} = \text{Partial Reduction App Temp Error}$$

The standard deviation and the generic value were then used to determine the optimized material parameters value that should be used in the actual DIRSIG scene.

The results of the optimization are shown in the charts below. The apparent temperature error between the generic material DIRSIG imagery and the truth imagery is listed first. This represented the error that needed to be eliminated through the optimization of the material parameters. The expected temperature change resulting from the optimized material parameters is shown next. Within the tables, the sensitivity of each material parameter, expressed as an apparent temperature error, is provided first. This is followed by the generic material parameter value, and the standard deviation of the input parameter. Finally, the optimization values are listed. This includes the standard deviation required to reduce the error between the truth and the synthetic imagery, and the final optimized material parameter value that was used to create the validation imagery.

Building Construction Materials

Aluminum - ID #50

Error - 0.23

$\Delta T_{\text{optimum}} - 0.085$

Input	ΔT_{exp}	GEN	σ	$\Delta \sigma_{\text{opt}}$	OPT
HC	-0.0031	0.55	0.1	-1.000	0.45
TC	0.0	1909	155.0	1.000	2064
TH	-0.0131	0.275	0.225	-0.667	0.125
VE	0.0	0.50	0.20	0.000	0.50
TE	-0.0182	0.72	0.08	0.000	0.72
EXP	0.184	-0.40	0.25	0.400	-0.30
SGP	3.845	0.00	5.00	0.000	0.00

Asphalt Shingle - ID #60-69

Error - 0.25

$\Delta T_{\text{optimum}} - 0.162$

Input	ΔT_{exp}	GEN	σ	$\Delta \sigma_{\text{opt}}$	OPT
HC	-0.0334	0.3575	0.098	0.194	0.3765
TC	0.0013	6.145	0.215	0.465	6.245
TH	-0.1240	0.85	0.65	-0.615	0.45
VE	0.0	0.84	0.11	0.000	0.84
TE	-0.0109	0.91	0.015	0.000	0.91
EXP	0.765	-0.40	0.25	0.120	-0.37
SGP	3.805	0.00	5.00	0.000	0.00

Roof Gravel - ID #12

Error - 0.48

$\Delta T_{\text{optimum}} - 0.534$

Input	ΔT_{exp}	GEN	σ	$\Delta \sigma_{\text{opt}}$	OPT
HC	0.0618	0.35	0.05	0.600	0.38
TC	0.1357	12.1	5.10	0.784	16.10
TH	0.0724	6.0	4.00	0.625	8.50
VE	0.0016	0.8	0.10	0.000	0.80
TE	-0.0446	0.9	0.02	0.000	0.90
EXP	1.4410	-0.5	0.25	0.240	-0.44
SGP	3.564	0.0	5.00	0.000	0.00

Steel - ID #52

Error - 0.62

$\Delta T_{\text{optimum}} - 0.257$

Input	ΔT_{exp}	GEN	OPT	σ	$\Delta \sigma_{\text{opt}}$
HC	-0.0117	0.825	0.805	0.045	-0.444
TC	0.0	511.5	551.5	47.50	0.842
TH	-0.0810	0.40	0.20	0.225	-0.889
VE	0.0	0.825	0.825	0.085	0.000
TE	-0.1213	0.79	0.79	0.120	0.000
EXP	0.903	-0.40	-0.35	0.250	0.200
SGP	3.448	0.00	0.00	5.00	0.000

Brick - ID #70-79

Error - 0.80

$\Delta T_{\text{optimum}} - 0.206$

Input	ΔT_{exp}	GEN	σ	$\Delta \sigma_{\text{opt}}$	OPT
HC	0.0277	0.2818	0.121	0.083	0.2918
TC	0.0447	5.935	2.235	0.470	6.985
TH	-0.05	10.00	10.000	-0.300	7.00
VE	0.00	0.795	0.165	0.030	0.80
TE	-0.0152	0.930	0.030	-0.100	0.927
EXP	0.378	-0.40	0.250	0.440	-0.29
SGP	3.855	0.000	5.000	0.000	0.00

Wall Concrete - ID #53

Error - 0.87

$\Delta T_{\text{optimum}} - 0.460$

Input	ΔT_{exp}	GEN	σ	$\Delta \sigma_{\text{opt}}$	OPT
HC	0.0405	0.3105	0.055	0.073	0.3145
TC	0.0079	15.48	1.10	0.182	15.68
TH	0.0628	6.00	4.00	0.750	9.00
VE	0.0002	0.725	0.125	0.000	0.725
TE	-0.0377	0.925	0.065	-0.308	0.905
EXP	0.331	-0.50	0.25	1.200	-0.20
SGP	4.336	0.00	5.00	0.000	0.00

Wall Wood - ID #80-89

Error - 0.73

$\Delta T_{\text{optimum}} - 0.119$

Input	ΔT_{exp}	GEN	σ	$\Delta \sigma_{\text{opt}}$	OPT
HC	0.0026	0.5124	0.245	-0.082	0.5324
TC	0.0036	0.98	0.120	0.083	0.99
TH	-0.0170	4.50	2.50	-0.400	3.50
VE	0.0	0.80	0.195	0.000	0.80
TE	-0.0377	0.865	0.085	-0.625	0.829
EXP	0.341	-0.40	0.25	0.400	-0.26
SGP	3.281	0.00	5.00	0.000	0.00

Window Glass - ID #54

Error - 1.03

$\Delta T_{\text{optimum}} - 0.119$

Input	ΔT_{exp}	GEN	σ	$\Delta \sigma_{\text{opt}}$	OPT
HC	-0.0101	0.3505	0.170	-0.059	0.3405
TC	0.0020	12.00	4.00	0.750	15.00
TH	-0.0113	0.525	0.225	-0.444	0.425
VE	0.0	0.70	0.120	0.000	0.70
TE	-0.0191	0.87	0.080	-0.625	0.82
EXP	0.252	-0.40	0.25	0.400	-0.30
SGP	4.188	0.00	5.00	0.000	0.00

Soils

Gray clay - ID #40

Error - 1.37

$\Delta T_{\text{optimum}} - 0.425$

Input	ΔT_{exp}	GEN	σ	$\Delta\sigma_{\text{opt}}$	OPT
HC	0.0172	0.3202	0.12	0.417	0.3802
TC	0.0276	4.162	0.720	0.972	4.762
TH	-0.1012	9.85	6.85	-0.715	4.85
VE	0.0001	0.795	0.095	0.000	0.795
TE	-0.0230	0.965	0.015	0.000	0.955
EXP	1.738	-0.30	0.25	0.200	-0.20
SGP	3.433	0.00	5.00	0.000	0.00

Red clay - ID #41

Error - 1.84

$\Delta T_{\text{optimum}} - 0.816$

Input	ΔT_{exp}	GEN	σ	$\Delta\sigma_{\text{opt}}$	OPT
HC	0.0244	0.3202	0.12	0.500	0.3702
TC	0.0308	4.162	0.720	0.833	4.862
TH	-0.0817	9.85	6.85	-0.730	4.95
VE	0.0001	0.825	0.075	0.000	0.825
TE	-0.0191	0.95	0.015	-0.667	0.95
EXP	1.636	-0.25	0.25	0.400	-0.20
SGP	3.401	0.00	5.00	0.000	0.00

Brown dirt - ID #13

Error - 2.03

$\Delta T_{\text{optimum}} - 0.777$

Input	ΔT_{exp}	GEN	σ	$\Delta\sigma_{\text{opt}}$	OPT
HC	0.0209	0.3222	0.042	0.909	0.3422
TC	0.0821	6.117	1.659	0.776	7.417
TH	-0.0801	9.85	6.85	-0.584	4.85
VE	0.0004	0.825	0.095	0.000	0.825
TE	-0.0335	0.925	0.025	0.000	0.925
EXP	1.579	-0.25	0.25	0.200	-0.22
SGP	3.541	0.00	5.00	0.000	0.00

Lt brown gravel - ID #43

Error - 1.42

$\Delta T_{\text{optimum}} - 0.322$

Input	ΔT_{exp}	GEN	σ	$\Delta\sigma_{\text{opt}}$	OPT
HC	0.1283	0.41	0.110	0.476	0.51
TC	0.3795	10.76	6.44	0.784	15.76
TH	-0.0993	9.85	6.85	-0.730	5.85
VE	0.0024	0.85	0.05	0.000	0.85
TE	-0.0403	0.915	0.025	0.000	0.915
EXP	1.543	-0.25	0.25	0.120	-0.20
SGP	3.797	0.00	5.00	0.000	0.00

Surface Construction Materials

Asphalt Street - ID #5

Error - -0.27

$\Delta T_{\text{optimum}} - -0.02$

Input	ΔT_{exp}	GEN	σ	$\Delta\sigma_{\text{opt}}$	OPT
HC	0.1008	0.3625	0.103	-0.182	0.4325
TC	0.1833	9.243	3.313	0.000	11.243
TH	-0.0980	9.55	7.15	-0.331	7.55
VE	0.0002	0.86	0.09	0.800	0.87
TE	-0.0373	0.955	0.025	0.000	0.945
EXP	1.656	-0.25	0.50	0.040	-0.22
SGP	3.809	0.00	5.00	0.000	0.00

Concrete - ID #6

Error - 0.53

$\Delta T_{\text{optimum}} - 0.320$

Input	ΔT_{exp}	GEN	σ	$\Delta\sigma_{\text{opt}}$	OPT
HC	0.1108	0.3105	0.055	-0.182	0.3005
TC	0.0233	15.50	1.10	0.000	15.50
TH	0.2131	6.565	5.435	-0.331	4.765
VE	0.0034	0.725	0.125	0.800	0.825
TE	-0.0787	0.935	0.055	0.000	0.935
EXP	1.518	-0.25	0.50	0.040	-0.23
SGP	4.122	0.00	5.00	0.000	0.00

Vegetation

Grass - ID #4

Error - -1.17

$\Delta T_{\text{optimum}} - -0.721$

Input	ΔT_{exp}	GEN	σ	$\Delta\sigma_{\text{opt}}$	OPT
HC	0.1038	1.00	0.20	-1.000	0.8
TC	0.0512	12.5	7.50	-0.933	5.5
TH	0.4710	1.275	1.225	-1.000	0.05
VE	0.0008	0.79	0.12	0.000	0.79
TE	-0.0575	0.93	0.05	0.200	0.94
EXP	1.456	-0.25	0.50	-0.060	-0.28
SGP	4.560	0.00	5.00	0.000	0.00

Tree-deciduous - ID #25

Error - -0.21

$\Delta T_{\text{optimum}} - 0.114$

Input	ΔT_{exp}	GEN	σ	$\Delta\sigma_{\text{opt}}$	OPT
HC	0.0457	1.0	0.2	0.000	1.00
TC	0.0228	12.5	7.5	0.000	12.5
TH	0.2062	1.00	0.9	0.556	1.50
VE	0.00	0.935	0.055	0.000	0.935
TE	-0.0063	0.95	0.01	0.000	0.95
EXP	0.918	-0.25	0.5	0.000	-0.25
SGP	4.683	0.00	5.0	0.000	0.00

The following chart summarizes the optimization results. It reveals the amount of change in the input parameter that was required to reduce the apparent temperature error. The optimization of each material parameter improved the radiometric accuracy of DIRSIG.

Table 6.3 Optimized material parameter changes
- expressed as standard deviations

<i>Material Name</i>	<i>Heat Capacity (W/m²)</i>	<i>Thermal Conductivity (L·cm/hr·°C)</i>	<i>Thickness (cm)</i>	<i>Visible Emissivity (unitless)</i>	<i>Thermal Emissivity (unitless)</i>	<i>Exposed Area (unitless)</i>
BCM						
aluminum	-1.00	1.00	-0.67	0.00	0.00	0.40
asphalt	0.19	0.47	-0.62	0.00	0.00	0.12
roof gravel	0.60	0.78	0.63	0.00	0.00	0.24
roof steel	-0.44	0.84	-0.89	0.00	0.00	0.20
brick	0.083	0.470	-0.30	0.17	-0.10	0.44
wall concrete	0.07	0.18	0.75	0.00	-0.31	1.2
wall wood	-0.082	0.083	-0.40	0.00	-0.63	0.40
window glass	-0.059	0.75	-0.44	0.00	-0.63	0.40
Soils						
gray clay	0.42	0.97	-0.72	0.00	0.00	0.20
red clay	0.50	0.83	-0.73	0.00	-0.67	0.40
brown dirt	0.90	0.77	-0.58	0.00	0.00	0.20
lt brown gravel	0.47	0.78	-0.72	0.00	0.00	0.12
SCM						
asphalt street	-0.18	0.00	-0.33	0.80	0.00	0.04
concrete	0.67	0.60	-0.28	0.11	-0.40	0.06
Vegetation						
Grass	0	-0.93	-1.00	0.00	0.20	-0.06
Tree deciduous	0.00	0.00	0.56	0.00	0.00	0.00

These changes in the input parameters helped to reduce the error in the synthetic image. They could have been better with more time and more DIRSIG synthetic imagery, but time prevented further optimization of the input parameters. The visible emissivity was often left its generic values because of its low expected temperature error. Without additional information to modify the visible emissivity, the initial estimated value from the databases seemed to be the best value. Following the rule that the first estimate is sometimes the best, very little effort was spent in optimizing the trees. It was known that this material was not correct as all the trees in the scene were coniferous. Similarly, a sensitivity analysis was conducted of water, but in the end, the temperature of the of water was set to 4.0°C. THERM simply cannot determine the temperature of a material whose temperature is based on seasonal factors.

The optimization of the materials still ended up being ad hoc. The sensitivity analysis helped to reduce some of the guesswork as it provided insight into the direction a material parameter should be changed, but there was usually a difference between the expected change and the actual change. Most of this discrepancy can be attributed to the approximations in the running of the off-line version of THERM. The errors and constant state of change of DIRSIG also made it difficult to determine the error source. DIRSIG was under a constant state of change during the validation. As a result, it was difficult to obtain a solid baseline from which to optimize the parameters.

It was originally planned to use both the primary and secondary sets of imagery in an interactive manner to minimize the error in common materials and points. This method could not be used due to a combination of factors. The primary materials in the Inframetrics imagery of Hawkeye were concrete siding, red brick, and glass windows. Because of the nadir viewpoint in the Bendix imagery, these materials could not be distinguished from each other, but windows could be seen in the houses. These windows were used to estimate the material parameters of the Hawkeye windows. However, a direct comparison was still not possible because the glass windows were not visible in any of the nadir synthetic imagery. These problems precluded the use of the combined imagery in optimizing the material parameters.

The optimization of the material parameters is an endless process, especially if every single material in the scene is modeled. One roof gravel was used in the scene where in reality, there were numerous roof gravel materials, asphalt shingles, wood sidings, and colored bricks. While it is still somewhat of a trial and error approach, the sensitivity analysis provided the tools to reduce some of the guesswork. The presented results were a balance between error and time.

6.5 Input Parameter Modification & Sensitivity Analysis Summary

The steps and methodology followed in optimizing the inputs to the Hawkeye scene can be applied to the development of any synthetic image. The procedure for modifying the input parameters is outlined by the following steps:

1. Determine limiting bounds of input parameters.
2. Do a sensitivity analysis of the input parameters.
3. Do a histogram comparison between the truth imagery and the synthetic imagery.

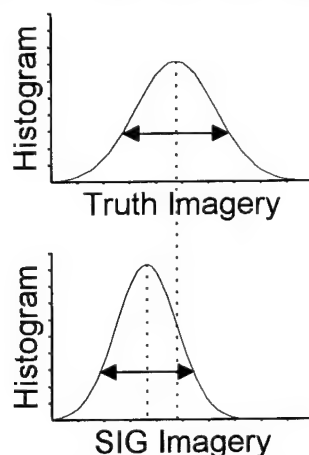


Figure 6.14 Histogram Comparison Summary

4. Optimize the input parameters that affect the overall scene.
5. Optimize the input parameters that affect individual objects.

**Table 6.4 Input Parameter Effect Summary
(Increase in the value of the input parameter)**

Sensitivity Parameter	Overall Scene Effect	Individual Material Effect
Air Temperature	+ mean temp	+ temp
Wind speed	- mean temp	- temp
Direct & Diffuse Insolation	+ mean temp	+ temp
Transmission	+ mean temp	+ temp
Upwelled Radiance	+ mean temp	+ temp
Downwelled Radiance	+ mean temp	+ temp
Heat Capacity	---	± temp
Thermal Conductivity	---	+ temp
Thickness	---	± temp
Visible Emissivity	---	+ temp
Thermal Emissivity	---	- temp
Exposed Area	---	± temp
Self Generated Power	---	+ temp

7.0 Recommendations & Conclusions

The primary goal of this validation was to advance the assessment of DIRSIG from established test targets in a relatively controlled environment to a scene where relatively little was known. This truly tested the robustness of DIRSIG to model the real world. In the end, DIRSIG was able to model the real world with a RMS error of 1.0782 degrees and a ROC coefficient of 0.9214 for the primary truth imagery. However, when the optimized material parameters from the primary truth imagery were used in the creation of the secondary truth imagery, the ROC coefficients decreased to 0.4395 for the imagery of Hawkeye and 0.400 for the imagery of the church. This decrease in accuracy of the synthetic imagery resulted from the optimization of the material parameters during the night. The effects of the visible characteristics on the self emission of a material are minimal at night so little effort was spent in optimizing the visible material parameters. In contrast, these visible characteristics dominate the self emission of an object during the day, leading to poor results in the daytime imagery. Despite the problem of using the optimized material parameters with the daytime imagery, the sensitivity analysis and optimization was successful in reducing the RMS error in the nighttime synthetic imagery from 6.87 to 1.08 RMS and increasing the ROC coefficient from 0.89 to 0.92.

7.1 DIRSIG

Throughout the validation, many obstacles were encountered that revealed the limitations of DIRSIG. These obstacles ranged from hardware memory problems to basic user mistakes. Because of these problems, DIRSIG proved to be a very labor intensive program, requiring constant assistance from the developers. In addition, the constant state of change and upgrades being made to DIRSIG meant that new problems were encountered regularly. As a result, much of the validation was spent in finding user input errors as well as DIRSIG logic errors. While this was not the primary goal of the thesis, it did help determine the robustness of DIRSIG. Despite all the problems, the true capabilities of DIRSIG could be exploited once the scene was created. This included changing the look angles, resolution, or any of the imaging parameters.

The errors and problems associated with DIRSIG could be reduced with improvements in the following areas:

THERM: A better thermal model is needed for DIRSIG. A thermal model should be able to determine the conduction between neighboring facets. While research was conducted on internal heat sources, they still have not been integrated into THERM. Therefore, self-generated power is still used as a fudge factor to account for the heating of facets. Also, it would be nice to have a thermal model that referenced the internal temperature of an object in determining the external temperature. THERM also fails in modeling the upper air temperature, wind effects, and surface objects. These problems lead to recommending an entirely new thermal model. It also had a problem modeling the upper air temperature. It also did not model wind effects.

Speed Improvements: Currently, it takes about 2 days to create a 512x512 image for a scene containing over 100,000 facets. While it would be nice to have results in only minutes or seconds, realistic generation times in the order of hours instead of days would be a great improvement.

Wavelength/Wavenumbers: DIRSIG currently operates in wavenumber units. It would be nice if DIRSIG could accept either wavelengths or wavenumbers as inputs.

Trees: The ability of DIRSIG to model trees is limited, but this is not a problem unique to DIRSIG. It is extremely difficult to model organic things are in constant states of change. Work is currently being conducted in this area in the visible and NIR regions, but analysis is still needed in the other regions of the electromagnetic spectrum. Trees are also extremely difficult to incorporate into a scene because of the large number of facets that are needed to create realistic looking trees. While it is often possible to create several trees, it becomes extremely difficult when trying to model many trees or a forest. This is where a balance between the number of facets and the realism must be made.

Graphical Interface: A graphical interface that prompts the user for inputs and also displays error messages would aid in the generation of synthetic images.

Directional Wind & Interference: A directional wind with the interference from neighboring buildings would also improve the results in the LWIR. Preliminary testing and analysis has been done in this area, but it still needs to be incorporated into the actual DIRSIG program. It is not known how much this will affect the results but is a consideration.

CAD Program: A better CAD program is needed. AutoCad had difficulties handling the large number of facets in the scene. In addition, CAD programs are available that can read in images. These images can then be used as templates or at least references when constructing the facets.

7.2 Sensitivity Analysis & Input Parameter Optimization

The next step in advancing the sensitivity study would involve automating the entire process. While the C-shell batch files saved a great deal of time, the MathCad analysis slowed the process. An alternative programming or analysis package should be used that is more adaptive to changes. This would allow the entire sensitivity study to run with less inputs from the user. Eventually, it might be possible to automate the procedure. A program could iterate through this process of optimizing the input parameters and arrive at the optimized material input values with minimal input from the user, similar to a user defining training polygons in a classification program. An interactive programming environment such as AVS might be the solution to automating the optimization of the input parameters.

More importantly, better sets of imagery would be useful in analyzing the input parameters. More imagery similar to the Bendix imagery would be needed. The Inframetrics imagery simply did not provide the resolution, field of view, or accuracy that was needed. In addition, the primary imagery should be daytime imagery. This will allow the input parameters to be optimized at a time when all the material parameters have a noticeable affect on the apparent temperature of a material, especially the visible characteristics of a material. The time history sensitivity analysis helped to show the increase in the sensitivity of the material parameters during the day. These optimized material parameters can then be used in validating a nighttime scene. If possible, the ideal solution would include several images of the same region taken throughout the day, to include morning, afternoon, evening, and night. Then, the multiple sets of imagery can be used in optimizing the input parameters.

7.3 Conclusion

DIRSIG was able to closely simulate the nighttime imaging conditions present in the primary truth imagery. A low RMS error, 1.08 °C, and high ROC coefficient, 0.92, resulted after the optimization of the input parameters. However, it was difficult to properly model the angular and background effects seen in the real imagery. In addition, poor results were evident when the optimized material parameters from the primary truth imagery were used in the validation with the secondary truth imagery. The validation and sensitivity analysis showed that imagery acquired at different times of the day, *morning*, *noon*, *evening*, and *night*, would be more useful in optimizing the input parameters.

Synthetic imagery will never replace real imagery, but it can be used in a wide variety of applications and scenarios to reduce costs. Specifically, synthetic imagery allows for the testing of image algorithms and analysis techniques. It offers a unique platform for testing these new tools that real imagery can never offer; the input parameters and variables can be controlled throughout the image generation process. This control of the variables allows the inputs to be changed one at a time to incrementally add complexity in testing the algorithms and techniques. Then, if errors occur, they can quickly be detected because the truth values and control variables are known at all stages in the synthetic image process. This image cube was constructed using DIRSIG synthetic imagery for the analysis of a new hyper-spectral fusion technique. It is just one of the many possible uses of DIRSIG synthetic imagery.



8.0 References

- Cathcart, J.M. and A.D. Sheffer, "Target and background infrared signature modeling for complex synthetic scenes" *Proceedings of the SPIE, Infrared Systems and Components II*, Vol. 890, 1988 a.
- Cathcart, J.M. and A.D. Sheffer, "Computer generated IR imagery: a first principles modeling approach," *Proceedings of the SPIE*, Vol. 933, 1988 b.
- Cathcart, J.M. and A.D. Sheffer, "Generation and application of high-resolution infrared computer imagery," *Optical Engineering*, Vol. 30 No. 11, November 1991.
- Engel, Michael and Y. Bushlin, "Field test validation of the TTIM sensor Model: Results of comparison with a real sensor," *Proceedings of the SPIE*, Vol 2224.
- Incropera, Frank P. *Fundamentals of Heat and Mass Transfer*. New York, NY, 1990.
- Gonda, Terry and G.R. Gerhart, "A comprehensive methodology for thermal signature simulation of targets and backgrounds," *Proceedings of the SPIE, Aerospace Pattern Recognition*, Vol. 1098, 1989.
- Lashansky, S.N. N. Ben-Yosef, A. Weitz, "Simulation of ground-based infrared cloudy sky images," *Optical Engineering*, Vol. 32 No. 6, June 1993.
- Lindahl, Charles, A. Cockcroft, T. Drryberry, J. Sigler, M. Yablonski, "Synthetic, multisensor database generation and validation," *Proceedings of the SPIE, Signal and Image Processing Systems Performance Evaluation*, Vol. 1310, 1990.
- Lyons, J.T. *SIRIM User Reference Manual Version 1.0*, February 1991.
- Mason, J.E., Schott, J.R. and Rankin-Parobek, D., "Validation analysis of the thermal and radiometric integrity of RIT's synthetic image generation model, DIRSIG," Presented at the SPIE Thermosense XVI, Orlando, April 1994.
- Rankin, D.K., "Validation of DIRSIG, an Infrared Synthetic Scene Generation Model" M.S. Thesis, Rochester Institute of Technology, Center for Imaging Science, 1992.
- Salacain, J. M., "Application of Imaging System Geometric Models to a Synthetic Image Generation System" M.S. Thesis, Rochester Institute of Technology, Center for Imaging Science, 1995.
- Schott, J.R., J. Mason, C. Salvaggio, J. Sirianni, "Validation of contrast and phenomenology in the Digital Imaging and Remote Sensing (DIRS) lab's Image Generation (DIRSIG) model" *Proceedings of the SPIE Annual Meeting on Optics, Imaging, & Instrumentation*, Vol. 2269, #72, San Diego, CA 1994.
- Schott, J.R., J. Mason, C. Salvaggio, J. Sirianni, R. Rose, E. Kulp, D. Rankin, "DIRSIG - Digital Imaging and Remote Sensing Image Generation Model: Description, Enhancements, and Validation" RIT/DIRS Report 92/93 -51-146, July 1993.
- Schott, John R. *Remote Sensing: The Image Chain Approach*, Oxford, NY, 1996.
- Scott, Herman, "Simulations 'picture' IR scenes" *Aerospace America*, January 1990.

Shor, E.H., "3-D Longwave Infrared Synthetic Scene Simulation" M.S. Thesis, Rochester Institute of Technology, Center for Imaging Science, 1990.

Sirianni, J.D., "Heat Transfer in DIRSIG an Infrared Synthetic Scene Generation Model" M.S. Thesis, Rochester Institute of Technology, Center for Imaging Science, 1994.

Stets, J., J. Conant, J. Gruninger and B. Ryali, "Synthetic IR scene generation," *Proceedings of the SPIE, Infrared Systems and Components II*, Vol. 890, 1988.

Appendix A

Validation Analysis

Image Evaluation - Bendix

Point Number	Point Description	DC value	BENDIX Radiance	BENDIX Apparent Temp	DIRSIG Generic Apparent Temp	Generic Radiance	DIRSIG Optimized Radiance	DIRSIG Optimized Apparent Temp	F-G Generic Ap Temp Er	F-J Optimum Ap Temp Er	Error Calc	Error Calc
50	Aluminum (50)	105.20	23.73298	-3.96	-12.67	19.2	23.94	-3.56	-8.71	0.40	75.90578	0.15831457
65	Asphalt shingles (65)	102.70	23.56236	-4.29	-12.71	19.18	23.53	-4.35	-8.42	-0.06	70.94509	0.003867735
12	Roof gravel (12)	93.46	22.93173	-5.50	-12.90	19.08	23.04	-5.29	-7.40	0.21	54.80471	0.043305504
75	Brick (75)	115.72	24.45097	-2.58	-9.73	20.73	25.12	-1.29	-7.15	1.29	51.14694	1.653463856
53	Concrete wall (53)	149.34	26.74554	1.83	-3.70	23.87	25.17	-1.20	-5.53	-3.03	30.54533	9.169892736
85	Wood (85)	111.72	24.17797	-3.10	-10.21	20.48	24.55	-2.39	-7.11	0.72	50.5166	0.511277704
40	Gray clay (40)	138.65	26.01595	0.43	-3.56	23.94	25.28	-0.99	-3.99	-1.41	15.91983	2.000771465
41	Red clay (41)	138.77	26.02414	0.44	-1.99	24.76	25.46	-0.64	-2.43	-1.08	5.903284	1.175635947
13	Dirt (13)	120.20	24.75673	-1.99	-11.50	19.81	24.67	-2.16	-9.51	-0.17	90.39484	0.027788845
43	Gravel (43)	128.87	25.34866	-0.85	-2.33	24.58	25.67	-0.24	-1.48	0.62	2.182633	0.381437604
2	Water (2)	182.91	29.03669	6.23	4.11	27.93	29.49	7.11	-2.13	0.87	4.524377	0.759097159
5	Asphalt street (5)	119.38	24.70077	-2.10	-10.77	20.19	25.05	-1.43	-8.67	0.67	75.16361	0.450542819
6	Concrete (6)	119.306	24.69572	-2.11	-10.33	20.42	25.02	-1.49	-8.22	0.62	67.53434	0.388467894
4	Grass (4)	111.05	24.13225	-3.19	-11.33	19.9	24.06	-3.33	-8.13	-0.14	66.16805	0.01928068
25	Tree (25)	120.34	24.76629	-1.97	-8.79	21.22	25.2	-1.14	-6.82	0.83	46.45737	0.694881333
											6.870773	1.07820919

Rank Order Correlation Results - Bendix

Validation Point	Truth		Truth Rank	DIRSIG Generic		Validation Point	DIRSIG Optimum		Compare Rank
	Truth DC	App Temp		App Temp	Validation Point		App Temp	Validation Point	
2 Water (2)	182.91	6.23451818	1	2	4.10746	2	7.10578	2	1
53 Concrete wall (53)	149.34	1.830923075	2	41	-1.98528	43	-0.23626	43	6
41 Red clay (41)	138.77	0.44438747	3	43	-2.33124	41	-0.63988	41	3
40 Gray clay (40)	138.65	0.42864629	4	40	-3.56132	40	-0.98584	40	4
43 Gravel (43)	128.87	-0.85386635	5	53	-3.69586	25	-1.1396	25	2
25 Tree (25)	120.34	-1.97319543	6	25	-8.78916	53	-1.19726	53	5
13 Dirt (13)	120.20	-1.99156013	7	75	-9.73094	75	-1.29336	75	10
5 Asphalt street (5)	119.38	-2.09912487	8	85	-10.21144	5	-1.4279	5	8
6 Concrete (6)	119.306	-2.10883193	9	6	-10.32676	6	-1.48556	6	9
75 Brick (75)	115.72	-2.57923085	10	5	-10.76882	13	-2.15826	13	7
85 Wood (85)	111.72	-3.10393686	11	4	-11.3262	85	-2.3889	85	11
4 Grass (4)	111.05	-3.19182511	12	13	-11.49918	4	-3.33068	4	12
50 Aluminum (50)	105.20	-3.95920763	13	50	-12.6716	50	-3.66132	50	13
65 Asphalt shingles (65)	102.70	-4.28714889	14	65	-12.71004	65	-4.439	65	14
12 Roof gravel (12)	93.46	-5.49921975	15	12	-12.90224	12	-5.29112	12	15

Bendix

Phenomenology Analysis

		Bendix APP	DIRSIG App	Rad	Error
Asphalt 1	119.4	24.70213	-2.097	-2.06	25.07
Asphalt 2	119.38	24.70077	-2.099	-2.10	25.05
Asphalt 3	125.7	25.13211	-1.270	-2.06	25.07
Asphalt 4	122.07	24.88436	-1.746	-1.87	25.17
Asphalt 5	119.61	24.71647	-2.069	-2.33	24.93
Asphalt 6	119.22	24.68985	-2.120	-2.19	25
Asphalt 7	121.18	24.82362	-1.863	-2.31	24.94
					0.3607848
Building - left	104.9133333	23.71342	-3.997	-4.14	23.61
Building - right	102.3133333	23.53597	-4.338	-3.96	23.7
Building - top	99.955	23.37501	-4.647	-3.46	23.96
Building - bottom	103.955	23.64801	-4.123	-4.65	23.34
					0.6792987
Gravel 1	91.78	22.81707	-5.720	-5.86	24.27
Gravel 2	102.74	23.56509	-4.282	-5.17	24.63
Gravel 3	95.81	23.09212	-5.191	-5.72	24.34
Gravel 4	97.81	23.22862	-4.929	-5.65	24.38
Gravel 5	128.2	25.30273	-0.942	-5.34	24.54
Gravel 6	90	22.69558	-5.953	-5.95	24.22
Gravel 7	105.66	23.76438	-3.899	-5.97	24.21
Gravel 8	97.25	23.1904	-5.002	-5.84	24.28
Grass 1	106.96	23.8531	-3.728	-2.53	24.55
Grass 2	106.89	23.84833	-3.738	-2.57	24.53
Grass 3	128.45	25.3198	-0.909	-1.01	25.34
Grass 4	124.33	25.03861	-1.450	-0.78	25.46
					1.80

Bendix

Phenomenology Analysis - ROC

	Roc		ROC			
Asphalt 3	-1.27008939	1	3 Asphalt 4	-1.86726	1	4
Asphalt 4	-1.74626008	2	1 Asphalt 1	-2.05946	2	1
Asphalt 7	-1.86300717	3	6 Asphalt 3	-2.05946	3	9
Asphalt 5	-2.06895427	4	7 Asphalt 2	-2.0979	4	9
Asphalt 1	-2.09650134	5	2 Asphalt 6	-2.194	5	9
Asphalt 2	-2.09912487	6	4 Asphalt 7	-2.30932	6	4
Asphalt 6	-2.12011311	7	5 Asphalt 5	-2.32854	7	4
						0.285714
Building - left	-3.99681157	1	3 Building - top	-3.46288	1	4
Building - botto	-4.12252238	2	4 Building - right	-3.9626	2	4
Building - right	-4.33787047	3	2 Building - left	-4.13558	3	1
Building - top	-4.64722838	4	1 Building - botto	-4.65452	4	9
						-0.8
Gravel 5	-0.94214814	1	2 Gravel 2	-5.16514	1	1
Gravel 7	-3.89886645	2	8 Gravel 5	-5.33812	2	36
Gravel 2	-4.28190183	3	1 Gravel 4	-5.64564	3	4
Gravel 4	-4.92860197	4	3 Gravel 3	-5.72252	4	1
Gravel 8	-5.00206081	5	5 Gravel 8	-5.83784	5	0
Gravel 3	-5.19095497	6	4 Gravel 1	-5.85706	6	4
Gravel 1	-5.71959627	7	6 Gravel 6	-5.95316	7	1
Gravel 6	-5.95309044	8	7 Gravel 7	-5.97238	8	1
Grass 3	-0.90935401	1	2 Grass 4	-0.77988	1	0.428571
Grass 4	-1.44980119	2	1 Grass 3	-1.01052	2	1
Grass 1	-3.728337	3	3 Grass 1	-2.5289	3	0
Grass 2	-3.73751935	4	4 Grass 2	-2.56734	4	0
						0.8

Church

[illegible]

Hawkeye

[illegible]

Appendix B

DIRSIG Files

Bendix Line Scanner DIRSIG Batch File (*.bat)

```
#!/bin/csh
#####
# Set up environment based on machine architecture
#####

if ($HOSTARCH == aux) then
    setenv TIMER /bin/time
else if ($HOSTARCH == alpha) then
    setenv TIMER /bin/time
else if ($HOSTARCH == mips) then
    setenv TIMER /usr/bin/time
else if ($HOSTARCH == paragon) then
    setenv TIMER /usr/bin/time
else if ($HOSTARCH == sun4) then
    setenv TIMER /bin/time
else if ($HOSTARCH == sgi) then
    setenv TIMER /bin/time
else
    echo " "
    echo "Unsupported architecture for dirsig2.5"
    echo " "
    exit
endif
endif

#####
# Current run information
#####

setenv DIRSIG_HOME /dirs/pkg
setenv DIRSIG_EMISSIVITY ../z_materials/emissivity_angular
setenv DIRSIG_EXTINCTION ../z_materials/extinction
setenv DIRSIG_TEXTURE ../z_materials
setenv DIRSIG_TEXTURE_MIN_WAVELENGTH 0.4
setenv DIRSIG_TEXTURE_MAX_WAVELENGTH 0.7

$TIMER $DIRSIG_HOME/bin/dirsig -f\
    10nov_hawkeye.adv \
    10nov_hawkeye.snd \
    ../z_weather/10nov_hawkeye_optimum.wth \
    ../z_materials/hawkeye_optimum.mat \
    ../z_scene/hawkeye_subarea34.gdb \
    10nov_hawkeye.rad \
    bendix.sen \
    10nov_hawkeye_final.dat \
>& 10nov_hawkeye_final.LOG
```

Bendix Line Scanner
AutoCad view files (*.adv)

Hawkeye

10nov_hawkeye.adv
2650 1600 465
2650 1600 1500
90 -90 0.0
35
600 600

Church

10nov_church.adv
644 890 460
644 1300 1500
68.48 90.00 0.0
58.33
300 300

Strip Mall

10nov_mall.adv
1225 890 460
1225 1300 1500
68.48 90 0.0
58.33
300 300

Garden

10nov_garden.adv
1200 1445 490
1200 1600 1500
81.28 90 0.0
58.33
300 300

Gorge

10nov_gorge.adv
1940 700 250
1940 1400 1500
60.75 90 0.0
60.0
200 200

Flyover

10nov_nadir.adv
1800 1600 240.0
1800 1600 240.0
90 -90 0.0
55.0
512 512

Bendix Line Scanner

Scene node files (*.snd)

Hawkeye

10nov_hawkeye.snd

0.522

1

696.28 1250.0 13.5

-54.0 54.0 6.0

11 10 91

7.0

5.0

43.1833 77.621

Church

10nov_church.adv

0.522

1

696.28 1250.0 13.5

-11.0 55.0 3.0

11 10 91

7.0

5.0

43.1833 77.621

Strip Mall

10nov_mall.adv

0.522

1

696.28 1250.0 13.5

-11.0 55.0 3.0

11 10 91

7.0

5.0

43.1833 77.621

Garden

10nov_garden.snd

0.522

1

696.28 1250.0 13.5

-24.0 44.0 4.0

11 10 91

7.0

5.0

43.1833 77.621

Gorge

10nov_gorge.snd

0.522

1

696.28 1250.0 13.5

-3.0 62.0 2.5

11 10 91

7.0

5.0

43.1833 77.621

Flyover

10nov_nadir.snd

0.522

1

696.28 1250.0 13.5

-64.0 64.0 6.0

11 10 91

7.0

5.0

43.1833 77.621

Bendix Line Scanner

Platform motion profile (*.prf)

```
#  
# DIRSIG flight description ...  
#  
FLIGHT_SIMPLE_BEGIN  
  
NUMBER_OF_SCANS = 512  
  
SCAN_RATE = 0.0229  
  
FLIGHT_HEADING = 0.0  
  
FLIGHT_ALTITUDE = 381.0  
  
AVERAGE_SPEED = 90.0  
  
AVERAGE_ROLL = 0.0  
  
AVERAGE_PITCH = 0.0  
  
AVERAGE_YAW = 0.0  
  
FLIGHT_SIMPLE_END
```

Bendix Line Scanner

Platform specification file (*.psf)

```
#
# DIRSIG Platform Specification file
#
SYSTEM_BEGIN

PLATFORM_ID = BENDIX

PLATFORM_TYPE = 2
#      1 -> FIXED
#      2 -> AIRBORN
#      3 -> ORBITAL

ORBITAL_ALTITUDE = -1
#      +n -> ALTITUDE (meters)
#      -1 -> N/A (PLATFORM_TYPE cannot be ORBITAL)

ORBITAL_INCLINATION = -1
#      +n -> INCLINATION (meters)
#      -1 -> N/A (PLATFORM_TYPE cannot be ORBITAL)

SCANNER_TYPE = 2
#      1 -> FRAME
#      2 -> LINE SCANNER
#      3 -> PUSHBROOM SCANNER

SCANNER_DUTY_CYCLE = 0.30
#      +n -> DUTY CYCLE (%)
#      -1 -> N/A (SCANNER_TYPE must be FRAME)

SCAN_RATE = 0.0229
#      +n -> SCAN RATE (ms)
#      -1 -> N/A (SCANNER_TYPE must be FRAME)

FOCAL_LENGTH = 0.1524
#      n -> FOCAL LENGTH (meters)

NUMBER_OF_BANDS = 1
#      n -> NUMBER OF BANDS

SYSTEM_END

BAND_BEGIN = 1
#      n -> NEW BAND (2)

BAND_ID = TEST_BAND1
#      n -> BAND_ID

SAMPLES_PER_LINE = 512
#      n -> SAMPLES_PER_LINE

LINES_PER_SCAN = 1
#      n = LINES_PER_SCAN

CROSS_TRACK_PITCH = 0.0
#      n = CROSS_TRACK_PITCH (um)

ALONG_TRACK_PITCH = 0.0
#      n = ALONG_TRACK_PITCH (um)

BAND_OFFSET = 0.0
#      n = BAND_OFFSET (radians)

DETECTOR_OFFSET = 0.0
#      n = DETECTOR_OFFSET (radians)

BAND_END
```

Bendix Line Scanner Modeling file (*modeling*)

```
#  
# DIRSIG Modeling Description ...  
#  
MODELING_BEGIN  
  
MODEL_EARTH_ROTATION = 0  
  
MODEL_LINE_SKEW = 0  
  
CENTER_TARGET = 0  
  
REGISTER_BANDS = 0  
  
REGISTER_DETECTORS = 0  
  
ALONG_TRACK_LOOK_ANGLE = 0.0  
  
CROSS_TRACK_LOOK_ANGLE = 0.0  
  
PLATFORM_FILENAME = todd_bendix.psf  
  
PROFILE_FILENAME = todd_simple.prf  
  
IMAGE_SIZE = 512 512  
  
MODELING_END
```

Bendix Line Scanner
Sensor file (*.sen)

42
1
0
0.28
0.33125
0.375
0.43
0.48
0.55
0.605
0.64
0.670
0.685
0.6975
0.700
0.733
0.75
0.77
0.805
0.825
0.85
0.875
0.90
0.925
0.94
0.9525
0.96
0.975
0.987
0.995
0.98
0.9675
0.945
0.927
0.885
0.835
0.79
0.755
0.715
0.68
0.61
0.535
0.4875
0.325
0.20

Bendix Line Scanner - generic weather file

10nov_hawkeye_generic.wth

52	1												
0	-6.11111	1033.7	0.882	-1	2.539773	0	0	0.9	5	0	0	0	0
1	-6.11111	1033.7	0.882	-1	2.539773	0	0	0.9	5	0	0	0	0
2	-6.66667	1034.2	0.919	-1	3.047727	0	0	0.9	5	0	0	0	0
3	-6.66667	1034.3	0.919	-1	3.047727	0	0	0.9	5	0	0	0	0
4	-6.66667	1034.3	0.919	-1	3.047727	0	0	0.9	5	0	0	0	0
5	-7.22222	1034.6	0.919	-1	2.031818	0	0	0.9	5	0	0	0	0
6	-7.77778	1034.7	0.918	-1	2.539773	0	0	1	5	0	0	0	0
7	-7.77778	1035.6	0.918	-1	2.031818	67.06	0.74	0.9	5	0	0	0	0
8	-7.22222	1035.9	0.919	-1	2.031818	80.55	2.65	0.9	5	0	0	0	0
9	-4.44444	1035.8	0.812	-1	3.047727	85.91	3.95	1	5	0	0	0	0
10	-1.66667	1035.8	0.72	-1	2.539777	88.86	4.69	1	5	0	0	0	0
11	1.66667	1035.4	0.567	-1	0.000000	90.26	5.01	1	5	0	0	0	0
12	2.77778	1034.7	0.482	-1	2.031818	90.33	5.02	0.7	5	0	0	0	0
13	1.66667	1034	0.499	-1	3.555682	89.07	4.73	0.5	5	0	0	0	0
14	2.22222	1033.2	0.501	-1	2.539773	86.3	4.04	0.6	5	0	0	0	0
15	2.77778	1033.5	0.503	-1	3.047727	81.27	2.81	0.7	5	0	0	0	0
16	1.66667	1032.7	0.544	-1	3.047727	76.36	1.98	0.8	1	0	0	0	0
17	0.000000	1032.4	0.612	-1	3.047727	0	0	0.9	1	0	0	0	0
18	-0.55556	1032.4	0.637	-1	2.539773	0	0	1	0	0	0	0	0
19	-1.11111	1032.1	0.663	-1	1.523864	0	0	1	0	0	0	0	0
20	-2.22222	1031.7	0.75	-1	0.000000	0	0	1	0	0	0	0	0
21	-5.00000	1031.1	0.846	-1	0.000000	0	0	1	0	0	0	0	0
22	-4.44444	1031	0.847	-1	1.523864	0	0	1	0	0	0	0	0
23	-5.55556	1030.6	0.92	-1	2.031818	0	0	1	0	0	0	0	0
24	-6.11111	1029.8	0.882	-1	0.000000	0	0	1	0	0	0	0	0
25	-6.66667	1029	0.881	-1	0.000000	0	0	1	0	0	0	0	0
26	-6.66667	1029.2	0.919	-1	0.000000	0	0	1	0	0	0	0	0
27	-7.22222	1028.8	0.959	-1	0.000000	0	0	1	0	0	0	0	0
28	-7.22222	1030.3	0.919	-1	3.047727	0	0	0.9	5	0	0	0	0
29	-7.22222	1034.6	0.919	-1	2.031818	0	0	0.9	5	0	0	0	0
30	-7.77778	1034.7	0.918	-1	2.539773	0	0	1	5	0	0	0	0
31	-7.77778	1035.6	0.918	-1	2.031818	67.06	0.74	0.9	5	0	0	0	0
32	-7.22222	1035.9	0.919	-1	2.031818	80.55	2.65	0.9	5	0	0	0	0
33	-4.44444	1035.8	0.812	-1	3.047727	85.91	3.95	1	5	0	0	0	0
34	-1.66667	1035.8	0.72	-1	2.539777	88.86	4.69	1	5	0	0	0	0
35	1.66667	1035.4	0.567	-1	0.000000	90.26	5.01	1	5	0	0	0	0
36	2.77778	1034.7	0.482	-1	2.031818	90.33	5.02	0.7	5	0	0	0	0
37	1.66667	1034	0.499	-1	3.555682	89.07	4.73	0.5	5	0	0	0	0
38	2.22222	1033.2	0.501	-1	2.539773	86.3	4.04	0.6	5	0	0	0	0
39	2.77778	1033.5	0.503	-1	3.047727	81.27	2.81	0.7	5	0	0	0	0
40	1.66667	1032.7	0.544	-1	3.047727	76.36	1.98	0.8	1	0	0	0	0
41	0.000000	1032.4	0.612	-1	3.047727	0	0	0.9	1	0	0	0	0
42	-0.55556	1032.4	0.637	-1	2.539773	0	0	1	0	0	0	0	0
43	-1.11111	1032.1	0.663	-1	1.523864	0	0	1	0	0	0	0	0
44	-2.22222	1031.7	0.75	-1	0.000000	0	0	1	0	0	0	0	0
45	-5.00000	1031.1	0.846	-1	0.000000	0	0	1	0	0	0	0	0
46	-4.44444	1031	0.847	-1	1.523864	0	0	1	0	0	0	0	0
47	-5.55556	1030.6	0.92	-1	2.031818	0	0	1	0	0	0	0	0
48	-6.11111	1029.8	0.882	-1	0.000000	0	0	1	0	0	0	0	0
49	-6.66667	1029	0.881	-1	0.000000	0	0	1	0	0	0	0	0
50	-6.66667	1029.2	0.919	-1	0.000000	0	0	1	0	0	0	0	0
51	-7.22222	1028.8	0.959	-1	0.000000	0	0	1	0	0	0	0	0

Bendix Line Scanner - optimum weather file

10nov_hawkeye_optimum.wth

52	1												
0	-2.11111	1033.7	0.882	-1	2.539773	0	0	0.9	5	0	0	0	0
1	-2.11111	1033.7	0.882	-1	2.539773	0	0	0.9	5	0	0	0	0
2	-2.66667	1034.2	0.919	-1	3.047727	0	0	0.9	5	0	0	0	0
3	-2.66667	1034.3	0.919	-1	3.047727	0	0	0.9	5	0	0	0	0
4	-2.66667	1034.3	0.919	-1	3.047727	0	0	0.9	5	0	0	0	0
5	-3.22222	1034.6	0.919	-1	2.031818	0	0	0.9	5	0	0	0	0
6	-3.77778	1034.7	0.918	-1	2.539773	0	0	1	5	0	0	0	0
7	-3.77778	1035.6	0.918	-1	2.031818	67.06	0.74	0.9	5	0	0	0	0
8	-3.22222	1035.9	0.919	-1	2.031818	80.55	2.65	0.9	5	0	0	0	0
9	-0.44444	1035.8	0.812	-1	3.047727	85.91	3.95	1	5	0	0	0	0
10	2.66667	1035.8	0.72	-1	2.539777	88.86	4.69	1	5	0	0	0	0
11	5.66667	1035.4	0.567	-1	0.000000	90.26	5.01	1	5	0	0	0	0
12	6.77778	1034.7	0.482	-1	2.031818	90.33	5.02	0.7	5	0	0	0	0
13	5.66667	1034	0.499	-1	3.555682	89.07	4.73	0.5	5	0	0	0	0
14	6.22222	1033.2	0.501	-1	2.539773	86.3	4.04	0.6	5	0	0	0	0
15	6.77778	1033.5	0.503	-1	3.047727	81.27	2.81	0.7	5	0	0	0	0
16	5.66667	1032.7	0.544	-1	3.047727	76.36	1.98	0.8	1	0	0	0	0
17	4.00000	1032.4	0.612	-1	3.047727	0	0	0.9	1	0	0	0	0
18	3.55556	1032.4	0.637	-1	2.539773	0	0	1	0	0	0	0	0
19	3.11111	1032.1	0.663	-1	1.523864	0	0	1	0	0	0	0	0
20	1.22222	1031.7	0.75	-1	0.000000	0	0	1	0	0	0	0	0
21	-1.00000	1031.1	0.846	-1	0.000000	0	0	1	0	0	0	0	0
22	-0.44444	1031	0.847	-1	1.523864	0	0	1	0	0	0	0	0
23	-1.55556	1030.6	0.92	-1	2.031818	0	0	1	0	0	0	0	0
24	-2.11111	1029.8	0.882	-1	0.000000	0	0	1	0	0	0	0	0
25	-2.36667	1029	0.881	-1	0.000000	0	0	1	0	0	0	0	0
26	-2.36667	1029.2	0.919	-1	0.000000	0	0	1	0	0	0	0	0
27	-2.88888	1028.8	0.959	-1	0.000000	0	0	1	0	0	0	0	0
28	-3.22222	1030.3	0.919	-1	3.047727	0	0	0.9	5	0	0	0	0
29	-3.22222	1034.6	0.919	-1	2.031818	0	0	0.9	5	0	0	0	0
30	-3.77778	1034.7	0.918	-1	2.539773	0	0	1	5	0	0	0	0
31	-3.77778	1035.6	0.918	-1	2.031818	67.06	0.74	0.9	5	0	0	0	0
32	-3.22222	1035.9	0.919	-1	2.031818	80.55	2.65	0.9	5	0	0	0	0
33	-0.44444	1035.8	0.812	-1	3.047727	85.91	3.95	1	5	0	0	0	0
34	2.66667	1035.8	0.72	-1	2.539777	88.86	4.69	1	5	0	0	0	0
35	5.66667	1035.4	0.567	-1	0.000000	90.26	5.01	1	5	0	0	0	0
36	6.77778	1034.7	0.482	-1	2.031818	90.33	5.02	0.7	5	0	0	0	0
37	5.66667	1034	0.499	-1	3.555682	89.07	4.73	0.5	5	0	0	0	0
38	6.22222	1033.2	0.501	-1	2.539773	86.3	4.04	0.6	5	0	0	0	0
39	6.77778	1033.5	0.503	-1	3.047727	81.27	2.81	0.7	5	0	0	0	0
40	5.66667	1032.7	0.544	-1	3.047727	76.36	1.98	0.8	1	0	0	0	0
41	4.00000	1032.4	0.612	-1	3.047727	0	0	0.9	1	0	0	0	0
42	3.55556	1032.4	0.637	-1	2.539773	0	0	1	0	0	0	0	0
43	3.11111	1032.1	0.663	-1	1.523864	0	0	1	0	0	0	0	0
44	1.22222	1031.7	0.75	-1	0.000000	0	0	1	0	0	0	0	0
45	-1.00000	1031.1	0.846	-1	0.000000	0	0	1	0	0	0	0	0
46	-0.44444	1031	0.847	-1	1.523864	0	0	1	0	0	0	0	0
47	-1.55556	1030.6	0.92	-1	2.031818	0	0	1	0	0	0	0	0
48	-2.11111	1029.8	0.882	-1	0.000000	0	0	1	0	0	0	0	0
49	-2.36667	1029	0.881	-1	0.000000	0	0	1	0	0	0	0	0
50	-2.36667	1029.2	0.919	-1	0.000000	0	0	1	0	0	0	0	0
51	-2.88888	1028.8	0.959	-1	0.000000	0	0	1	0	0	0	0	0

Bendix Line Scanner Modtran card deck (*.cdk)

```

7 2 2 1 0 0 0 0 0 0 1 1 1 0.000 0.00
5 2 0 1 0 0 24.000 0.000 0.000 0.000 0.218
33 0 0TEMP
0.218 0.103E+04-0.722E+01-0.777E+01 0.000E+00 0.000E+00ABG
0.242 0.997E+03-0.610E+01-0.108E+02 0.000E+00 0.000E+00ABG
0.290 0.991E+03-0.370E+01-0.640E+01 0.000E+00 0.000E+00ABG
0.365 0.982E+03-0.180E+01-0.720E+01 0.000E+00 0.000E+00ABG
0.461 0.970E+03-0.200E+01-0.960E+01 0.000E+00 0.000E+00ABG
0.767 0.933E+03-0.360E+01-0.960E+01 0.000E+00 0.000E+00ABG
1.019 0.904E+03-0.300E+00-0.180E+02 0.000E+00 0.000E+00ABG
1.208 0.883E+03 0.310E+01-0.173E+02 0.000E+00 0.000E+00ABG
1.516 0.850E+03 0.360E+01-0.168E+02 0.000E+00 0.000E+00ABG
1.864 0.814E+03 0.300E+01-0.173E+02 0.000E+00 0.000E+00ABG
2.113 0.790E+03 0.420E+01-0.166E+02 0.000E+00 0.000E+00ABG
2.531 0.750E+03 0.240E+01-0.179E+02 0.000E+00 0.000E+00ABG
3.085 0.700E+03-0.400E+00-0.200E+02 0.000E+00 0.000E+00ABG
3.735 0.645E+03-0.390E+01-0.207E+02 0.000E+00 0.000E+00ABG
4.400 0.593E+03-0.660E+01-0.212E+02 0.000E+00 0.000E+00ABG
4.982 0.550E+03-0.980E+01-0.265E+02 0.000E+00 0.000E+00ABG
5.710 0.500E+03-0.150E+02-0.310E+02 0.000E+00 0.000E+00ABG
6.834 0.430E+03-0.229E+02-0.359E+02 0.000E+00 0.000E+00ABG
7.834 0.374E+03-0.304E+02-0.401E+02 0.000E+00 0.000E+00ABG
8.892 0.322E+03-0.399E+02-0.490E+02 0.000E+00 0.000E+00ABG
10.808 0.241E+03-0.539E+02-0.674E+02 0.000E+00 0.000E+00ABG
11.667 0.211E+03-0.566E+02-0.708E+02 0.000E+00 0.000E+00ABG
12.543 0.183E+03-0.574E+02-0.718E+02 0.000E+00 0.000E+00ABG
13.033 0.170E+03-0.597E+02-0.746E+02 0.000E+00 0.000E+00ABG
14.065 0.144E+03-0.599E+02-0.749E+02 0.000E+00 0.000E+00ABG
15.033 0.123E+03-0.625E+02-0.781E+02 0.000E+00 0.000E+00ABG
16.629 0.950E+02-0.618E+02-0.773E+02 0.000E+00 0.000E+00ABG
17.887 0.774E+02-0.629E+02-0.786E+02 0.000E+00 0.000E+00ABG
19.230 0.623E+02-0.626E+02-0.783E+02 0.000E+00 0.000E+00ABG
20.848 0.480E+02-0.576E+02-0.720E+02 0.000E+00 0.000E+00ABG
23.791 0.300E+02-0.599E+02-0.749E+02 0.000E+00 0.000E+00ABG
25.769 0.219E+02-0.602E+02-0.753E+02 0.000E+00 0.000E+00ABG
27.133 0.176E+02-0.574E+02-0.718E+02 0.000E+00 0.000E+00ABG
0.000 0.000 0.000 0.000 0.000 0.000 0
1 2 1 0
0.000 0.000 0.000 0.000 0.000 0.000 0.000 0.000
5000.000 10000.000 12.626
0

```

Bendix Line Scanner
Radiosonde data - (*.rsd)

0.218	1028.8	-7.22	-7.77
0.242	997	-6.1	-10.8
0.29	990.9	-3.7	-6.4
0.365	981.6	-1.8	-7.2
0.461	969.8	-2	-9.6
0.767	933.1	-3.6	-9.6
1.019	903.8	-0.3	-18
1.208	882.9	3.1	-17.3
1.516	850	3.6	-16.8
1.864	814.3	3	-17.3
2.113	789.7	4.2	-16.6
2.531	750	2.4	-17.9
3.085	700	-0.4	-20
3.735	645	-3.9	-20.7
4.4	592.7	-6.6	-21.2
4.982	550	-9.8	-26.5
5.71	500	-15	-31
6.834	430	-22.9	-35.9
7.834	374.3	-30.4	-40.1
8.892	321.6	-39.9	-49
10.808	240.8	-53.9	-67.375
11.667	210.5	-56.6	-70.75
12.543	183.4	-57.4	-71.75
13.033	169.7	-59.7	-74.625
14.065	143.7	-59.9	-74.875
15.033	123	-62.5	-78.125
16.629	95	-61.8	-77.25
17.887	77.4	-62.9	-78.625
19.23	62.3	-62.6	-78.25
20.848	48	-57.6	-72
23.791	30	-59.9	-74.875
25.769	21.9	-60.2	-75.25
27.133	17.6	-57.4	-71.75

Inframetrics Camera DIRSIG Batch File (*.bat)

```
#!/bin/csh
#####
# Set up environment based on machine architecture
#####

if ($HOSTARCH == aux) then
    setenv TIMER /bin/time
else if ($HOSTARCH == alpha) then
    setenv TIMER /bin/time
else if ($HOSTARCH == mips) then
    setenv TIMER /usr/bin/time
else if ($HOSTARCH == paragon) then
    setenv TIMER /usr/bin/time
else if ($HOSTARCH == sun4) then
    setenv TIMER /bin/time
else if ($HOSTARCH == sgi) then
    setenv TIMER /bin/time
else
    echo " "
    echo "Unsupported architecture for dirsig2.5"
    echo " "
    exit
endif
endif

#####
# Current run information
#####

setenv DIRSIG_HOME /dirs/pkg
setenv DIRSIG_EMISSIVITY ../z_materials/emissivity_angular
setenv DIRSIG_EXTINCTION ../z_materials/extinction
setenv DIRSIG_TEXTURE ../z_materials
setenv DIRSIG_TEXTURE_MIN_WAVELENGTH 0.4
setenv DIRSIG_TEXTURE_MAX_WAVELENGTH 0.7

STIMER /dirs/src/dirsig/src/dirsig/main/dirsig -f\
    12oct_church.adv \
    12oct_church.snd \
    ../z_weather/12oct_hawkeye_generic.wth \
    ../z_materials/hawkeye_optimum.mat \
    ../z_scene/inframetrics_church_scene.gdb \
    12oct_church.rad \
    inframetrics.sen \
    12oct_church_final.dat \
>& 12oct_church_final.LOG
```

Inframetrics Camera
AutoCad view files (*.adv)

Hawkeye

12oct_hawkeye.adv

2347 1470 450

1208 1029 497

2.20 -158.83 0.0

87

200 256

Church

12oct_church.adv

1350 1110 430

2346 1433 585

8.42 17.97 0.0

90

256 256

Inframetrics Camera

Scene node files (*.snd)

Hawkeye

12oct_hawkeye.snd

0.369

1

833.3 1250.0 20

64.0 112.0 4.0

10 12 95

19

5.0

43.1833 77.621

Church

12oct_church.snd

0.395

1

833.3 1250.0 20.0

58.0 106.0 4.0

10 12 95

19.0

5.0

43.1833 77.621

Inframetrics Camera
Sensor file (*.sen)

22
1
0
0.59
0.68
0.75
0.83
0.895
0.91
0.925
0.94
0.945
0.955
0.96
0.968
0.97
0.975
0.98
0.98
0.99
1.0
0.99
0.95
0.90
0.82

Inframetrics Camera- generic weather file

12oct_hawkeye_generic.wth

40	1											
0	12.78	1029.52	-1	9.44	3.048	0.0	0.0	0.5	3	0	0	0
1	11.67	1029.52	-1	8.89	3.048	0.0	0.0	0.7	5	0	0	0
2	10.00	1029.52	-1	7.78	3.048	0.0	0.0	0.9	3	0	0	0
3	11.11	1029.54	-1	7.78	2.540	0.0	0.0	1	0	0	0	0
4	10.56	1029.55	-1	7.22	3.048	0.0	0.0	1	0	0	0	0
5	10.56	1029.56	-1	8.33	3.048	0.0	0.0	1	0	0	0	0
6	10.56	1029.59	-1	8.89	3.048	0.0	0.0	1	0	0	0	0
7	10.56	1029.61	-1	10.00	1.524	73.5	2.04	1	0	0	0	0
8	10.00	1029.62	-1	9.44	2.032	81.40	3.71	0.9	8	0	0	0
9	11.67	1029.63	-1	10.56	2.540	85.81	4.74	0.9	1	0	0	0
10	15.00	1029.64	-1	11.11	4.064	88.48	5.26	0.5	1	0	0	0
11	17.22	1029.64	-1	11.11	4.064	89.82	5.45	0.4	1	0	0	0
12	19.44	1029.64	-1	11.11	4.064	89.95	5.47	0.7	1	0	0	0
13	21.11	1029.62	-1	8.33	4.572	88.88	5.32	0.9	1	0	0	0
14	22.78	1029.59	-1	8.33	5.588	86.52	4.89	0.9	1	0	0	0
15	22.78	1029.57	-1	7.78	5.080	82.55	3.98	0.7	1	0	0	0
16	23.33	1029.56	-1	6.11	7.111	75.74	2.45	0.5	1	0	0	0
17	22.22	1029.56	-1	7.78	7.111	54.17	0.35	0.8	1	0	0	0
18	21.11	1029.56	-1	7.78	5.080	0.0	0.0	0.8	1	0	0	0
19	18.33	1029.56	-1	6.67	2.540	0.0	0.0	0.9	1	0	0	0
20	16.11	1029.56	-1	7.22	2.540	0.0	0.0	1	0	0	0	0
21	14.44	1029.56	-1	7.78	3.048	0.0	0.0	1	0	0	0	0
22	13.33	1029.56	-1	7.78	1.524	0.0	0.0	1	0	0	0	0
23	12.22	1029.56	-1	7.78	2.032	0.0	0.0	1	0	0	0	0
24	11.67	1029.55	-1	6.67	1.524	0.0	0.0	1	0	0	0	0
25	11.67	1029.54	-1	6.67	2.032	0.0	0.0	1	0	0	0	0
26	11.67	1029.54	-1	7.78	3.556	0.0	0.0	1	0	0	0	0
27	11.11	1029.53	-1	7.22	3.556	0.0	0.0	1	0	0	0	0
28	10.56	1029.52	-1	6.11	3.048	0.0	0.0	1	0	0	0	0
29	10.56	1029.52	-1	6.67	2.540	0.0	0.0	1	0	0	0	0
30	10.56	1029.52	-1	5.56	3.048	0.0	0.0	1	0	0	0	0
31	10.56	1029.52	-1	6.11	3.048	73.63	1.99	0.9	1	0	0	0
32	11.11	1029.53	-1	5.56	4.572	81.60	3.67	0.9	1	0	0	0
33	15.00	1029.53	-1	7.78	3.556	86.02	4.70	0.9	1	0	0	0
34	18.33	1029.54	-1	8.33	3.048	88.69	5.22	0.9	1	0	0	0
35	21.67	1029.53	-1	9.44	5.588	90.03	5.42	1	0	0	0	0
36	23.89	1029.52	-1	11.11	5.080	90.15	5.44	1	0	0	0	0
37	25.00	1029.52	-1	11.11	5.080	89.07	5.28	1	0	0	0	0
38	26.67	1029.50	-1	12.78	6.095	86.70	4.84	1	0	0	0	0
39	26.67	1029.49	-1	12.22	6.095	82.81	3.93	1	0	0	0	0

```

7 2 2 1 0 0 0 0 0 0 1 1 1 0.000 0.00
5 2 0 1 0 0 32.000 0.000 0.000 0.000 0.218
19 0 012OCT.RAD
0.218 0.987E+03 0.267E+02 0.122E+02 0.000E+00 0.000E+00ABG
0.545 0.950E+03 0.230E+02 0.900E+01 0.000E+00 0.000E+00ABG
1.002 0.900E+03 0.170E+02 0.690E+01 0.000E+00 0.000E+00ABG
1.480 0.850E+03 0.106E+02-0.400E+00 0.000E+00 0.000E+00ABG
1.982 0.800E+03 0.119E+02-0.144E+02 0.000E+00 0.000E+00ABG
2.515 0.750E+03 0.790E+01-0.171E+02 0.000E+00 0.000E+00ABG
3.086 0.700E+03 0.460E+01-0.204E+02 0.000E+00 0.000E+00ABG
3.669 0.650E+03 0.130E+01-0.234E+02 0.000E+00 0.000E+00ABG
4.299 0.600E+03-0.370E+01-0.266E+02 0.000E+00 0.000E+00ABG
4.983 0.550E+03-0.900E+01-0.301E+02 0.000E+00 0.000E+00ABG
5.733 0.500E+03-0.149E+02-0.192E+02 0.000E+00 0.000E+00ABG
6.512 0.450E+03-0.204E+02-0.355E+02 0.000E+00 0.000E+00ABG
7.383 0.400E+03-0.269E+02-0.419E+02 0.000E+00 0.000E+00ABG
8.316 0.350E+03-0.344E+02-0.407E+02 0.000E+00 0.000E+00ABG
9.393 0.300E+03-0.421E+02-0.521E+02 0.000E+00 0.000E+00ABG
10.603 0.250E+03-0.501E+02-0.626E+02 0.000E+00 0.000E+00ABG
12.023 0.200E+03-0.589E+02-0.736E+02 0.000E+00 0.000E+00ABG
13.803 0.150E+03-0.639E+02-0.799E+02 0.000E+00 0.000E+00ABG
16.283 0.100E+03-0.621E+02-0.776E+02 0.000E+00 0.000E+00ABG
0.000 0.000 0.000 0.000 0.000 0.000 0
1 2 1 0
0.000 0.000 0.000 0.000 0.000 0.000 0.000 0.000
5000.000 10000.000 12.626
0

```

Inframetrics Camera
Radiosonde data - (*.rsd)

0.218	987	26.667	12.22
0.545	950	23	9
1.002	900	17	6.9
1.48	850	10.6	-0.4
1.982	800	11.9	-14.4
2.515	750	7.9	-17.1
3.086	700	4.6	-20.4
3.669	650	1.3	-23.4
4.299	600	-3.7	-26.6
4.983	550	-9	-30.1
5.733	500	-14.9	-19.2
6.512	450	-20.4	-35.5
7.383	400	-26.9	-41.9
8.316	350	-34.4	-40.7
9.393	300	-42.1	-52.1
10.603	250	-50.1	-62.625
12.023	200	-58.9	-73.625
13.803	150	-63.9	-79.875
16.283	100	-62.1	-77.625

Appendix C

AutoCad Scene
Construction
&
Image Generation

AutoCad Drawing Notes

The following guidelines were documented to help others in drawing a complex scene and using the scene that was created by myself and Russell White.

Streets: When doing an AutoCad scene that involves streets and terrain, one should start with laying the foundation for the streets. Streets are relatively flat and the natural terrain has been modified to make the streets flat. Determine the elevation of the streets from intersections of the contour lines and the streets. If there is a large region where there are no intersections, the elevation of the street can be estimated. If possible, each side of the road should be the same elevation as this will prevent 'earthquake roads'. Depending on the resolution, the foundation for the streets should be wider than the actual street so that sidewalks can also be placed into the drawing. Having a foundation with roads placed on top of the foundation will show the grass between the road and the sidewalk while reducing the number of overall facets required to create this appearance. In addition, at the intersection of two roads, a separate facet should be created for the intersection. Each corner of this facet will have the same elevation. This will also help prevent the uneven or 'earthquake' roads mentioned earlier. Once the foundation for the roads has been laid, streets can be placed over the foundation of the roads.

Terrain: Terrain should be added after the roads have been constructed. Whenever feasible, it is best to use polylines and rulesurf to create undulating terrain. However, rulesurf can only be used between two polylines that are of similar length. If one attempts to rulesurf between a long and short line, facets can be created that overlap on themselves. A polyline can be used for multiple rulesurf meshes by creating the polylines in different layers and alternating the state of the layer (freeze/thaw). Finally, if a mistake or change is needed within a rulesurf, explode can be used to separate the rulesurf into individual facets. 3dfaces can then be used in other areas to fill in the rest of the terrain. There may be a better method with AutoCad 13, but this method worked well for AutoCad 11.

Houses: Generic houses can easily be created and modified in AutoCad. By creating houses that were approximately 1x1x1, it was then possible to scale the houses to exact dimensions. When a house was inserted, 'xyz' scaling was selected. This allowed the 1x1x1 house to be made the proper dimensions in the x and y axes. The proper height of the house, depending on whether it was a one or two story house, could then be typed into AutoCad. This ensured that each house could have different widths and lengths, but all houses would have similar heights. Houses that were not traditional or did not fit the models that were developed could then be created individually and inserted into the scene.

As each house was inserted into the scene, a list was done on the insertion. This showed the location, scaling, and rotation of the inserted object. This information was taken from AutoCad and pasted into a separate document using the VI editor. This procedure was repeated for each house in the region. After all the houses had been inserted into the scene, the document containing all the house insertion information was

modified into an AutoCad script file. This allowed the region or even a particular house to be changed in the future without having to manually reinsert all the houses.

Object Creation: The scene was divided into 20 different regions to reduce the size of the bounding volumes. This was also done to reduce the run time of DIRSIG. Another useful tool in creating the objects was the use of script files. Script files were used to create each of the 20 regions. Each of the objects consisted of several different parts. The parts usually included:

- terrain
- streets
- sidewalks
- houses

This allowed the scene and each of the 20 objects to be easily modified and reconstructed if necessary.

Script files were developed for the creation of each object. These script files should not have to be modified. The only problem is that the **objects must be created using AutoCad 13**. After the object has been assembled using the script file, **it must be saved as AutoCad 12 format**. This is because there is a memory problem with AutoCad 13 and it cannot assemble the entire scene (***this problem may have been fixed but I would recommend this method**). Remember, the trees are inserted at the scene level of the DIRSIG hierarchy.

The object must be recreated if any change is made to a part in that object. This includes changing the material ID number, SGP, or facet temperature. The material parameters of any material can be changed in the material file without having to rebuild the scene. Also, the emissivity curves can be changed without having to rebuild the scene. In particular, I created my version of the scene with 10 colored asphalt shingles, 10 colored wood sidings, and 10 colored bricks. However, I used the same emissivity file for all these materials. The visible portion of the emissivity curve can be modified to produce different colors in the visible region of the electromagnetic spectrum without any modifications to the actual scene.

Scene Creation: The final scene can also be created using script files. Each region was inserted into the scene as an object. In addition, the Hawkeye plant and the driving part bridge were inserted into the scene as objects. Multiple trees, which were treated as objects -- each individual tree representing one part, were also inserted at the scene level. The trees were placed into script files to allow for easy removal of the trees from the scene. This was especially important since the addition of trees greatly added to the number of facets in the scene.

Separate script files can be created from the original scene script file if necessary. This is important if examining a small part of the scene. A separate script file can be created that does not insert all the objects into the scene, just the ones in the desired

subscene. This greatly reduces the run time of DIRSIG. In doing this, I recommend copying the entire scene script file and then deleting the objects from the scene that you do not want inserted. If you retype the script files, you usually end up with a lot of errors in the script file. It is much easier to just delete lines.

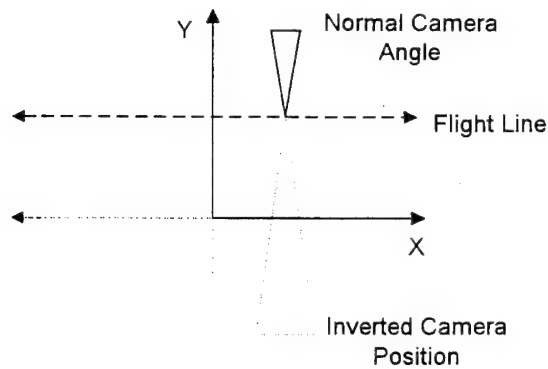
The scene must be rebuilt in AutoCad 11. If the problem with AutoCad 13 that was experience during the scene creation is resolved, then AutoCad 13 can be used for everything.

General Drawing Guidelines: When drawing in three dimensions, it is best to type in the coordinates if they are known. If the coordinates are not exactly known, it is useful to use the '.xy' feature in AutoCad and then type in the z coordinate. This ensures accurate drawings in three dimensions. If the '.xy' is not chosen, then the z coordinate will be set to 0.0 when drawing in three dimensions. In addition, when joining facets, the 'nea' and 'int' features of AutoCad ensure that there will not be any 'holes' in the resulting DIRSIG scene. These features can be set to the default by using the DOSNAP feature. Finally, it is best to use triangular facets if the points are non-coplanar. AutoCad will make a non-coplanar rectangular facet into two triangular facets. This can cause problems when trying to lay objects on top of the facet. As a result, it is best to make the facet triangular when you do the initial drawing.

When drawing complex objects, it is best to draw the objects using different layers. Each complex piece of an object is a part. Each part should be the same material type. This allows for easy material selection and modification at later times. After the entire object is finished and each part is represented by a different layer, use the 'Write blocks' feature in AutoCad to make each layer a separate file. This method of drawing complex objects reduces the chances of holes or problems when joining the parts.

DVIEW: When using DVIEW in AutoCad, select only the boundaries of the scene, or a sample of objects in the desired scene. Selecting all objects in a scene makes it difficult for AutoCad to redraw the scene. It will often crash as it runs of memory.

A major problem arose when using DVIEW. If the camera and targets points were typed into the scene, **DVIEW would sometimes provide camera angles that were incorrect.** It is not possible to rotate the camera upside down, or invert, in DVIEW. The DVIEW camera is always upright. However, if the 'points' are typed in, recording the camera angles, DVIEW will provide you with camera angles that are upside down. The result is a scene that does not appear as it does in DVIEW. The solution is to slightly alter the camera angle when typing in 'camera angles'. This will flip the camera upright and provide the appropriate view point. This problem is illustrated in the following picture. The z axis is coming out of the page. The inverted camera position is when the camera angles must be modified slightly in DVIEW.



Also, remember to type 'distance' when using DVIEW to see the appropriate view of the scene. You must make sure the zoom is correct. Otherwise, the field of view will not be correct. As a final note, the field of view in DVIEW is smaller than in the DIRSIG rendering. As a result, you will see more in the DIRSIG output than what you thought when the parameters were selected in DVIEW.

Converting to DIRSIG format: Make sure that the -c option is used when building a complex scene that has facets that are noncoplanar. The -c option will break the facet up into two triangular facets. The division of the facet seemed random and was difficult to predict within AutoCad. It may be necessary to create only triangular facets when doing objects such as terrain to avoid having to convert the facets. In addition, this increases the number of facets in the scene and should be considered if one is close the maximum number of allowable facets because of memory limitations. This became a key consideration when drawing the trees. All trees were made of triangular facets to avoid problems when rotating or scaling a tree which could make a 4 sided facet noncoplanar.

Problems: The scene that I created must be converted from AutoCad format to DIRSIG format using translate. In addition, the DONORMS feature that has been added to AutoCad will not work with the scene that I created. If you want to put a new building into the scene or modify the normals of an existing part, you must do it manually. **The automated DONORMS feature is not compatible with translate.**

Hopefully, these notes will make it easier for those using the scene that we created easier to use and help future people using DIRSIG to develop scenes.

Using the Scene

These notes are for those people using the Hawkeye scene. They may be a little cryptic, but they are only meant for people experienced in the use of DIRSIG.

Weather files: Several weather files were created during this validation. They are referred to in a specified manner. The date that the weather file is valid is listed first. The 10 November 1991 data was cold, -5°C, clear, and calm. The 12 October 1995 data was warm, 26°C, clear, and calm. The exact format of the weather files is found in the DIRSIG User's Manual or Tutorial.

10nov_hawkeye_optimum.wth
10nov_hawkeye_generic.wth
12oct_hawkeye_generic.wth

Radiance files: These are the outputs from Modtran, based on the card deck and the scene node file. Any time that the scene node file is changed, the radiance file must be recreated. This includes changes in the imaging time, wavelength increments, or altitude. As an additional area of concern, the radiance file must be referenced when creating the sensor responsivity file. The sensor responsivity file must match the wavelengths for which the radiance data is generated. The radiance is not in equal wavelengths, but equal wavenumbers.

Errors sometime occur from the radiance file if the incremental angle for the sensor field of view does not closely fall near the maximum field of view angle. To solve this problem, the field of view within the *.snd file must be fixed. Simply increase or decrease the field of view angles so that the maximum value falls at a field of view increment. The easiest thing to do is use whole numbers and increase the minimum, maximum, or both field of view angles to achieve a whole number of increments. For example, if the field of view angles are -4.0 and 43.0, increase the angles to -4.0 and 44.0. Then, use an incremental angle of 4, 6, or 8. This will eliminate the problem.

GDB: When creating scenes, it is sometimes best to create smaller GDB files that only contain the regions that are field of view. This greatly reduces the run times of DIRSIG. For example, the Inframetrics Hawkeye scene only contained regions 23, 24, 33, 34, 43, and 44. This reduced the size of the GDB by more than 1/2. In addition, it is sometimes best to create the scene without the use of the trees. Simply do not include the tree references in the scene script file if they are not needed.

Because Jim Salicain's Hawkeye building was not rebuilt, it was necessary to modify the GDB file after the translation. The temperature of the concrete tower had to be reduced. The concrete tower was set to 350° and needs to be changed so that THERM calculates the temperature (there are 128 substitutions). Within vi, type the following command:

`:%s/^350$/-1/gc`

The temperature of the vent in Hawkeye also needed to be changed. It was set to 320° but should be calculated by THERM. Within vi, type the following command:

```
:%s/^320$/-1/gc
```

The roof of Hawkeye also had to be modified because one the material attributes was assigned incorrectly. The material should be roof gravel, but it was assigned concrete. In vi, do a search:

```
:/BLDG12_10
```

This facet's material ID number needs to be changed from 6 to 12.

Batch files: Batch files were used to run all DIRSIG scenes. Within the batch files, the reference files needed to run DIRSIG are defined. These were all established using absolute paths. If the directories are moved around, the batch files must be modified.

Radiosonde data: This information was obtained from actual data. It should not have to be modified. The radiosonde data is corrected for local surface conditions at the imaging time.

Scene node file: Various scene node files were created for use with the DIRSIG scene. These are all listed later. Remember that any change in the scene node file requires rebuilding the radiance. If the field of view is too large or too small, the focal length of the camera can be changed within the *.adv files. Changing the focal length does not require a change in the scene node file or the radiance file. Also, remember to choose the field of view angles to prevent problems with the radiance file.

AutoCad view file: The AutoCad view files contained the camera point, targets points, and camera angles for various Hawkeye scenes. The resolution of the DIRSIG scene is also contained in this file. The resolution can be changed without affecting any other DIRSIG input files. The AutoCad view files that were used in the validation are listed later.

Line Scanner files: The line scanner requires more inputs than the pinhole camera; the platform specification, motion profile, and modeling files are all needed. Because the sensor geometry effects have not been fully incorporated into DIRSIG, a special version was created for the validation. There was a problem getting the appropriate field of view and resolution using the actual motion profile data. Therefore, a simple motion profile was created. In order to determine the resolution, speed of the plane, and scan rate, some simple equations and knowledge of the scene were required.

The first step is to determine the desired resolution. In the validation, a 512x512 image was created. Then, figure out the ground distance that this resolution must cover. For the entire scene, this distance is approximately 3500 ft (see the drawing on the next page for more information). Convert this distance into meters and divide by the speed of the plane. The speed of the plane should be the actual speed of the plane in m/s or an arbitrary value can be used if necessary. The speed of the plane is a constant that is used

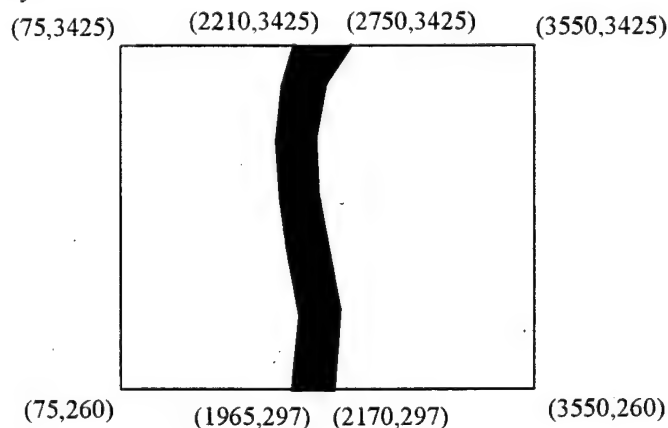
to determine the other values. Therefore, any reasonable value can be chosen. The result is a time to cover the ground distance. Divide this time by the desired resolution (512). This provides the time per scan. The inverse of this number is the scan rate needed in the DIRSIG files.

Required Values: Desired resolution in flight path direction (pixels)
 Speed of Plane (m/s)
 Ground Distance (m)

Calculated Values: Ground Distance (ft) \Rightarrow Ground Distance (m)
 Ground Distance (m)/Speed of Plane (m/s) \Rightarrow Total Flight Time (s)
 Total Flight Time (s)/Resolution (pixels) \Rightarrow Time per pixel (s)
 1/Time per pixel (s) \Rightarrow Scan Rate

The other parameters, focal length and scanner duty cycle are taken from the actual Bendix Line Scanner. The other input files are essentially the same as the pinhole camera. The AutoCad dview file provides the center points for the line scanner. It should be selected the same as one would do for the pinhole camera. Although, the field of view will be larger with the line scanner. In addition, the focal length in the AutoCad dview file is replaced with the data from the line scanner files. Hopefully, this provides a little documentation to obtaining an image using the line scanner.

AutoCad Drawings: There are numerous AutoCad drawings used in the creation of the scene. These drawings should not have to be altered. The only thing that might be required is the changing of the material assigned to a facet. This can be accomplished using the pick routine. The facet normals should not have to be modified, but if they do, using the old DIRSIG routines. The new addnorms feature does not work with the old translate. The drawing below shows the approximate coordinates of the AutoCad scene. This is especially useful when using the line scanner and determining ground resolution of the DIRSIG imagery.



Appendix D

Material Files

Generic

Optimum

Angular Emissivity Factor

```
#
# FILE TYPE:      DIRSIG Materials file
# CREATEOR:      'convert_materials' utility
# DATE:          Wed Oct 4 12:37:27 EDT 1995
# NOTES: Entries can be arranged in any order
#              Tags within any entry can be in any order
#              A minimal set of tags are required (see below)
#
```

```
# Required Tags:
# MATERIAL_ENTRY_BEGIN      start an entry
# MATERIAL_NAME             name of the material
# MATERIAL_ID               #ID of the material
# SPECIFIC_HEAT             specific heat
# THERMAL_CONDUCTIVITY      thermal conductivity
# MASS_DENSITY              mass density
# SPECULARITY               specularity of the material surface
#                           0.0 = 100% diffuse and 1.0 = 100% specular
# VISIBLE_EMISSIVITY        solar/incident emissivity
# THERMAL_EMISSIVITY        thermal/exit emissivity
# EXPOSED_AREA              DCS/THERM surface area term
# OPTICAL_DESCRIPTION        OPAQUE, UNIFORM_TRANSMISSION, or
#                           NONUNIFORM_TRANSMISSION
# EMISSIVITY_FILE           name of emissivity file
# MATERIAL_ENTRY_END        end of entry
```

```
# Optional/Additional Tags:
# EXTINCTION_FILE           extinction file -- required for transmission
# TEXTURE_FILE              name DIRSIG Texture Image file for material
# USE_GAUSSIAN_TEXTURE      flag to generate gaussian texture
#                           (default is FALSE)
#
```

```
# New material organization and development for Hawkeye scene
```

``` # ----- # Building Construction Materials # ----- ```

```
MATERIAL_ENTRY_BEGIN
MATERIAL_NAME = roof_aluminum
MATERIAL_ID = 50
SPECIFIC_HEAT = 0.55
THERMAL_CONDUCTIVITY = 1909
MASS_DENSITY = 1.00
SPECULARITY = 0.30
VISIBLE_EMISSIVITY = 0.5
THERMAL_EMISSIVITY = 0.72
EXPOSED_AREA = -0.4
THICKNESS = 0.275
OPTICAL_DESCRIPTION = OPAQUE
EMISSIVITY_FILE = roof_aluminum.ems
EXTINCTION_FILE =
TEXTURE_FILE =
USE_GAUSSIAN_TEXTURE = FALSE
MATERIAL_ENTRY_END
```

```
MATERIAL_ENTRY_BEGIN
MATERIAL_NAME = roof_gravel
MATERIAL_ID = 12
SPECIFIC_HEAT = 0.35
THERMAL_CONDUCTIVITY = 12.1
MASS_DENSITY = 1.00
SPECULARITY = 0.30
VISIBLE_EMISSIVITY = 0.80
THERMAL_EMISSIVITY = 0.90
EXPOSED_AREA = -0.5
THICKNESS = 6.00
OPTICAL_DESCRIPTION = OPAQUE
EMISSIVITY_FILE = roof_gravel.ems
EXTINCTION_FILE =
TEXTURE_FILE =
USE_GAUSSIAN_TEXTURE = FALSE
MATERIAL_ENTRY_END
```

```
MATERIAL_ENTRY_BEGIN
MATERIAL_NAME = roof_steel
MATERIAL_ID = 52
SPECIFIC_HEAT = 0.825
THERMAL_CONDUCTIVITY = 511.5
MASS_DENSITY = 1.00
SPECULARITY = 0.30
VISIBLE_EMISSIVITY = 0.825
THERMAL_EMISSIVITY = 0.79
EXPOSED_AREA = -0.4
THICKNESS = 0.4
OPTICAL_DESCRIPTION = OPAQUE
EMISSIVITY_FILE = roof_steel.ems
EXTINCTION_FILE =
TEXTURE_FILE =
USE_GAUSSIAN_TEXTURE = FALSE
MATERIAL_ENTRY_END
```

```
MATERIAL_ENTRY_BEGIN
MATERIAL_NAME = wall_concrete
MATERIAL_ID = 53
SPECIFIC_HEAT = 0.3105
THERMAL_CONDUCTIVITY = 15.48
MASS_DENSITY = 1.00
SPECULARITY = 0.30
VISIBLE_EMISSIVITY = 0.725
THERMAL_EMISSIVITY = 0.925
EXPOSED_AREA = -0.5
THICKNESS = 6.0
OPTICAL_DESCRIPTION = OPAQUE
EMISSIVITY_FILE = wall_concrete.ems
EXTINCTION_FILE =
TEXTURE_FILE =
USE_GAUSSIAN_TEXTURE = FALSE
MATERIAL_ENTRY_END
```

```
MATERIAL_ENTRY_BEGIN
MATERIAL_NAME = window_glass
MATERIAL_ID = 54
SPECIFIC_HEAT = 0.3505
THERMAL_CONDUCTIVITY = 12.0
MASS_DENSITY = 1.00
SPECULARITY = 0.30
VISIBLE_EMISSIVITY = 0.7
THERMAL_EMISSIVITY = 0.87
EXPOSED_AREA = -0.4
THICKNESS = 0.525
OPTICAL_DESCRIPTION = OPAQUE
EMISSIVITY_FILE = window_glass.ems
EXTINCTION_FILE =
TEXTURE_FILE =
USE_GAUSSIAN_TEXTURE = FALSE
MATERIAL_ENTRY_END
```

```
MATERIAL_ENTRY_BEGIN
MATERIAL_NAME = roof_asphalt_shingles_color
MATERIAL_ID = 60
SPECIFIC_HEAT = 0.3575
THERMAL_CONDUCTIVITY = 6.145
MASS_DENSITY = 1.00
SPECULARITY = 0.10
VISIBLE_EMISSIVITY = 0.73
THERMAL_EMISSIVITY = .91
EXPOSED_AREA = -0.4
THICKNESS = 0.85
OPTICAL_DESCRIPTION = OPAQUE
EMISSIVITY_FILE = roof_asphalt_shingles_color.ems
EXTINCTION_FILE =
TEXTURE_FILE =
USE_GAUSSIAN_TEXTURE = FALSE
MATERIAL_ENTRY_END
```

MATERIAL_ENTRY_BEGIN
 MATERIAL_NAME = roof_asphalt_shingles_color
 MATERIAL_ID = 61
 SPECIFIC_HEAT = 0.3575
 THERMAL_CONDUCTIVITY = 6.145
 MASS_DENSITY = 1.00
 SPECULARITY = 0.10
 VISIBLE_EMISSIVITY = 0.76
 THERMAL_EMISSIVITY = .91
 EXPOSED_AREA = -0.4
 THICKNESS = 0.85
 OPTICAL_DESCRIPTION = OPAQUE
 EMISSIVITY_FILE = roof_asphalt_shingles_color.ems
 EXTINCTION_FILE =
 TEXTURE_FILE =
 USE_GAUSSIAN_TEXTURE = FALSE
 MATERIAL_ENTRY_END

MATERIAL_ENTRY_BEGIN
 MATERIAL_NAME = roof_asphalt_shingles_color
 MATERIAL_ID = 62
 SPECIFIC_HEAT = 0.3575
 THERMAL_CONDUCTIVITY = 6.145
 MASS_DENSITY = 1.000
 SPECULARITY = 0.10
 VISIBLE_EMISSIVITY = 0.78
 THERMAL_EMISSIVITY = .91
 EXPOSED_AREA = -0.4
 THICKNESS = 0.85
 OPTICAL_DESCRIPTION = OPAQUE
 EMISSIVITY_FILE = roof_asphalt_shingles_color.ems
 EXTINCTION_FILE =
 TEXTURE_FILE =
 USE_GAUSSIAN_TEXTURE = FALSE
 MATERIAL_ENTRY_END

MATERIAL_ENTRY_BEGIN
 MATERIAL_NAME = roof_asphalt_shingles_color
 MATERIAL_ID = 63
 SPECIFIC_HEAT = 0.3575
 THERMAL_CONDUCTIVITY = 6.145
 MASS_DENSITY = 1.00
 SPECULARITY = 0.10
 VISIBLE_EMISSIVITY = 0.81
 THERMAL_EMISSIVITY = .91
 EXPOSED_AREA = -0.4
 THICKNESS = 0.85
 OPTICAL_DESCRIPTION = OPAQUE
 EMISSIVITY_FILE = roof_asphalt_shingles_color.ems
 EXTINCTION_FILE =
 TEXTURE_FILE =
 USE_GAUSSIAN_TEXTURE = FALSE
 MATERIAL_ENTRY_END

MATERIAL_ENTRY_BEGIN
 MATERIAL_NAME = roof_asphalt_shingles_color
 MATERIAL_ID = 64
 SPECIFIC_HEAT = 0.3575
 THERMAL_CONDUCTIVITY = 6.145
 MASS_DENSITY = 1.000
 SPECULARITY = 0.10
 VISIBLE_EMISSIVITY = 0.83
 THERMAL_EMISSIVITY = .91
 EXPOSED_AREA = -0.4
 THICKNESS = 0.85
 OPTICAL_DESCRIPTION = OPAQUE
 EMISSIVITY_FILE = roof_asphalt_shingles_color.ems
 EXTINCTION_FILE =
 TEXTURE_FILE =
 USE_GAUSSIAN_TEXTURE = FALSE
 MATERIAL_ENTRY_END

MATERIAL_ENTRY_BEGIN
 MATERIAL_NAME = roof_asphalt_shingles_color
 MATERIAL_ID = 65
 SPECIFIC_HEAT = 0.3575
 THERMAL_CONDUCTIVITY = 6.145
 MASS_DENSITY = 1.000
 SPECULARITY = 0.10
 VISIBLE_EMISSIVITY = 0.86
 THERMAL_EMISSIVITY = .91
 EXPOSED_AREA = -0.4
 THICKNESS = 0.85
 OPTICAL_DESCRIPTION = OPAQUE
 EMISSIVITY_FILE = roof_asphalt_shingles_color.ems
 EXTINCTION_FILE =
 TEXTURE_FILE =
 USE_GAUSSIAN_TEXTURE = FALSE
 MATERIAL_ENTRY_END

MATERIAL_ENTRY_BEGIN
 MATERIAL_NAME = roof_asphalt_shingles_color
 MATERIAL_ID = 66
 SPECIFIC_HEAT = 0.3575
 THERMAL_CONDUCTIVITY = 6.145
 MASS_DENSITY = 1.000
 SPECULARITY = 0.10
 VISIBLE_EMISSIVITY = 0.89
 THERMAL_EMISSIVITY = .91
 EXPOSED_AREA = -0.4
 THICKNESS = 0.85
 OPTICAL_DESCRIPTION = OPAQUE
 EMISSIVITY_FILE = roof_asphalt_shingles_color.ems
 EXTINCTION_FILE =
 TEXTURE_FILE =
 USE_GAUSSIAN_TEXTURE = FALSE
 MATERIAL_ENTRY_END

MATERIAL_ENTRY_BEGIN
 MATERIAL_NAME = roof_asphalt_shingles_color
 MATERIAL_ID = 67
 SPECIFIC_HEAT = 0.3575
 THERMAL_CONDUCTIVITY = 6.145
 MASS_DENSITY = 1.000
 SPECULARITY = 0.10
 VISIBLE_EMISSIVITY = 0.91
 THERMAL_EMISSIVITY = .91
 EXPOSED_AREA = -0.4
 THICKNESS = 0.85
 OPTICAL_DESCRIPTION = OPAQUE
 EMISSIVITY_FILE = roof_asphalt_shingles_color.ems
 EXTINCTION_FILE =
 TEXTURE_FILE =
 USE_GAUSSIAN_TEXTURE = FALSE
 MATERIAL_ENTRY_END

MATERIAL_ENTRY_BEGIN
 MATERIAL_NAME = roof_asphalt_shingles_color
 MATERIAL_ID = 68
 SPECIFIC_HEAT = 0.3575
 THERMAL_CONDUCTIVITY = 6.145
 MASS_DENSITY = 1.00
 SPECULARITY = 0.10
 VISIBLE_EMISSIVITY = 0.93
 THERMAL_EMISSIVITY = .91
 EXPOSED_AREA = -0.4
 THICKNESS = 0.85
 OPTICAL_DESCRIPTION = OPAQUE
 EMISSIVITY_FILE = roof_asphalt_shingles_color.ems
 EXTINCTION_FILE =
 TEXTURE_FILE =
 USE_GAUSSIAN_TEXTURE = FALSE
 MATERIAL_ENTRY_END

MATERIAL_ENTRY_BEGIN
 MATERIAL_NAME = roof_asphalt_shingles_color
 MATERIAL_ID = 69
 SPECIFIC_HEAT = 0.3575
 THERMAL_CONDUCTIVITY = 6.145
 MASS_DENSITY = 1.000
 SPECULARITY = 0.10
 VISIBLE_EMISSIVITY = 0.95
 THERMAL_EMISSIVITY = .91
 EXPOSED_AREA = -0.4
 THICKNESS = 0.85
 OPTICAL_DESCRIPTION = OPAQUE
 EMISSIVITY_FILE = roof_asphalt_shingles_color.ems
 EXTINCTION_FILE =
 TEXTURE_FILE =
 USE_GAUSSIAN_TEXTURE = FALSE
 MATERIAL_ENTRY_END

MATERIAL_ENTRY_BEGIN
 MATERIAL_NAME = wall_brick_color
 MATERIAL_ID = 70
 SPECIFIC_HEAT = 0.2818
 THERMAL_CONDUCTIVITY = 5.935
 MASS_DENSITY = 1.0
 SPECULARITY = 0.10
 VISIBLE_EMISSIVITY = 0.65
 THERMAL_EMISSIVITY = .93
 EXPOSED_AREA = -0.4
 THICKNESS = 10.0
 OPTICAL_DESCRIPTION = OPAQUE
 EMISSIVITY_FILE = wall_brick_color.ems
 EXTINCTION_FILE =
 TEXTURE_FILE =
 USE_GAUSSIAN_TEXTURE = FALSE
 MATERIAL_ENTRY_END

```

MATERIAL_ENTRY_BEGIN
MATERIAL_NAME = wall_brick_color
MATERIAL_ID = 75
SPECIFIC_HEAT = 0.2818
THERMAL_CONDUCTIVITY = 5.935
MASS_DENSITY = 1.0
SPECULARITY = 0.10
VISIBLE_EMISSIVITY = 0.8
THERMAL_EMISSIVITY = .93
EXPOSED_AREA = -0.4
THICKNESS = 10.0
OPTICAL_DESCRIPTION = OPAQUE
EMISSIVITY_FILE = wall_brick_color.ems
EXTINCTION_FILE =
TEXTURE_FILE =
USE_GAUSSIAN_TEXTURE = FALSE
MATERIAL_ENTRY_END

```

```

MATERIAL_ENTRY_BEGIN
MATERIAL_NAME = wall_brick_hawk_red
MATERIAL_ID = 90
SPECIFIC_HEAT = 0.2818
THERMAL_CONDUCTIVITY = 5.935
MASS_DENSITY = 1.0
SPECULARITY = 0.10
VISIBLE_EMISSIVITY = 0.92
THERMAL_EMISSIVITY = .93
EXPOSED_AREA = -0.4
THICKNESS = 10.0
OPTICAL_DESCRIPTION = OPAQUE
EMISSIVITY_FILE = wall_brick_color.ems
EXTINCTION_FILE =
TEXTURE_FILE =
USE_GAUSSIAN_TEXTURE = FALSE
MATERIAL_ENTRY_END

```

MATERIAL_ENTRY_BEGIN
 MATERIAL_NAME = wall_brick_hawk_cream
 MATERIAL_ID = 15
 SPECIFIC_HEAT = 0.2818
 THERMAL_CONDUCTIVITY = 5.935
 MASS_DENSITY = 1.0
 SPECULARITY = 0.10
 VISIBLE_EMISSIVITY = 0.92
 THERMAL_EMISSIVITY = .93
 EXPOSED_AREA = -0.4
 THICKNESS = 10.0
 OPTICAL_DESCRIPTION = OPAQUE
 EMISSIVITY_FILE = wall_brick_color.ems
 EXTINCTION_FILE =
 TEXTURE_FILE =
 USE_GAUSSIAN_TEXTURE = FALSE
 MATERIAL_ENTRY_END

MATERIAL_ENTRY_BEGIN
 MATERIAL_NAME = wall_brick_hawk_church
 MATERIAL_ID = 92
 SPECIFIC_HEAT = 0.2818
 THERMAL_CONDUCTIVITY = 5.935
 MASS_DENSITY = 1.0
 SPECULARITY = 0.10
 VISIBLE_EMISSIVITY = 0.92
 THERMAL_EMISSIVITY = .93
 EXPOSED_AREA = -0.4
 THICKNESS = 10.0
 OPTICAL_DESCRIPTION = OPAQUE
 EMISSIVITY_FILE = wall_brick_color.ems
 EXTINCTION_FILE =
 TEXTURE_FILE =
 USE_GAUSSIAN_TEXTURE = FALSE
 MATERIAL_ENTRY_END

MATERIAL_ENTRY_BEGIN
 MATERIAL_NAME = wall_wood_color
 MATERIAL_ID = 80
 SPECIFIC_HEAT = 0.5124
 THERMAL_CONDUCTIVITY = 0.98
 MASS_DENSITY = 1.0
 SPECULARITY = 0.15
 VISIBLE_EMISSIVITY = 0.7
 THERMAL_EMISSIVITY = 0.865
 EXPOSED_AREA = -0.4
 THICKNESS = 4.5
 OPTICAL_DESCRIPTION = OPAQUE
 EMISSIVITY_FILE = wall_wood_color.ems
 EXTINCTION_FILE =
 TEXTURE_FILE =
 USE_GAUSSIAN_TEXTURE = FALSE
 MATERIAL_ENTRY_END

MATERIAL_ENTRY_BEGIN
 MATERIAL_NAME = wall_wood_color
 MATERIAL_ID = 81
 SPECIFIC_HEAT = 0.5124
 THERMAL_CONDUCTIVITY = 0.98
 MASS_DENSITY = 1.0
 SPECULARITY = 0.15
 VISIBLE_EMISSIVITY = 0.72
 THERMAL_EMISSIVITY = 0.865
 EXPOSED_AREA = -0.4
 THICKNESS = 4.5
 OPTICAL_DESCRIPTION = OPAQUE
 EMISSIVITY_FILE = wall_wood_color.ems
 EXTINCTION_FILE =
 TEXTURE_FILE =
 USE_GAUSSIAN_TEXTURE = FALSE
 MATERIAL_ENTRY_END

MATERIAL_ENTRY_BEGIN
 MATERIAL_NAME = wall_wood_color
 MATERIAL_ID = 82
 SPECIFIC_HEAT = 0.5124
 THERMAL_CONDUCTIVITY = 0.98
 MASS_DENSITY = 1.0
 SPECULARITY = 0.15
 VISIBLE_EMISSIVITY = 0.74
 THERMAL_EMISSIVITY = 0.865
 EXPOSED_AREA = -0.4
 THICKNESS = 4.5
 OPTICAL_DESCRIPTION = OPAQUE
 EMISSIVITY_FILE = wall_wood_color.ems
 EXTINCTION_FILE =
 TEXTURE_FILE =
 USE_GAUSSIAN_TEXTURE = FALSE
 MATERIAL_ENTRY_END

MATERIAL_ENTRY_BEGIN
 MATERIAL_NAME = wall_wood_color
 MATERIAL_ID = 83
 SPECIFIC_HEAT = 0.5124
 THERMAL_CONDUCTIVITY = 0.98
 MASS_DENSITY = 1.0
 SPECULARITY = 0.15
 VISIBLE_EMISSIVITY = 0.76
 THERMAL_EMISSIVITY = 0.865
 EXPOSED_AREA = -0.4
 THICKNESS = 4.5
 OPTICAL_DESCRIPTION = OPAQUE
 EMISSIVITY_FILE = wall_wood_color.ems
 EXTINCTION_FILE =
 TEXTURE_FILE =
 USE_GAUSSIAN_TEXTURE = FALSE
 MATERIAL_ENTRY_END

MATERIAL_ENTRY_BEGIN
 MATERIAL_NAME = wall_wood_color
 MATERIAL_ID = 84
 SPECIFIC_HEAT = 0.5124
 THERMAL_CONDUCTIVITY = 0.98
 MASS_DENSITY = 1.0
 SPECULARITY = 0.15
 VISIBLE_EMISSIVITY = 0.78
 THERMAL_EMISSIVITY = 0.865
 EXPOSED_AREA = -0.4
 THICKNESS = 4.5
 OPTICAL_DESCRIPTION = OPAQUE
 EMISSIVITY_FILE = wall_wood_color.ems
 EXTINCTION_FILE =
 TEXTURE_FILE =
 USE_GAUSSIAN_TEXTURE = FALSE
 MATERIAL_ENTRY_END

MATERIAL_ENTRY_BEGIN
 MATERIAL_NAME = wall_wood_color
 MATERIAL_ID = 85
 SPECIFIC_HEAT = 0.5124
 THERMAL_CONDUCTIVITY = 0.98
 MASS_DENSITY = 1.0
 SPECULARITY = 0.15
 VISIBLE_EMISSIVITY = 0.80
 THERMAL_EMISSIVITY = 0.865
 EXPOSED_AREA = -0.4
 THICKNESS = 4.5
 OPTICAL_DESCRIPTION = OPAQUE
 EMISSIVITY_FILE = wall_wood_color.ems
 EXTINCTION_FILE =
 TEXTURE_FILE =
 USE_GAUSSIAN_TEXTURE = FALSE
 MATERIAL_ENTRY_END

MATERIAL_ENTRY_BEGIN
 MATERIAL_NAME = wall_wood_color
 MATERIAL_ID = 86
 SPECIFIC_HEAT = 0.5124
 THERMAL_CONDUCTIVITY = 0.98
 MASS_DENSITY = 1.0
 SPECULARITY = 0.15
 VISIBLE_EMISSIVITY = 0.82
 THERMAL_EMISSIVITY = 0.865
 EXPOSED_AREA = -0.4
 THICKNESS = 4.5
 OPTICAL_DESCRIPTION = OPAQUE
 EMISSIVITY_FILE = wall_wood_color.ems
 EXTINCTION_FILE =
 TEXTURE_FILE =
 USE_GAUSSIAN_TEXTURE = FALSE
 MATERIAL_ENTRY_END

MATERIAL_ENTRY_BEGIN
 MATERIAL_NAME = wall_wood_color
 MATERIAL_ID = 87
 SPECIFIC_HEAT = 0.5124
 THERMAL_CONDUCTIVITY = 0.98
 MASS_DENSITY = 1.0
 SPECULARITY = 0.15
 VISIBLE_EMISSIVITY = 0.84
 THERMAL_EMISSIVITY = 0.865
 EXPOSED_AREA = -0.4
 THICKNESS = 4.5
 OPTICAL_DESCRIPTION = OPAQUE
 EMISSIVITY_FILE = wall_wood_color.ems
 EXTINCTION_FILE =
 TEXTURE_FILE =
 USE_GAUSSIAN_TEXTURE = FALSE
 MATERIAL_ENTRY_END

MATERIAL_ENTRY_BEGIN
 MATERIAL_NAME = wall_wood_color
 MATERIAL_ID = 88
 SPECIFIC_HEAT = 0.5124
 THERMAL_CONDUCTIVITY = 0.98
 MASS_DENSITY = 1.0
 SPECULARITY = 0.15
 VISIBLE_EMISSIVITY = 0.86
 THERMAL_EMISSIVITY = 0.865
 EXPOSED_AREA = -0.4
 THICKNESS = 4.5
 OPTICAL_DESCRIPTION = OPAQUE
 EMISSIVITY_FILE = wall_wood_color.ems
 EXTINCTION_FILE =
 TEXTURE_FILE =
 USE_GAUSSIAN_TEXTURE = FALSE
 MATERIAL_ENTRY_END

MATERIAL_ENTRY_BEGIN
 MATERIAL_NAME = wall_wood_color
 MATERIAL_ID = 89
 SPECIFIC_HEAT = 0.5124
 THERMAL_CONDUCTIVITY = 0.98
 MASS_DENSITY = 1.0
 SPECULARITY = 0.15
 VISIBLE_EMISSIVITY = 0.88
 THERMAL_EMISSIVITY = 0.865
 EXPOSED_AREA = -0.4
 THICKNESS = 4.5
 OPTICAL_DESCRIPTION = OPAQUE
 EMISSIVITY_FILE = wall_wood_color.ems
 EXTINCTION_FILE =
 TEXTURE_FILE =
 USE_GAUSSIAN_TEXTURE = FALSE
 MATERIAL_ENTRY_END

#-----
 # Soils/Water Materials
 #-----

MATERIAL_ENTRY_BEGIN
 MATERIAL_NAME = soil_clay_gray
 MATERIAL_ID = 40
 SPECIFIC_HEAT = .3202
 THERMAL_CONDUCTIVITY = 4.162
 MASS_DENSITY = 1.00
 SPECULARITY = 0.0
 VISIBLE_EMISSIVITY = 0.795
 THERMAL_EMISSIVITY = 0.965
 EXPOSED_AREA = -0.3
 THICKNESS = 9.85
 OPTICAL_DESCRIPTION = OPAQUE
 EMISSIVITY_FILE = soil_clay_gray.ems
 EXTINCTION_FILE =
 TEXTURE_FILE =
 USE_GAUSSIAN_TEXTURE = FALSE
 MATERIAL_ENTRY_END

MATERIAL_ENTRY_BEGIN
 MATERIAL_NAME = soil_clay_red
 MATERIAL_ID = 41
 SPECIFIC_HEAT = 0.3202
 THERMAL_CONDUCTIVITY = 4.162
 MASS_DENSITY = 1.0
 SPECULARITY = 0.0
 VISIBLE_EMISSIVITY = 0.825
 THERMAL_EMISSIVITY = 0.95
 EXPOSED_AREA = -0.25
 THICKNESS = 9.85
 OPTICAL_DESCRIPTION = OPAQUE
 EMISSIVITY_FILE = soil_clay_red.ems
 EXTINCTION_FILE =
 TEXTURE_FILE =
 USE_GAUSSIAN_TEXTURE = FALSE
 MATERIAL_ENTRY_END

MATERIAL_ENTRY_BEGIN
 MATERIAL_NAME = soil_dirt_brown
 MATERIAL_ID = 13
 SPECIFIC_HEAT = 0.3222
 THERMAL_CONDUCTIVITY = 6.117
 MASS_DENSITY = 1.0
 SPECULARITY = 0.0
 VISIBLE_EMISSIVITY = 0.825
 THERMAL_EMISSIVITY = 0.925
 EXPOSED_AREA = -0.25
 THICKNESS = 9.85
 OPTICAL_DESCRIPTION = OPAQUE
 EMISSIVITY_FILE = soil_dirt_brown.ems
 EXTINCTION_FILE =
 TEXTURE_FILE =
 USE_GAUSSIAN_TEXTURE = FALSE
 MATERIAL_ENTRY_END

MATERIAL_ENTRY_BEGIN
 MATERIAL_NAME = soil_gravel_light_brown
 MATERIAL_ID = 43
 SPECIFIC_HEAT = 0.41
 THERMAL_CONDUCTIVITY = 10.76
 MASS_DENSITY = 1.0
 SPECULARITY = 0.0
 VISIBLE_EMISSIVITY = 0.85
 THERMAL_EMISSIVITY = 0.915
 EXPOSED_AREA = -0.25
 THICKNESS = 9.85
 OPTICAL_DESCRIPTION = OPAQUE
 EMISSIVITY_FILE = soil_gravel_light_brown
 EXTINCTION_FILE =
 TEXTURE_FILE =
 USE_GAUSSIAN_TEXTURE = FALSE
 MATERIAL_ENTRY_END

MATERIAL_ENTRY_BEGIN
 MATERIAL_NAME = water_genesee_river
 MATERIAL_ID = 2
 SPECIFIC_HEAT = 0.9841
 THERMAL_CONDUCTIVITY = 5.1
 MASS_DENSITY = 1.0
 SPECULARITY = 0.0
 VISIBLE_EMISSIVITY = 0.98
 THERMAL_EMISSIVITY = 0.975
 EXPOSED_AREA = -0.5
 THICKNESS = 5.1
 OPTICAL_DESCRIPTION = OPAQUE
 EMISSIVITY_FILE = water_genesee_river.ems
 EXTINCTION_FILE =
 TEXTURE_FILE =
 USE_GAUSSIAN_TEXTURE = FALSE
 MATERIAL_ENTRY_END

#-----
 # Surface Construction Materials
 #-----

MATERIAL_ENTRY_BEGIN
 MATERIAL_NAME = asphalt_parking_dark
 MATERIAL_ID = 30
 SPECIFIC_HEAT = 0.36254
 THERMAL_CONDUCTIVITY = 9.243
 MASS_DENSITY = 1.0
 SPECULARITY = 0.1
 VISIBLE_EMISSIVITY = 0.91
 THERMAL_EMISSIVITY = 0.955
 EXPOSED_AREA = -0.25
 THICKNESS = 9.55
 OPTICAL_DESCRIPTION = OPAQUE
 EMISSIVITY_FILE = asphalt_parking_dark.ems
 EXTINCTION_FILE =
 TEXTURE_FILE =
 USE_GAUSSIAN_TEXTURE = FALSE
 MATERIAL_ENTRY_END

MATERIAL_ENTRY_BEGIN
 MATERIAL_NAME = asphalt_parking_old
 MATERIAL_ID = 31
 SPECIFIC_HEAT = 0.36254
 THERMAL_CONDUCTIVITY = 9.243
 MASS_DENSITY = 1.0
 SPECULARITY = 0.1
 VISIBLE_EMISSIVITY = 0.775
 THERMAL_EMISSIVITY = 0.955
 EXPOSED_AREA = -0.25
 THICKNESS = 9.55
 OPTICAL_DESCRIPTION = OPAQUE
 EMISSIVITY_FILE = asphalt_parking_old.ems
 EXTINCTION_FILE =
 TEXTURE_FILE =
 USE_GAUSSIAN_TEXTURE = FALSE
 MATERIAL_ENTRY_END

MATERIAL_ENTRY_BEGIN
 MATERIAL_NAME = asphalt_street
 MATERIAL_ID = 5
 SPECIFIC_HEAT = 0.36254
 THERMAL_CONDUCTIVITY = 9.243
 MASS_DENSITY = 1.0
 SPECULARITY = 0.1
 VISIBLE_EMISSIVITY = 0.86
 THERMAL_EMISSIVITY = 0.955
 EXPOSED_AREA = -0.25
 THICKNESS = 9.55
 OPTICAL_DESCRIPTION = OPAQUE
 EMISSIVITY_FILE = asphalt_street.ems
 EXTINCTION_FILE =
 TEXTURE_FILE =
 USE_GAUSSIAN_TEXTURE = FALSE
 MATERIAL_ENTRY_END

MATERIAL_ENTRY_BEGIN
 MATERIAL_NAME = concrete_sidewalk
 MATERIAL_ID = 6
 SPECIFIC_HEAT = 0.3105
 THERMAL_CONDUCTIVITY = 15.5
 MASS_DENSITY = 1.0
 SPECULARITY = 0.1
 VISIBLE_EMISSIVITY = 0.725
 THERMAL_EMISSIVITY = 0.935
 EXPOSED_AREA = -0.25
 THICKNESS = 6.565
 OPTICAL_DESCRIPTION = OPAQUE
 EMISSIVITY_FILE = concrete_sidewalk.ems
 EXTINCTION_FILE =
 TEXTURE_FILE =
 USE_GAUSSIAN_TEXTURE = FALSE
 MATERIAL_ENTRY_END

#-----
 # Vegetation
 #-----

MATERIAL_ENTRY_BEGIN
 MATERIAL_NAME = grass
 MATERIAL_ID = 4
 SPECIFIC_HEAT = 1
 THERMAL_CONDUCTIVITY = 12.5
 MASS_DENSITY = 1.0
 SPECULARITY = 0.0
 VISIBLE_EMISSIVITY = 0.79
 THERMAL_EMISSIVITY = 0.93
 EXPOSED_AREA = -0.25
 THICKNESS = 1.275
 OPTICAL_DESCRIPTION = OPAQUE
 EMISSIVITY_FILE = grass.ems
 EXTINCTION_FILE =
 TEXTURE_FILE =
 USE_GAUSSIAN_TEXTURE = FALSE
 MATERIAL_ENTRY_END

MATERIAL_ENTRY_BEGIN
 MATERIAL_NAME = tree_deciduous
 MATERIAL_ID = 25
 SPECIFIC_HEAT = 1
 THERMAL_CONDUCTIVITY = 12.5
 MASS_DENSITY = 1.0
 SPECULARITY = 0.0
 VISIBLE_EMISSIVITY = 0.935
 THERMAL_EMISSIVITY = 0.95
 EXPOSED_AREA = -0.25
 THICKNESS = 1.0
 OPTICAL_DESCRIPTION = OPAQUE
 EMISSIVITY_FILE = tree_deciduous.ems
 EXTINCTION_FILE =
 TEXTURE_FILE =
 USE_GAUSSIAN_TEXTURE = FALSE
 MATERIAL_ENTRY_END

MATERIAL_ENTRY_BEGIN
 MATERIAL_NAME = tree_trunk
 MATERIAL_ID = 18
 SPECIFIC_HEAT = 0.429
 THERMAL_CONDUCTIVITY = 0.85
 MASS_DENSITY = 1.0
 SPECULARITY = 0.0
 VISIBLE_EMISSIVITY = 0.87
 THERMAL_EMISSIVITY = 0.955
 EXPOSED_AREA = -0.5
 THICKNESS = 0.65
 OPTICAL_DESCRIPTION = OPAQUE
 EMISSIVITY_FILE = tree_trunk.ems
 EXTINCTION_FILE =
 TEXTURE_FILE =
 USE_GAUSSIAN_TEXTURE = FALSE
 MATERIAL_ENTRY_END

Hawkeye Optimum Materials

```
# FILE TYPE:      DIRSIG Materials file
# CREATEOR:       `convert_materials' utility
# DATE            Wed Oct 4 12:37:27 EDT 1995
# NOTES: Entries can be arranged in any order
#               Tags within any entry can be in any order
#               A minimal set of tags are required (see below)
```

Required Tags:

```
# MATERIAL_ENTRY_BEGIN  start an entry
# MATERIAL_NAME          name of the material
# MATERIAL_ID            #ID of the material
# SPECIFIC_HEAT          specific heat
# THERMAL_CONDUCTIVITY   thermal conductivity
# MASS_DENSITY           mass density
# SPECULARITY            specularity of the material surface
#                       0.0 = 100% diffuse and 1.0 = 100% specular
# VISIBLE_EMISSIVITY     solar/incident emissivity
# THERMAL_EMISSIVITY     thermal/exit emissivity
# EXPOSED_AREA           DCS/THERM surface area term
# OPTICAL_DESCRIPTION    OPAQUE, UNIFORM_TRANSMISSION, or
#                       NONUNIFORM_TRANSMISSION
# EMISSIVITY_FILE        name of emissivity file
# MATERIAL_ENTRY_END     end of entry
```

Optional/Additional Tags:

```
# EXTINCTION_FILE        extinction file -- required for transmission
# TEXTURE_FILE           name DIRSIG Texture Image file for material
# USE_GAUSSIAN_TEXTURE   flag to generate gaussian texture
#                       (default is FALSE)
```

```
MATERIAL_ENTRY_BEGIN
MATERIAL_NAME = painted_steel_roof
MATERIAL_ID = 1
SPECIFIC_HEAT = 0.089
THERMAL_CONDUCTIVITY = 464.4
MASS_DENSITY = 7.8330
SPECULARITY = 0.3
VISIBLE_EMISSIVITY = 0.88
THERMAL_EMISSIVITY = 0.7
EXPOSED_AREA = -0.4
THICKNESS = 1
OPTICAL_DESCRIPTION = OPAQUE
EMISSIVITY_FILE = painted_steel_roof.ems
EXTINCTION_FILE =
TEXTURE_FILE =
USE_GAUSSIAN_TEXTURE = FALSE
MATERIAL_ENTRY_END
```

```
MATERIAL_ENTRY_BEGIN
MATERIAL_NAME = water_genesee_river
MATERIAL_ID = 2
SPECIFIC_HEAT = 0.9841
THERMAL_CONDUCTIVITY = 5.1
MASS_DENSITY = 1.0
SPECULARITY = 0.0
VISIBLE_EMISSIVITY = 0.98
THERMAL_EMISSIVITY = 0.975
EXPOSED_AREA = -0.5
THICKNESS = 5.1
OPTICAL_DESCRIPTION = OPAQUE
EMISSIVITY_FILE = water_genesee_river.ems
EXTINCTION_FILE =
TEXTURE_FILE =
USE_GAUSSIAN_TEXTURE = FALSE
MATERIAL_ENTRY_END
```

```
MATERIAL_ENTRY_BEGIN
MATERIAL_NAME = grass
MATERIAL_ID = 4
SPECIFIC_HEAT = 0.8
THERMAL_CONDUCTIVITY = 5.5
MASS_DENSITY = 1.0
SPECULARITY = 0.0
VISIBLE_EMISSIVITY = 0.79
THERMAL_EMISSIVITY = 0.94
EXPOSED_AREA = -0.27
THICKNESS = 0.05
OPTICAL_DESCRIPTION = OPAQUE
EMISSIVITY_FILE = grass.ems
EXTINCTION_FILE =
TEXTURE_FILE =
USE_GAUSSIAN_TEXTURE = FALSE
MATERIAL_ENTRY_END
```

```
MATERIAL_ENTRY_BEGIN
MATERIAL_NAME = asphalt_street
MATERIAL_ID = 5
SPECIFIC_HEAT = 0.43254
THERMAL_CONDUCTIVITY = 11.243
MASS_DENSITY = 1.0
SPECULARITY = 0.1
VISIBLE_EMISSIVITY = 0.87
THERMAL_EMISSIVITY = 0.945
EXPOSED_AREA = -0.22
THICKNESS = 7.55
OPTICAL_DESCRIPTION = OPAQUE
EMISSIVITY_FILE = asphalt_old.ems
EXTINCTION_FILE =
TEXTURE_FILE =
USE_GAUSSIAN_TEXTURE = FALSE
MATERIAL_ENTRY_END
```

```
MATERIAL_ENTRY_BEGIN
MATERIAL_NAME = concrete_sidewalk
MATERIAL_ID = 6
```

SPECIFIC_HEAT = 0.3005
THERMAL_CONDUCTIVITY = 15.5
MASS_DENSITY = 1.0
SPECULARITY = 0.1
VISIBLE_EMISSIVITY = 0.825
THERMAL_EMISSIVITY = 0.935
EXPOSED_AREA = -0.23
THICKNESS = 4.765
OPTICAL_DESCRIPTION = OPAQUE
EMISSIVITY_FILE = concrete_sidewalk.cms
EXTINCTION_FILE =
TEXTURE_FILE =
USE_GAUSSIAN_TEXTURE = FALSE
MATERIAL_ENTRY_END

MATERIAL_ENTRY_BEGIN
MATERIAL_NAME = roof_gravel
MATERIAL_ID = 12
SPECIFIC_HEAT = 0.35
THERMAL_CONDUCTIVITY = 13.1
MASS_DENSITY = 1.00
SPECULARITY = 0.30
VISIBLE_EMISSIVITY = 0.80
THERMAL_EMISSIVITY = 0.90
EXPOSED_AREA = -0.50
THICKNESS = 7.50
OPTICAL_DESCRIPTION = OPAQUE
EMISSIVITY_FILE = roof_gravel.cms
EXTINCTION_FILE =
TEXTURE_FILE =
USE_GAUSSIAN_TEXTURE = FALSE
MATERIAL_ENTRY_END

MATERIAL_ENTRY_BEGIN
MATERIAL_NAME = soil_dirt_brown
MATERIAL_ID = 13
SPECIFIC_HEAT = 0.3422
THERMAL_CONDUCTIVITY = 7.417
MASS_DENSITY = 1.0
SPECULARITY = 0.0
VISIBLE_EMISSIVITY = 0.825
THERMAL_EMISSIVITY = 0.925
EXPOSED_AREA = -0.22
THICKNESS = 4.85
OPTICAL_DESCRIPTION = OPAQUE
EMISSIVITY_FILE = soil_dirt_brown.cms
EXTINCTION_FILE =
TEXTURE_FILE =
USE_GAUSSIAN_TEXTURE = FALSE
MATERIAL_ENTRY_END

MATERIAL_ENTRY_BEGIN
MATERIAL NAME = wall_brick_hawk_cream
MATERIAL_ID = 15
SPECIFIC_HEAT = 0.2918
THERMAL_CONDUCTIVITY = 6.935
MASS_DENSITY = 1.0
SPECULARITY = 0.10
VISIBLE_EMISSIVITY = 0.92
THERMAL_EMISSIVITY = .93
EXPOSED_AREA = -0.2
THICKNESS = 7.0
OPTICAL_DESCRIPTION = OPAQUE
EMISSIVITY_FILE = brick.cms
EXTINCTION_FILE =
TEXTURE_FILE =
USE_GAUSSIAN_TEXTURE = FALSE
MATERIAL_ENTRY_END

MATERIAL_ENTRY_BEGIN
MATERIAL NAME = aluminum_vent_hawkeye
MATERIAL_ID = 16
SPECIFIC_HEAT = 0.55
THERMAL_CONDUCTIVITY = 1909
MASS_DENSITY = 1
SPECULARITY = 0.3
VISIBLE_EMISSIVITY = 0.5
THERMAL_EMISSIVITY = 0.72
EXPOSED_AREA = -0.3
THICKNESS = 0.275
OPTICAL_DESCRIPTION = OPAQUE
EMISSIVITY_FILE = aluminum_weathered.cms
EXTINCTION_FILE =
TEXTURE_FILE =
USE_GAUSSIAN_TEXTURE = FALSE
MATERIAL_ENTRY_END

MATERIAL_ENTRY_BEGIN
MATERIAL NAME = tree_trunk
MATERIAL_ID = 18
SPECIFIC_HEAT = 0.429
THERMAL_CONDUCTIVITY = 0.85
MASS_DENSITY = 1.0
SPECULARITY = 0.0
VISIBLE_EMISSIVITY = 0.87
THERMAL_EMISSIVITY = 0.955
EXPOSED_AREA = -0.3
THICKNESS = 0.65
OPTICAL_DESCRIPTION = OPAQUE
EMISSIVITY_FILE = tree_trunk.cms
EXTINCTION_FILE =
TEXTURE_FILE =
USE_GAUSSIAN_TEXTURE = FALSE
MATERIAL_ENTRY_END

MATERIAL_ENTRY_BEGIN
MATERIAL NAME = tree_deciduous
MATERIAL_ID = 25
SPECIFIC_HEAT = 1
THERMAL_CONDUCTIVITY = 12.5
MASS_DENSITY = 1.0
SPECULARITY = 0.0
VISIBLE_EMISSIVITY = 0.935
THERMAL_EMISSIVITY = 0.95
EXPOSED_AREA = -0.22
THICKNESS = 1.5
OPTICAL_DESCRIPTION = OPAQUE
EMISSIVITY_FILE = tree_deciduous.cms
EXTINCTION_FILE =
TEXTURE_FILE =
USE_GAUSSIAN_TEXTURE = FALSE
MATERIAL_ENTRY_END

MATERIAL_ENTRY_BEGIN
MATERIAL NAME = asphalt_parking_new
MATERIAL_ID = 30
SPECIFIC_HEAT = 0.44254
THERMAL_CONDUCTIVITY = 11.243
MASS_DENSITY = 1.0
SPECULARITY = 0.1
VISIBLE_EMISSIVITY = 0.91
THERMAL_EMISSIVITY = 0.94
EXPOSED_AREA = -0.21
THICKNESS = 7.55
OPTICAL_DESCRIPTION = OPAQUE
EMISSIVITY_FILE = asphalt_new.cms
EXTINCTION_FILE =
TEXTURE_FILE =

USE_GAUSSIAN_TEXTURE = FALSE
MATERIAL_ENTRY_END

MATERIAL_ENTRY_BEGIN
MATERIAL_NAME = asphalt_old
MATERIAL_ID = 31
SPECIFIC_HEAT = 0.42254
THERMAL_CONDUCTIVITY = 11.443
MASS_DENSITY = 1.0
SPECULARITY = 0.1
VISIBLE_EMISSIVITY = 0.775
THERMAL_EMISSIVITY = 0.943
EXPOSED_AREA = -0.21
THICKNESS = 7.55
OPTICAL_DESCRIPTION = OPAQUE
EMISSIVITY_FILE = asphalt_old.ems
EXTINCTION_FILE =
TEXTURE_FILE =
USE_GAUSSIAN_TEXTURE = FALSE
MATERIAL_ENTRY_END

MATERIAL_ENTRY_BEGIN
MATERIAL_NAME = soil_clay_gray
MATERIAL_ID = 40
SPECIFIC_HEAT = .3802
THERMAL_CONDUCTIVITY = 4.762
MASS_DENSITY = 1.00
SPECULARITY = 0.0
VISIBLE_EMISSIVITY = 0.795
THERMAL_EMISSIVITY = 0.955
EXPOSED_AREA = -0.20
THICKNESS = 4.85
OPTICAL_DESCRIPTION = OPAQUE
EMISSIVITY_FILE = soil_clay_gray.ems
EXTINCTION_FILE =
TEXTURE_FILE =
USE_GAUSSIAN_TEXTURE = FALSE
MATERIAL_ENTRY_END

MATERIAL_ENTRY_BEGIN
MATERIAL NAME = soil_clay_red
MATERIAL_ID = 41
SPECIFIC_HEAT = 0.3702
THERMAL_CONDUCTIVITY = 4.862
MASS_DENSITY = 1.0
SPECULARITY = 0.0
VISIBLE_EMISSIVITY = 0.825
THERMAL_EMISSIVITY = 0.95
EXPOSED_AREA = -0.20
THICKNESS = 4.95
OPTICAL_DESCRIPTION = OPAQUE
EMISSIVITY_FILE = soil_clay_red.ems
EXTINCTION_FILE =
TEXTURE_FILE =
USE_GAUSSIAN_TEXTURE = FALSE
MATERIAL_ENTRY_END

MATERIAL_ENTRY_BEGIN
MATERIAL NAME = soil_gravel_light_brown
MATERIAL_ID = 43
SPECIFIC_HEAT = 0.51
THERMAL_CONDUCTIVITY = 15.76
MASS_DENSITY = 1.0
SPECULARITY = 0.0
VISIBLE_EMISSIVITY = 0.85
THERMAL_EMISSIVITY = 0.915
EXPOSED_AREA = -0.20
THICKNESS = 5.85
OPTICAL_DESCRIPTION = OPAQUE
EMISSIVITY_FILE = soil_gravel_brown.ems

EXTINCTION_FILE =
TEXTURE_FILE =
USE_GAUSSIAN_TEXTURE = FALSE
MATERIAL_ENTRY_END

MATERIAL_ENTRY_BEGIN
MATERIAL NAME = roof_aluminum
MATERIAL_ID = 50
SPECIFIC_HEAT = 0.45
THERMAL_CONDUCTIVITY = 2309
MASS_DENSITY = 1.00
SPECULARITY = 0.30
VISIBLE_EMISSIVITY = 0.5
THERMAL_EMISSIVITY = 0.72
EXPOSED_AREA = -0.3
THICKNESS = 0.125
OPTICAL_DESCRIPTION = OPAQUE
EMISSIVITY_FILE = aluminum_weathered.ems
EXTINCTION_FILE =
TEXTURE_FILE =
USE_GAUSSIAN_TEXTURE = FALSE
MATERIAL_ENTRY_END

MATERIAL_ENTRY_BEGIN
MATERIAL NAME = roof_steel
MATERIAL_ID = 52
SPECIFIC_HEAT = 0.805
THERMAL_CONDUCTIVITY = 511.5
MASS_DENSITY = 1.00
SPECULARITY = 0.30
VISIBLE_EMISSIVITY = 0.825
THERMAL_EMISSIVITY = 0.79
EXPOSED_AREA = -0.35
THICKNESS = 0.2
OPTICAL_DESCRIPTION = OPAQUE
EMISSIVITY_FILE = steel.ems
EXTINCTION_FILE =
TEXTURE_FILE =
USE_GAUSSIAN_TEXTURE = FALSE
MATERIAL_ENTRY_END

MATERIAL_ENTRY_BEGIN
MATERIAL NAME = wall_concrete
MATERIAL_ID = 53
SPECIFIC_HEAT = 0.3145
THERMAL_CONDUCTIVITY = 15.68
MASS_DENSITY = 1.00
SPECULARITY = 0.30
VISIBLE_EMISSIVITY = 0.725
THERMAL_EMISSIVITY = 0.905
EXPOSED_AREA = -0.20
THICKNESS = 9.0
OPTICAL_DESCRIPTION = OPAQUE
EMISSIVITY_FILE = concrete_wall.ems
EXTINCTION_FILE =
TEXTURE_FILE =
USE_GAUSSIAN_TEXTURE = FALSE
MATERIAL_ENTRY_END

MATERIAL_ENTRY_BEGIN
MATERIAL NAME = window_glass
MATERIAL_ID = 54
SPECIFIC_HEAT = 0.3405
THERMAL_CONDUCTIVITY = 15.0
MASS_DENSITY = 1.00
SPECULARITY = 0.20
VISIBLE_EMISSIVITY = 0.85
THERMAL_EMISSIVITY = 0.82
EXPOSED_AREA = -0.38
THICKNESS = 0.425
OPTICAL_DESCRIPTION = OPAQUE

EMISSIONITY_FILE = window_glass.ems
EXTINCTION_FILE =
TEXTURE_FILE =
USE_GAUSSIAN_TEXTURE = FALSE
MATERIAL_ENTRY_END

MATERIAL_ENTRY_BEGIN
MATERIAL_NAME = roof_asphalt_shingles_color
MATERIAL_ID = 60
SPECIFIC_HEAT = 0.3775
THERMAL_CONDUCTIVITY = 6.145
MASS_DENSITY = 1.00
SPECULARITY = 0.10
VISIBLE_EMISSIONITY = 0.73
THERMAL_EMISSIONITY = .90
EXPOSED_AREA = -0.36
THICKNESS = 0.75
OPTICAL_DESCRIPTION = OPAQUE
EMISSIONITY_FILE = asphalt_shingle.ems
EXTINCTION_FILE =
TEXTURE_FILE =
USE_GAUSSIAN_TEXTURE = FALSE
MATERIAL_ENTRY_END

MATERIAL_ENTRY_BEGIN
MATERIAL NAME = roof_asphalt_shingles_color
MATERIAL_ID = 61
SPECIFIC_HEAT = 0.3775
THERMAL_CONDUCTIVITY = 6.045
MASS_DENSITY = 1.00
SPECULARITY = 0.10
VISIBLE_EMISSIONITY = 0.76
THERMAL_EMISSIONITY = .91
EXPOSED_AREA = -0.374
THICKNESS = 0.65
OPTICAL_DESCRIPTION = OPAQUE
EMISSIONITY_FILE = asphalt_shingle.ems
EXTINCTION_FILE =
TEXTURE_FILE =
USE_GAUSSIAN_TEXTURE = FALSE
MATERIAL_ENTRY_END

MATERIAL_ENTRY_BEGIN
MATERIAL NAME = roof_asphalt_shingles_color
MATERIAL_ID = 62
SPECIFIC_HEAT = 0.3775
THERMAL_CONDUCTIVITY = 6.075
MASS_DENSITY = 1.000
SPECULARITY = 0.10
VISIBLE_EMISSIONITY = 0.78
THERMAL_EMISSIONITY = .911
EXPOSED_AREA = -0.37
THICKNESS = 0.685
OPTICAL_DESCRIPTION = OPAQUE
EMISSIONITY_FILE = asphalt_shingle.ems
EXTINCTION_FILE =
TEXTURE_FILE =
USE_GAUSSIAN_TEXTURE = FALSE
MATERIAL_ENTRY_END

MATERIAL_ENTRY_BEGIN
MATERIAL NAME = roof_asphalt_shingles_color
MATERIAL_ID = 63
SPECIFIC_HEAT = 0.3775
THERMAL_CONDUCTIVITY = 6.065
MASS_DENSITY = 1.00
SPECULARITY = 0.10
VISIBLE_EMISSIONITY = 0.81
THERMAL_EMISSIONITY = .913
EXPOSED_AREA = -0.374
THICKNESS = 0.85
OPTICAL_DESCRIPTION = OPAQUE

EMISSIONITY_FILE = asphalt_shingle.ems
EXTINCTION_FILE =
TEXTURE_FILE =
USE_GAUSSIAN_TEXTURE = FALSE
MATERIAL_ENTRY_END

MATERIAL_ENTRY_BEGIN
MATERIAL NAME = roof_asphalt_shingles_color
MATERIAL_ID = 64
SPECIFIC_HEAT = 0.3795
THERMAL_CONDUCTIVITY = 6.045
MASS_DENSITY = 1.000
SPECULARITY = 0.10
VISIBLE_EMISSIONITY = 0.83
THERMAL_EMISSIONITY = .913
EXPOSED_AREA = -0.373
THICKNESS = 0.79
OPTICAL_DESCRIPTION = OPAQUE
EMISSIONITY_FILE = asphalt_shingle.ems
EXTINCTION_FILE =
TEXTURE_FILE =
USE_GAUSSIAN_TEXTURE = FALSE
MATERIAL_ENTRY_END

MATERIAL_ENTRY_BEGIN
MATERIAL NAME = roof_asphalt_shingles_color
MATERIAL_ID = 65
SPECIFIC_HEAT = 0.3765
THERMAL_CONDUCTIVITY = 6.145
MASS_DENSITY = 1.000
SPECULARITY = 0.10
VISIBLE_EMISSIONITY = 0.86
THERMAL_EMISSIONITY = .91
EXPOSED_AREA = -0.376
THICKNESS = 0.45
OPTICAL_DESCRIPTION = OPAQUE
EMISSIONITY_FILE = asphalt_shingle.ems
EXTINCTION_FILE =
TEXTURE_FILE =
USE_GAUSSIAN_TEXTURE = FALSE
MATERIAL_ENTRY_END

MATERIAL_ENTRY_BEGIN
MATERIAL NAME = roof_asphalt_shingles_color
MATERIAL_ID = 66
SPECIFIC_HEAT = 0.3675
THERMAL_CONDUCTIVITY = 6.245
MASS_DENSITY = 1.000
SPECULARITY = 0.10
VISIBLE_EMISSIONITY = 0.89
THERMAL_EMISSIONITY = .907
EXPOSED_AREA = -0.372
THICKNESS = 0.55
OPTICAL_DESCRIPTION = OPAQUE
EMISSIONITY_FILE = asphalt_shingle.ems
EXTINCTION_FILE =
TEXTURE_FILE =
USE_GAUSSIAN_TEXTURE = FALSE
MATERIAL_ENTRY_END

MATERIAL_ENTRY_BEGIN
MATERIAL NAME = roof_asphalt_shingles_color
MATERIAL_ID = 67
SPECIFIC_HEAT = 0.3575
THERMAL_CONDUCTIVITY = 6.185
MASS_DENSITY = 1.000
SPECULARITY = 0.10
VISIBLE_EMISSIONITY = 0.91
THERMAL_EMISSIONITY = .914
EXPOSED_AREA = -0.37
THICKNESS = 0.65
OPTICAL_DESCRIPTION = OPAQUE

EMISSIONITY_FILE = asphalt_shingle.ems
EXTINCTION_FILE =
TEXTURE_FILE =
USE_GAUSSIAN_TEXTURE = FALSE
MATERIAL_ENTRY_END

MATERIAL_ENTRY_BEGIN
MATERIAL_NAME = roof_asphalt_shingles_color
MATERIAL_ID = 68
SPECIFIC_HEAT = 0.3595
THERMAL_CONDUCTIVITY = 6.125
MASS_DENSITY = 1.00
SPECULARITY = 0.10
VISIBLE_EMISSIONITY = 0.93
THERMAL_EMISSIONITY = .905
EXPOSED_AREA = -0.371
THICKNESS = 0.57
OPTICAL_DESCRIPTION = OPAQUE
EMISSIONITY_FILE = asphalt_shingle.ems
EXTINCTION_FILE =
TEXTURE_FILE =
USE_GAUSSIAN_TEXTURE = FALSE
MATERIAL_ENTRY_END

MATERIAL_ENTRY_BEGIN
MATERIAL NAME = roof_asphalt_shingles_color
MATERIAL_ID = 69
SPECIFIC_HEAT = 0.3575
THERMAL_CONDUCTIVITY = 6.145
MASS_DENSITY = 1.000
SPECULARITY = 0.10
VISIBLE_EMISSIONITY = 0.95
THERMAL_EMISSIONITY = .912
EXPOSED_AREA = -0.282
THICKNESS = 0.67
OPTICAL_DESCRIPTION = OPAQUE
EMISSIONITY_FILE = asphalt_shingle.ems
EXTINCTION_FILE =
TEXTURE_FILE =
USE_GAUSSIAN_TEXTURE = FALSE
MATERIAL_ENTRY_END

MATERIAL_ENTRY_BEGIN
MATERIAL NAME = wall_brick_color
MATERIAL_ID = 70
SPECIFIC_HEAT = 0.3818
THERMAL_CONDUCTIVITY = 6.935
MASS_DENSITY = 1.0
SPECULARITY = 0.10
VISIBLE_EMISSIONITY = 0.65
THERMAL_EMISSIONITY = .93
EXPOSED_AREA = -0.287
THICKNESS = 6.0
OPTICAL_DESCRIPTION = OPAQUE
EMISSIONITY_FILE = brick.ems
EXTINCTION_FILE =
TEXTURE_FILE =
USE_GAUSSIAN_TEXTURE = FALSE
MATERIAL_ENTRY_END

MATERIAL_ENTRY_BEGIN
MATERIAL NAME = wall_brick_color
MATERIAL_ID = 71
SPECIFIC_HEAT = 0.2918
THERMAL_CONDUCTIVITY = 5.935
MASS_DENSITY = 1.0
SPECULARITY = 0.10
VISIBLE_EMISSIONITY = 0.68
THERMAL_EMISSIONITY = .93
EXPOSED_AREA = -0.3
THICKNESS = 7.0

OPTICAL_DESCRIPTION = OPAQUE
EMISSIONITY_FILE = brick.ems
EXTINCTION_FILE =
TEXTURE_FILE =
USE_GAUSSIAN_TEXTURE = FALSE
MATERIAL_ENTRY_END

MATERIAL_ENTRY_BEGIN
MATERIAL NAME = wall_brick_color
MATERIAL_ID = 72
SPECIFIC_HEAT = 0.2998
THERMAL_CONDUCTIVITY = 6.835
MASS_DENSITY = 1.0
SPECULARITY = 0.10
VISIBLE_EMISSIONITY = 0.71
THERMAL_EMISSIONITY = .93
EXPOSED_AREA = -0.29
THICKNESS = 8.0
OPTICAL_DESCRIPTION = OPAQUE
EMISSIONITY_FILE = brick.ems
EXTINCTION_FILE =
TEXTURE_FILE =
USE_GAUSSIAN_TEXTURE = FALSE
MATERIAL_ENTRY_END

MATERIAL_ENTRY_BEGIN
MATERIAL NAME = wall_brick_color
MATERIAL_ID = 73
SPECIFIC_HEAT = 0.3818
THERMAL_CONDUCTIVITY = 7.335
MASS_DENSITY = 1.0
SPECULARITY = 0.10
VISIBLE_EMISSIONITY = 0.74
THERMAL_EMISSIONITY = .93
EXPOSED_AREA = -0.29
THICKNESS = 7.0
OPTICAL_DESCRIPTION = OPAQUE
EMISSIONITY_FILE = brick.ems
EXTINCTION_FILE =
TEXTURE_FILE =
USE_GAUSSIAN_TEXTURE = FALSE
MATERIAL_ENTRY_END

MATERIAL_ENTRY_BEGIN
MATERIAL NAME = wall_brick_color
MATERIAL_ID = 74
SPECIFIC_HEAT = 0.2818
THERMAL_CONDUCTIVITY = 6.735
MASS_DENSITY = 1.0
SPECULARITY = 0.10
VISIBLE_EMISSIONITY = 0.77
THERMAL_EMISSIONITY = .93
EXPOSED_AREA = -0.3
THICKNESS = 6.0
OPTICAL_DESCRIPTION = OPAQUE
EMISSIONITY_FILE = brick.ems
EXTINCTION_FILE =
TEXTURE_FILE =
USE_GAUSSIAN_TEXTURE = FALSE
MATERIAL_ENTRY_END

MATERIAL_ENTRY_BEGIN
MATERIAL NAME = wall_brick_color
MATERIAL_ID = 75
SPECIFIC_HEAT = 0.2918
THERMAL_CONDUCTIVITY = 6.985
MASS_DENSITY = 1.0
SPECULARITY = 0.10

VISIBLE_EMISSIVITY = 0.8
THERMAL_EMISSIVITY = .927
EXPOSED_AREA = -0.287
THICKNESS = 7.0
OPTICAL_DESCRIPTION = OPAQUE
EMISSIVITY_FILE = brick.ems
EXTINCTION_FILE =
TEXTURE_FILE =
USE_GAUSSIAN_TEXTURE = FALSE
MATERIAL_ENTRY_END

MATERIAL_ENTRY_BEGIN
MATERIAL_NAME = wall_brick_color
MATERIAL_ID = 76
SPECIFIC_HEAT = 0.2818
THERMAL_CONDUCTIVITY = 5.935
MASS_DENSITY = 1.0
SPECULARITY = 0.10
VISIBLE_EMISSIVITY = 0.83
THERMAL_EMISSIVITY = .918
EXPOSED_AREA = -0.3
THICKNESS = 7.2
OPTICAL_DESCRIPTION = OPAQUE
EMISSIVITY_FILE = brick.ems
EXTINCTION_FILE =
TEXTURE_FILE =
USE_GAUSSIAN_TEXTURE = FALSE
MATERIAL_ENTRY_END

MATERIAL_ENTRY_BEGIN
MATERIAL_NAME = wall_brick_color
MATERIAL_ID = 77
SPECIFIC_HEAT = 0.3218
THERMAL_CONDUCTIVITY = 7.935
MASS_DENSITY = 1.0
SPECULARITY = 0.10
VISIBLE_EMISSIVITY = 0.86
THERMAL_EMISSIVITY = .92
EXPOSED_AREA = -0.3
THICKNESS = 8.3
OPTICAL_DESCRIPTION = OPAQUE
EMISSIVITY_FILE = brick.ems
EXTINCTION_FILE =
TEXTURE_FILE =
USE_GAUSSIAN_TEXTURE = FALSE
MATERIAL_ENTRY_END

MATERIAL_ENTRY_BEGIN
MATERIAL NAME = wall_brick_color
MATERIAL_ID = 78
SPECIFIC_HEAT = 0.2898
THERMAL_CONDUCTIVITY = 6.335
MASS_DENSITY = 1.0
SPECULARITY = 0.10
VISIBLE_EMISSIVITY = 0.89
THERMAL_EMISSIVITY = .925
EXPOSED_AREA = -0.278
THICKNESS = 6.0
OPTICAL_DESCRIPTION = OPAQUE
EMISSIVITY_FILE = brick.ems
EXTINCTION_FILE =
TEXTURE_FILE =
USE_GAUSSIAN_TEXTURE = FALSE
MATERIAL_ENTRY_END

MATERIAL_ENTRY_BEGIN
MATERIAL NAME = wall_brick_color
MATERIAL_ID = 79

SPECIFIC_HEAT = 0.2918
THERMAL_CONDUCTIVITY = 6.935
MASS_DENSITY = 1.0
SPECULARITY = 0.10
VISIBLE_EMISSIVITY = 0.92
THERMAL_EMISSIVITY = .932
EXPOSED_AREA = -0.28
THICKNESS = 7.0
OPTICAL_DESCRIPTION = OPAQUE
EMISSIVITY_FILE = brick.ems
EXTINCTION_FILE =
TEXTURE_FILE =
USE_GAUSSIAN_TEXTURE = FALSE
MATERIAL_ENTRY_END

MATERIAL_ENTRY_BEGIN
MATERIAL NAME = wall_wood_color
MATERIAL_ID = 80
SPECIFIC_HEAT = 0.5194
THERMAL_CONDUCTIVITY = 1.02
MASS_DENSITY = 1.0
SPECULARITY = 0.15
VISIBLE_EMISSIVITY = 0.7
THERMAL_EMISSIVITY = 0.858
EXPOSED_AREA = -0.28
THICKNESS = 4.0
OPTICAL_DESCRIPTION = OPAQUE
EMISSIVITY_FILE = wood.ems
EXTINCTION_FILE =
TEXTURE_FILE =
USE_GAUSSIAN_TEXTURE = FALSE
MATERIAL_ENTRY_END

MATERIAL_ENTRY_BEGIN
MATERIAL NAME = wall_wood_color
MATERIAL_ID = 81
SPECIFIC_HEAT = 0.5184
THERMAL_CONDUCTIVITY = 0.96
MASS_DENSITY = 1.0
SPECULARITY = 0.15
VISIBLE_EMISSIVITY = 0.72
THERMAL_EMISSIVITY = 0.848
EXPOSED_AREA = -0.286
THICKNESS = 3.85
OPTICAL_DESCRIPTION = OPAQUE
EMISSIVITY_FILE = wood.ems
EXTINCTION_FILE =
TEXTURE_FILE =
USE_GAUSSIAN_TEXTURE = FALSE
MATERIAL_ENTRY_END

MATERIAL_ENTRY_BEGIN
MATERIAL NAME = wall_wood_color
MATERIAL_ID = 82
SPECIFIC_HEAT = 0.5124
THERMAL_CONDUCTIVITY = 0.98
MASS_DENSITY = 1.0
SPECULARITY = 0.15
VISIBLE_EMISSIVITY = 0.74
THERMAL_EMISSIVITY = 0.865
EXPOSED_AREA = -0.3
THICKNESS = 4.5
OPTICAL_DESCRIPTION = OPAQUE
EMISSIVITY_FILE = wood.ems
EXTINCTION_FILE =
TEXTURE_FILE =
USE_GAUSSIAN_TEXTURE = FALSE
MATERIAL_ENTRY_END

MATERIAL_ENTRY_BEGIN
MATERIAL_NAME = wall_wood_color
MATERIAL_ID = 83
SPECIFIC_HEAT = 0.5284
THERMAL_CONDUCTIVITY = 1.04
MASS_DENSITY = 1.0
SPECULARITY = 0.15
VISIBLE_EMISSIVITY = 0.76
THERMAL_EMISSIVITY = 0.865
EXPOSED_AREA = -0.28
THICKNESS = 3.75
OPTICAL_DESCRIPTION = OPAQUE
EMISSIVITY_FILE = wood.ems
EXTINCTION_FILE =
TEXTURE_FILE =
USE_GAUSSIAN_TEXTURE = FALSE
MATERIAL_ENTRY_END

MATERIAL_ENTRY_BEGIN
MATERIAL_NAME = wall_wood_color
MATERIAL_ID = 84
SPECIFIC_HEAT = 0.5124
THERMAL_CONDUCTIVITY = 0.98
MASS_DENSITY = 1.0
SPECULARITY = 0.15
VISIBLE_EMISSIVITY = 0.78
THERMAL_EMISSIVITY = 0.865
EXPOSED_AREA = -0.3
THICKNESS = 4.5
OPTICAL_DESCRIPTION = OPAQUE
EMISSIVITY_FILE = wood.ems
EXTINCTION_FILE =
TEXTURE_FILE =
USE_GAUSSIAN_TEXTURE = FALSE
MATERIAL_ENTRY_END

MATERIAL_ENTRY_BEGIN
MATERIAL_NAME = wall_wood_color
MATERIAL_ID = 85
SPECIFIC_HEAT = 0.5324
THERMAL_CONDUCTIVITY = 0.98
MASS_DENSITY = 1.0
SPECULARITY = 0.15
VISIBLE_EMISSIVITY = 0.80
THERMAL_EMISSIVITY = 0.829
EXPOSED_AREA = -0.26
THICKNESS = 2.5
OPTICAL_DESCRIPTION = OPAQUE
EMISSIVITY_FILE = wood.ems
EXTINCTION_FILE =
TEXTURE_FILE =
USE_GAUSSIAN_TEXTURE = FALSE
MATERIAL_ENTRY_END

MATERIAL_ENTRY_BEGIN
MATERIAL_NAME = wall_wood_color
MATERIAL_ID = 86
SPECIFIC_HEAT = 0.5024
THERMAL_CONDUCTIVITY = 0.97
MASS_DENSITY = 1.0
SPECULARITY = 0.15
VISIBLE_EMISSIVITY = 0.82
THERMAL_EMISSIVITY = 0.868
EXPOSED_AREA = -0.3
THICKNESS = 4.8
OPTICAL_DESCRIPTION = OPAQUE
EMISSIVITY_FILE = wood.ems
EXTINCTION_FILE =
TEXTURE_FILE =

USE_GAUSSIAN_TEXTURE = FALSE
MATERIAL_ENTRY_END

MATERIAL_ENTRY_BEGIN
MATERIAL_NAME = wall_wood_color
MATERIAL_ID = 87
SPECIFIC_HEAT = 0.5284
THERMAL_CONDUCTIVITY = 0.11
MASS_DENSITY = 1.0
SPECULARITY = 0.15
VISIBLE_EMISSIVITY = 0.84
THERMAL_EMISSIVITY = 0.860
EXPOSED_AREA = -0.289
THICKNESS = 4.5
OPTICAL_DESCRIPTION = OPAQUE
EMISSIVITY_FILE = wood.ems
EXTINCTION_FILE =
TEXTURE_FILE =
USE_GAUSSIAN_TEXTURE = FALSE
MATERIAL_ENTRY_END

MATERIAL_ENTRY_BEGIN
MATERIAL_NAME = wall_wood_color
MATERIAL_ID = 88
SPECIFIC_HEAT = 0.5324
THERMAL_CONDUCTIVITY = 0.99
MASS_DENSITY = 1.0
SPECULARITY = 0.15
VISIBLE_EMISSIVITY = 0.86
THERMAL_EMISSIVITY = 0.855
EXPOSED_AREA = -0.29
THICKNESS = 3.9
OPTICAL_DESCRIPTION = OPAQUE
EMISSIVITY_FILE = wood.ems
EXTINCTION_FILE =
TEXTURE_FILE =
USE_GAUSSIAN_TEXTURE = FALSE
MATERIAL_ENTRY_END

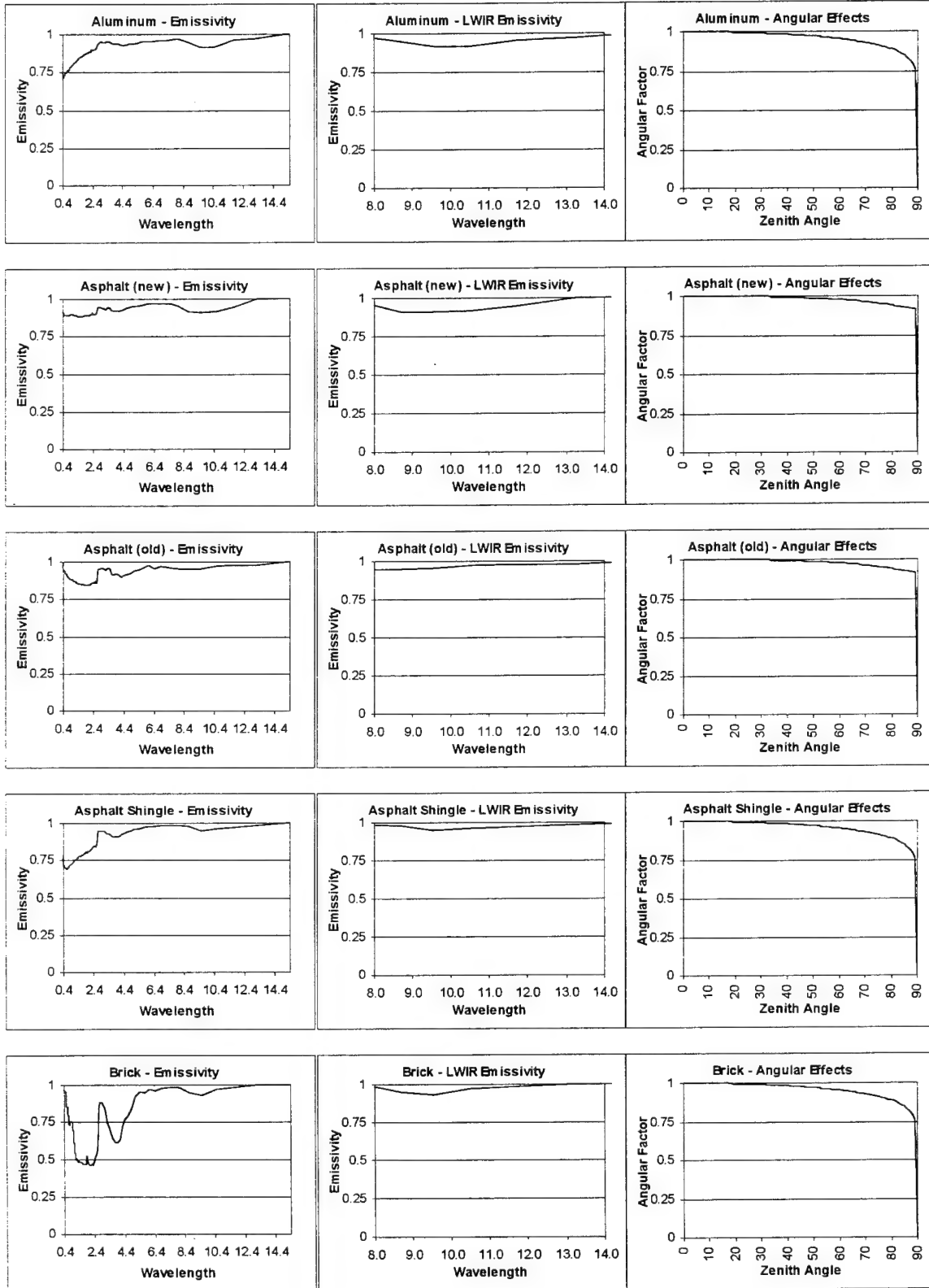
MATERIAL_ENTRY_BEGIN
MATERIAL_NAME = wall_wood_color
MATERIAL_ID = 89
SPECIFIC_HEAT = 0.6524
THERMAL_CONDUCTIVITY = 0.108
MASS_DENSITY = 1.0
SPECULARITY = 0.15
VISIBLE_EMISSIVITY = 0.88
THERMAL_EMISSIVITY = 0.835
EXPOSED_AREA = -0.27
THICKNESS = 3.5
OPTICAL_DESCRIPTION = OPAQUE
EMISSIVITY_FILE = wood.ems
EXTINCTION_FILE =
TEXTURE_FILE =
USE_GAUSSIAN_TEXTURE = FALSE
MATERIAL_ENTRY_END

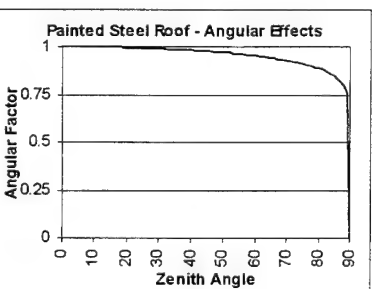
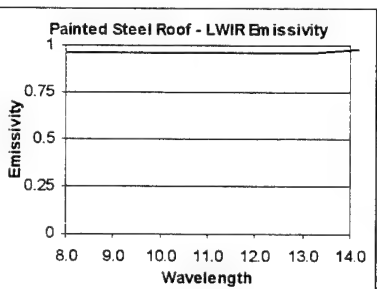
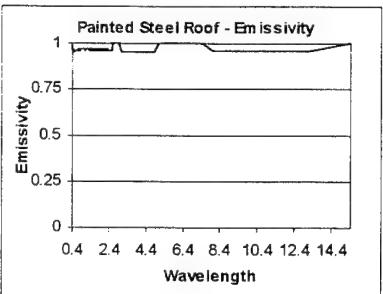
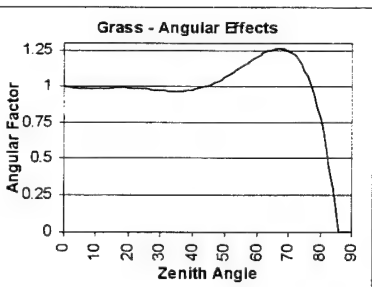
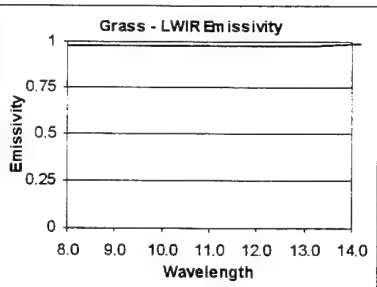
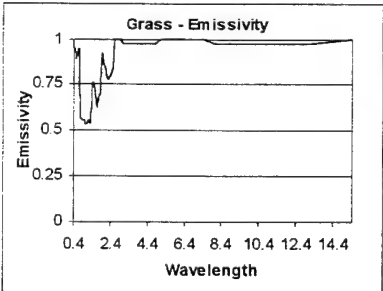
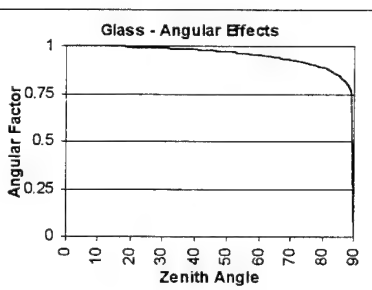
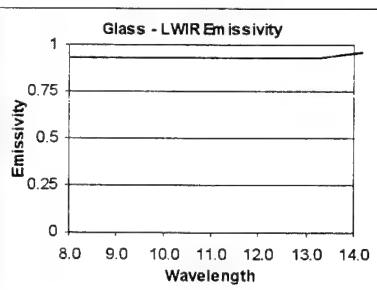
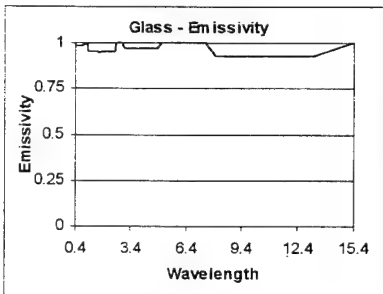
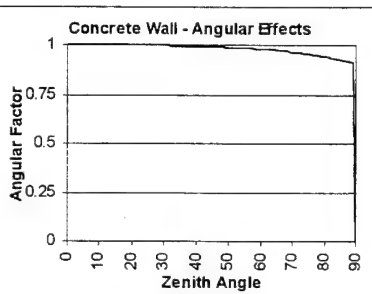
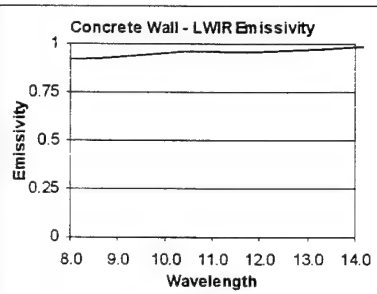
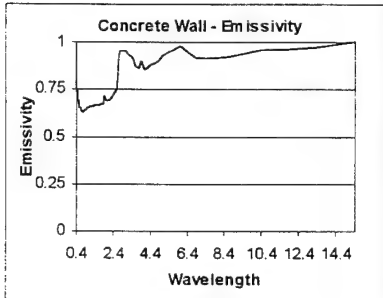
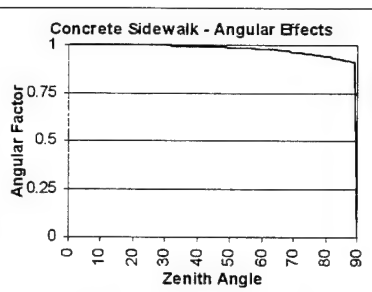
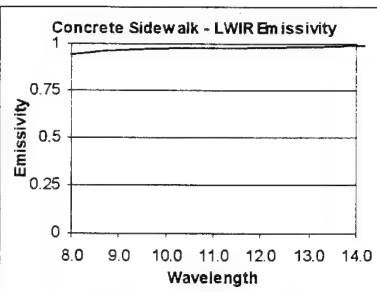
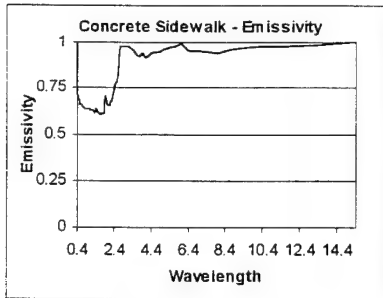
MATERIAL_ENTRY_BEGIN
MATERIAL_NAME = wall_brick_hawk_red
MATERIAL_ID = 90
SPECIFIC_HEAT = 0.2978
THERMAL_CONDUCTIVITY = 7.235
MASS_DENSITY = 1.0
SPECULARITY = 0.10
VISIBLE_EMISSIVITY = 0.915
THERMAL_EMISSIVITY = .925
EXPOSED_AREA = -0.25
THICKNESS = 6.0
OPTICAL_DESCRIPTION = OPAQUE

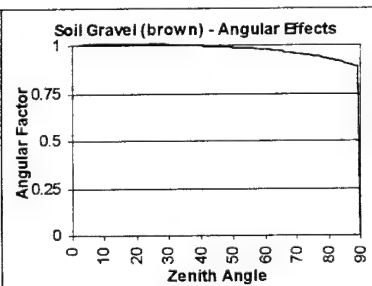
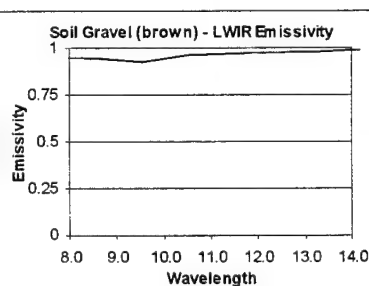
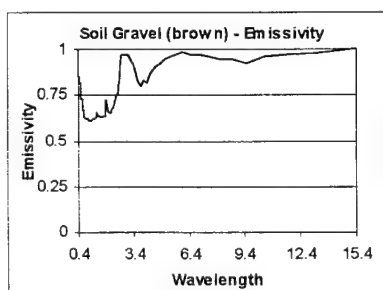
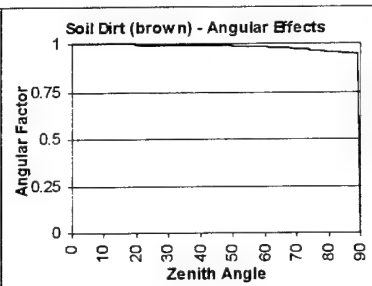
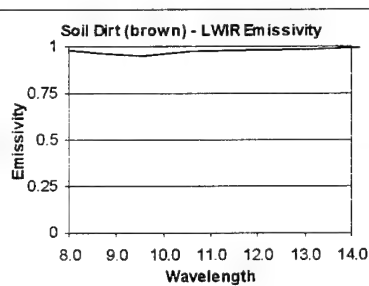
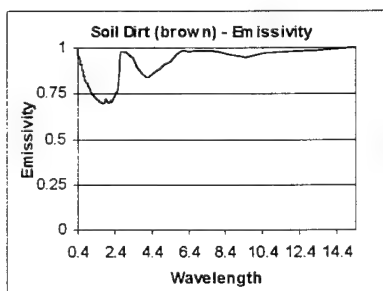
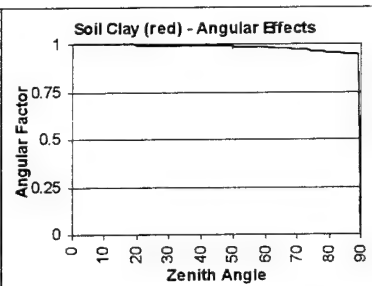
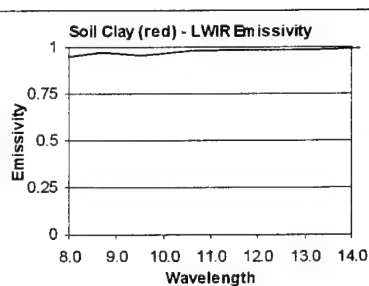
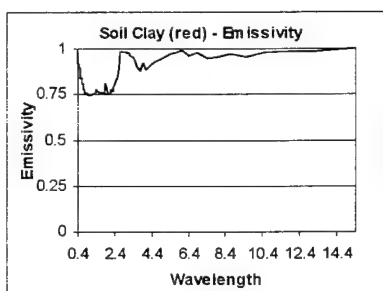
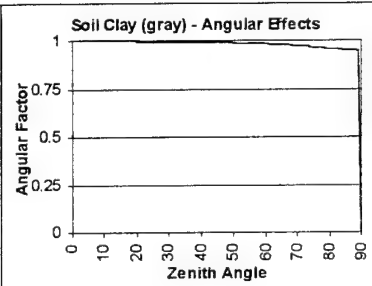
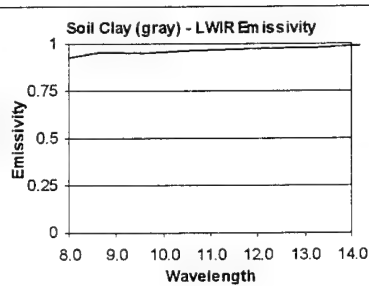
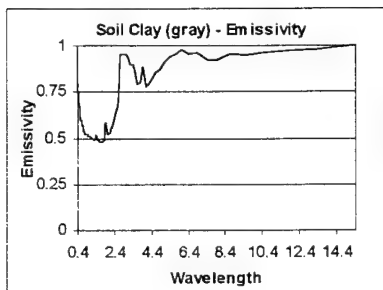
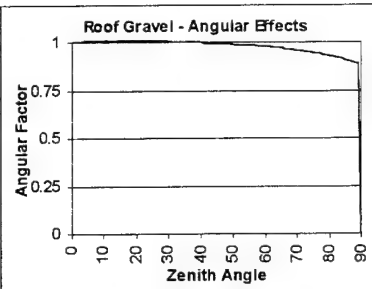
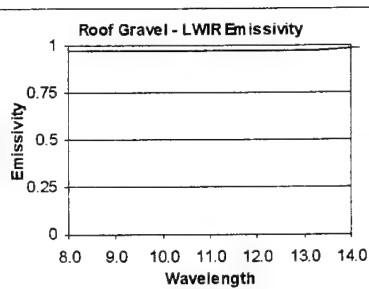
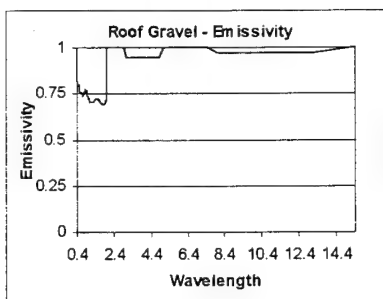
EMISSIONITY_FILE = brick.ems
EXTINCTION_FILE =
TEXTURE_FILE =
USE_GAUSSIAN_TEXTURE = FALSE
MATERIAL_ENTRY_END

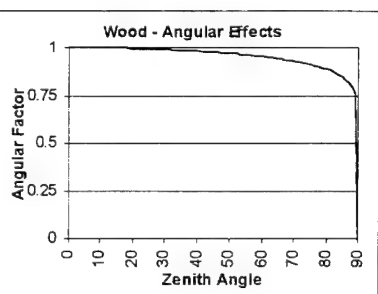
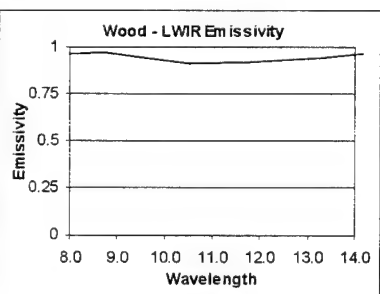
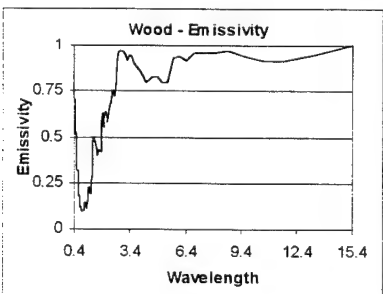
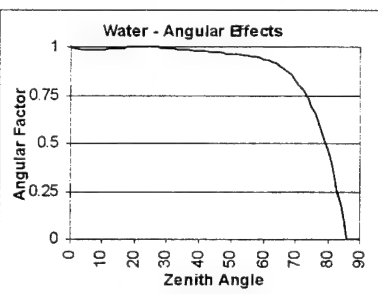
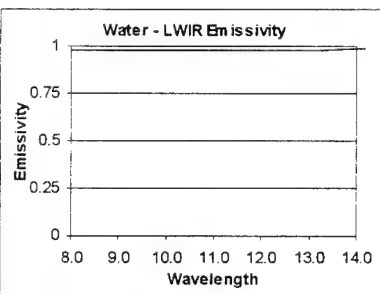
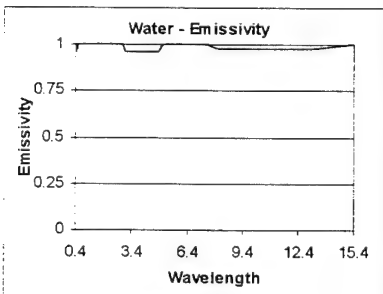
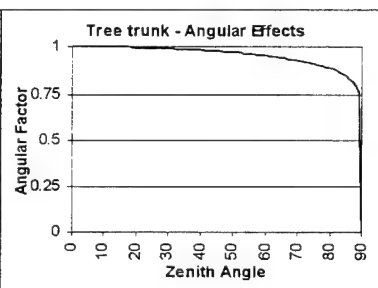
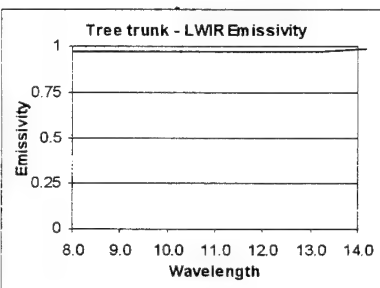
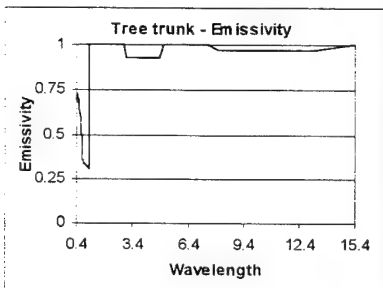
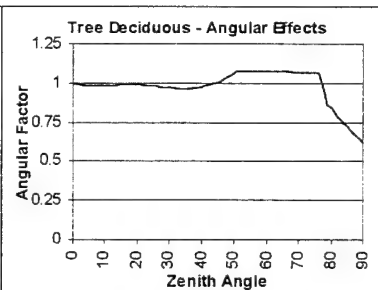
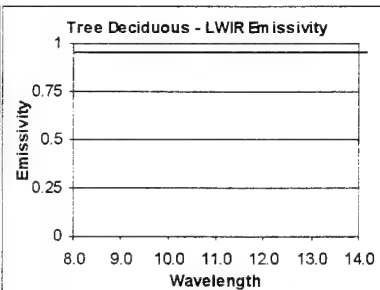
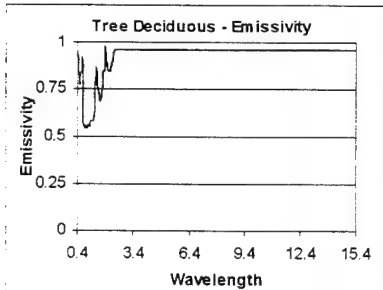
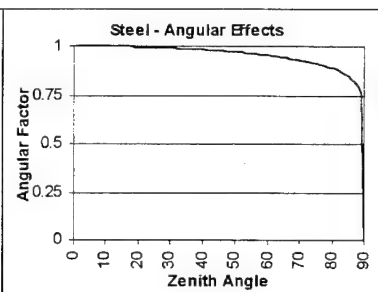
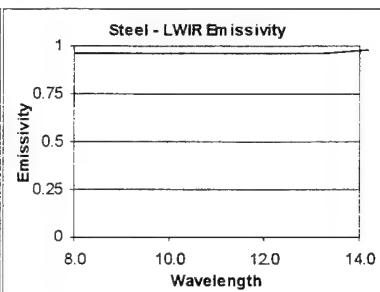
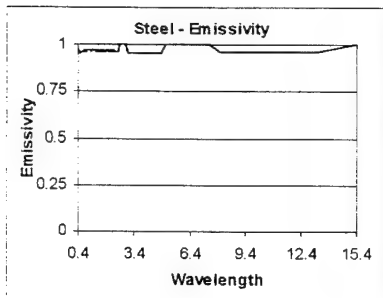
MATERIAL_ENTRY_BEGIN
MATERIAL_NAME = wall_brick_hawk_church
MATERIAL_ID = 92
SPECIFIC_HEAT = 0.2818
THERMAL_CONDUCTIVITY = 5.935
MASS_DENSITY = 1.0
SPECULARITY = 0.10
VISIBLE_EMISSIONITY = 0.92
THERMAL_EMISSIONITY = .93
EXPOSED_AREA = -0.26
THICKNESS = 7.5
OPTICAL_DESCRIPTION = OPAQUE
EMISSIONITY_FILE = brick.ems
EXTINCTION_FILE =
TEXTURE_FILE =
USE_GAUSSIAN_TEXTURE = FALSE
MATERIAL_ENTRY_END

Material Emissivity Curves









Appendix E

Actual Weather Data

10 November 1991

12 October 1995

MF1-10A

U.S. DEPARTMENT OF COMMERCE, NOAA
NATIONAL WEATHER SERVICE

Station: WSO ROCHESTER NY
Surface Weather Observations Date: OCT 10, 1995 To convert LST to UTC: +5

Type Time Sky&Ceiling Vsbty&Wx&Obsns Slp/Temp/Dp/Wnd/Asi/ Remarks&SupplementalCodedData

Add 1 hour
for LST

SA 0050 CLR 20 215/43/30/1903/016/ 50005 10051 20043 (DA 05:51Z)

72529 32920 01923 10061 20333 30010 40215 50005 333 10170 20061 70000 555 91006= (DA05:52Z)

SA 0153 CLR 15 216/42/30/2203/016 (DA 06:53Z)

SA 0251 CLR 15 216/40/36/2103/016/ 90417 (DA 07:52Z)

SA 0350 CLR 12 216/40/37/2103/016/ 55000 (DA 08:51Z)

SA 0450 CLR 6F 216/40/33/2104/016/ SC VCNTY STN W (DA 09:51Z)

SA 0550 CLR 6F 217/41/39/2003/016/ SC VCNTY STN W-N (DA 10:51Z)

SA 0650 CLR 7 217/43/42/2103/016/ 54000 10043 20040 (RM 11:50Z)

SCT = $\frac{1}{10} - \frac{5}{10}$

BKN = $\frac{6}{10} - \frac{9}{10}$

OVC = $\frac{10}{10}$

72529 32961 02103 10059 20056 30010 40217 54000 333 10170 20044 555 91012= (RM11:59Z)

SA 0751 CLR 7 222/40/47/1504/010/ FG PRSHT/ LX TMP 55 (CT 12:53Z)

SA 0850 CLR 10 221/54/50/1705/010 (CT 13:50Z)

SA 0951 CLR 15 220/60/47/1405/010/ 51005 (CT 14:53Z)

SA 1051 250 -SCT 20 210/65/51/2104/017 (CT 15:52Z)

SA 1151 250 -SCT 25 214/71/45/2306/016 (CT 16:53Z)

SA 1250 250 -SCT 25 207/73/49/1907/014/ 0/001/ 50012 10073 20043 (CT 17:52Z)

72529 32902 21907 10220 20094 30003 40207 50012 00001 333 10220 20044 555 91010= (CT17:53Z)

SA 1350 250 -BKN 25 190/75/49/2204/012 (CT 18:52Z)

SA 1451 270 -BKN 25 192/73/50/1506/009 (CT 19:53Z)

SA 1551 270 SCT 25 192/73/50/1505/009/ 0/001/ 56015 (EM/KR 20:53Z)

SA 1652 270 SCT 25 192/72/49/1704/009 (EM/KR 21:55Z)

SA 1751 270 SCT 15 196/65/50/2003/010 (EM/KR 22:54Z)

SA 1851 270 SCT 15 197/61/50/2003/010/ 0/001/ 53003 10075 20061 (EM/KR 23:56Z)

72529 32974 12003 10162 20100 39992 40197 53003 00001 333 10239 20044 555 91100= (EM/KR00:00Z)

SA 1951 000 BKN 15 190/59/51/2303/011 (EM/KR 00:54Z)

SA 2050 05 SCT 15 199/56/50/2104/011 (EM/KR 01:52Z)

SA 2151 05 SCT 15 199/55/50/2104/011/ 0/070/ 51003 (EM/KR 02:54Z)

SA 2251 05 SCT 15 190/55/49/2204/011 (EM/KR 03:53Z)

SA 2350 70 SCT 15 196/53/40/2106/011/ 400750040 (DA 04:51Z)

MF1-10B

U.S. DEPARTMENT OF COMMERCE, NOAA
NATIONAL WEATHER SERVICE

Station: WSO ROCHESTER NY
Surface Weather Observations Date: OCT 10, 1995 To convert LST to UTC: +5

Time	Station Pressure	Dry Bulb	Wet Bulb	[pressure]		Preci- pitation
				tend- ency	net chg	
-16-	-17-	-18-	-19-	-37-	-38-	-40-
0050	29.560			0	005	
0153	29.560					
0250	29.560					
0350	29.560			5	000	
0450	29.560					
0550	29.560					
0650	29.560	42.7	42.4	4	000	
0751	29.575					
0850	29.575					
0951	29.575	60.0	53.1	1	005	
1051	29.570					
1151	29.560	70.5	56.5			
1250	29.540			0	012	
1350	29.515					
1451	29.495					
1551	29.495			6	015	
1652	29.495	72.2	50.2			
1751	29.505	65.4	56.3			
1851	29.505	61.1	55.0	3	003	
1951	29.510	58.9	54.5			
2050	29.515	56.0	52.0			
2151	29.515	54.9	52.2	1	003	
2251	29.515	55.4	52.0			
2350	29.510	53.4	50.7			

[CLOUD LAYERS AND OBSCURING PHENOMENA]

[illegible]

Synoptic Observations

Time	No.	Precip.	Fall	Snow	Depth	Max.	Min.	State	Soil	[Station Pressure]	
(LST)		(ins.)	(ins.)	(ins.)		Temp	Temp	of	Temp	[Computations]	
						(F)	(F)	Grnd.	(F)	Barograph Corr.	
-42-	-43-	-44-	-45-	-46-	-47-	-48-	-49-	-50-	-56-	-64-	-65-

Mid to

0049		0.00	0.0			44	43			
0049	1	0.00	0.0	0		51	43		29.575	-0.015
0647	2	0.00	0.0	0		43	40		29.580	-0.020
1258	3	0.00	0.0	0		73	43		29.540	0.000
1858	4	0.00	0.0	0		75	61		29.510	-0.005
Mid.		0.00	0.0	0		61	53			

Summary of Day (Midnight to midnight)

[TEMPS]		24-hr	Snow	Snow	[Peak Wind]		[Sky Cover]		Water	Sun-	Sun-	Total	%	[Fastest Wind]	
Max	Min	Precip	Unaltd	Depth	Spd	Dir.	Time	SR-SS	Mid-Mid	Equiv.	Rise	Set	Sun	Psb1	Spd Dir. Time
(F)	(F)	(ins.)	(ins.)	(ins.)	(kts.)	(LST)				(ins.)					(mph) (LST)
-66-	-67-	-68-	-69-	-70-	-71	72	73-	-78-	-79-	-88-					
75	40	0.00	0.0	0	10	S	1240	2	2		0618	1737	676	100	8 19 1250

Weather & Obstruction to Vision

Type	began	end
-82-	-83-	-84-

F 0441 0646

98. Remarks, Notes & Miscellaneous Phenomena

Character of Sunrise: FOGGY Character of Sunset: CLEAR

Time Check: 0100/0650//

H0-83 CONT OTS//

MF1-10A

U.S. DEPARTMENT OF COMMERCE, NOAA
NATIONAL WEATHER SERVICE

Station: WSO ROCHESTER NY

Surface Weather Observations Date: OCT 11, 1995 To convert LST to UTC: +5

Type Time Sky/Ceiling Vsbty&Wx&Obsns Slp/Temp/Dp/Wnd/Asi/ Remarks&SupplementalCodedData

SA 0050 75 SCT 15 199/50/46/2106/012/ 8/070/ 53002 10061 20050 (DA 05:51Z)

72529 32074 12105 10102 20070 39997 40199 53002 01070 333 10239 20044 70000 555 91106= (DA05:53Z)

SA 0150 CLR 13 206/52/46/2305/014 (DA 06:51Z)

SA 0252 CLR 12 209/51/45/2406/015/ 90676 (DA 07:53Z)

SA 0350 CLR 6F 213/51/47/2406/016/ 52014 (DA 08:51Z)

SA 0450 CLR 4F 222/51/40/2306/019 (DA 09:51Z)

SP 0536 CLR 21/2F 2205/020/ R04VR06V60+/ VSBY E-SW 3/4 (DA 10:37Z)

SA 0551 CLR 21/2F 231/51/50/2103/021/ VSBY E-SW 11/2 (DA 10:52Z)

SP 0607 -X 2VF 2104/021/ F2/ VSBY 1V3 (BN 11:00Z)

SP 0619 -X 3/4VF 2103/021/ R22VR20V60+/ F3 / VSBY 1/2V2 (BN 11:20Z)

SP 0645 -X 11/2VF 2104/022/ F1/ VSBY 1V2 (BN 11:47Z)

SA 0651 -X 11/2VF 235/50/49/2104/022/ F1/ 52020 10052 20050/ VSBY 1V2 (BN 11:53Z)

72529 31924 02104 10099 20094 30030 40235 52020 74240 333 10239 20100 555 91112= (BN11:55Z)

SA 0750 250 -SCT 11/2F 239/53/51/2305/023/ LK TNP 56 (TD 12:50Z)

SP 0822 250 -SCT 3F 2205/024/ TWR VSBY 4 (TD 13:23Z)

SA 0851 250 -SCT 4H 242/59/52/2300/024 (TD 13:52Z)

SA 0952 250 -BKN 7 241/63/52/2300/024/ 8/001/ 51007 (TD 14:53Z)

SA 1052 250 -SCT 10 239/67/52/2300/024/ CU VCNTY STN SW-NW (TD 15:54Z)

SA 1152 250 -SCT 15 232/70/47/2209/021/ CU VCNTY STN AL0DS (TD 16:54Z)

SA 1255 250 -SCT 20 223/73/47/2511/019/ CU VCNTY STN AL0DS/ 8/101/ 56017 10073 20050 (TD 17:56Z)

72529 31600 12511 10226 20003 30020 40223 56017 70244 01101 333 10220 20100 555 91110= (TD17:58Z)

SA 1351 250 -SCT 20 216/73/46/2510/017/ CU VCNTY STN AL0DS (TD 18:53Z)

SA 1450 250 SCT 25 213/74/43/2514/016/ CU VCNTY STN N-E (TD 19:51Z)

SA 1554 250 -SCT 25 213/72/46/2514/016/ 0/001/ 56010 (EM/KR 20:59Z)

SA 1650 250 -SCT 25 213/70/46/2610/016 (EM/KR 21:51Z)

SA 1752 250 SCT 15 214/65/44/2305/016 (EM/KR 22:55Z)

SA 1851 CLR 15 213/61/45/2405/016/ CI NW/ 8/001/ 50002 10074 20061 (EM/KR 23:57Z)

72529 32974 12405 10162 20072 30000 40213 50002 00001 333 10233 20100 555 91200= (EM/KR00:03Z)

SA 1952 CLR 15 215/50/46/2006/016 (EM/KR 00:55Z)

SA 2051 CLR 15 214/56/46/2003/016 (EM/KR 01:52Z)

SA 2151 CLR 15 212/54/46/2204/016/ 54000 (EM/KR 02:52Z)

SA 2250 CLR 15 210/53/44/1903/015 (EM/KR 03:52Z)

SA 2351 CLR 15 204/53/44/2204/013/ 400740050 (BN 04:52Z)

NF1-10B

U.S. DEPARTMENT OF COMMERCE, NOAA
NATIONAL WEATHER SERVICE

Station: WSD ROCHESTER NY

Surface Weather Observations

Date: OCT 11, 1995 To convert LST to UTC: +5

Time	Station Pressure	Dry Bulb	Wet Bulb	[pressure]		Preci- pitation
				tend- ency	net chg	
-16-	-17-	-18-	-19-	-37-	-38-	-48-
0050	29.520	50.4	48.2	3	002	
0150	29.540	51.6	48.5			
0251	29.550	51.4	48.1			
0350	29.560	51.1	48.7	2	014	
0450	29.505	50.8	49.4			
0551	29.610	50.8	50.2			
0651	29.620	49.9	49.5	2	020	
0750	29.630	53.2	51.8			
0851	29.640	58.5	54.9			
0952	29.640	63.2	56.5	1	007	
1052	29.635	67.3	58.2			
1152	29.615	70.3	57.0			
1255	29.590	72.6	57.8	6	017	
1351	29.570	73.4	58.0			
1450	29.560	73.9	57.0			
1554	29.560			6	010	
1650	29.560					
1752	29.560	65.1	53.7			
1851	29.555	61.1	52.3	0	032	
1952	29.560	50.3	51.5			
2051	29.560	55.9	50.5			
2151	29.555	53.9	49.8	4	000	
2250	29.550	53.1	48.5			
2351	29.535	52.5	40.2			

[illegible]

Synoptic Observations

Time	No.	Precip.	Snow Fall	Snow Depth	Max. Temp	Min. Temp	State of Temp	Soil Temp	[Station Pressure]
(LST)		(ins.)	(ins.)	(ins.)	(F)	(F)	Grnd. (F)	(F)	Barograph Corr.
-42-	-43-	- 44 -	- 45 -	- 46 -	- 47 -	- 48 -	- 50 -	- 56 -	- 64 - -65 -

Mid to

0049		0.00	0.0		53	50			
0049	1	0.00	0.0	0	61	50		29.525	-0.005
0647	2	0.00	0.0	0	52	50		29.625	-0.005
1254	3	0.00	0.0	0	73	50		29.600	-0.010
1850	4	0.00	0.0	0	74	61		29.560	-0.005
Mid.		0.00	0.0	0	61	53			

Summary of Day (Midnight to midnight)

		24-hr		[Peak Wind]		[Sky Cover]		Water	Sun-	Sun-	Total	%	[Fastest Wind]		
Max	Min	Precip	Unmtd Depth	Spd	Dir.	Time	SR-SS Mid-Mid	Equiv.	Rise	Set	Sun	Ptbl	Spd	Dir.	Time
(F)	(F)	(ins.)	(ins.)	(kts.)		(LST)		(ins.)					(mph)		(LST)
-66-	-67-	-68-	-69-	-70-	-71	72	73-	-78-	-79-	-80-					
74	50	0.00	0.0	0	20	W 1540	3	1	0619	1735	605	89	16	25	1554

Weather & Obstruction to Vision

Type	began	end
-02-	-03-	-04-

F	0333	0049
H	0049	0740

90. Remarks, Notes & Miscellaneous Phenomena

Character of Sunrise: FOGGY Character of Sunset: CLEAR

Time Check: 0100/0645//

//H0-03 OTS CONT//FASTEST 2-MIN WND LAST OF SEVERAL OCCURRENCES//

MF1-10A

U.S. DEPARTMENT OF COMMERCE, NOAA
NATIONAL WEATHER SERVICE

Station: WSO ROCHESTER NY

Surface Weather Observations Date: OCT 12, 1995 To convert LST to UTC: +5

Type Time Sky&Ceiling Vsbty&Wx&Obsns Slp/Temp/Dp/Wnd/Asi/ Remarks&SupplementalCodedData

SA 0054 CLR 15 204/53/46/2107/013/ 57007 10061 20053 (BN 05:56Z)

72529 32974 02107 10116 20070 30002 40204 57007 333 10233 20100 70000 555 91206= (BN05:56Z)

SA 0154 CLR 15 202/52/45/2107/013 (BN 06:56Z)

SA 0250 CLR 15 199/51/43/2006/012/ 90605 (DA 07:51Z)

SA 0350 CLR 15 199/51/44/2005/012/ 56005 (DA 08:51Z)

SA 0450 CLR 15 199/51/42/2106/012 (DA 09:51Z)

SA 0550 250 -SCT 20 200/51/43/2206/012 (DA 10:52Z)

SA 0650 250 -SCT 20 202/52/42/2209/013/ 8/001/ 53002 10053 20051 (DA 11:51Z)

72529 32900 12209 10113 20056 39990 40202 53002 00001 333 10233 20106 555 91212= (DA11:52Z)

SA 0750 250 -SCT 20 203/59/46/2107/013/ LK TNP 57 (TD 12:51Z)

SA 0850 250 -SCT 20 206/65/47/2306/014 (TD 13:51Z)

SA 0952 CLR 20 203/71/49/2511/013/ CI E/ 8/001/ 50002 (TD 14:53Z)

SA 1051 CLR 20 199/75/52/2410/012 (TD 15:52Z)

SA 1151 CLR 20 197/77/52/2510/011 (TD 16:52Z)

SA 1251 CLR 20 191/80/55/2512/010/ 50010 10000 20052 (TD 17:53Z)

72529 32900 02512 10264 20120 39990 40191 50010 333 10267 20106 555 91218= (TD17:56Z)

SA 1351 CLR 20 180/00/54/2412/009 (TD 18:52Z)

SA 1450 CLR 20 180/01/54/2511/009 (TD 19:51Z)

SA 1550 CLR 20 180/79/50/2512/009/ 57003 (NP 20:51Z)

SA 1650 CLR 20 187/70/57/2500/000 (NP 22:17Z)

SA 1750 CLR 20 187/70/56/2105/000 (NP 22:53Z)

SA 1850 CLR 20 189/60/57/2205/009/ 54000 10001 20060 (NP 23:49Z)

72529 31900 02205 10200 20139 39906 40109 54000 70200 333 10272 20106 555 91300= (NP23:51Z)

SA 1950 CLR 20 190/66/55/2106/009 (NP 00:49Z)

SA 2050 CLR 20 190/62/53/2106/009 (NP 01:49Z)

SA 2151 CLR 20 180/61/54/1906/009/ 54000 (NP 02:52Z)

SA 2250 CLR 20 180/50/53/2105/009 (NP 03:40Z)

SA 2350 CLR 20 194/57/49/2004/000/ 400010051 (DA 04:51Z)

MF1-10B

U.S. DEPARTMENT OF COMMERCE, NOAA
NATIONAL WEATHER SERVICE

Surface Weather Observations

Station: WSD ROCHESTER NY
Date: OCT 12, 1995 To convert LST to UTC: +5

Time	Station Pressure	Dry Bulb	Wet Bulb	[pressure]		Preci- pitation
				tend- ency	net chg	
-16-	-17-	-18-	-19-	-37-	-38-	-40-
0054	29.535	52.9	49.1	7	007	
0154	29.530	52.3	48.5			
0250	29.520	51.2	47.1			
0350	29.520	50.6	47.2	6	005	
0450	29.520	50.6	46.5			
0550	29.520	50.5	46.0			
0650	29.525	52.4	47.3	3	002	
0750	29.530	50.5	51.6			
0850	29.540	65.0	55.1			
0952	29.530	71.1	50.2	0	002	
1051	29.520	75.1	61.0			
1151	29.515	77.4	62.1			
1251	29.500	79.5	64.2	0	010	
1351	29.490	80.4	64.0			
1450	29.490	80.6	64.0			
1550	29.490			7	003	
1650	29.485					
1750	29.485					
1850	29.490			4	000	
1950	29.495					
2050	29.495					
2151	29.490			4	000	
2250	29.490					
2350	29.400					

[illegible]

Synoptic Observations

Time	No.	Precip.	Snow	Snow	Max.	Min.	State	Soil	[Station Pressure]
(LST)		(ins.)	Fall	Depth	Temp	Temp	of	Temp	[Computations]
			(ins.)	(ins.)	(F)	(F)	Grnd.	(F)	Barograph Corr.
-42-	-43-	- 44 -	- 45 -	- 46 -	- 47 -	- 48 -	- 50 -	- 56 -	- 64 -
									- 65 -

Mid to

0047		0.00	0.0		53	53			
0047	1	0.00	0.0	0	61	53		29.540	-0.005
0649	2	0.00	0.0	0	53	51		29.525	0.000
1249	3	0.00	0.0	0	00	52		29.500	0.000
1850	4	0.00	0.0	0	81	68		29.495	-0.005
Mid.		0.00	0.0	0	68	57			

Summary of Day (Midnight to midnight)

[TEMPS]		24-hr	Snow	Snow	[Peak Wind]		[Sky Cover]		Water	Sun-	Sun-	Total	%	[Fastest Wind]	
Max	Min	Precip	Unmtd	Depth	Spd	Dir.	Time	SR-SS	Mid-Mid	Equiv.	Rise	Set	Sun	Psb1	Spd Dir. Time
(F)	(F)	(ins.)	(ins.)	(ins.)	(kts.)	(LST)				(ins.)					(mph) (LST)
-66-	-67-	-68-	-69-	-70-	-71	72	73-	-78-	-79-	-80-					
01	51	0.00	0.0	0	10	SW	1240	0	0		0620	1734	617	92	14 25 1550

Weather & Obstruction to Vision

Type	began	end
-82-	-83-	-84-

<<< None Logged >>>

98. Remarks, Notes & Miscellaneous Phenomena

Character of Sunrise: CLEAR Character of Sunset: CLEAR

Time Check: 0111/0646//

HO-83 OTS CONT//FASTEST 2-MIN WIND SPEED WAS LAST OF SEVERAL OCCURRENCES

Single-Station RAOB data for: RUF

Date: 10/12/95 Time: 12 UTC

Page - 1

*****CONVECTIVE INDICES*****

Lifted Index @ 500mb...	6	Cross Totals (CT).....	14
@ 300mb...	9	Vertical Totals (VT)....	26
		Total Totals.....	40
Shower Index.....	7	B+.....	0 J/kg
Sweat Index.....	153	B-.....	0 J/kg
TEI.....	4.5	Max UVV.....	0 m/s
K Index.....	0		
Precipitable Water.....	0.57 in	BRN.....	0
700-500mb Lapse Rate...	7.4 C/km	Energy/Helicity Index..	0.00

***** STORM ENVIRONMENT *****

STORM MOTION: 243/ 35

DEPTH: AGL m	SHEAR			HELICITY				Rel	MEAN WIND		MEAN STORM		VORTICITY	
	Pos	Neg	Tot	Pos	Neg	Tot	Ave		Vector	Inflow	Horiz	Stream		
	(10-3 s-1)			(m/s)^2					(Dir/kt)	(Dir/kt)	(10-3 s-1)			
1000	14.1	7.4	21.5	184	-7	177	177.0	0.90	213/29	116/18	33.94	30.48		
2000	9.1	4.3	13.5	192	-17	175	87.5	0.49	214/36	140/18	21.42	10.52		
3000	4.8	3.0	7.8	212	-37	175	58.3	0.52	212/40	150/20	12.86	6.73		
4000	4.8	2.3	7.1	249	-37	212	53.0	0.62	213/43	157/21	10.58	6.54		
5000	3.9	2.0	6.6	264	-41	223	44.6	0.53	213/45	162/22	10.12	5.35		
6000	3.3	2.4	5.7	273	-52	221	36.8	0.54	213/47	166/24	8.02	4.31		

***** WIND DATA *****

HEIGHT AGL (m)	dir	GROUND RELATIVE				dir	STORM RELATIVE			
		speed	u-mag	v-mag			speed	u-mag	v-mag	
		kt	m/s	m/s			kt	m/s	m/s	
0.0	190.0	14.0	7.2	-1.3	-7.1	85.2	29.2	15.0	15.0	1.3
285.0	203.0	33.0	17.0	-6.6	-15.6	127.2	23.4	12.0	9.6	-7.3
785.0	229.0	43.0	22.1	-16.7	-14.5	184.4	12.0	6.2	-0.5	-6.2
1285.0	219.0	44.0	22.7	-14.3	-17.6	168.0	18.4	9.5	2.0	-9.3
1785.0	210.0	53.0	27.3	-13.6	-23.6	170.4	30.1	15.5	2.6	-15.3
2285.0	210.0	54.0	27.8	-13.7	-24.1	171.6	30.9	15.9	2.3	-15.7
2785.0	210.0	50.0	25.7	-12.9	-22.3	166.5	27.9	14.3	3.4	-13.9
3285.0	214.0	54.0	27.8	-15.5	-23.0	177.3	28.6	14.7	0.7	-14.7
3785.0	215.0	55.0	28.3	-16.2	-23.2	180.0	28.8	14.8	-0.0	-14.8
4285.0	215.0	57.0	29.3	-16.8	-24.0	182.2	30.5	15.7	-0.6	-15.7
4785.0	214.0	61.0	31.4	-17.6	-26.0	184.3	34.4	17.7	-1.3	-17.7
5285.0	211.0	65.0	33.5	-17.2	-28.7	182.8	39.5	20.4	-1.0	-20.3
5785.0	210.0	66.0	34.0	-17.0	-29.4	182.1	41.0	21.1	-0.8	-21.1
6285.0	213.0	64.0	32.9	-17.9	-27.6	185.1	37.6	19.4	-1.7	-19.3
6785.0	217.0	62.0	31.9	-19.2	-25.5	189.9	33.8	17.4	-3.0	-17.1
7285.0	223.0	60.0	30.9	-21.1	-22.6	198.8	29.2	15.0	-4.8	-14.2
7785.0	225.0	61.0	31.4	-22.2	-22.2	203.3	29.3	15.1	-6.0	-13.9
8285.0	225.0	61.0	31.4	-22.2	-22.2	203.3	29.3	15.1	-6.0	-13.9
8785.0	225.0	65.0	33.5	-23.7	-23.7	205.9	33.1	17.0	-7.4	-15.3

Single-Station RAOB data for: BUF

Date: 10/12/95 Time: 12 UTC

Page - 2

*****THERMODYNAMIC DATA*****

LEVEL	PRES	HGT (AGL)	TEMP		DEWPT		TH-W	TH-E
	mb	ft m	C	F	C	F	K	K
SFC	987	0 0	15.4	59.7	4.4	39.9	283.4	306.1
LPL	925	1811 552	13.2	55.8	3.4	38.1	284.7	309.6
LCL	832	4720 1439	11.1	51.9	0.1	32.1	286.6	315.1
WBZ	767	6927 2112	9.3	48.7	-17.0	1.3	284.9	310.3
FZL	637	11841 3610	-0.0	32.0	-24.7	-12.5	286.5	314.7
EL	-999	-999 -999	-999.0	-999.0	-999.0	-999.0	-999.0	-999.0
TROP	163	42873 13071	-62.6	-80.7	-999.0	-999.0	-999.0	-999.0
MPL	-999	-999 -999	-999.0	-999.0	-999.0	-999.0	-999.0	-999.0

PRESSURE	HEIGHT (AGL)	TEMP		DEWPT		TH-W	TH-E	WETB.	w
mb	ft m	C	F	C	F	K	K	C	
987	0 0	15.4	59.7	4.4	39.9	283.4	306.2	9.7	5.3
950	1073 327	14.7	58.5	4.9	40.8	284.9	310.1	9.5	5.7
900	2572 784	11.7	53.1	6.9	44.4	286.6	315.3	9.0	7.0
850	4139 1262	10.6	51.1	-0.4	31.3	285.4	311.8	5.2	4.4
800	5786 1764	11.9	53.4	-14.4	6.1	284.9	310.4	1.7	1.6
750	7534 2297	7.9	46.2	-17.1	1.2	285.1	310.9	-1.1	1.3
700	9407 2868	4.6	40.3	-20.4	-4.7	285.6	312.4	-3.7	1.1
650	11319 3451	1.3	34.3	-23.4	-10.1	286.4	314.7	-6.3	0.9
600	13386 4081	-3.7	25.3	-26.6	-15.9	286.8	315.6	-9.9	0.7
550	15629 4765	-9.0	15.8	-30.1	-22.2	287.0	316.5	-14.0	0.6
500	18089 5515	-14.9	5.2	-19.2	-2.6	288.8	321.9	-16.2	1.7
450	20644 6294	-20.4	-4.7	-35.5	-31.9	288.1	320.0	-23.1	0.4
400	23501 7165	-26.9	-16.4	-41.9	-43.4	288.6	321.6	-28.9	0.2
350	26561 8098	-34.4	-29.9	-40.7	-41.3	289.4	324.2	-35.2	0.3
300	30094 9175	-42.1	-43.8	-52.1	-61.8	290.3	327.0	-42.8	0.1
250	34063 10385	-50.1	-58.2	-999.0	-999.0	-999.0	-999.0	-999.0	-99.9
200	38720 11805	-58.9	-74.0	-999.0	-999.0	-999.0	-999.0	-999.0	-99.9
150	44559 13585	-63.9	-83.0	-999.0	-999.0	-999.0	-999.0	-999.0	-99.9
100	52693 16065	-62.1	-79.8	-999.0	-999.0	-999.0	-999.0	-999.0	-99.9

NOAA Form 34-326T
(Rev. 1-93)

TRANSMITTAL

NO PAYMENT DUE - PAID IN FULL

U.S. Department of Commerce
National Oceanic and Atmospheric Administration
National Environmental Satellite, Data and Information Service
NATIONAL CLIMATIC DATA CENTER
Asheville NC 28801-5001
Phone (704) 271-4800
Federal Tax ID 52-0821608

INDIVIDUAL

ORDER #	PAYMENT METHOD	PRINTED	CUSTOMER #	PHONE/MAIL TYPE	MAIL ACCT	PAGE	CBRAD
162750		10/31/1995 09:54	66807	FIRST CLASS		1	1CNTR BN3ANPAA InvDt 103195

Ship to Attn:

TODD KRASKA
226 BENNINGTON HILLS COURT
WEST HENRIETTA NY 14586

Bill to Attn: TODD KRASKA

TODD KRASKA
226 BENNINGTON HILLS COURT
WEST HENRIETTA NY 14586

DESCRIPTION	AMOUNT
01 UPPER-AIR WEATHER OBSERVATION BUFFALO, NEW YORK 11/10/1991 00:00 MICRO PRINTS 11/11/1991 12:00	\$ 7.00
02 SURFACE WEATHER OBSERVATIONS ROCHESTER, NEW YORK 11/09/1991 MICRO PRINTS 11/11/1991	\$ 0.00
98 SERVICE CHARGE OTHER	\$ 5.00

The National Climatic Data Center (NCDC) guarantees its data and information to be of readable quality (except in cases where the disclaimer statement, "Best Available Copy," accompanies the data). If the data or information are not legible, the original purchaser may return the data to the NCDC within 60 days of the transmittal date. NCDC will replace it at no charge to the customer. This guarantee does not apply to data delivered via telecopier.

NO PAYMENT DUE - PAID IN FULL
TOTAL \$ 12.00
LESS PREPAID \$ 12.00
AMOUNT OWED \$ 0.00

KEY TO AVIATION
WEATHER OBSERVATIONS

[illegible]

COLUMN 1. TYPE OF OBSERVATION

AVGA is an acronym standing for "Aviation Aviation". "Surface", means the observation was taken at ground level and "Aviation", means the observation was taken in the aviation field. These observations are taken within the 10 minute period that prior to the hour. This is an observation detailing all conditions observed at that particular site.

SSP means "Special". This is an observation taken anytime during the hour when meteorological conditions change enough to warrant a special notation. These observations are generally limited to sky and ceiling conditions, visibility, weather and obstructions to vision, wind, and pressure.

RS means "Record Special". This is a normally scheduled hourly observation in which one or more of the meteorological elements has changed significantly since the last observation to warrant special notation.

COLUMN 2. TIME OF OBSERVATION

The actual time of observation entered in *Local standard Time. (see conversion table at end of text)

COLUMN 3. SKY AND CEILING

sky cover contractions are for each layer of clouds in ascending order. Figures preceding contractions are the heights of the base of the cloud layer in hundreds of feet above the station elevation. Sky cover contractions used are:

CLR = Clear. Less than 0.1 tenth of sky cover. - = Thin when prefixed to SCT, BKN, or OVC.
SCT = Scattered. One tenth to 0.5 sky cover. -X = Partly obscured. Nine tenths or less of sky hidden by precipitation or obstruction to vision. (bases at surface)
BKN = Broken. Six to 0.9 sky cover. X = Obscured. Ten tenths of sky hidden by precipitation or obstruction to vision. (bases at surface)
OVC = Overcast. More than 0.9 sky cover.

vision. (bases at surface)
 A letter preceding the height of a base. Identifies a ceiling layer, and indicates how the ceiling height was determined. Thus:

E = Estimated M = Measured W = Vertical visibility into obscured sky
V = Immediately following the height of a base indicates a variable ceiling height.

COLUMN 4. SURFACE VISIBILITY 4a. TOWER VISIBILITY

Reported in statute miles and fractions. (V = variable)

COLUMN 5. WEATHER AND OBSTRUCTION TO VISION SYMBOLS

A	Hail	IC	Ice crystals	B	Snow	BC	Blowing dust	IF	Ice fog
BU	Snow grain	BM	Blowing sand	IP	Ice pellets	BP	Snow pellets	DS	Blowing snow
IPM	Ice pellet showers	L	Snow showers	D	Dust	K	Smoke	T	Thunderstorms
F	Fog	BR	Drizzle	T	Severe T-storm	QF	Ground fog	R	Rain
ZL	Freezing drizzle	B	Haze	RM	Rain showers	ZA	Freezing rain		

Precipitation intensities are indicated thus:
 - - light, (no sign) - moderate, + - heavy

COLUMN 6. SEA LEVEL PRESSURE

Measured in hectopascals (millibars) using only the tens, units, and tenths digits, e.g. 1013.2 as 132

COLUMN 7. TEMPERATURE COLUMN 8. DEW-POINT TEMPERATURE

Measured in whole degrees Fahrenheit.

COLUMN 9, 10, & 11 WIND, DIRECTION, SPEED, & CHARACTER

Direction is reported in tens of degrees from true north.
 Speed is reported in knots. 0000 indicates calm, 0 gusty.
 0 equals. Peak wind speed in the past 10 minutes follows
 0 or 0 when gusts or equals are reported. The contraction
 MSHFT, followed by GMT time in remarks, indicates windshift and it's time of occurrence. (Knots x 1.15 = statute mi/hr)

EXAMPLES: 3627 - wind from 360 Degrees at 27 knots.
 3627040 - wind from 360 Degrees at 27 knots, peak
 gust of 40 knots.

COLUMN 12. ALTIMETER SETTING

The first figure of the actual altimeter setting is always omitted from the report, e.g. 933 = 29.93

COLUMN 13. REMARKS AND CODED DATA

Entries in this column are made to record operationally significant information not recorded elsewhere or to elaborate on preceding coded data.

FOR EXAMPLE

STANDARD TIME FROM	TO CONVERT TO GMT ADD	1200 LEX EQUALS
Atlantic Standard Time	4 hours	1600 GMT
Eastern Standard Time	5 hours	1700 GMT
Central Standard Time	6 hours	1800 GMT
Mountain Standard Time	7 hours	1900 GMT
Pacific Standard Time	8 hours	2000 GMT
Yukon Standard Time	9 hours	2100 GMT
Alaska-Hawaii Standard Time	10 hours	2200 GMT
Bering Standard Time	11 hours	2300 GMT

U.S. DEPARTMENT OF COMMERCE NATIONAL OCEANIC AND ATMOSPHERIC ADMINISTRATION NATIONAL WEATHER SERVICE										STATION ROCHESTER, NY		DATE NOVEMBER 9, 1991		TO CONVERT LST TO GMT ADD .05 hrs. SUBTRACT hrs.												
SURFACE WEATHER OBSERVATIONS																										
TIME (LST)	STATION (INS)	PRESSURE (deg. f.)	WET BULB RELATIVE HUMIDITY	TOTAL SKY COVER	CLOUDS AND OBSCURING PHENOMENA				TOTAL SKY COVER	CLOUDS AND OBSCURING PHENOMENA				PRECIP- ITATION (INS)												
					LOWEST LAYER	SECOND LAYER	THIRD LAYER	FOURTH LAYER		LOWEST LAYER	SECOND LAYER	THIRD LAYER	FOURTH LAYER													
					AMT	TYPE	HGT	AMT	TYPE	HGT	AMT	TYPE	HGT	AMT	TYPE	HGT	AMT	TYPE	HGT	AMT	TYPE	HGT	AMT	TYPE	HGT	
00 50	29895	21.0	20.1	1	1	SC	55																			
01 50	29910	20.0	19.4	1	1	SC	55																			
02 50	29910	20.0	19.4	1	1	SC	55																			
03 50	29920	19.0	18.4	1	1	SC	55																			
04 50	29920	18.0	17.4	1	1	SC	55																			
05 50	29920	18.0	17.4	1	1	SC	55																			
06 50	29945	18.0	17.4	1	1	SC	55																			
07 50	29955	19.0	18.4	1	1	SC	55																			
08 51	29955	24.0	22.4	1	1	SC	55																			
09 50	29955	29.0	26.3	0	0	SC	50																			
10 52	29945	35.0	30.1	0	0	SC	45																			
11 51	29925	37.0	30.7	0	0	SC	41																			
12 51	29905	35.0	27.1	0	0	SC	40																			
13 52	29880	37.0	31.0	0	0	SC	39																			
14 53	29865	35.0	29.8	0	0	SC	40																			
15 53	29855	32.0	27.9	0	0	SC	40																			
16 53	29855	31.0	27.3	0	0	SC	40																			
17 53	29855	30.0	26.7	0	0	SC	40																			
18 54	29845	28.0	25.7	0	0	SC	40																			
19 53	29835	23.0	21.8	0	0	SC	40																			
20 50	29815	24.0	22.7	0	0	SC	40																			
21 54	29815	22.0	21.4	0	0	SC	40																			
22 55	29805	22.0	21.4	0	0	SC	40																			
23 50	29785	21.0	20.1	0	0	SC	40																			

SYNOPTIC OBSERVATIONS																	
TIME (GMT)	TIME (LST)	NO.	PRECIP (INS)	SNOW FALL (INS)	SNOW DEPTH (INS)	MAX TEMP (deg. f.)	MIN TEMP (deg. f.)	PRECIP ORIG.	STATE OF GRND.	51	52	53	54	55	56	57	58
	0048	1	0.00	0.00	0.0	22	21										
	0648	2	0.00	0.00	0.0	22	17										
	1245	3	0.00	0.00	0.0	30	30										
	1846	4	0.00	0.00	0.0	30	21										

STATION PRESSURE COMPUTATIONS													
TIME (LST)	53	0048	0648	1245	1846								
ATT. THERM.	60												
OBSVD. BAR.	61												
TOTAL CORR.	62												
STA. PRESS.	63												
BAROGRAPH	64	29.890	29.940	29.905	29.840								
BAR. CORR.	65	+ .005	+ .005	+ .000	+ .005								

WEATHER & OBSTRUCTIONS TO VISION													
TYPE	BEGAN	ENDED	TYPE	BEGAN	ENDED								
82	83	84	85	86	87								

90. REMARKS, NOTES AND MISCELLANEOUS PHENOMENA													
SUNSET 1655 CHARACTER OF SUNSET CLOUDY CHARACTER OF SUNSET CLEAR FASTEST OBSERVED 1-MINUTE WIND SPEED (MPH) 8 OR FASTEST 10-MILE TIME CHECK== 1805 // 175R*10//													

M1-10A (1-85)			U.S. DEPARTMENT OF COMMERCE NATIONAL OCEANIC AND ATMOSPHERIC ADMINISTRATION NATIONAL WEATHER SERVICE				STATION ROCHESTER, NY				TO CONVERT LST TO GMT ADD 05 hrs. SUBTRACT				OBSERVER'S INITIALS (15)
TYPE	TIME (12)	SKY AND CEILING (Hundreds of Feet) (3)	SURFACE WEATHER OBSERVATIONS		SEA LEVEL PRESS (Hrs) (6)	TEMP. (deg. F) (7)	DEW PT. (deg. F) (8)	WIND			REMARKS AND SUPPLEMENTAL CODED DATA (13)	ALTIMETER (Inches) (12)	CHAR- ACTER (11)	DATE NOVEMBER 9, 1991	hrs
			VISI- BILITY (Miles) (4)	WEATHER AND OBSTRUCTIONS to VISION (5)				DIR (100-36) (9)	SPEED (Kts.) (10)	CHARTER (11)					
SA 0050	555CT	32774 12305 11061 21078	15	55000 81500 333	337	21	18	23	05	90906	500 1500 36	050			
SA 0150	555CT		30124 40337		10022 21061	20	4/001	23	05		11005	10001			
SA 0250	555CT		15		342	20	18	23	06		98386	051			
SA 0350	555CT		15		343	20	18	23	06		105 1500	051			
SA 0450	555CT		12		346	19	17	22	04			052			
SA 0550	555CT		15		347	18	16	21	04		312 1500 17	053			
SA 0650	555CT	32774 12104 11078 21089	30141 40356	53012 81500 333	10022 21083	19	17	21	04	90912		10001			
SA 0750	555CT		12		359	24	19	21	06			056			
SA 0850	555CT		15		358	29	21	23	05		FEW SC/ LK TEMP 47	056			
SA 0950	555CT		15		354	35	21	00	00		FEW SC/ 103 1500	055			
SA 1052	555CT		25		347	37	19	36	04		FEW SC	055			
SA 1151	555CT		25		340	35	18	10	07		817 1500 17	051			
SA 1251	555CT		25		10033 21083	36	19	04	05			049			
SA 1352	555CT	32682 41007 10017 21078	30127 40340	58017 84500 333	332	36	20	05	06			049			
SA 1452	555CT		25		335	37	20	03	06			047			
SA 1552	555CT		25		327	35	20	03	06		FEW SC/ 814 1501	046			
SA 1652	555CT		25		324	32	20	04	06			046			
SA 1752	555CT		25		324	31	20	02	05		807 38	045			
SA 1854	555CT		15		321	30	20	11	03			045			
SA 1953	555CT	32974 01103 11011 21067	30107 40321	58007 333 10033	21083 555	28	21	00	00			044			
SA 2050	555CT		15		317	23	19	00	00			042			
SA 2154	555CT		15		310	24	20	17	03		610	042			
SA 2255	555CT		15		306	22	20	13	04			041			
SA 2350	555CT		15		298	21	18	00	00			039			

A synoptic observation, in WMO code format FM12-VII, is entered on line following related aviation observation.
 FM12-VII: 11111 1R1XHVW Nddff 1snTTT 2snTdTd 3p0p0p0 4pppp 5pppp 6RRRtR 7wHtH2 8NhCtCmCh

U.S. DEPARTMENT OF COMMERCE
NATIONAL OCEANIC AND ATMOSPHERIC ADMINISTRATION
NATIONAL WEATHER SERVICE

STATION ROCHESTER, NY

TO CONVERT LST TO GMT
ADD 05 hrs. SUBTRACT

hrs

SURFACE WEATHER OBSERVATIONS

[illegible]

SYNOPTIC OBSERVATIONS

[illegible]

0	0	40	37		
---	---	----	----	--	--

[illegible]

90. REMARKS, NOTES AND MISCELLANEOUS PHENOMENA

TIME: SUNRISE 0656		SUNSET 1654	
TOTAL		% OF POSSIBLE SUNSHINE (MIN) 493	CHARACTER OF SUNRISE CLOUDY
FASTEST OBSERVED		OR FASTEST	DIREC-
1-MINUTE WIND SPEED (MPH) 18		MILE	TION 02
			TIME 1453

TIME CHECKED 1806 11

STATION PRESSURE COMPUTATIONS

	TIME	ILST	59	0047	0648	1245	1846
ATT. THERM.	60						
OBSRVD BAR.	61						
TOTAL CORR.	62						
STA. PRESS.	63			29.780	29.720	29.610	29.525
BAROGRAPH	64			-.020	+.005	.000	+.005
BAR. CORR.	65						

WEATHER & OBSTRUCTIONS TO VISION

TYPE	BEGAN 83	ENDED 84	TYPE 86	BEGAN 87	ENDED 88
-	1901	2007			
-	2210	CONT			
-					

FM1-10A (1-85)		U.S. DEPARTMENT OF COMMERCE NATIONAL OCEANIC AND ATMOSPHERIC ADMINISTRATION NATIONAL WEATHER SERVICE				STATION ROCHESTER, NY		DATE NOVEMBER 10, 1991		TO CONVERT LST TO GMT ADD 05 hrs. SUBTRACT		hrs													
SURFACE WEATHER OBSERVATIONS		SKY AND CEILING (Hundreds of Feet)		VISI- BILITY (Miles)		WEATHER AND OBSTRUCTIONS TO VISION		SEA LEVEL PRESS (Hrs)		TEMP. (deg. F.)		DEM (ft.)		WIND SPEED (Kts.)		HIND (00-36)		CHAR- ACTER		AL SETTING		REMARKS AND SUPPLEMENTAL CODED DATA		OBSERVER'S INITIALS	
(1)	(2)	(3)	(4)	(5)	(6)	(7)	(8)	(9)	(10)	(11)	(12)	(13)	(14)	(15)	(16)	(17)	(18)	(19)	(20)	(21)	(22)	(23)	(24)	(25)	(26)
SA 0050	CLR	72529 32974 00000 11067 21083	15	30078	40290	58019 333 10033	290	21083	70000	20	17	00	LOXDA	00	00	036	819 38								
SA 0150	CLR	72529 32974 00000 11067 21083	15	30078	40290	58019 333 10033	292	21083	70000	20	18	00	LOXDA	00	00	037	98570								
SA 0250	CLR	72529 32974 00000 11067 21083	15	30078	40290	58019 333 10033	288	21083	70000	19	18	00	LOXDA	00	00	036	803								
SA 0350	CLR	72529 32974 00000 11067 21083	15	30078	40290	58019 333 10033	287	21083	70000	19	17	00	LOXDA	00	00	035									
SA 0450	CLR	72529 32974 00000 11067 21083	12	30078	40290	58019 333 10033	284	21083	70000	17	14	00	LOXDA	00	00	034									
SA 0550	CLR	72529 32974 00000 11067 21083	12	30078	40290	58019 333 10033	284	21083	70000	18	15	19	LOXDA	04	04	034									
SA 0650	CLR	72529 32974 00000 11067 21083	8	30066	40280	58008 81070 333	280	21083	70000	15	13	23	LOXDA	03	03	033	808 1070 15								
SA 0750	100SCT	72529 32962 12303 11094 21106	8	30066	40280	58008 81070 333	10033	21084	555	19	18	22	LOXDA	04	04	032	LK TEMP 47								
SA 0850	120SCT	72529 32962 12303 11094 21106	8	30066	40280	58008 81070 333	276	21084	555	25	22	00	LOXDA	00	00	036	FEW AC/ 812 1071								
SA 0950	120SCT	72529 32962 12303 11094 21106	8	30066	40280	58008 81070 333	276	21084	555	25	22	00	LOXDA	00	00	036	FEW AC								
SA 1050	120SCT	72529 32962 12303 11094 21106	25	30066	40280	58008 81070 333	259	21084	555	36	20	11	LOXDA	08	08	027									
SA 1150	120SCT	72529 32962 12303 11094 21106	25	30066	40280	58008 81070 333	251	21084	555	41	24	06	LOXDA	08	08	025									
SA 1251	100SCT	72529 32962 12303 11094 21106	25	30066	40280	58008 81070 333	238	21084	555	41	24	02	LOXDA	14	14	021	727 1071 15								
SA 1353	100SCT	72529 32962 12303 11094 21106	25	30066	40280	58008 81070 333	10056	21094	555	41	24	02	LOXDA	14	14	021									
SA 1453	100SCT	72529 32962 12303 11094 21106	25	30066	40280	58008 81070 333	227	21094	555	41	25	03	LOXDA	10	10	018									
SA 1550	100SCT	72529 32962 12303 11094 21106	25	30066	40280	58008 81070 333	221	21094	555	39	25	02	LOXDA	16	16	016									
SA 1652	100SCT	72529 32962 12303 11094 21106	25	30066	40280	58008 81070 333	219	21094	555	38	25	03	LOXDA	12	12	015	719 1054								
SA 1753	100SCT	72529 32962 12303 11094 21106	15	30066	40280	58008 81070 333	218	21094	555	38	27	06	LOXDA	08	08	015									
SA 1852	100SCT	72529 32962 12303 11094 21106	15	30066	40280	58008 81070 333	214	21094	555	39	27	04	LOXDA	08	08	014	708 1071 42								
SA 1950	100SCT	72529 32966 80311 10044 21028	10	30000	40211	57008 88071 333	211	21094	555	40	27	03	LOXDA	11	11	013									
SA 2054	100SCT	72529 32966 80311 10044 21028	7	30000	40211	57008 88071 333	10056	21094	555	38	30	03	LOXDA	10	10	009	RB01								
SA 2155	100SCT	72529 32966 80311 10044 21028	10	30000	40211	57008 88071 333	189	21094	555	39	30	03	LOXDA	11	11	007	REC7								
SA 2254	100SCT	72529 32966 80311 10044 21028	10	30000	40211	57008 88071 333	185	21094	555	39	30	03	LOXDA	11	11	006	B2402 1071								
SA 2350	100SCT	72529 32966 80311 10044 21028	7	30000	40211	57008 88071 333	176	21094	555	37	31	02	LOXDA	12	12	003	RB10								
							172	21094	555	37	31	03	LOXDA	13	13	002									

A synoptic observation, in HMO code format FM12-VII, is entered on line following related aviation observation.
 FM12-VII: 11111 RHVV Nddff 1sn111 2sn1d1d7 3PoPoPoPo 4pppp 5appp 6RRRR 7HHH1H2 8NNC1CmCh

BUFFALO, NEW YORK
RADIOSONDE/RAMINSONDE OBSERVATION WBAN NO. 14733 10 NOVEMBER 1991
TIME (UTC) 12
RELEASE TIME (UTC) 1102
TROPOPAUSE DATA - PRESS (hPa): 159.6 HEIGHT (M-MSL): 13415 TEMP (DEG C):-61.8
* NCDC GENERATED LEVELS : ELAPSED TIMES MAY VARY + OR - .09 MINUTE FROM ACTUAL TIME.

ELAPSED TIME (MIN)	PRESSURE (hPa)	HEIGHT (M-MSL)	TEMP (DEG C)	DEW POINT (DEG C)	RH %	WIND DIR (DEG)	WIND SPD (KTS)
.0	1000.0	218	-7.0	-7.8	94	080	006
.1	997.0	242	-6.1	-10.8	69	079	006
.3	990.9	290	-3.7	-6.4	81	077	008
.6	981.6	365	-1.8	-7.2	66	076	008
1.0	969.8	461	-2.0	-9.6	56	080	006
* 1.6	950.0	625	-2.8	-9.6	59	072	012
2.2	933.1	767	-3.6	-9.6	63	072	014
2.6	919.7	881	-3.7	-12.4	51	073	012
2.8	913.2	937	-3.0	-14.3	41	074	012
3.1	903.8	1019	-0.3	-18.0	25	076	012
* 3.2	900.0	1053	0.7	-18.0	24	077	012
3.4	894.2	1105	2.3	-18.0	20	078	010
3.8	882.9	1208	3.1	-17.3	20	083	008
4.9	850.0	1516	3.6	-16.8	21	087	006
6.2	814.3	1864	3.0	-17.3	21	115	002
* 6.7	800.0	2008	3.6	-16.9	21	136	004
7.1	789.7	2113	4.2	-16.6	20	143	004
* 8.5	750.0	2531	2.4	-17.9	20	178	002
10.2	705.2	3026	0.1	-19.6	21	188	004
10.4	700.0	3085	-0.4	-20.0	21	188	004
11.0	684.8	3260	-1.3	-20.8	21	190	004
11.5	672.6	3403	-1.2	-19.2	24	193	004
* 12.4	650.0	3674	-3.4	-20.4	25	204	006
12.7	645.0	3735	-3.9	-20.7	26	210	006
12.9	641.0	3784	-3.7	-17.0	35	215	006
13.3	633.0	3883	-3.5	-19.8	27	219	008
* 14.8	600.0	4304	-6.0	-20.9	29	220	012
15.2	592.7	4400	-6.6	-21.2	30	221	012
15.5	586.1	4488	-6.4	-23.5	24	222	012
* 17.1	550.0	4982	-9.8	-26.5	24	226	016
19.6	500.0	5710	-15.0	-31.0	24	219	021
* 22.3	450.0	6498	-20.4	-35.3	24	223	025
22.8	442.2	6628	-21.3	-36.1	24	224	027
23.5	430.0	6834	-22.9	-35.9	29	221	031
25.0	403.3	7300	-27.2	-32.5	60	213	037
25.2	400.0	7359	-27.6	-33.2	58	213	037
25.7	391.6	7511	-28.5	-36.5	45	213	039
26.7	374.3	7834	-30.4	-40.1	37	217	043
* 28.1	350.0	8310	-34.7	-44.2	37	225	041
28.8	339.9	8511	-36.6	-46.0	36	227	041
30.0	321.6	8892	-39.9	-49.0	36	225	043
31.5	300.0	9363	-43.6			224	045
35.3	250.0	10566	-52.3			223	039
36.1	240.8	10808	-53.9			223	041
36.6	235.2	10959	-53.5			227	045
37.7	223.8	11277	-55.6			233	051
39.1	210.5	11667	-56.6			231	056
40.2	200.0	11992	-56.4			223	058
41.0	192.0	12252	-55.4			217	062
41.9	183.4	12543	-57.4			215	070

BUFFALO, NEW YORK
 RADIOSONDE/RAWINSONDE OBSERVATION WBAN NO. 14733 10 NOVEMBER 1991
 TIME (UTC) 12 (CONTO)
 RELEASE TIME (UTC) 1102
 TROPOPAUSE DATA - PRESS (hPa): 159.6 HEIGHT (M-MSL): 13415 TEMP (DEG C):-61.8
 * NCDC GENERATED LEVELS : ELAPSED TIMES MAY VARY + OR - .09 MINUTE FROM ACTUAL TIME.

ELAPSED TIME (MIN)	PRESSURE (hPa)	HEIGHT (M-MSL)	TEMP (DEG C)	DEW POINT (DEG C)	RH %	WIND DIR (DEG)	WIND SPD (KTS)
42.6	176.6	12782	-57.4			216	072
* 42.7	175.0	12839	-57.9			216	072
43.3	169.7	13033	-59.7			216	074
44.5	159.6	13415	-61.8			218	072
45.8	150.0	13799	-61.9			225	064
46.4	146.1	13962	-61.4			229	060
46.6	144.9	14013	-60.2			229	060
46.8	143.7	14065	-59.9			230	058
47.5	139.3	14259	-60.6			233	054
48.1	135.8	14418	-60.0			236	051
48.8	131.4	14623	-60.3			238	049
* 49.7	125.0	14933	-61.9			239	043
50.1	123.0	15033	-62.5			238	041
51.5	115.0	15449	-61.7			230	037
52.4	110.3	15707	-62.8			228	037
52.9	107.7	15854	-62.2			229	037
53.5	104.9	16017	-62.9			231	039
54.6	100.0	16312	-62.8			237	039
55.6	95.0	16629	-61.8			239	041
56.8	89.4	17003	-64.5			237	045
58.0	84.1	17376	-64.8			237	041
58.3	82.9	17464	-64.7			237	043
58.9	80.6	17637	-62.4			238	047
* 59.0	80.0	17683	-62.2			238	047
59.2	79.5	17722	-62.0			239	047
59.8	77.4	17887	-62.9			244	045
60.5	74.6	18115	-61.1			246	047
61.4	71.0	18421	-62.7			249	047
61.7	70.0	18509	-61.6			251	045
64.0	62.3	19230	-62.6			250	037
* 64.6	60.0	19463	-61.0			251	031
65.0	58.9	19578	-60.2			252	027
66.8	53.6	20162	-63.4			246	043
68.2	50.0	20592	-60.8			251	045
69.1	48.0	20848	-57.6			252	045
71.2	42.6	21598	-59.9			247	045
* 72.3	40.0	21993	-58.4			241	049
72.7	39.2	22120	-57.8			239	052
73.8	36.7	22533	-60.2			240	058
77.1	30.0	23791	-59.9			257	056
80.0	25.1	24912	-57.1			255	062
* 80.0	25.0	24937	-57.1			255	062
82.0	21.9	25769	-60.2			255	054
83.3	20.0	26335	-60.1			254	072
85.2	17.6	27133	-59.8				

Appendix F

Sensitivity Analysis

Meteorological Data

Material Parameter Data

Time History Data

Weather Parameter Sensitivity Analysis

Weather Parameter: Temperature

Read in the resulting output files from THERM for the Direct & Diffuse Insolation Sensitivity Analysis.

temp_2 := READPRN(temp_2)	values := 0..2
temp_4 := READPRN(temp_4)	Resp := READPRN(bendix)
temp_5 := READPRN(temp_5)	temp_43 := READPRN(temp_43)
temp_6 := READPRN(temp_6)	temp_50 := READPRN(temp_50)
temp_12 := READPRN(temp_12)	temp_52 := READPRN(temp_52)
temp_13 := READPRN(temp_13)	temp_53 := READPRN(temp_53)
temp_18 := READPRN(temp_18)	temp_54 := READPRN(temp_54)
temp_25 := READPRN(temp_25)	temp_65 := READPRN(temp_65)
temp_40 := READPRN(temp_40)	temp_75 := READPRN(temp_4)
temp_41 := READPRN(temp_41)	temp_85 := READPRN(temp_85)

Read in the variation in temperature that was caused by the variation in the material parameter values, treating THERM as a black box.

Parameter Array

sf ₁ := temp ₂ _{0,2}	emis ₁ := temp ₂ _{0,1}
sf ₂ := temp ₄ _{0,2}	emis ₂ := temp ₄ _{0,1}
sf ₃ := temp ₅ _{0,2}	emis ₃ := temp ₅ _{0,1}
sf ₄ := temp ₆ _{0,2}	emis ₄ := temp ₆ _{0,1}
sf ₅ := temp ₁₂ _{0,2}	emis ₅ := temp ₁₂ _{0,1}
sf ₆ := temp ₁₃ _{0,2}	emis ₆ := temp ₁₃ _{0,1}
sf ₇ := temp ₁₈ _{0,2}	emis ₇ := temp ₁₈ _{0,1}
sf ₈ := temp ₂₅ _{0,2}	emis ₈ := temp ₂₅ _{0,1}
sf ₉ := temp ₄₀ _{0,2}	emis ₉ := temp ₄₀ _{0,1}
sf ₁₀ := temp ₄₁ _{0,2}	emis ₁₀ := temp ₄₁ _{0,1}
sf ₁₁ := temp ₄₃ _{0,2}	emis ₁₁ := temp ₄₃ _{0,1}
sf ₁₂ := temp ₅₀ _{0,2}	emis ₁₂ := temp ₅₀ _{0,1}
sf ₁₃ := temp ₅₂ _{0,2}	emis ₁₃ := temp ₅₂ _{0,1}
sf ₁₄ := temp ₅₃ _{0,2}	emis ₁₄ := temp ₅₃ _{0,1}
sf ₁₅ := temp ₅₄ _{0,2}	emis ₁₅ := temp ₅₄ _{0,1}
sf ₁₆ := temp ₆₅ _{0,2}	emis ₁₆ := temp ₆₅ _{0,1}
sf ₁₇ := temp ₇₅ _{0,2}	emis ₁₇ := temp ₇₅ _{0,1}
sf ₁₈ := temp ₈₅ _{0,2}	emis ₁₈ := temp ₈₅ _{0,1}

Temperature Array - Converted from Celsius to Kelvin

T ₂ := temp ₂ ^{<3>} + 273.15
T ₄ := temp ₄ ^{<3>} + 273.15
T ₅ := temp ₅ ^{<3>} + 273.15
T ₆ := temp ₆ ^{<3>} + 273.15
T ₁₂ := temp ₁₂ ^{<3>} + 273.15
T ₁₃ := temp ₁₃ ^{<3>} + 273.15
T ₁₈ := temp ₁₈ ^{<3>} + 273.15
T ₂₅ := temp ₂₅ ^{<3>} + 273.15
T ₄₀ := temp ₄₀ ^{<3>} + 273.15
T ₄₁ := temp ₄₁ ^{<3>} + 273.15
T ₄₃ := temp ₄₃ ^{<3>} + 273.15
T ₅₀ := temp ₅₀ ^{<3>} + 273.15
T ₅₂ := temp ₅₂ ^{<3>} + 273.15
T ₅₃ := temp ₅₃ ^{<3>} + 273.15
T ₅₄ := temp ₅₄ ^{<3>} + 273.15
T ₆₅ := temp ₆₅ ^{<3>} + 273.15
T ₇₅ := temp ₇₅ ^{<3>} + 273.15
T ₈₅ := temp ₈₅ ^{<3>} + 273.15

The material properties and temperatures are shown below

sf =	0	emis =	0
	0		0
	1		0.975
	2		0.93
	3		0.955
	4		0.935
	5		0.9
	6		0.925
	7		0.955
	8		0.95
	9		0.965
	10		0.95
	11		0.915
	12		0.72
	13		0.79
	14		0.925

temp_{values} =

-2
0
2

$$T_2 = \begin{pmatrix} 263.036 \\ 261.026 \\ 259.031 \end{pmatrix}$$

$$T_{12} = \begin{pmatrix} 263.354 \\ 261.34 \\ 259.342 \end{pmatrix}$$

$$T_4 = \begin{pmatrix} 265.769 \\ 263.761 \\ 261.761 \end{pmatrix}$$

$$T_{65} = \begin{pmatrix} 267.287 \\ 265.875 \\ 264.465 \end{pmatrix}$$

$$T_5 = \begin{pmatrix} 265.558 \\ 263.556 \\ 261.562 \end{pmatrix}$$

ref := 0..1

T_{bb_ref} :=

300
301

Convert the temperatures to radiance values using the Plank equation.

$$k := 1.38 \cdot 10^{-23}$$

k - Boltzmann constant (J/K)

$$c := 2.99792459 \cdot 10^8$$

c - speed of light (m/sec)

$$h := 6.626176 \cdot 10^{-34}$$

h - Planck's constant (J/sec)

$$jmin := 8$$

jmin - minimum wavelength (μm) in the bandpass of interest

$$jmax := 14$$

jmax - maximum wavelength (μm) in the bandpass of interest

$$n := .1$$

n - wavelength increment for bandpass (μm)

$$p := \frac{jmax - jmin}{n}$$

p - number of steps in the bandpass of interest

$$j := 0..(p - 1)$$

j - index for the wavelength array

$$\lambda_j := (j \cdot n + jmin) \cdot 10^{-6} \quad \lambda - \text{in the bandpass of interest}$$

$$L_2(\lambda, T_2) := \frac{2 \cdot h \cdot c^2}{\lambda^5 \cdot \left(e^{\frac{h \cdot c}{\lambda \cdot k \cdot T_2}} - 1 \right)}$$

$$L_4(\lambda, T_4) := \frac{2 \cdot h \cdot c^2}{\lambda^5 \cdot \left(e^{\frac{h \cdot c}{\lambda \cdot k \cdot T_4}} - 1 \right)}$$

$$L_{bb}(\lambda, T_{bb}) := \frac{2 \cdot h \cdot c^2}{\lambda^5 \cdot \left(e^{\frac{h \cdot c}{\lambda \cdot k \cdot T_{bb}}} - 1 \right)}$$

$$L_5(\lambda, T_5) := \frac{2 \cdot h \cdot c^2}{\lambda^5 \cdot \left(e^{\frac{h \cdot c}{\lambda \cdot k \cdot T_5}} - 1 \right)}$$

$$L_12(\lambda, T_12) := \frac{2 \cdot h \cdot c^2}{\lambda^5 \cdot \left(e^{\frac{h \cdot c}{\lambda \cdot k \cdot T_12}} - 1 \right)}$$

$$L_18(\lambda, T_18) := \frac{2 \cdot h \cdot c^2}{\lambda^5 \cdot \left(e^{\frac{h \cdot c}{\lambda \cdot k \cdot T_18}} - 1 \right)}$$

$$L_40(\lambda, T_40) := \frac{2 \cdot h \cdot c^2}{\lambda^5 \cdot \left(e^{\frac{h \cdot c}{\lambda \cdot k \cdot T_40}} - 1 \right)}$$

$$L_43(\lambda, T_43) := \frac{2 \cdot h \cdot c^2}{\lambda^5 \cdot \left(e^{\frac{h \cdot c}{\lambda \cdot k \cdot T_43}} - 1 \right)}$$

$$L_52(\lambda, T_52) := \frac{2 \cdot h \cdot c^2}{\lambda^5 \cdot \left(e^{\frac{h \cdot c}{\lambda \cdot k \cdot T_52}} - 1 \right)}$$

$$L_54(\lambda, T_54) := \frac{2 \cdot h \cdot c^2}{\lambda^5 \cdot \left(e^{\frac{h \cdot c}{\lambda \cdot k \cdot T_54}} - 1 \right)}$$

$$L_75(\lambda, T_75) := \frac{2 \cdot h \cdot c^2}{\lambda^5 \cdot \left(e^{\frac{h \cdot c}{\lambda \cdot k \cdot T_75}} - 1 \right)}$$

$$L_6(\lambda, T_6) := \frac{2 \cdot h \cdot c^2}{\lambda^5 \cdot \left(e^{\frac{h \cdot c}{\lambda \cdot k \cdot T_6}} - 1 \right)}$$

$$L_13(\lambda, T_13) := \frac{2 \cdot h \cdot c^2}{\lambda^5 \cdot \left(e^{\frac{h \cdot c}{\lambda \cdot k \cdot T_13}} - 1 \right)}$$

$$L_25(\lambda, T_25) := \frac{2 \cdot h \cdot c^2}{\lambda^5 \cdot \left(e^{\frac{h \cdot c}{\lambda \cdot k \cdot T_25}} - 1 \right)}$$

$$L_41(\lambda, T_41) := \frac{2 \cdot h \cdot c^2}{\lambda^5 \cdot \left(e^{\frac{h \cdot c}{\lambda \cdot k \cdot T_41}} - 1 \right)}$$

$$L_50(\lambda, T_50) := \frac{2 \cdot h \cdot c^2}{\lambda^5 \cdot \left(e^{\frac{h \cdot c}{\lambda \cdot k \cdot T_50}} - 1 \right)}$$

$$L_53(\lambda, T_53) := \frac{2 \cdot h \cdot c^2}{\lambda^5 \cdot \left(e^{\frac{h \cdot c}{\lambda \cdot k \cdot T_53}} - 1 \right)}$$

$$L_65(\lambda, T_65) := \frac{2 \cdot h \cdot c^2}{\lambda^5 \cdot \left(e^{\frac{h \cdot c}{\lambda \cdot k \cdot T_65}} - 1 \right)}$$

$$L_85(\lambda, T_85) := \frac{2 \cdot h \cdot c^2}{\lambda^5 \cdot \left(e^{\frac{h \cdot c}{\lambda \cdot k \cdot T_85}} - 1 \right)}$$

$$L_2_ground_{values} := \sum_j Resp_j \cdot L_2(\lambda_j, T_{2_values}) \cdot (n \cdot 10^{-6})$$

$$L_4_ground_{values} := \sum_j Resp_j \cdot L_4(\lambda_j, T_{4_values}) \cdot (n \cdot 10^{-6})$$

$$L_5_ground_{values} := \sum_j Resp_j \cdot L_5(\lambda_j, T_{5_values}) \cdot (n \cdot 10^{-6})$$

$$L_6_ground_{values} := \sum_j Resp_j \cdot L_6(\lambda_j, T_{6_values}) \cdot (n \cdot 10^{-6})$$

$$L_12_ground_{values} := \sum_j Resp_j \cdot L_12(\lambda_j, T_{12_values}) \cdot (n \cdot 10^{-6})$$

$$L_13_ground_{values} := \sum_j Resp_j \cdot L_13(\lambda_j, T_{13_values}) \cdot (n \cdot 10^{-6})$$

$$L_18_ground_{values} := \sum_j Resp_j \cdot L_18(\lambda_j, T_{18_values}) \cdot (n \cdot 10^{-6})$$

$$L_25_ground_{values} := \sum_j Resp_j \cdot L_25(\lambda_j, T_{25_values}) \cdot (n \cdot 10^{-6})$$

$$L_40_ground_{values} := \sum_j Resp_j \cdot L_40(\lambda_j, T_{40_values}) \cdot (n \cdot 10^{-6})$$

$$L_41_ground_{values} := \sum_j Resp_j \cdot L_41(\lambda_j, T_{41_values}) \cdot (n \cdot 10^{-6})$$

$$L_43_ground_{values} := \sum_j Resp_j \cdot L_43(\lambda_j, T_{43_values}) \cdot (n \cdot 10^{-6})$$

$$L_50_ground_{values} := \sum_j Resp_j \cdot L_50(\lambda_j, T_{50_values}) \cdot (n \cdot 10^{-6})$$

$$L_52_ground_{values} := \sum_j Resp_j \cdot L_52(\lambda_j, T_{52_values}) \cdot (n \cdot 10^{-6})$$

$$L_53_ground_{values} := \sum_j Resp_j \cdot L_53(\lambda_j, T_{53_values}) \cdot (n \cdot 10^{-6})$$

$$L_54_ground_{values} := \sum_j Resp_j \cdot L_54(\lambda_j, T_{54_values}) \cdot (n \cdot 10^{-6})$$

$$L_65_ground_{values} := \sum_j Resp_j \cdot L_65(\lambda_j, T_{65_values}) \cdot (n \cdot 10^{-6})$$

$$L_75_ground_{values} := \sum_j Resp_j \cdot L_75(\lambda_j, T_{75_values}) \cdot (n \cdot 10^{-6})$$

Integrate the surface radiance across the bandpass of interest (8-14 μm) - including the sensor response function.

Calculated at .1 μm increments

$$L_{75_ground_values} := \sum_j \text{Resp}_j \cdot L_{75}(\lambda_j, T_{75_values}) \cdot (n \cdot 10^{-6})$$

$$L_{85_ground_values} := \sum_j \text{Resp}_j \cdot L_{85}(\lambda_j, T_{85_values}) \cdot (n \cdot 10^{-6})$$

$$L_{bb_ground_ref} := \sum_j \text{Resp}_j \cdot L_{bb}(\lambda_j, T_{bb_ref}) \cdot (n \cdot 10^{-6}) \quad \Delta L_{bb} := L_{bb_ground_1} - L_{bb_ground_0}$$

$$\Delta L_{bb} = 0.615$$

Propagate the radiance of the target to the radiance reaching the sensor using the big equation, simplified for use in the LWIR and assuming a shape factor of 1.0

$$\tau_2 := .9 \quad L_{\mu\epsilon} := 2.51 \quad L_{d\epsilon} := 4.289 \quad L_{b\epsilon} := 20.41 \quad \text{materials} := 0..18 \quad r_{\text{materials}} := 1 - \text{emis}_{\text{materials}}$$

$$L_{2_sensor_values} := [emis_1 \cdot L_{2_ground_values} + [sf_1 \cdot L_{d\epsilon} + (1 - sf_1) \cdot L_{b\epsilon}] \cdot r_1] \cdot \tau_2 + L_{\mu\epsilon}$$

$$L_{4_sensor_values} := [emis_2 \cdot L_{4_ground_values} + [sf_2 \cdot L_{d\epsilon} + (1 - sf_2) \cdot L_{b\epsilon}] \cdot r_2] \cdot \tau_2 + L_{\mu\epsilon}$$

$$L_{5_sensor_values} := [emis_3 \cdot L_{5_ground_values} + [sf_3 \cdot L_{d\epsilon} + (1 - sf_3) \cdot L_{b\epsilon}] \cdot r_3] \cdot \tau_2 + L_{\mu\epsilon}$$

$$L_{6_sensor_values} := [emis_4 \cdot L_{6_ground_values} + [sf_4 \cdot L_{d\epsilon} + (1 - sf_4) \cdot L_{b\epsilon}] \cdot r_4] \cdot \tau_2 + L_{\mu\epsilon}$$

$$L_{12_sensor_values} := [emis_5 \cdot L_{12_ground_values} + [sf_5 \cdot L_{d\epsilon} + (1 - sf_5) \cdot L_{b\epsilon}] \cdot r_5] \cdot \tau_2 + L_{\mu\epsilon}$$

$$L_{13_sensor_values} := [emis_6 \cdot L_{13_ground_values} + [sf_6 \cdot L_{d\epsilon} + (1 - sf_6) \cdot L_{b\epsilon}] \cdot r_6] \cdot \tau_2 + L_{\mu\epsilon}$$

$$L_{18_sensor_values} := [emis_7 \cdot L_{18_ground_values} + [sf_7 \cdot L_{d\epsilon} + (1 - sf_7) \cdot L_{b\epsilon}] \cdot r_7] \cdot \tau_2 + L_{\mu\epsilon}$$

$$L_{25_sensor_values} := [emis_8 \cdot L_{25_ground_values} + [sf_8 \cdot L_{d\epsilon} + (1 - sf_8) \cdot L_{b\epsilon}] \cdot r_8] \cdot \tau_2 + L_{\mu\epsilon}$$

$$L_{40_sensor_values} := [emis_9 \cdot L_{40_ground_values} + [sf_9 \cdot L_{d\epsilon} + (1 - sf_9) \cdot L_{b\epsilon}] \cdot r_9] \cdot \tau_2 + L_{\mu\epsilon}$$

$$L_{41_sensor_values} := [emis_{10} \cdot L_{41_ground_values} + [sf_{10} \cdot L_{d\epsilon} + (1 - sf_{10}) \cdot L_{b\epsilon}] \cdot r_{10}] \cdot \tau_2 + L_{\mu\epsilon}$$

$$L_{43_sensor_values} := [emis_{11} \cdot L_{43_ground_values} + [sf_{11} \cdot L_{d\epsilon} + (1 - sf_{11}) \cdot L_{b\epsilon}] \cdot r_{11}] \cdot \tau_2 + L_{\mu\epsilon}$$

$$L_{50_sensor_values} := [emis_{12} \cdot L_{50_ground_values} + [sf_{12} \cdot L_{d\epsilon} + (1 - sf_{12}) \cdot L_{b\epsilon}] \cdot r_{12}] \cdot \tau_2 + L_{\mu\epsilon}$$

$$L_{52_sensor_values} := [emis_{13} \cdot L_{52_ground_values} + [sf_{13} \cdot L_{d\epsilon} + (1 - sf_{13}) \cdot L_{b\epsilon}] \cdot r_{13}] \cdot \tau_2 + L_{\mu\epsilon}$$

$$L_{53_sensor_values} := [emis_{14} \cdot L_{53_ground_values} + [sf_{14} \cdot L_{d\epsilon} + (1 - sf_{14}) \cdot L_{b\epsilon}] \cdot r_{14}] \cdot \tau_2 + L_{\mu\epsilon}$$

$$L_{54_sensor_values} := [emis_{15} \cdot L_{54_ground_values} + [sf_{15} \cdot L_{d\epsilon} + (1 - sf_{15}) \cdot L_{b\epsilon}] \cdot r_{15}] \cdot \tau_2 + L_{\mu\epsilon}$$

$$L_65_sensor_values := \left[emis_{16} \cdot L_65_ground_values + \left[sf_{16} \cdot Ld\epsilon + (1 - sf_{16}) \cdot Lb\epsilon \right] \cdot r_{16} \right] \cdot \tau_2 + L\mu\epsilon$$

$$L_75_sensor_values := \left[emis_{17} \cdot L_75_ground_values + \left[sf_{17} \cdot Ld\epsilon + (1 - sf_{17}) \cdot Lb\epsilon \right] \cdot r_{17} \right] \cdot \tau_2 + L\mu\epsilon$$

$$L_85_sensor_values := \left[emis_{18} \cdot L_85_ground_values + \left[sf_{18} \cdot Ld\epsilon + (1 - sf_{18}) \cdot Lb\epsilon \right] \cdot r_{18} \right] \cdot \tau_2 + L\mu\epsilon$$

Write out the results of the sensitivity analysis

$$sens_1 := \text{slope}(\text{temp}, L_2_sensor) \quad sens_7 := \text{slope}(\text{temp}, L_18_sensor) \quad sens_{13} := \text{slope}(\text{temp}, L_52_sensor)$$

$$sens_2 := \text{slope}(\text{temp}, L_4_sensor) \quad sens_8 := \text{slope}(\text{temp}, L_25_sensor) \quad sens_{14} := \text{slope}(\text{temp}, L_53_sensor)$$

$$sens_3 := \text{slope}(\text{temp}, L_5_sensor) \quad sens_9 := \text{slope}(\text{temp}, L_40_sensor) \quad sens_{15} := \text{slope}(\text{temp}, L_54_sensor)$$

$$sens_4 := \text{slope}(\text{temp}, L_6_sensor) \quad sens_{10} := \text{slope}(\text{temp}, L_41_sensor) \quad sens_{16} := \text{slope}(\text{temp}, L_65_sensor)$$

$$sens_5 := \text{slope}(\text{temp}, L_12_sensor) \quad sens_{11} := \text{slope}(\text{temp}, L_43_sensor) \quad sens_{17} := \text{slope}(\text{temp}, L_75_sensor)$$

$$sens_6 := \text{slope}(\text{temp}, L_13_sensor) \quad sens_{12} := \text{slope}(\text{temp}, L_50_sensor) \quad sens_{18} := \text{slope}(\text{temp}, L_85_sensor)$$

$$sens^T = \begin{array}{|c|c|c|c|c|c|c|c|c|} \hline & 0 & 1 & 2 & 3 & 4 & 5 & 6 & 7 \\ \hline 0 & 0 & -0.354 & -0.349 & -0.357 & -0.35 & -0.328 & -0.345 & -0.154 \\ \hline \end{array}$$

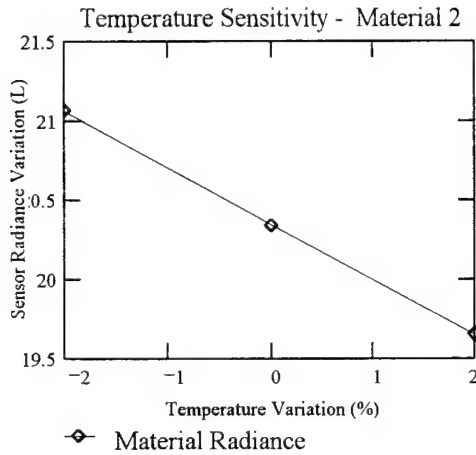
$$\text{temp_sens} := \frac{\text{sens}}{\Delta L_bb}$$

$$\text{temp_sens}^T = \begin{array}{|c|c|c|c|c|c|c|c|c|} \hline & 0 & 1 & 2 & 3 & 4 & 5 & 6 & 7 \\ \hline 0 & 0 & -0.575 & -0.568 & -0.58 & -0.57 & -0.534 & -0.561 & -0.25 \\ \hline \end{array}$$

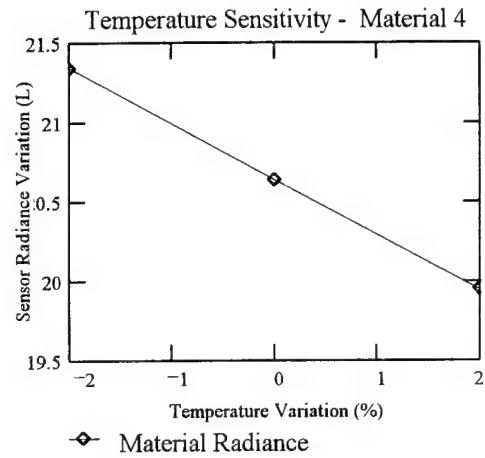
WRITEPRN(results_temp) := temp_sens

Meteorological Parameter Sensitivity Results - Temperature

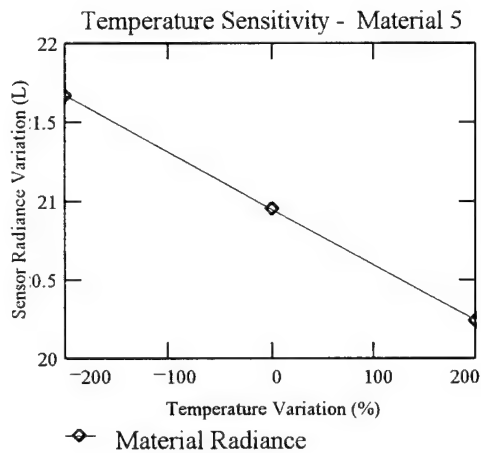
The following graphs show the change in radiance at the sensor as the material parameter of the object on the ground was varied. The resulting linear regression shows the final output sensitivity of the material parameter.



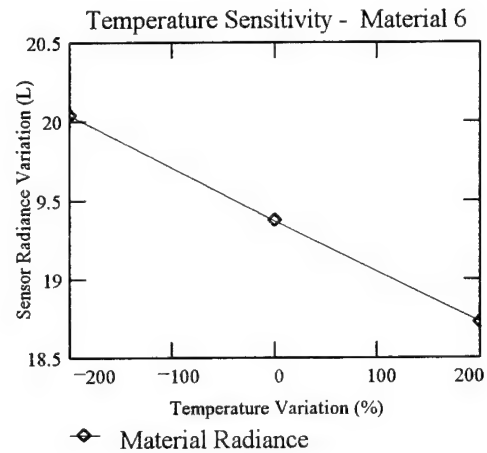
$$\text{sens}_1 = -0.354$$



$$\text{sens}_2 = -0.349$$



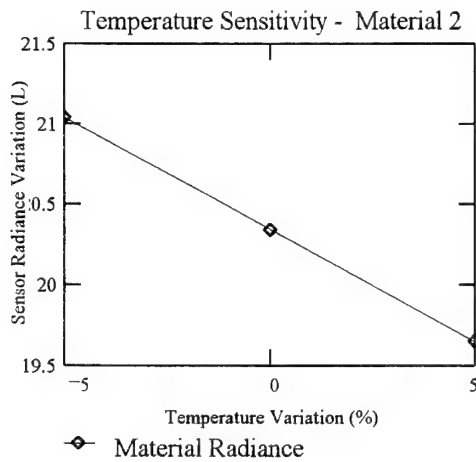
$$\text{sens}_3 = -0.357$$



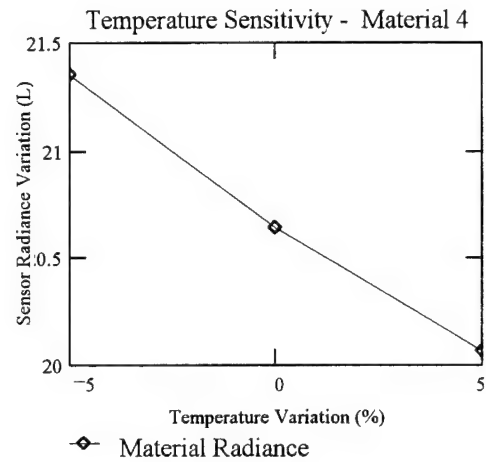
$$\text{sens}_4 = -0.35$$

Meteorological Parameter Sensitivity Results - *Wind Speed*

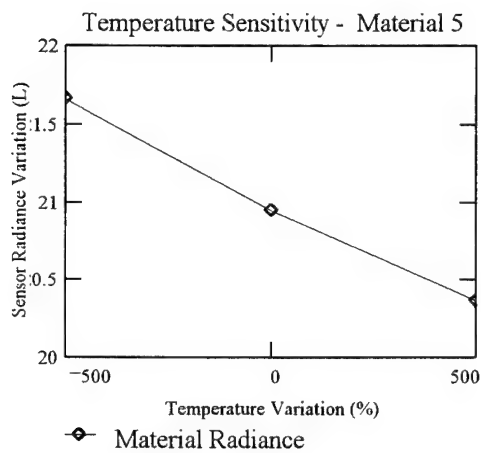
The following graphs show the change in radiance at the sensor as the material parameter of the object on the ground was varied. The resulting linear regression shows the final output sensitivity of the material parameter.



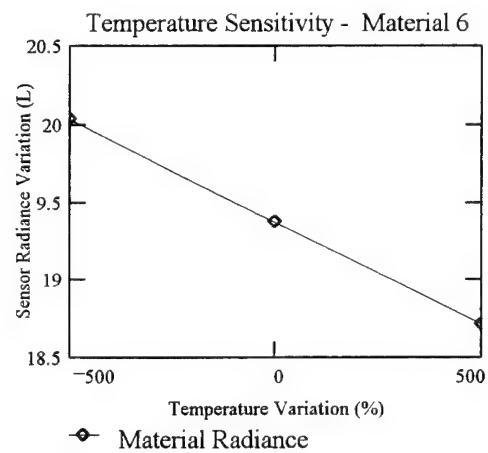
$$\text{sens}_1 = -0.139$$



$$\text{sens}_2 = -0.128$$



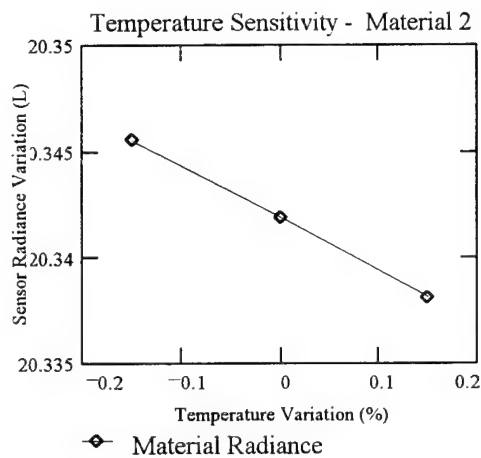
$$\text{sens}_3 = -0.13$$



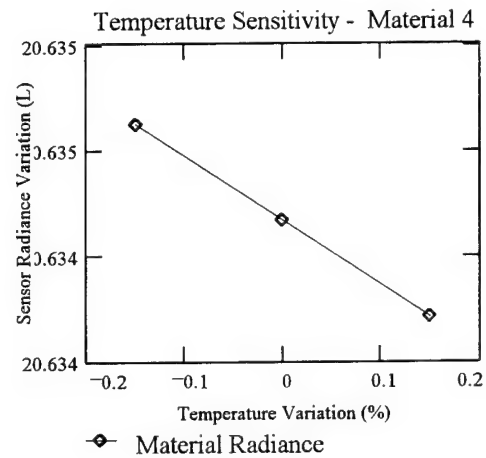
$$\text{sens}_4 = -0.122$$

Meteorological Parameter Sensitivity Results - *Insolation*

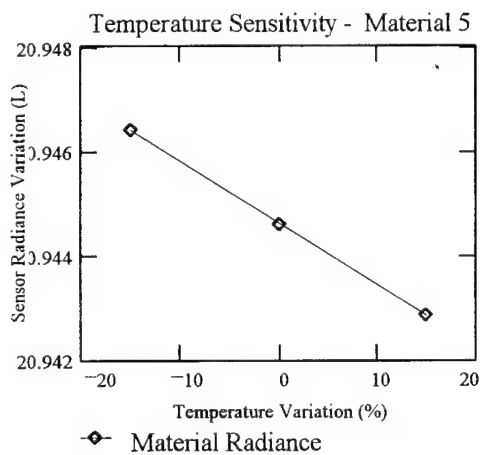
The following graphs show the change in radiance at the sensor as the material parameter of the object on the ground was varied. The resulting linear regression shows the final output sensitivity of the material parameter.



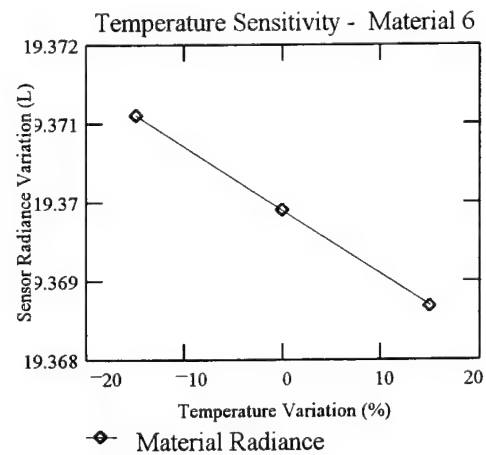
$$\text{sens}_1 = -0.024$$



$$\text{sens}_2 = -0.003$$



$$\text{sens}_3 = -0.012$$



$$\text{sens}_4 = -0.012$$

Meteorological Parameter Sensitivity Analysis

Transmission, Upwelled & Downwelled Radiance

Read in the resulting output files from THERM for the Direct & Diffuse Insolation Sensitivity Analysis.

atmos_2 := READPRN(insol_2)	mats := 0..18
atmos_4 := READPRN(insol_4)	Resp := READPRN(bendix)
atmos_5 := READPRN(insol_5)	atmos_43 := READPRN(insol_43)
atmos_6 := READPRN(insol_6)	atmos_50 := READPRN(insol_50)
atmos_12 := READPRN(temp_12)	atmos_52 := READPRN(insol_52)
atmos_13 := READPRN(insol_13)	atmos_53 := READPRN(insol_53)
atmos_18 := READPRN(insol_18)	atmos_54 := READPRN(insol_54)
atmos_25 := READPRN(insol_25)	atmos_65 := READPRN(insol_65)
atmos_40 := READPRN(insol_40)	atmos_75 := READPRN(insol_4)
atmos_41 := READPRN(insol_41)	atmos_85 := READPRN(insol_85)

Read in the variation in temperature that was caused by the variation in the material parameter values, treating THERM as a black box.

Temperature Array - Converted from Celsius to Kelvin

Parameter Array

sf ₁ := atmos_2 _{0,2}	emis ₁ := atmos_2 _{0,1}
sf ₂ := atmos_4 _{0,2}	emis ₂ := atmos_4 _{0,1}
sf ₃ := atmos_5 _{0,2}	emis ₃ := atmos_5 _{0,1}
sf ₄ := atmos_6 _{0,2}	emis ₄ := atmos_6 _{0,1}
sf ₅ := atmos_12 _{0,2}	emis ₅ := atmos_12 _{0,1}
sf ₆ := atmos_13 _{0,2}	emis ₆ := atmos_13 _{0,1}
sf ₇ := atmos_18 _{0,2}	emis ₇ := atmos_18 _{0,1}
sf ₈ := atmos_25 _{0,2}	emis ₈ := atmos_25 _{0,1}
sf ₉ := atmos_40 _{0,2}	emis ₉ := atmos_40 _{0,1}
sf ₁₀ := atmos_41 _{0,2}	emis ₁₀ := atmos_41 _{0,1}
sf ₁₁ := atmos_43 _{0,2}	emis ₁₁ := atmos_43 _{0,1}
sf ₁₂ := atmos_50 _{0,2}	emis ₁₂ := atmos_50 _{0,1}
sf ₁₃ := atmos_52 _{0,2}	emis ₁₃ := atmos_52 _{0,1}
sf ₁₄ := atmos_53 _{0,2}	emis ₁₄ := atmos_53 _{0,1}
sf ₁₅ := atmos_54 _{0,2}	emis ₁₅ := atmos_54 _{0,1}
sf ₁₆ := atmos_65 _{0,2}	emis ₁₆ := atmos_65 _{0,1}
sf ₁₇ := atmos_75 _{0,2}	emis ₁₇ := atmos_75 _{0,1}
sf ₁₈ := atmos_85 _{0,2}	emis ₁₈ := atmos_85 _{0,1}

atmos ₀ := 0 + 273.15	
atmos ₁ := atmos_2 _{1,3}	+ 273.15
atmos ₂ := atmos_4 _{1,3}	+ 273.15
atmos ₃ := atmos_5 _{1,3}	+ 273.15
atmos ₄ := atmos_6 _{1,3}	+ 273.15
atmos ₅ := atmos_12 _{1,3}	+ 273.15
atmos ₆ := atmos_13 _{1,3}	+ 273.15
atmos ₇ := atmos_18 _{1,3}	+ 273.15
atmos ₈ := atmos_25 _{1,3}	+ 273.15
atmos ₉ := atmos_40 _{1,3}	+ 273.15
atmos ₁₀ := atmos_41 _{1,3}	+ 273.15
atmos ₁₁ := atmos_43 _{1,3}	+ 273.15
atmos ₁₂ := atmos_50 _{1,3}	+ 273.15
atmos ₁₃ := atmos_52 _{1,3}	+ 273.15
atmos ₁₄ := atmos_53 _{1,3}	+ 273.15
atmos ₁₅ := atmos_54 _{1,3}	+ 273.15
atmos ₁₆ := atmos_65 _{1,3}	+ 273.15
atmos ₁₇ := atmos_75 _{1,3}	+ 273.15
atmos ₁₈ := atmos_85 _{1,3}	+ 273.15

The material properties and temperatures are shown below

sf =		0	emis =		0	atmos =		0	ref := 0..1	T_bb_ref :=
	0	0		0	0		1	261.026		
	1	1		1	0.975		2	263.761		
	2	1		2	0.93		3	263.556		
	3	1		3	0.955		4	263.842		
	4	1		4	0.935		5	261.34		
	5	1		5	0.9		6	263.277		
	6	1		6	0.925		7	269.189		
	7	0.4		7	0.955		8	266.701		
	8	0.7		8	0.95		9	262.463		
	9	1		9	0.965		10	263.051		
	10	1		10	0.95		11	263.9		
	11	1		11	0.915		12	269.61		
	12	0.4		12	0.72		13	262.775		
	13	1		13	0.79		14	269.407		
	14	0.4		14	0.925		15	269.527		

Convert the temperatures to radiance values using the Plank equation.

$k := 1.38 \cdot 10^{-23}$ k - Boltzmann constant (J/K)
 $c := 2.99792459 \cdot 10^8$ c - speed of light (m/sec)
 $h := 6.626176 \cdot 10^{-34}$ h - Planck's constant (J/sec)
 $jmin := 8$ $jmin$ - minimum wavelength (μm) in the bandpass of interest
 $jmax := 14$ $jmax$ - maximum wavelength (μm) in the bandpass of interest
 $n := 1$ n - wavelength increment for bandpass (μm)
 $p := \frac{jmax - jmin}{n}$ p - number of steps in the bandpass of interest
 $j := 0..(p - 1)$ j - index for the wavelength array
 $\lambda_j := (j \cdot n + jmin) \cdot 10^{-6}$ λ - in the bandpass of interest

$$L(\lambda, \text{atmos}) := \frac{2 \cdot h \cdot c^2}{\lambda^5 \cdot \left(e^{\frac{h \cdot c}{\lambda \cdot k \cdot \text{atmos}}} - 1 \right)}$$

$$L_bb(\lambda, T_bb) := \frac{2 \cdot h \cdot c^2}{\lambda^5 \cdot \left(e^{\frac{h \cdot c}{\lambda \cdot k \cdot T_bb}} - 1 \right)}$$

$$L_{\text{ground_mats}} := \sum_j \text{Resp}_j \cdot L(\lambda_j, \text{atmos_mats}) \cdot (n \cdot 10^{-6})$$

Integrate the surface radiance across the bandpass of interest (8-14 μm) - including the sensor response function.

Calculated at .1 μm increments

$$L_{\text{bb_ground_ref}} := \sum_j \text{Resp}_j \cdot L_{\text{bb}}(\lambda_j, T_{\text{bb_ref}}) \cdot (n \cdot 10^{-6})$$

$$\Delta L_{\text{bb}} := L_{\text{bb_ground}_1} - L_{\text{bb_ground}_0}$$

$$\Delta L_{\text{bb}} = 0.615$$

Propagate the radiance of the target to the radiance reaching the sensor using the big equation, simplified for use in the LWIR and assuming a shape factor of 1.0

$$\text{var} := 0..3$$

$$L_{\text{b}\epsilon} := 20.41$$

$$r_{\text{mats}} := 1 - \text{emis}_{\text{mats}}$$

$$\tau_2 := .92$$

$$L_{\mu\epsilon} := 2.51$$

$$L_{\text{d}\epsilon} := 4.289$$

$$\tau_{2\text{v_var}} := \quad L_{\text{uv_var}} := \quad L_{\text{dv_var}} :=$$

.89
.90
.91
.93

2
2.25
2.51
3

3.5
4
4.289
4.5

$$L_{\tau_1\text{_sensor_mats}} := [\text{emis}_{\text{mats}} \cdot L_{\text{ground_mats}} + [\text{sf}_{\text{mats}} \cdot L_{\text{d}\epsilon} + (1 - \text{sf}_{\text{mats}}) \cdot L_{\text{b}\epsilon}] \cdot r_{\text{mats}}] \cdot \tau_{2\text{v}_0} + L_{\mu\epsilon}$$

$$L_{\tau_2\text{_sensor_mats}} := [\text{emis}_{\text{mats}} \cdot L_{\text{ground_mats}} + [\text{sf}_{\text{mats}} \cdot L_{\text{d}\epsilon} + (1 - \text{sf}_{\text{mats}}) \cdot L_{\text{b}\epsilon}] \cdot r_{\text{mats}}] \cdot \tau_{2\text{v}_1} + L_{\mu\epsilon}$$

$$L_{\tau_3\text{_sensor_mats}} := [\text{emis}_{\text{mats}} \cdot L_{\text{ground_mats}} + [\text{sf}_{\text{mats}} \cdot L_{\text{d}\epsilon} + (1 - \text{sf}_{\text{mats}}) \cdot L_{\text{b}\epsilon}] \cdot r_{\text{mats}}] \cdot \tau_{2\text{v}_2} + L_{\mu\epsilon}$$

$$L_{\tau_4\text{_sensor_mats}} := [\text{emis}_{\text{mats}} \cdot L_{\text{ground_mats}} + [\text{sf}_{\text{mats}} \cdot L_{\text{d}\epsilon} + (1 - \text{sf}_{\text{mats}}) \cdot L_{\text{b}\epsilon}] \cdot r_{\text{mats}}] \cdot \tau_{2\text{v}_3} + L_{\mu\epsilon}$$

$$L_{\text{lu}_1\text{_sensor_mats}} := [\text{emis}_{\text{mats}} \cdot L_{\text{ground_mats}} + [\text{sf}_{\text{mats}} \cdot L_{\text{d}\epsilon} + (1 - \text{sf}_{\text{mats}}) \cdot L_{\text{b}\epsilon}] \cdot r_{\text{mats}}] \cdot \tau_2 + L_{\text{uv}_0}$$

$$L_{\text{lu}_2\text{_sensor_mats}} := [\text{emis}_{\text{mats}} \cdot L_{\text{ground_mats}} + [\text{sf}_{\text{mats}} \cdot L_{\text{d}\epsilon} + (1 - \text{sf}_{\text{mats}}) \cdot L_{\text{b}\epsilon}] \cdot r_{\text{mats}}] \cdot \tau_2 + L_{\text{uv}_1}$$

$$L_{\text{lu}_3\text{_sensor_mats}} := [\text{emis}_{\text{mats}} \cdot L_{\text{ground_mats}} + [\text{sf}_{\text{mats}} \cdot L_{\text{d}\epsilon} + (1 - \text{sf}_{\text{mats}}) \cdot L_{\text{b}\epsilon}] \cdot r_{\text{mats}}] \cdot \tau_2 + L_{\text{uv}_2}$$

$$L_{\text{lu}_4\text{_sensor_mats}} := [\text{emis}_{\text{mats}} \cdot L_{\text{ground_mats}} + [\text{sf}_{\text{mats}} \cdot L_{\text{d}\epsilon} + (1 - \text{sf}_{\text{mats}}) \cdot L_{\text{b}\epsilon}] \cdot r_{\text{mats}}] \cdot \tau_2 + L_{\text{uv}_3}$$

$$L_{\text{ld}_1\text{_sensor_mats}} := [\text{emis}_{\text{mats}} \cdot L_{\text{ground_mats}} + [\text{sf}_{\text{mats}} \cdot L_{\text{dv}_0} + (1 - \text{sf}_{\text{mats}}) \cdot L_{\text{b}\epsilon}] \cdot r_{\text{mats}}] \cdot \tau_2 + L_{\mu\epsilon}$$

$$L_{\text{ld}_2\text{_sensor_mats}} := [\text{emis}_{\text{mats}} \cdot L_{\text{ground_mats}} + [\text{sf}_{\text{mats}} \cdot L_{\text{dv}_1} + (1 - \text{sf}_{\text{mats}}) \cdot L_{\text{b}\epsilon}] \cdot r_{\text{mats}}] \cdot \tau_2 + L_{\mu\epsilon}$$

$$L_{\text{ld}_3\text{_sensor_mats}} := [\text{emis}_{\text{mats}} \cdot L_{\text{ground_mats}} + [\text{sf}_{\text{mats}} \cdot L_{\text{dv}_2} + (1 - \text{sf}_{\text{mats}}) \cdot L_{\text{b}\epsilon}] \cdot r_{\text{mats}}] \cdot \tau_2 + L_{\mu\epsilon}$$

$$L_{\text{ld}_4\text{_sensor_mats}} := [\text{emis}_{\text{mats}} \cdot L_{\text{ground_mats}} + [\text{sf}_{\text{mats}} \cdot L_{\text{dv}_3} + (1 - \text{sf}_{\text{mats}}) \cdot L_{\text{b}\epsilon}] \cdot r_{\text{mats}}] \cdot \tau_2 + L_{\mu\epsilon}$$

Join the individual sensitivity arrays so that the final sensitivity can be found.

$$\begin{aligned} Lt1 &:= \text{stack}(L_{\tau1_sensor}^T, L_{\tau2_sensor}^T) & Lt2 &:= \text{stack}(L_{\tau3_sensor}^T, L_{\tau4_sensor}^T) \\ Ld1 &:= \text{stack}(L_{ld1_sensor}^T, L_{ld2_sensor}^T) & Ld2 &:= \text{stack}(L_{ld3_sensor}^T, L_{ld4_sensor}^T) \\ Lu1 &:= \text{stack}(L_{lu1_sensor}^T, L_{lu2_sensor}^T) & Lu2 &:= \text{stack}(L_{lu3_sensor}^T, L_{lu4_sensor}^T) \\ Lt &:= \text{stack}(Lt1, Lt2) & Lu &:= \text{stack}(Lu1, Lu2) & Ld &:= \text{stack}(Ld1, Ld2) \end{aligned}$$

Write out the results of the sensitivity analysis

$$\begin{aligned} \text{sens}_{\tau_1} &:= \text{slope}(\tau_{2v}, Lt^{<1>}) & \text{sens}_{\tau_7} &:= \text{slope}(\tau_{2v}, Lt^{<7>}) & \text{sens}_{\tau_{13}} &:= \text{slope}(\tau_{2v}, Lt^{<13>}) \\ \text{sens}_{\tau_2} &:= \text{slope}(\tau_{2v}, Lt^{<2>}) & \text{sens}_{\tau_8} &:= \text{slope}(\tau_{2v}, Lt^{<8>}) & \text{sens}_{\tau_{14}} &:= \text{slope}(\tau_{2v}, Lt^{<14>}) \\ \text{sens}_{\tau_3} &:= \text{slope}(\tau_{2v}, Lt^{<3>}) & \text{sens}_{\tau_9} &:= \text{slope}(\tau_{2v}, Lt^{<9>}) & \text{sens}_{\tau_{15}} &:= \text{slope}(\tau_{2v}, Lt^{<15>}) \\ \text{sens}_{\tau_4} &:= \text{slope}(\tau_{2v}, Lt^{<4>}) & \text{sens}_{\tau_{10}} &:= \text{slope}(\tau_{2v}, Lt^{<10>}) & \text{sens}_{\tau_{16}} &:= \text{slope}(\tau_{2v}, Lt^{<16>}) \\ \text{sens}_{\tau_5} &:= \text{slope}(\tau_{2v}, Lt^{<5>}) & \text{sens}_{\tau_{11}} &:= \text{slope}(\tau_{2v}, Lt^{<11>}) & \text{sens}_{\tau_{17}} &:= \text{slope}(\tau_{2v}, Lt^{<17>}) \\ \text{sens}_{\tau_6} &:= \text{slope}(\tau_{2v}, Lt^{<6>}) & \text{sens}_{\tau_{12}} &:= \text{slope}(\tau_{2v}, Lt^{<12>}) & \text{sens}_{\tau_{18}} &:= \text{slope}(\tau_{2v}, Lt^{<18>}) \\ \\ \text{sens}_{Lu_1} &:= \text{slope}(Luv, Lu^{<1>}) & \text{sens}_{Lu_7} &:= \text{slope}(Luv, Lu^{<7>}) & \text{sens}_{Lu_{13}} &:= \text{slope}(Luv, Lu^{<13>}) \\ \text{sens}_{Lu_2} &:= \text{slope}(Luv, Lu^{<2>}) & \text{sens}_{Lu_8} &:= \text{slope}(Luv, Lu^{<8>}) & \text{sens}_{Lu_{14}} &:= \text{slope}(Luv, Lu^{<14>}) \\ \text{sens}_{Lu_3} &:= \text{slope}(Luv, Lu^{<3>}) & \text{sens}_{Lu_9} &:= \text{slope}(Luv, Lu^{<9>}) & \text{sens}_{Lu_{15}} &:= \text{slope}(Luv, Lu^{<15>}) \\ \text{sens}_{Lu_4} &:= \text{slope}(Luv, Lu^{<4>}) & \text{sens}_{Lu_{10}} &:= \text{slope}(Luv, Lu^{<10>}) & \text{sens}_{Lu_{16}} &:= \text{slope}(Luv, Lu^{<16>}) \\ \text{sens}_{Lu_5} &:= \text{slope}(Luv, Lu^{<5>}) & \text{sens}_{Lu_{11}} &:= \text{slope}(Luv, Lu^{<11>}) & \text{sens}_{Lu_{17}} &:= \text{slope}(Luv, Lu^{<17>}) \\ \text{sens}_{Lu_6} &:= \text{slope}(Luv, Lu^{<6>}) & \text{sens}_{Lu_{12}} &:= \text{slope}(Luv, Lu^{<12>}) & \text{sens}_{Lu_{18}} &:= \text{slope}(Luv, Lu^{<18>}) \\ \\ \text{sens}_{Ld_1} &:= \text{slope}(Ldv, Ld^{<1>}) & \text{sens}_{Ld_7} &:= \text{slope}(Ldv, Ld^{<7>}) & \text{sens}_{Ld_{13}} &:= \text{slope}(Ldv, Ld^{<13>}) \\ \text{sens}_{Ld_2} &:= \text{slope}(Ldv, Ld^{<2>}) & \text{sens}_{Ld_8} &:= \text{slope}(Ldv, Ld^{<8>}) & \text{sens}_{Ld_{14}} &:= \text{slope}(Ldv, Ld^{<14>}) \\ \text{sens}_{Ld_3} &:= \text{slope}(Ldv, Ld^{<3>}) & \text{sens}_{Ld_9} &:= \text{slope}(Ldv, Ld^{<9>}) & \text{sens}_{Ld_{15}} &:= \text{slope}(Ldv, Ld^{<15>}) \\ \text{sens}_{Ld_4} &:= \text{slope}(Ldv, Ld^{<4>}) & \text{sens}_{Ld_{10}} &:= \text{slope}(Ldv, Ld^{<10>}) & \text{sens}_{Ld_{16}} &:= \text{slope}(Ldv, Ld^{<16>}) \\ \text{sens}_{Ld_5} &:= \text{slope}(Ldv, Ld^{<5>}) & \text{sens}_{Ld_{11}} &:= \text{slope}(Ldv, Ld^{<11>}) & \text{sens}_{Ld_{17}} &:= \text{slope}(Ldv, Ld^{<17>}) \\ \text{sens}_{Ld_6} &:= \text{slope}(Ldv, Ld^{<6>}) & \text{sens}_{Ld_{12}} &:= \text{slope}(Ldv, Ld^{<12>}) & \text{sens}_{Ld_{18}} &:= \text{slope}(Ldv, Ld^{<18>}) \end{aligned}$$

$$\text{tsens}_{\tau} := \frac{\text{sens}_{\tau}}{\Delta L_{bb}} \quad \text{tsens}_{Lu} := \frac{\text{sens}_{Lu}}{\Delta L_{bb}} \quad \text{tsens}_{Ld} := \frac{\text{sens}_{Ld}}{\Delta L_{bb}}$$

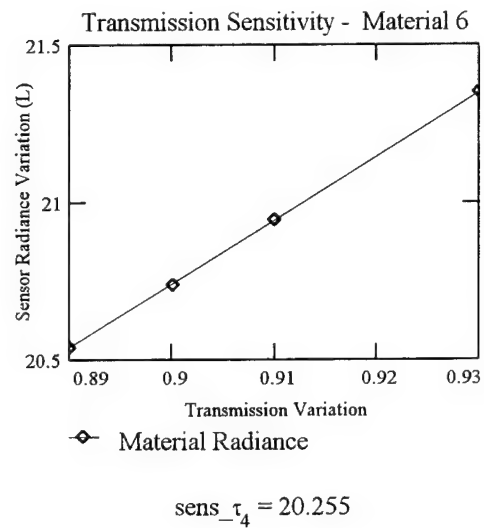
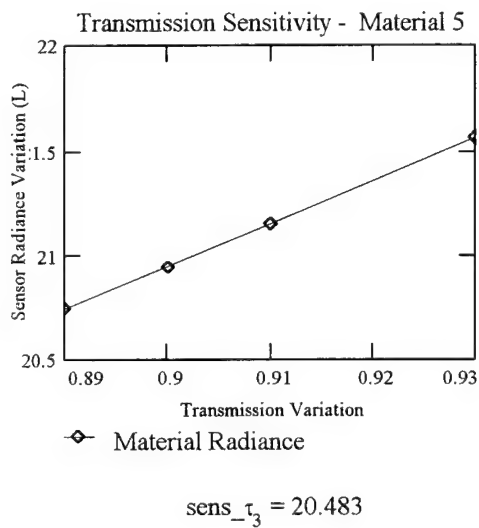
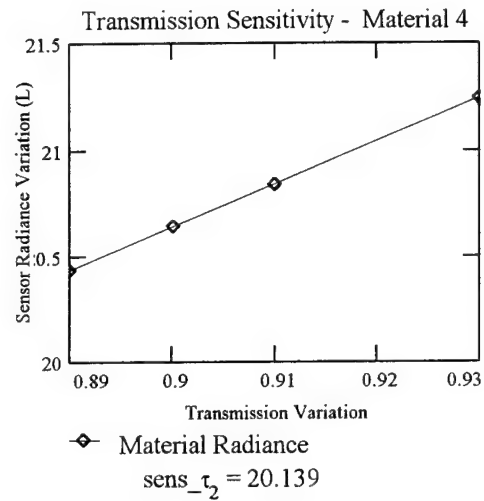
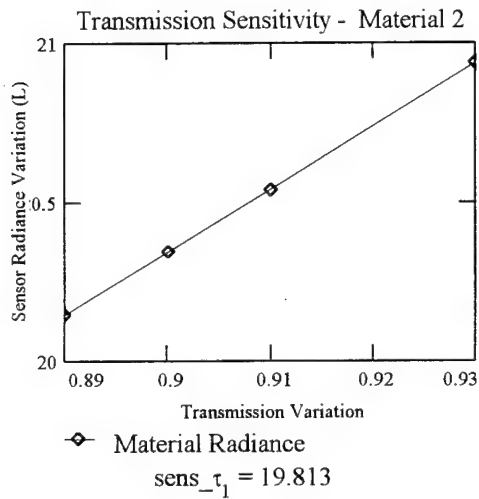
$$\text{tsens}_{\tau}^T = \begin{array}{c|cccccc} & 0 & 1 & 2 & 3 & 4 & 5 & 6 \\ \hline 0 & 0 & 32.202 & 32.731 & 33.291 & 32.921 & 30.447 & 32.29 \end{array}$$

$$\text{sens}_{Lu}^T = \begin{array}{c|cccccccccccc} & 0 & 1 & 2 & 3 & 4 & 5 & 6 & 7 & 8 & 9 & 10 & 11 \\ \hline 0 & 0 & 1 & 1 & 1 & 1 & 1 & 1 & 1 & 1 & 1 & 1 & 1 \end{array}$$

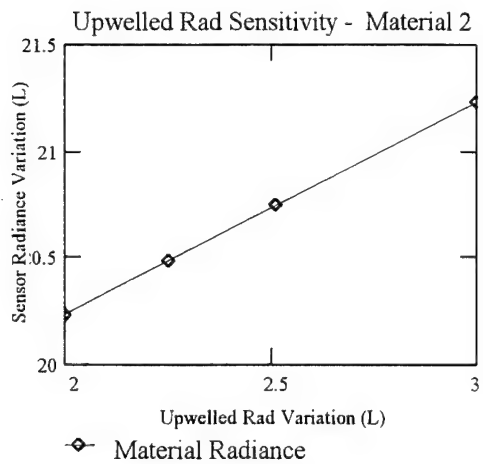
$$\text{tsens}_{Ld}^T = \begin{array}{c|cccccccc} & 0 & 1 & 2 & 3 & 4 & 5 & 6 & 7 & 8 \\ \hline 0 & 0 & 0.037 & 0.105 & 0.067 & 0.097 & 0.15 & 0.112 & 0.027 & 0.052 \end{array}$$

Meteorological Parameter Sensitivity Results - *Transmission*

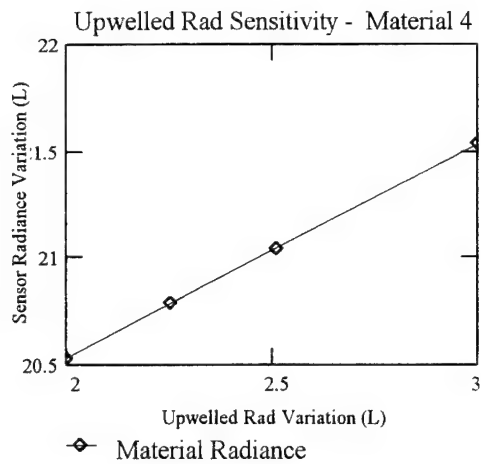
The following graphs show the change in radiance at the sensor as the material parameter of the object on the ground was varied. The resulting linear regression shows the final output sensitivity of the material parameter.



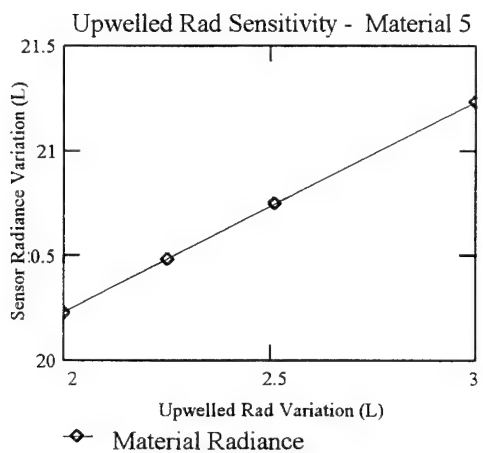
Meteorological Parameter Sensitivity Results - *Upwelled Radaince*



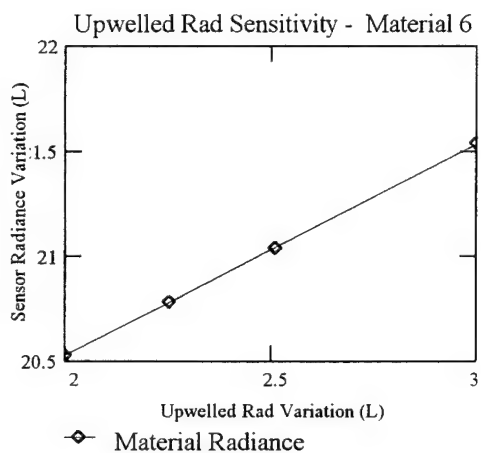
$$\text{sens_Lu}_1 = 1$$



$$\text{sens_Lu}_2 = 1$$

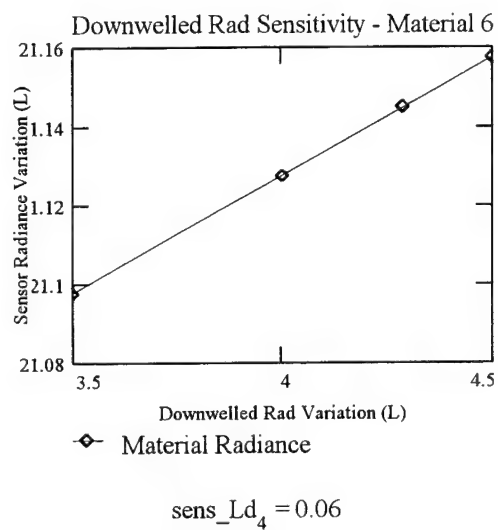
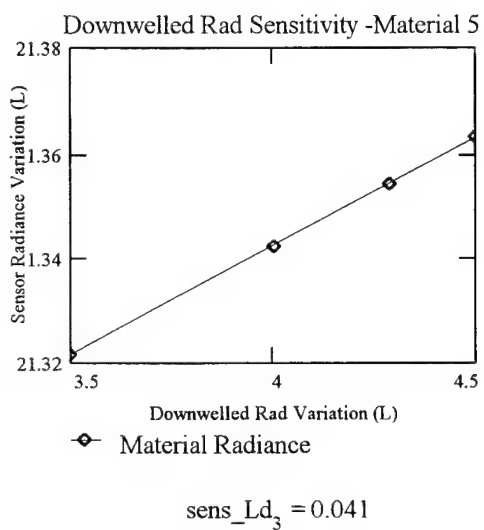
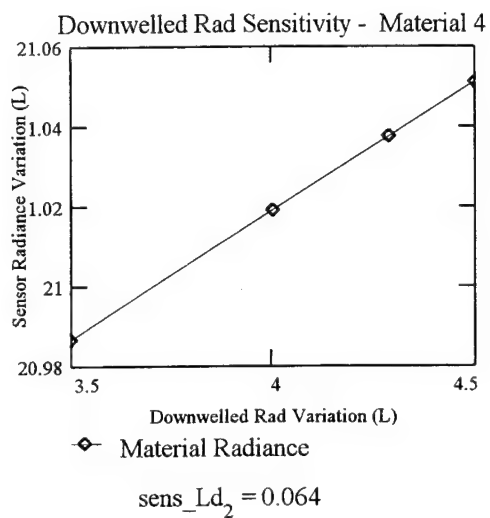
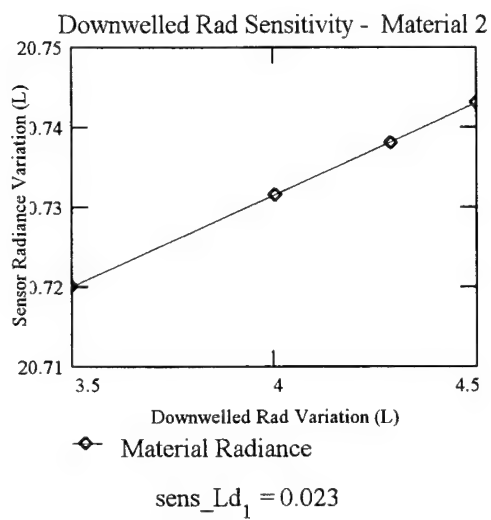


$$\text{sens_Lu}_3 = 1$$



$$\text{sens_Lu}_4 = 1$$

Meteorological Parameter Sensitivity Results - *Downwelled Radaince*



```

#!/bin/csh

set path=( $path /dirs/pkg/bin )

set INPUT_FILE='input.tmp'
set OUTPUT_FILE='output.tmp'
set MAT_FILE='material.tmp'
set READ_FILE='mats.dat'
set MASTER='./z_master'

# Input files that are needed for sensitivity analysis
#

set SND_FILE=${MASTER}/hawkeye.snd'
set DIRSIG_MAT_FILE=${MASTER}/toddd_mat.mat'

# change the weather file multiple times and record the
# output in the corresponding output file
#

set weather_var_max=3
set weather_counter=1

# while not at the end of the file
while ($COUNTER <= $STOP)

# Set the material ID, thickness, orientation for the sensitivity analysis
#
set MATIDS_ARRAY=cat $READ_FILE | cut -f1 | tr "\012" " "
set ORIENT_ARRAY=cat $READ_FILE | cut -f2 | tr "\012" " "

set STOP=${#MATIDS_ARRAY}
set COUNTER=1

set ORIENTATION_FILE=${MASTER}/or_$(ORIENTATION)'.dat'
set junk=cat $ORIENTATION_FILE | paste - - -
set SHAPE_FACTOR=${junk[1]}
set ZENITH=${junk[2]}
set AZIMUTH=${junk[3]}

# Scene specific variables
#
set AVG_TEMP=0.00
set TIME_INCR=24.0
set SGP=0.0

# Read in the generic material parameters from the DIRSIG material file
# and set those values to variables in the shell program
#
nawk -f ${MASTER}/test.awk ID=${MATID} $DIRSIG_MAT_FILE > $MAT_FILE
set line=cat $MAT_FILE | paste - - - - -
set SP_HEAT=${line[1]}
set TCOND=${line[2]}
set MASS_DENSITY=${line[3]}
set E_VIS=${line[4]}
set E_THERM=${line[5]}
set EXP_AREA=${line[6]}
set THICKNESS=${line[7]}
set HCAP=echo "$MASS_DENSITY * $SP_HEAT" | bc -l

```

```

set MATIDS_ARRAY=cat $READ_FILE | cut -f1 | tr "\012" " "
set ORIENT_ARRAY=cat $READ_FILE | cut -f2 | tr "\012" " "

```

```

set STOP=${#MATIDS_ARRAY}
set COUNTER=1

```

```

#while not at the end of the file
while ($COUNTER <= $STOP)

```

```

# # Set the material ID, thickness, orientation for the sensitivity analysis
#
set MATIDS_ARRAY=${COUNTER}
set ORIENTATION=${ORIENT_ARRAY[COUNTER]}

```

```

set ORIENTATION_FILE=${MASTER}/or_$(ORIENTATION)'.dat'
set junk=cat $ORIENTATION_FILE | paste - - -
set SHAPE_FACTOR=${junk[1]}
set ZENITH=${junk[2]}
set AZIMUTH=${junk[3]}

```



```

#-----
# # Insolation Sensitivity Analysis
# #
# #
# #
# # clear a new FINAL output file which contains the
# # material parameter and the resulting temperature
set FINAL_FILE=insol_${MATID}.pmi
echo -n "" > $FINAL_FILE

#reinitialize the weather counter
set weather_counter=1

#while not done for all the weather parameter variations
while ($weather_counter <= $weather_var_max)

    set WITH_FILE=${MASTER}/${awkeyc}_insol_${weather_counter}.whi

    #create a temporary file with these parameters in it ...
    echo $SND_FILE > $INPUT_FILE
    echo $WITH_FILE >> $INPUT_FILE
    echo $OUTPUT_FILE >> $INPUT_FILE
    echo $AVG_TEMP >> $INPUT_FILE
    echo $SHAPE_FACTOR >> $INPUT_FILE
    echo $ZENITH >> $INPUT_FILE
    echo $AZIMUTH >> $INPUT_FILE
    echo $TIME_INCR >> $INPUT_FILE
    echo $HCAP >> $INPUT_FILE
    echo $TCOND >> $INPUT_FILE
    echo $THICKNESS >> $INPUT_FILE
    echo $E_VIS >> $INPUT_FILE
    echo $E_THERM >> $INPUT_FILE
    echo $EXP_AREA >> $INPUT_FILE
    echo $SGP >> $INPUT_FILE

    # call thermal_model(1)
    thermal_model < $INPUT_FILE > /dev/null

    # add the last run to the file for this material
    echo -n $MATID >> $FINAL_FILE
    echo -n " " >> $FINAL_FILE
    echo -n $E_THERM >> $FINAL_FILE
    echo -n " " >> $FINAL_FILE
    echo -n $SHAPE_FACTOR >> $FINAL_FILE
    echo -n " " >> $FINAL_FILE
    awk '{ printf "%6.4f\n", $2 }' $OUTPUT_FILE >> $FINAL_FILE

    #iterate and go to the next material number
    set weather_counter= echo $weather_counter + 1 | bc -l
end

set COUNTER=`echo $COUNTER + 1 | bc -l`
end

rm *.tmp

```

Material Parameter Modifications & Sensitivity Analysis

Material Type: Asphalt Shingle

Read in the resulting output file from THERM for each of the material parameters & determine the number of elements in the array.

heat_capacity := READPRN(hc_65)	hc := 0..rows(heat_capacity) - 1
thermal_conductivity := READPRN(tc_65)	tc := 0..rows(thermal_conductivity) - 1
thickness := READPRN(th_65)	th := 0..rows(thickness) - 1
vis_emissivity := READPRN(visem_65)	visem := 0..rows(vis_emissivity) - 1
therm_emissivity := READPRN(them_65)	them := 0..rows(therm_emissivity) - 1
exposed_area_p := READPRN(xpp_65)	expp := 0..rows(exposed_area_p) - 1
exposed_area_n := READPRN(xpn_65)	expn := 0..rows(exposed_area_n) - 1
SGP := READPRN(sgp_65)	sgp := 0..rows(SGP) - 1
shape_factor := READPRN(sf_65)	sf := 0..rows(shape_factor) - 1

Read in the material ID, shape factor, emissivity, and baseline temperature for used in the 'Big Equation'

generic_file := READPRN(gen_65)

Create a reference blackbody temperature difference to relate the sensitivity values of all the material parameters

ref := 0..1 T_{bb_ref} :=

300
301

Read in the sensor responsivity file - Bendix line scanner

Resp := READPRN(bendix)

Parameter		Temperature		Parameter		Temperature	
heat_capacity =	0.26	-7.207		thermal_conductivity =	5.93	-7.278	
	0.288	-7.229			5.991	-7.277	
	0.316	-7.249			6.053	-7.276	
	0.343	-7.267			6.114	-7.276	
	0.371	-7.283			6.176	-7.275	
	0.399	-7.298			6.237	-7.274	
	0.427	-7.312			6.298	-7.274	
vis_emissivity =	0.455	-7.324			6.36	-7.273	
	0.73	-7.275		therm_emissivity =	0.9	-7.263	
	0.761	-7.275			0.904	-7.268	
	0.793	-7.275			0.908	-7.273	
	0.824	-7.275			0.913	-7.279	
	0.856	-7.275			0.917	-7.284	
	0.887	-7.275			0.921	-7.29	
	0.918	-7.275			0.925	-7.295	
SGP =	0.95	-7.275			0.929	-7.3	
	0	0	-7.275	thickness =	0.2	-6.983	
	1	1	-5.986		0.386	-7.08	
	2	2	-4.712		0.571	-7.169	
	3	3	-3.438		0.757	-7.244	
	4	4	-2.181		0.943	-7.304	
	5	5	-0.934		1.129	-7.352	
	6	6	0.304		1.314	-7.391	
exposed_area_p =	7	7	1.527		1.5	-7.42	
	8	8	2.741	exposed_area_n =	-0.5	-7.707	
	9	9	3.945		-0.4	-7.275	
	10	10	5.144		-0.3	-6.801	
					-0.2	-6.276	
					-0.1	-5.677	
					0	-5.046	
				shape_factor =	0	0	
					0.25	-2.691	
					0.5	-5.28	
					0.75	-7.766	
					1	-10.17	

Read in the variation in temperature that was caused by the variation in the material parameter values, treating THERM as a black box.

Parameter Array

$P_{hc} := \text{heat_capacity}^{<0>}$
 $P_{tc} := \text{thermal_conductivity}^{<0>}$
 $P_{th} := \text{thickness}^{<0>}$
 $P_{visem} := \text{vis_emissivity}^{<0>}$
 $P_{them} := \text{therm_emissivity}^{<0>}$
 $P_{expp} := \text{exposed_area_p}^{<0>}$
 $P_{expn} := \text{exposed_area_n}^{<0>}$
 $P_{sgp} := \text{SGP}^{<0>}$
 $P_{sf} := \text{shape_factor}^{<0>}$

Temperature Array - Converted from Celsius to Kelvin

$T_{hc} := \text{heat_capacity}^{<1>} + 273.15$
 $T_{tc} := \text{thermal_conductivity}^{<1>} + 273.15$
 $T_{th} := \text{thickness}^{<1>} + 273.15$
 $T_{visem} := \text{vis_emissivity}^{<1>} + 273.15$
 $T_{them} := \text{therm_emissivity}^{<1>} + 273.15$
 $T_{expp} := \text{exposed_area_p}^{<1>} + 273.15$
 $T_{expn} := \text{exposed_area_n}^{<1>} + 273.15$
 $T_{sgp} := \text{SGP}^{<1>} + 273.15$
 $T_{sf} := \text{shape_factor}^{<1>} + 273.15$

Convert the temperatures to radiance values using the Plank equation.

$k := 1.38 \cdot 10^{-23}$ k - Boltzmann constant (J/K)
 $c := 2.99792459 \cdot 10^8$ c - speed of light (m/sec)
 $h := 6.626176 \cdot 10^{-34}$ h - Planck's constant (J/sec)
 $jmin := 8$ $jmin$ - minimum wavelength (μm) in the bandpass of interest
 $jmax := 14$ $jmax$ - maximum wavelength (μm) in the bandpass of interest
 $n := 1$ n - wavelength increment for bandpass (μm)

$p := \frac{jmax - jmin}{n}$ p - number of steps in the bandpass of interest

$j := 0..(p - 1)$ j - index for the wavelength array

$\lambda_j := (j \cdot n + jmin) \cdot 10^{-6}$ λ - in the bandpass of interest

$$L_{hc}(\lambda, T_{hc}) := \frac{2 \cdot h \cdot c^2}{\lambda^5 \cdot \left(e^{\frac{h \cdot c}{\lambda \cdot k \cdot T_{hc}}} - 1 \right)}$$

$$L_{tc}(\lambda, T_{tc}) := \frac{2 \cdot h \cdot c^2}{\lambda^5 \cdot \left(e^{\frac{h \cdot c}{\lambda \cdot k \cdot T_{tc}}} - 1 \right)}$$

$$L_{th}(\lambda, T_{th}) := \frac{2 \cdot h \cdot c^2}{\lambda^5 \cdot \left(e^{\frac{h \cdot c}{\lambda \cdot k \cdot T_{th}}} - 1 \right)}$$

$$L_{visem}(\lambda, T_{visem}) := \frac{2 \cdot h \cdot c^2}{\lambda^5 \cdot \left(e^{\frac{h \cdot c}{\lambda \cdot k \cdot T_{visem}}} - 1 \right)}$$

$$L_{\text{them}}(\lambda, T_{\text{them}}) := \frac{2 \cdot h \cdot c^2}{\lambda^5 \cdot \left(e^{\frac{h \cdot c}{\lambda \cdot k \cdot T_{\text{them}}}} - 1 \right)}$$

$$L_{\text{expp}}(\lambda, T_{\text{expp}}) := \frac{2 \cdot h \cdot c^2}{\lambda^5 \cdot \left(e^{\frac{h \cdot c}{\lambda \cdot k \cdot T_{\text{expp}}}} - 1 \right)}$$

$$L_{\text{sgp}}(\lambda, T_{\text{sgp}}) := \frac{2 \cdot h \cdot c^2}{\lambda^5 \cdot \left(e^{\frac{h \cdot c}{\lambda \cdot k \cdot T_{\text{sgp}}}} - 1 \right)}$$

$$L_{\text{expn}}(\lambda, T_{\text{expn}}) := \frac{2 \cdot h \cdot c^2}{\lambda^5 \cdot \left(e^{\frac{h \cdot c}{\lambda \cdot k \cdot T_{\text{expn}}}} - 1 \right)}$$

$$L_{\text{sf}}(\lambda, T_{\text{sf}}) := \frac{2 \cdot h \cdot c^2}{\lambda^5 \cdot \left(e^{\frac{h \cdot c}{\lambda \cdot k \cdot T_{\text{sf}}}} - 1 \right)}$$

$$L_{\text{bb}}(\lambda, T_{\text{bb}}) := \frac{2 \cdot h \cdot c^2}{\lambda^5 \cdot \left(e^{\frac{h \cdot c}{\lambda \cdot k \cdot T_{\text{bb}}}} - 1 \right)}$$

Integrate the surface radiance across the bandpass of interest (8-14 μm) - including the sensor response function. **Calculated at 1 μm increments**

$$L_{\text{hc_ground}}_{\text{hc}} := \sum_j \text{Resp}_j \cdot L_{\text{hc}}(\lambda_j, T_{\text{hc}}_{\text{hc}}) \cdot (n \cdot 10^{-6})$$

$$L_{\text{th_ground}}_{\text{th}} := \sum_j \text{Resp}_j \cdot L_{\text{th}}(\lambda_j, T_{\text{th}}_{\text{th}}) \cdot (n \cdot 10^{-6})$$

$$L_{\text{visem_ground}}_{\text{visem}} := \sum_j \text{Resp}_j \cdot L_{\text{visem}}(\lambda_j, T_{\text{visem}}_{\text{visem}}) \cdot (n \cdot 10^{-6})$$

$$L_{\text{them_ground}}_{\text{them}} := \sum_j \text{Resp}_j \cdot L_{\text{them}}(\lambda_j, T_{\text{them}}_{\text{them}}) \cdot (n \cdot 10^{-6})$$

$$L_{\text{tc_ground}}_{\text{tc}} := \sum_j \text{Resp}_j \cdot L_{\text{tc}}(\lambda_j, T_{\text{tc}}_{\text{tc}}) \cdot (n \cdot 10^{-6})$$

$$L_{\text{expp_ground}}_{\text{expp}} := \sum_j \text{Resp}_j \cdot L_{\text{expp}}(\lambda_j, T_{\text{expp}}_{\text{expp}}) \cdot (n \cdot 10^{-6})$$

$$L_{\text{expn_ground}}_{\text{expn}} := \sum_j \text{Resp}_j \cdot L_{\text{expn}}(\lambda_j, T_{\text{expn}}_{\text{expn}}) \cdot (n \cdot 10^{-6})$$

$$L_{\text{sgp_ground}}_{\text{sgp}} := \sum_j \text{Resp}_j \cdot L_{\text{sgp}}(\lambda_j, T_{\text{sgp}}_{\text{sgp}}) \cdot (n \cdot 10^{-6})$$

$$L_{\text{sf_ground}}_{\text{sf}} := \sum_j \text{Resp}_j \cdot L_{\text{sf}}(\lambda_j, T_{\text{sf}}_{\text{sf}}) \cdot (n \cdot 10^{-6})$$

$$L_{\text{bb_ground}}_{\text{ref}} := \sum_j \text{Resp}_j \cdot L_{\text{bb}}(\lambda_j, T_{\text{bb}}_{\text{ref}}) \cdot (n \cdot 10^{-6}) \quad \Delta L_{\text{bb}} := L_{\text{bb_ground}}_1 - L_{\text{bb_ground}}_0$$

$$\Delta L_{\text{bb}} = 0.615$$

Propagate the radiance of the target to the radiance reaching the sensor using the big equation, simplified for use in the LWIR and assuming a shape factor of 1.0

$$\varepsilon := \text{generic_file}_{0,1} \quad L_{\mu\varepsilon} := 2.51 \quad L_{d\varepsilon} := 4.289 \quad \tau_2 := .9 \quad L_{b\varepsilon} := 20.41 \quad r := 1 - \varepsilon \quad F := \text{generic_file}_{0,2}$$

$$L_{\text{hc_sensor_hc}} := [\varepsilon \cdot L_{\text{hc_ground_hc}} + (F \cdot L_{d\varepsilon} + (1 - F) \cdot L_{b\varepsilon}) \cdot r] \cdot \tau_2 + L_{\mu\varepsilon}$$

$$L_{\text{tc_sensor_tc}} := [\varepsilon \cdot L_{\text{tc_ground_tc}} + (F \cdot L_{d\varepsilon} + (1 - F) \cdot L_{b\varepsilon}) \cdot r] \cdot \tau_2 + L_{\mu\varepsilon}$$

$$L_{\text{th_sensor_th}} := [\varepsilon \cdot L_{\text{th_ground_th}} + (F \cdot L_{d\varepsilon} + (1 - F) \cdot L_{b\varepsilon}) \cdot r] \cdot \tau_2 + L_{\mu\varepsilon}$$

$$L_{\text{visem_sensor_visem}} := [\varepsilon \cdot L_{\text{visem_ground_visem}} + (F \cdot L_{d\varepsilon} + (1 - F) \cdot L_{b\varepsilon}) \cdot r] \cdot \tau_2 + L_{\mu\varepsilon}$$

$$L_{\text{them_sensor_them}} := [\varepsilon \cdot L_{\text{them_ground_them}} + (F \cdot L_{d\varepsilon} + (1 - F) \cdot L_{b\varepsilon}) \cdot r] \cdot \tau_2 + L_{\mu\varepsilon}$$

$$L_{\text{expp_sensor_expp}} := [\varepsilon \cdot L_{\text{expp_ground_expp}} + (F \cdot L_{d\varepsilon} + (1 - F) \cdot L_{b\varepsilon}) \cdot r] \cdot \tau_2 + L_{\mu\varepsilon}$$

$$L_{\text{expn_sensor_expn}} := [\varepsilon \cdot L_{\text{expn_ground_expn}} + (F \cdot L_{d\varepsilon} + (1 - F) \cdot L_{b\varepsilon}) \cdot r] \cdot \tau_2 + L_{\mu\varepsilon}$$

$$L_{\text{sgp_sensor_sgp}} := [\varepsilon \cdot L_{\text{sgp_ground_sgp}} + (F \cdot L_{d\varepsilon} + (1 - F) \cdot L_{b\varepsilon}) \cdot r] \cdot \tau_2 + L_{\mu\varepsilon}$$

$$L_{\text{sf_sensor_sf}} := [\varepsilon \cdot L_{\text{sf_ground_sf}} + (F \cdot L_{d\varepsilon} + (1 - F) \cdot L_{b\varepsilon}) \cdot r] \cdot \tau_2 + L_{\mu\varepsilon}$$

Write out the results of the sensitivity analysis to an output file

$$\text{sens}_0 := \text{slope}(P_{\text{th}}, L_{\text{th_sensor}})$$

$$\text{sens}_4 := \text{slope}(P_{\text{them}}, L_{\text{them_sensor}})$$

$$\text{sens}_1 := \text{slope}(P_{\text{tc}}, L_{\text{tc_sensor}})$$

$$\text{sens}_5 := \text{slope}(P_{\text{expp}}, L_{\text{expp_sensor}})$$

$$\text{sens}_2 := \text{slope}(P_{\text{hc}}, L_{\text{hc_sensor}})$$

$$\text{sens}_6 := \text{slope}(P_{\text{expn}}, L_{\text{expn_sensor}})$$

$$\text{sens}_3 := \text{slope}(P_{\text{visem}}, L_{\text{visem_sensor}})$$

$$\text{sens}_7 := \text{slope}(P_{\text{sgp}}, L_{\text{sgp_sensor}})$$

$$\text{temp_sens} := \frac{\text{sens}}{\Delta L_{\text{bb}}} \quad \text{temp_sens}_9 := 65$$

$$\text{sens}_8 := \text{slope}(P_{\text{sf}}, L_{\text{sf_sensor}})$$

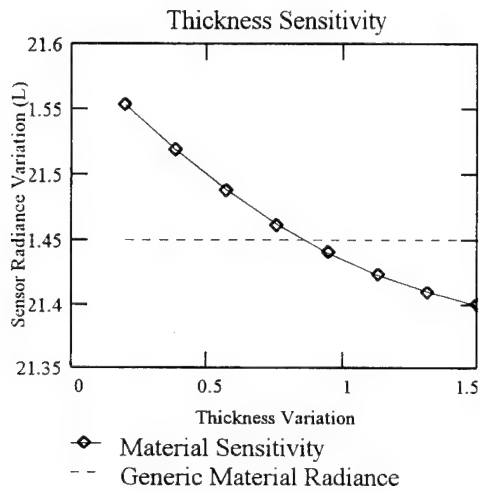
$$\text{sens}^T = \begin{pmatrix} -0.117 & 0.004 & -0.209 & -6.863 \cdot 10^{-13} & -0.449 & -1.459 & 1.883 & 0.468 & -3.654 \end{pmatrix}$$

$$\text{temp_sens}^T = \begin{array}{|c|c|c|c|c|c|c|c|c|c|} \hline & 0 & 1 & 2 & 3 & 4 & 5 & 6 & 7 & 8 \\ \hline 0 & -0.191 & 0.006 & -0.34 & -1.116 \cdot 10^{-12} & -0.729 & -2.372 & 3.061 & 0.761 & -5.939 \\ \hline \end{array}$$

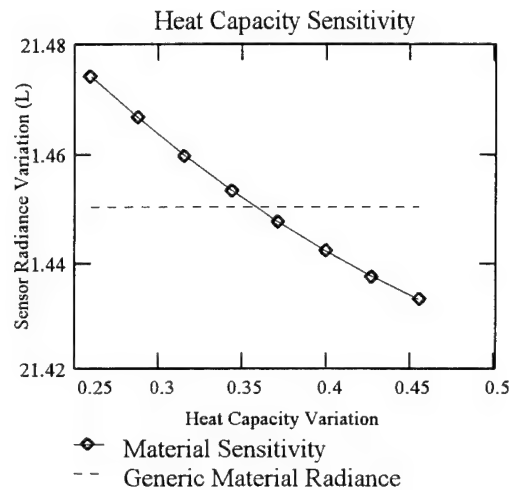
$$\text{APPENDPRN}(\text{materials}) := \text{temp_sens}^T$$

Material Parameter Sensitivity Results - Asphalt shingle

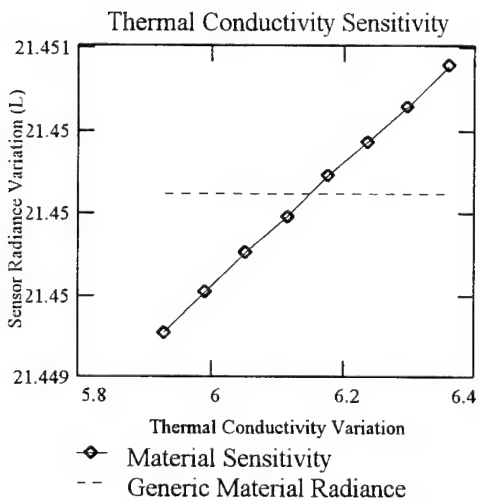
The following graphs show the change in radiance at the sensor as the material parameter of the object on the ground was varied. The resulting linear regression shows the final output sensitivity of the material parameter.



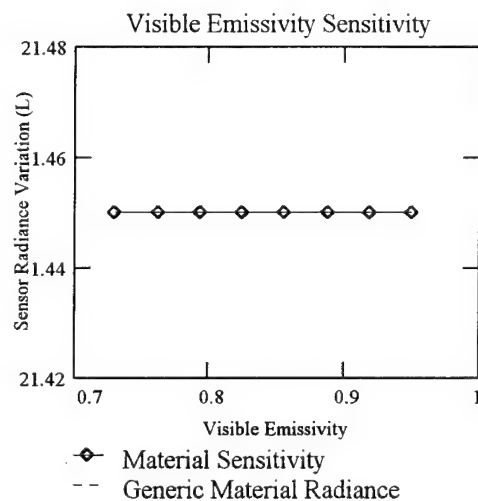
$$\text{sens}_0 = -0.117$$



$$\text{sens}_2 = -0.209$$



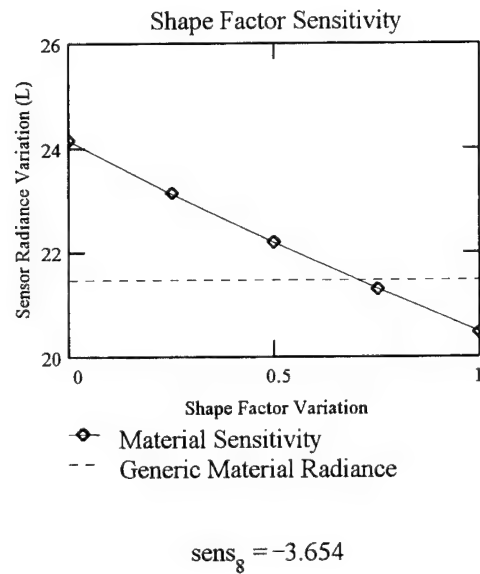
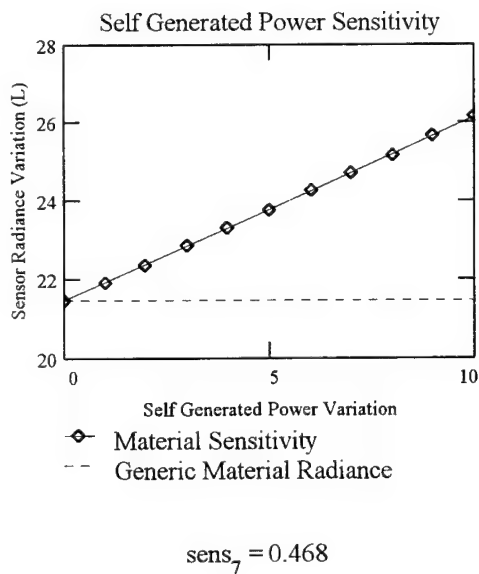
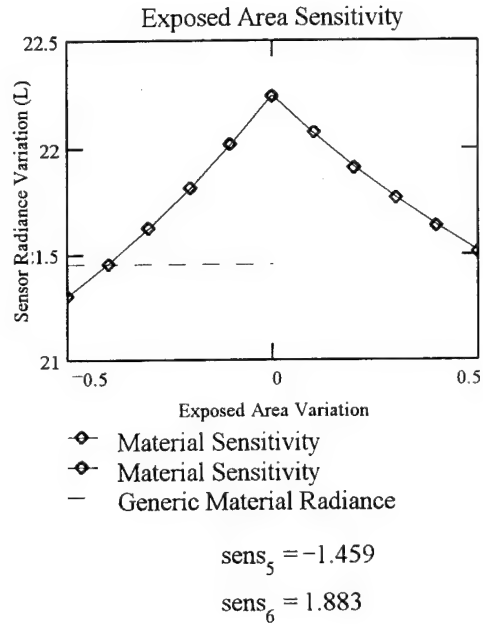
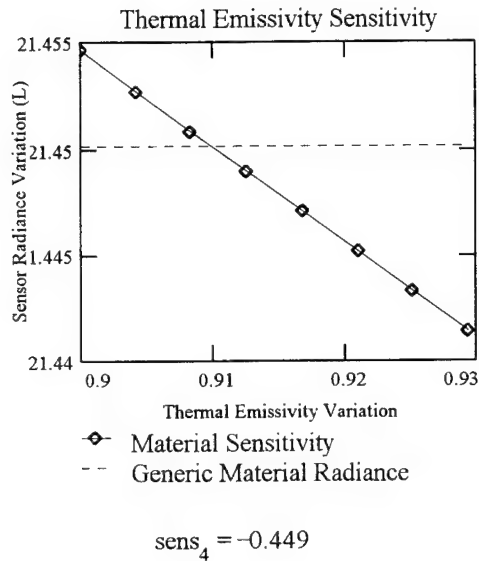
$$\text{sens}_1 = 0.004$$



$$\text{sens}_3 = -6.863 \cdot 10^{-13}$$

Material Parameter Sensitivity Results - *Asphalt shingle*

Continued



```

# /bin/csh
set path=( $path /dirs/pkg/min)
set MASTER="/h_master"
set INPUT_FILE="input.tmp"
set OUTPUT_FILE="output.tmp"
set MAT_FILE="material.tmp"

# Read in the material ID and the thickness for the sensitivity analysis
#
#
set MATID=$1
set ORIENTATION=$2

# Input files that are needed for sensitivity analysis
#
set SND_FILE=$(MASTER)/hawkeye.snd"
set WITH_FILE=$(MASTER)/hawkeye.with"
set DIRSIG_MAT_FILE=$(MASTER)/todd_mat_var.mat"
set ORIENTATION_FILE=$(MASTER)/or_$(ORIENTATION).dat"

# Scene specific variables
#
set AVG_TEMP=0.00
set TIME_INCR=24.0
set SGP=0.0

set junk="cat $ORIENTATION_FILE | paste .....
set SHAPE_FACTOR=$junk[1]
set ZENITH=$junk[2]
set AZIMUTH=$junk[3]

# Variation Parameters for Sensitivity Analysis of the Material Parameters
#
set NUM_INCREMENTS=7.0

# Read in the generic material parameters from the DIRSIG material file
# and set those values to variables in the shell program
#
nawk -f $(MASTER)/testvar.awk ID=$MATID $DIRSIG_MAT_FILE > $MAT_FILE
set line1="head -6 $MAT_FILE | paste .....
set line2="tail +7 $MAT_FILE | head -6 | paste .....
set line3="tail +13 $MAT_FILE | paste .....
set line=($line1 $line2 $line3)

set SP_HEAT=$line[1]
set TCOND=$line[2]
set MASS_DENSITY=$line[3]
set E_VIS=$line[4]
set E_THERM=$line[5]
set EXP_AREA=$line[6]
set THICKNESS=$line[7]
set HC_MIN=$line[8]

set HC_MAX=$line[9]
set TC_MIN=$line[10]
set TC_MAX=$line[11]
set VE_MIN=$line[12]
set VE_MAX=$line[13]
set TE_MIN=$line[14]
set TE_MAX=$line[15]
set TH_MIN=$line[16]
set TH_MAX=$line[17]
set HCAP="echo '$MASS DENSITY * $SP HEAT' | bc -l"

# -----
# # Material Parameter Variation: Thickness ...
#
set VAR_INCR="echo '4k $TH_MAX $TH_MIN - $NUM INCREMENTS / p' | dc"

# set the initial thickness variation value
set THICKNESS_VAR=$TH_MIN

set FINAL_FILE="th_$(MATID).prm"

# clear a new FINAL output file which contains the
# material parameter and the resulting temperature
echo -n "" > $FINAL_FILE

# loop around for while, varying one parameter
while (0 == "echo 't($THICKNESS_VAR,$TH_MAX)' | bc -l $(MASTER)/test.bc")

# create a temporary file with these parameters in it ...
echo $SND_FILE > $INPUT_FILE
echo $WITH_FILE > $INPUT_FILE
echo $OUTPUT_FILE > $INPUT_FILE
echo $AVG_TEMP > $INPUT_FILE
echo $SHAPE_FACTOR > $INPUT_FILE
echo $ZENITH > $INPUT_FILE
echo $AZIMUTH > $INPUT_FILE
echo $TIME_INCR > $INPUT_FILE
echo $HCAP > $INPUT_FILE
echo $TCOND > $INPUT_FILE
echo $THICKNESS_VAR > $INPUT_FILE
echo $E_VIS > $INPUT_FILE
echo $E_THERM > $INPUT_FILE
echo $EXP_AREA > $INPUT_FILE
echo $SGP > $INPUT_FILE

# call thermal_model(1)
thermal_model < $INPUT_FILE > /dev/null

# add the last run to the file for this material
echo -n $THICKNESS_VAR >> $FINAL_FILE
echo -n " " >> $FINAL_FILE
awk '{ printf( "%6.4f\n", $2 ) }' $OUTPUT_FILE >> $FINAL_FILE

# increment the thickness
set THICKNESS_VAR="echo $THICKNESS_VAR + $VAR_INCR | bc -l"

end

```

```

# -----
# # Material Parameter Variation: Thermal Conductivity ...
#
set VAR_INCR="echo "4k $TC_MAX $TC_MIN - $NUM_INCREMENTS / p" | dc"
# set the initial thermal conductivity
set TCOND_VAR=$TC_MIN
set FINAL_FILE="tc_${MATID}.pm"

# clear a new FINAL output file which contains the
# material parameter and the resulting temperature
echo -n "" > $FINAL_FILE

# loop around for while, varying one parameter
while (0 == `echo "${TCOND_VAR,$TC_MAX}" | bc -l ${MASTER}/test.bc`)
# create a temporary file with these parameters in it ...
echo $SSND_FILE > $INPUT_FILE
echo $SWTH_FILE > $INPUT_FILE
echo $SOUTPUT_FILE > $INPUT_FILE
echo $AVG_TEMP > $INPUT_FILE
echo $SHAPE_FACTOR > $INPUT_FILE
echo $ZENITH > $INPUT_FILE
echo $AZIMUTH > $INPUT_FILE
echo $TIME_INCR > $INPUT_FILE
echo $HCAP_VAR > $INPUT_FILE
echo $TCOND > $INPUT_FILE
echo $THICKNESS > $INPUT_FILE
echo $E_VIS > $INPUT_FILE
echo $E_THERM > $INPUT_FILE
echo $EXP_AREA > $INPUT_FILE
echo $SSGP > $INPUT_FILE

# call thermal_model()
thermal_model < $INPUT_FILE > /dev/null

# add the last run to the file for this material
echo -n " " > $FINAL_FILE
awk '{ print( "%6.4f\n", $2 ) }' $SOUTPUT_FILE >> $FINAL_FILE

# increment the heat capacity
set HCAP_VAR="echo $HCAP_VAR + $VAR_INCR | bc -l"

end

# -----
# # Material Parameter Variation: Visible Emissivity ...
#
set VAR_INCR="echo "4k $SVE_MAX $SVE_MIN - $NUM_INCREMENTS / p" | dc"
# set the initial visible emissivity
set E_VIS_VAR=$SVE_MIN
set FINAL_FILE="viscm_${MATID}.pm"

# clear a new FINAL output file which contains the
# material parameter and the resulting temperature
echo -n "" > $FINAL_FILE

# loop around for while, varying one parameter
while (0 == `echo "${E_VIS_VAR,$SVE_MAX}" | bc -l ${MASTER}/test.bc`)
# create a temporary file with these parameters in it ...
echo $SSND_FILE > $INPUT_FILE
echo $SWTH_FILE > $INPUT_FILE
echo $SOUTPUT_FILE > $INPUT_FILE

# -----
# # Material Parameter Variation: Heat Capacity ...
#
set VAR_INCR="echo "4k $HC_MAX $HC_MIN - $NUM_INCREMENTS / p" | dc"
# set the initial heat capacity
set HCAP_VAR=$HC_MIN
set FINAL_FILE="hc_${MATID}.pm"

```

```

echo $AVG_TEMP >> $INPUT_FILE
echo $SHAPE_FACTOR >> $INPUT_FILE
echo $ZENITH >> $INPUT_FILE
echo $AZIMUTH >> $INPUT_FILE
echo $HCAP >> $INPUT_FILE
echo $THICKNESS >> $INPUT_FILE
echo $TCOND >> $INPUT_FILE
echo $E_VIS >> $INPUT_FILE
echo $THERM_VAR >> $INPUT_FILE
echo $EXP_AREA >> $INPUT_FILE
echo $SGP >> $INPUT_FILE

# call thermal_model(1)
thermal_model < $INPUT_FILE > /dev/null

# add the last run to the file for this material
echo -n $E_THERM_VAR >> $FINAL_FILE
echo -n " " >> $FINAL_FILE
awk '{ print( "%6.4f\n", $2 ) }' $OUTPUT_FILE >> $FINAL_FILE

# increment the thermal emissivity
set E_THERM_VAR=echo $E_THERM_VAR + $VAR_INCR | bc -l
end

# -----
# # Material Parameter Variation: Exposed Area (positive)...
#
set MIN_VAR=0.0
set MAX_VAR=0.5
set VAR_INCR=0.1
# set the initial exposed area
set EXP_AREA_VAR=$MIN_VAR

set FINAL_FILE=$pp.$[MATID].pm

# clear a new FINAL output file which contains the
# material parameter and the resulting temperature
echo -n "" > $FINAL_FILE

# loop around for while, varying one parameter
while (0 == echo "($EXP_AREA_VAR,$MAX_VAR)" | bc -l $(MASTER)/test.bc)

# create a temporary file with these parameters in it ...
echo $SSND_FILE > $INPUT_FILE
echo $WITH_FILE >> $INPUT_FILE
echo $OUTPUT_FILE >> $INPUT_FILE
echo $AVG_TEMP >> $INPUT_FILE
echo $SHAPE_FACTOR >> $INPUT_FILE
echo $ZENITH >> $INPUT_FILE
echo $AZIMUTH >> $INPUT_FILE
echo $TIME_INCR >> $INPUT_FILE
echo $HCAP >> $INPUT_FILE
echo $THICKNESS >> $INPUT_FILE
echo $E_VIS >> $INPUT_FILE
echo $THERM_VAR >> $INPUT_FILE
echo $EXP_AREA_VAR >> $INPUT_FILE
echo $SGP >> $INPUT_FILE

# call thermal_model(1)
thermal_model < $INPUT_FILE > /dev/null

# add the last run to the file for this material
echo -n $EXP_AREA_VAR >> $FINAL_FILE
echo -n " " >> $FINAL_FILE
awk '{ print( "%6.4f\n", $2 ) }' $OUTPUT_FILE >> $FINAL_FILE

# increment the exposed area
set EXP_AREA_VAR=echo $EXP_AREA_VAR + $VAR_INCR | bc -l
end

```

```

echo $AVG_TEMP >> $INPUT_FILE
echo $SHAPE_FACTOR >> $INPUT_FILE
echo $ZENITH >> $INPUT_FILE
echo $AZIMUTH >> $INPUT_FILE
echo $HCAP >> $INPUT_FILE
echo $THICKNESS >> $INPUT_FILE
echo $TCOND >> $INPUT_FILE
echo $E_VIS >> $INPUT_FILE
echo $THERM_VAR >> $INPUT_FILE
echo $EXP_AREA >> $INPUT_FILE
echo $SGP >> $INPUT_FILE

# call thermal_model(1)
thermal_model < $INPUT_FILE > /dev/null

# add the last run to the file for this material
echo -n $E_THERM_VAR >> $FINAL_FILE
echo -n " " >> $FINAL_FILE
awk '{ print( "%6.4f\n", $2 ) }' $OUTPUT_FILE >> $FINAL_FILE

# increment the visible emissivity
set E_VIS_VAR=echo $E_VIS_VAR + $VAR_INCR | bc -l
end

# -----
# # Material Parameter Variation: Thermal Emissivity ...
#
set VAR_INCR=echo "4k $E_MAX $E_MIN - $NUM_INCREMENTS / p" | dc
# set the initial thermal emissivity
set E_THERM_VAR=$E_MIN

set FINAL_FILE=$them.$[MATID].pm

# clear a new FINAL output file which contains the
# material parameter and the resulting temperature
echo -n "" > $FINAL_FILE

# loop around for while, varying one parameter
while (0 == echo "($E_THERM_VAR,$E_MAX)" | bc -l $(MASTER)/test.bc)

# create a temporary file with these parameters in it ...
echo $SSND_FILE > $INPUT_FILE
echo $WITH_FILE >> $INPUT_FILE
echo $OUTPUT_FILE >> $INPUT_FILE
echo $AVG_TEMP >> $INPUT_FILE
echo $SHAPE_FACTOR >> $INPUT_FILE
echo $ZENITH >> $INPUT_FILE
echo $AZIMUTH >> $INPUT_FILE
echo $TIME_INCR >> $INPUT_FILE
echo $HCAP >> $INPUT_FILE
echo $THICKNESS >> $INPUT_FILE
echo $E_VIS >> $INPUT_FILE
echo $THERM_VAR >> $INPUT_FILE
echo $EXP_AREA >> $INPUT_FILE
echo $SGP >> $INPUT_FILE

# call thermal_model(1)

```

```

# -----
# Material Parameter Variation: Exposed Area (negative)...
#
set MIN_VAR=0.5
set MAX_VAR=0.0
set VAR_INCR=0.1
set EXP_AREA_VAR=$MIN_VAR

set FINAL_FILE=xpn_${MATID}.pm

# clear a new FINAL output file which contains the
# material parameter and the resulting temperature
echo -n "" > $FINAL_FILE

# loop around for while, varying one parameter
while (0 == `echo "${($SGP_VAR,$MAX_VAR)" | bc -l ${MASTER}/test.bc`)

# create a temporary file with these parameters in it ...
echo $SND_FILE > $INPUT_FILE
echo $WTH_FILE >> $INPUT_FILE
echo $OUTPUT_FILE >> $INPUT_FILE
echo $AVG_TEMP >> $INPUT_FILE
echo $SHAPE_FACTOR >> $INPUT_FILE
echo $ZENITH >> $INPUT_FILE
echo $AZIMUTH >> $INPUT_FILE
echo $TIME_INCR >> $INPUT_FILE
echo $HCAP >> $INPUT_FILE
echo $THICKNESS >> $INPUT_FILE
echo $E_VIS >> $INPUT_FILE
echo $E_THERM >> $INPUT_FILE
echo $EXP_AREA >> $INPUT_FILE
echo $SGP_VAR >> $INPUT_FILE

# call thermal_model(1)
thermal_model < $INPUT_FILE > /dev/null

# add the last run to the file for this material
echo -n $SGP_VAR >> $FINAL_FILE
echo -n " " >> $FINAL_FILE
awk '{ printf "%6.4f\n", $2 }' $OUTPUT_FILE >> $FINAL_FILE

# increment the self generated power
set SGP_VAR=echo $SGP_VAR + $VAR_INCR | bc -l

end

# -----
# Material Parameter Variation: Shape Factor ...
#
set MIN_VAR=0.0
set MAX_VAR=1.0
set VAR_INCR=0.25

# set the initial shape factor
set SHAPE_FACTOR_VAR=$MIN_VAR

set FINAL_FILE=sc_${MATID}.pm

# clear a new FINAL output file which contains the
# material parameter and the resulting temperature
echo -n "" > $FINAL_FILE

# loop around for while, varying one parameter
while (0 == `echo "${($SHAPE_FACTOR_VAR,$MAX_VAR)" | bc -l ${MASTER}/test.bc`)

# create a temporary file with these parameters in it ...

```

```

# -----
# Material Parameter Variation: Self Generated Power ...
#
set MIN_VAR=0.0
set MAX_VAR=10.0
set VAR_INCR=1.0

# set the initial self generated power
set SGP_VAR=$MIN_VAR

# -----
# Material Parameter Variation: Exposed Area (negative)...
#
set MIN_VAR=0.5
set MAX_VAR=0.0
set VAR_INCR=0.1
set EXP_AREA_VAR=$MIN_VAR

set FINAL_FILE=xpn_${MATID}.pm

# clear a new FINAL output file which contains the
# material parameter and the resulting temperature
echo -n "" > $FINAL_FILE

# loop around for while, varying one parameter
while (0 == `echo "${($EXP_AREA_VAR,$MAX_VAR)" | bc -l ${MASTER}/test.bc`)

# create a temporary file with these parameters in it ...
echo $SND_FILE > $INPUT_FILE
echo $WTH_FILE >> $INPUT_FILE
echo $OUTPUT_FILE >> $INPUT_FILE
echo $AVG_TEMP >> $INPUT_FILE
echo $SHAPE_FACTOR >> $INPUT_FILE
echo $ZENITH >> $INPUT_FILE
echo $AZIMUTH >> $INPUT_FILE
echo $TIME_INCR >> $INPUT_FILE
echo $HCAP >> $INPUT_FILE
echo $THICKNESS >> $INPUT_FILE
echo $E_VIS >> $INPUT_FILE
echo $E_THERM >> $INPUT_FILE
echo $EXP_AREA_VAR >> $INPUT_FILE
echo $SGP >> $INPUT_FILE

# call thermal_model(1)
thermal_model < $INPUT_FILE > /dev/null

# add the last run to the file for this material
echo -n $EXP_AREA_VAR >> $FINAL_FILE
echo -n " " >> $FINAL_FILE
awk '{ printf "%6.4f\n", $2 }' $OUTPUT_FILE >> $FINAL_FILE

# increment the exposed area
set EXP_AREA_VAR=echo $EXP_AREA_VAR + $VAR_INCR | bc -l

end

# -----
# Material Parameter Variation: Self Generated Power ...
#
set MIN_VAR=0.0
set MAX_VAR=10.0
set VAR_INCR=1.0

# set the initial self generated power
set SGP_VAR=$MIN_VAR

```

```

# add the last run to the file for this material
echo -n $MATID >> $FINAL_FILE
echo -n " " >> $FINAL_FILE
echo -n " " >> $FINAL_FILE
echo -n $E_THERM >> $FINAL_FILE
echo -n " " >> $FINAL_FILE
echo -n $SHAPE_FACTOR >> $FINAL_FILE
echo -n " " >> $FINAL_FILE
awk '{ printf "%6.4f\n", $2 }' $OUTPUT_FILE >> $FINAL_FILE

```

```
rm *.tmp
```

```

echo $SND_FILE > $INPUT_FILE
echo $WITH_FILE >> $INPUT_FILE
echo $OUTPUT_FILE >> $INPUT_FILE
echo $AVG_TEMP >> $INPUT_FILE
echo $SHAPE_FACTOR >> $INPUT_FILE
echo $ZENITH >> $INPUT_FILE
echo $AZIMUTH >> $INPUT_FILE
echo $TIME_INCR >> $INPUT_FILE
echo $HCAP >> $INPUT_FILE
echo $THICKNESS >> $INPUT_FILE
echo $E_VIS >> $INPUT_FILE
echo $E_THERM >> $INPUT_FILE
echo $EXP_AREA >> $INPUT_FILE
echo $SGP >> $INPUT_FILE

```

```

# call thermal_model(1)
thermal_model < $INPUT_FILE > /dev/null

```

```

# add the last run to the file for this material
echo -n $SHAPE_FACTOR_VAR >> $FINAL_FILE
echo -n " " >> $FINAL_FILE
awk '{ printf "%6.4f\n", $2 }' $OUTPUT_FILE >> $FINAL_FILE

```

```

# increment the shape factor
set SHAPE_FACTOR_VAR= echo $SHAPE_FACTOR_VAR + $VAR_INCR | bc -l
end

```

```

# -----
# Material Parameter Variation: Generic Materials ...
#

```

```
set FINAL_FILE=gen_$(MATID).pm
```

```

# clear a new FINAL output file which contains the
# material parameter and the resulting temperature
echo -n "" > $FINAL_FILE

```

```

# create a temporary file with these parameters in it ...
echo $SND_FILE > $INPUT_FILE
echo $WITH_FILE >> $INPUT_FILE
echo $OUTPUT_FILE >> $INPUT_FILE
echo $AVG_TEMP >> $INPUT_FILE
echo $SHAPE_FACTOR >> $INPUT_FILE
echo $ZENITH >> $INPUT_FILE
echo $AZIMUTH >> $INPUT_FILE
echo $TIME_INCR >> $INPUT_FILE
echo $HCAP >> $INPUT_FILE
echo $THICKNESS >> $INPUT_FILE
echo $E_VIS >> $INPUT_FILE
echo $E_THERM >> $INPUT_FILE
echo $EXP_AREA >> $INPUT_FILE
echo $SGP >> $INPUT_FILE

```

```

# call thermal_model(1)
thermal_model < $INPUT_FILE > /dev/null

```

Time Dependent Material Parameter Sensitivity Analysis

Material Type: Asphalt - 0600

Read in the resulting output file from THERM for each of the material parameters & determine the number of elements in the array.

heat_capacity := READPRN(hc_5_06)	hc := 0..rows(heat_capacity) - 1
thermal_conductivity := READPRN(tc_5_06)	tc := 0..rows(thermal_conductivity) - 1
thickness := READPRN(th_5_06)	th := 0..rows(thickness) - 1
vis_emissivity := READPRN(vem_5_06)	visem := 0..rows(vis_emissivity) - 1
therm_emissivity := READPRN(tem_5_06)	them := 0..rows(therm_emissivity) - 1
exposed_area_p := READPRN(xpp_5_06)	expp := 0..rows(exposed_area_p) - 1
exposed_area_n := READPRN(xpn_5_06)	expn := 0..rows(exposed_area_n) - 1
SGP := READPRN(sgp_5_06)	sgp := 0..rows(SGP) - 1
shape_factor := READPRN(sf_5_06)	sf := 0..rows(shape_factor) - 1

Read in the material ID, shape factor, emissivity, and baseline temperature for used in the 'Big Equation'

generic_file := READPRN(gen_5)

Create a reference blackbody temperature difference to relate the sensitivity values of all the material parameters

ref := 0..1 $T_{bb_{ref}}$:=

300
301

Read in the sensor responsivity file - Bendix line scanner

Resp := READPRN(bendix)

	Parameter	Temperature
heat_capacity =	0.26	-10.066
	0.289	-10.05
	0.318	-10.033
	0.348	-10.015
	0.377	-9.997
	0.406	-9.979
	0.435	-9.96
	0.464	-9.941

vis_emissivity =	0.77	-10.014
	0.796	-10.012
	0.821	-10.009
	0.847	-10.007
	0.873	-10.005
	0.898	-10.002
	0.924	-10
	0.95	-9.998

	0	1
SGP =	0	-10.006
	1	-8.937
	2	-7.87
	3	-6.818
	4	-5.76
	5	-4.71
	6	-3.666
	7	-2.627
	8	-1.594
	9	-0.565
	10	0.459

exposed_area_n =	-0.5	-11.669
	-0.4	-11.098
	-0.3	-10.407
	-0.2	-9.562
	-0.1	-8.522
	0	-7.373

exposed_area_p =	0	-7.373
	0.1	-8.488
	0.2	-9.409
	0.3	-10.177
	0.4	-10.819
	0.5	-11.361

shape_factor =	0	0
	0.25	-2.59
	0.5	-5.129
	0.75	-7.598
	1	-10.006

	Parameter	Temperature
thermal_conductivity =	5.93	-10.152
	6.877	-10.111
	7.823	-10.069
	8.77	-10.027
	9.716	-9.985
	10.663	-9.943
	11.609	-9.902
	12.556	-9.86

therm_emissivity =	0.93	-9.953
	0.937	-9.968
	0.944	-9.983
	0.951	-9.998
	0.958	-10.013
	0.966	-10.028
	0.973	-10.042
	0.98	-10.057

thickness =	6.486	-9.953
	8.528	-9.986
	10.571	-10.025
	12.614	-10.06
	14.657	-10.089
	16.7	-10.113

Read in the variation in temperature that was caused by the variation in the material parameter values, treating THERM as a black box.

Parameter Array

$P_{hc} := \text{heat_capacity}^{<0>}$
 $P_{tc} := \text{thermal_conductivity}^{<0>}$
 $P_{th} := \text{thickness}^{<0>}$
 $P_{visem} := \text{vis_emissivity}^{<0>}$
 $P_{them} := \text{therm_emissivity}^{<0>}$
 $P_{expp} := \text{exposed_area_p}^{<0>}$
 $P_{expn} := \text{exposed_area_n}^{<0>}$
 $P_{sgp} := \text{SGP}^{<0>}$
 $P_{sf} := \text{shape_factor}^{<0>}$

Temperature Array - Converted from Celsius to Kelvin

$T_{hc} := \text{heat_capacity}^{<1>} + 273.15$
 $T_{tc} := \text{thermal_conductivity}^{<1>} + 273.15$
 $T_{th} := \text{thickness}^{<1>} + 273.15$
 $T_{visem} := \text{vis_emissivity}^{<1>} + 273.15$
 $T_{them} := \text{therm_emissivity}^{<1>} + 273.15$
 $T_{expp} := \text{exposed_area_p}^{<1>} + 273.15$
 $T_{expn} := \text{exposed_area_n}^{<1>} + 273.15$
 $T_{sgp} := \text{SGP}^{<1>} + 273.15$
 $T_{sf} := \text{shape_factor}^{<1>} + 273.15$

Convert the temperatures to radiance values using the Plank equation.

$k := 1.38 \cdot 10^{-23}$ k - Boltzmann constant (J/K)
 $c := 2.99792459 \cdot 10^8$ c - speed of light (m/sec)
 $h := 6.626176 \cdot 10^{-34}$ h - Planck's constant (J/sec)
 $jmin := 8$ $jmin$ - minimum wavelength (μm) in the bandpass of interest
 $jmax := 14$ $jmax$ - maximum wavelength (μm) in the bandpass of interest
 $n := .1$ n - wavelength increment for bandpass (μm)
 $p := \frac{jmax - jmin}{n}$ p - number of steps in the bandpass of interest
 $j := 0..(p - 1)$ j - index for the wavelength array
 $\lambda_j := (j \cdot n + jmin) \cdot 10^{-6}$ λ - in the bandpass of interest

$$L_{hc}(\lambda, T_{hc}) := \frac{2 \cdot h \cdot c^2}{\lambda^5 \cdot \left(e^{\frac{h \cdot c}{\lambda \cdot k \cdot T_{hc}}} - 1 \right)}$$

$$L_{tc}(\lambda, T_{tc}) := \frac{2 \cdot h \cdot c^2}{\lambda^5 \cdot \left(e^{\frac{h \cdot c}{\lambda \cdot k \cdot T_{tc}}} - 1 \right)}$$

$$L_{th}(\lambda, T_{th}) := \frac{2 \cdot h \cdot c^2}{\lambda^5 \cdot \left(e^{\frac{h \cdot c}{\lambda \cdot k \cdot T_{th}}} - 1 \right)}$$

$$L_{visem}(\lambda, T_{visem}) := \frac{2 \cdot h \cdot c^2}{\lambda^5 \cdot \left(e^{\frac{h \cdot c}{\lambda \cdot k \cdot T_{visem}}} - 1 \right)}$$

$$L_{\text{them}}(\lambda, T_{\text{them}}) := \frac{2 \cdot h \cdot c^2}{\lambda^5 \cdot \left(e^{\frac{h \cdot c}{\lambda \cdot k \cdot T_{\text{them}}}} - 1 \right)}$$

$$L_{\text{expp}}(\lambda, T_{\text{expp}}) := \frac{2 \cdot h \cdot c^2}{\lambda^5 \cdot \left(e^{\frac{h \cdot c}{\lambda \cdot k \cdot T_{\text{expp}}}} - 1 \right)}$$

$$L_{\text{sgp}}(\lambda, T_{\text{sgp}}) := \frac{2 \cdot h \cdot c^2}{\lambda^5 \cdot \left(e^{\frac{h \cdot c}{\lambda \cdot k \cdot T_{\text{sgp}}}} - 1 \right)}$$

$$L_{\text{expn}}(\lambda, T_{\text{expn}}) := \frac{2 \cdot h \cdot c^2}{\lambda^5 \cdot \left(e^{\frac{h \cdot c}{\lambda \cdot k \cdot T_{\text{expn}}}} - 1 \right)}$$

$$L_{\text{sf}}(\lambda, T_{\text{sf}}) := \frac{2 \cdot h \cdot c^2}{\lambda^5 \cdot \left(e^{\frac{h \cdot c}{\lambda \cdot k \cdot T_{\text{sf}}}} - 1 \right)}$$

$$L_{\text{bb}}(\lambda, T_{\text{bb}}) := \frac{2 \cdot h \cdot c^2}{\lambda^5 \cdot \left(e^{\frac{h \cdot c}{\lambda \cdot k \cdot T_{\text{bb}}}} - 1 \right)}$$

Integrate the surface radiance across the bandpass of interest (8-14 μm) - including the sensor response function. **Calculated at .1 μm increments**

$$L_{\text{hc_ground}}_{\text{hc}} := \sum_j \text{Resp}_j \cdot L_{\text{hc}}(\lambda_j, T_{\text{hc}}_{\text{hc}}) \cdot (n \cdot 10^{-6})$$

$$L_{\text{th_ground}}_{\text{th}} := \sum_j \text{Resp}_j \cdot L_{\text{th}}(\lambda_j, T_{\text{th}}_{\text{th}}) \cdot (n \cdot 10^{-6})$$

$$L_{\text{visem_ground}}_{\text{visem}} := \sum_j \text{Resp}_j \cdot L_{\text{visem}}(\lambda_j, T_{\text{visem}}_{\text{visem}}) \cdot (n \cdot 10^{-6})$$

$$L_{\text{them_ground}}_{\text{them}} := \sum_j \text{Resp}_j \cdot L_{\text{them}}(\lambda_j, T_{\text{them}}_{\text{them}}) \cdot (n \cdot 10^{-6})$$

$$L_{\text{tc_ground}}_{\text{tc}} := \sum_j \text{Resp}_j \cdot L_{\text{tc}}(\lambda_j, T_{\text{tc}}_{\text{tc}}) \cdot (n \cdot 10^{-6})$$

$$L_{\text{expp_ground}}_{\text{expp}} := \sum_j \text{Resp}_j \cdot L_{\text{expp}}(\lambda_j, T_{\text{expp}}_{\text{expp}}) \cdot (n \cdot 10^{-6})$$

$$L_{\text{expn_ground}}_{\text{expn}} := \sum_j \text{Resp}_j \cdot L_{\text{expn}}(\lambda_j, T_{\text{expn}}_{\text{expn}}) \cdot (n \cdot 10^{-6})$$

$$L_{\text{sgp_ground}}_{\text{sgp}} := \sum_j \text{Resp}_j \cdot L_{\text{sgp}}(\lambda_j, T_{\text{sgp}}_{\text{sgp}}) \cdot (n \cdot 10^{-6})$$

$$L_{\text{sf_ground}}_{\text{sf}} := \sum_j \text{Resp}_j \cdot L_{\text{sf}}(\lambda_j, T_{\text{sf}}_{\text{sf}}) \cdot (n \cdot 10^{-6})$$

$$L_{\text{bb_ground}}_{\text{ref}} := \sum_j \text{Resp}_j \cdot L_{\text{bb}}(\lambda_j, T_{\text{bb}}_{\text{ref}}) \cdot (n \cdot 10^{-6})$$

$$\Delta L_{\text{bb}} := L_{\text{bb_ground}}_1 - L_{\text{bb_ground}}_0$$

$$\Delta L_{\text{bb}} = 0.615$$

Propagate the radiance of the target to the radiance reaching the sensor using the big equation, simplified for use in the LWIR and assuming a shape factor of 1.0

$$\varepsilon := \text{generic_file}_{0,1} \quad L_{\mu\varepsilon} := 2.51 \quad L_{d\varepsilon} := 4.289 \quad \tau_2 := .9 \quad L_{b\varepsilon} := 20.41 \quad r := 1 - \varepsilon \quad F := \text{generic_file}_{0,2}$$

$$L_{\text{hc_sensor}}_{\text{hc}} := [\varepsilon L_{\text{hc_ground}}_{\text{hc}} + (F \cdot L_{d\varepsilon} + (1 - F) \cdot L_{b\varepsilon}) \cdot r] \cdot \tau_2 + L_{\mu\varepsilon}$$

$$L_{\text{tc_sensor}}_{\text{tc}} := [\varepsilon L_{\text{tc_ground}}_{\text{tc}} + (F \cdot L_{d\varepsilon} + (1 - F) \cdot L_{b\varepsilon}) \cdot r] \cdot \tau_2 + L_{\mu\varepsilon}$$

$$L_{\text{th_sensor}}_{\text{th}} := [\varepsilon L_{\text{th_ground}}_{\text{th}} + (F \cdot L_{d\varepsilon} + (1 - F) \cdot L_{b\varepsilon}) \cdot r] \cdot \tau_2 + L_{\mu\varepsilon}$$

$$L_{\text{visem_sensor}}_{\text{visem}} := [\varepsilon L_{\text{visem_ground}}_{\text{visem}} + (F \cdot L_{d\varepsilon} + (1 - F) \cdot L_{b\varepsilon}) \cdot r] \cdot \tau_2 + L_{\mu\varepsilon}$$

$$L_{\text{them_sensor}}_{\text{them}} := [\varepsilon L_{\text{them_ground}}_{\text{them}} + (F \cdot L_{d\varepsilon} + (1 - F) \cdot L_{b\varepsilon}) \cdot r] \cdot \tau_2 + L_{\mu\varepsilon}$$

$$L_{\text{expp_sensor}}_{\text{expp}} := [\varepsilon L_{\text{expp_ground}}_{\text{expp}} + (F \cdot L_{d\varepsilon} + (1 - F) \cdot L_{b\varepsilon}) \cdot r] \cdot \tau_2 + L_{\mu\varepsilon}$$

$$L_{\text{expn_sensor}}_{\text{expn}} := [\varepsilon L_{\text{expn_ground}}_{\text{expn}} + (F \cdot L_{d\varepsilon} + (1 - F) \cdot L_{b\varepsilon}) \cdot r] \cdot \tau_2 + L_{\mu\varepsilon}$$

$$L_{\text{sgp_sensor}}_{\text{sgp}} := [\varepsilon L_{\text{sgp_ground}}_{\text{sgp}} + (F \cdot L_{d\varepsilon} + (1 - F) \cdot L_{b\varepsilon}) \cdot r] \cdot \tau_2 + L_{\mu\varepsilon}$$

$$L_{\text{sf_sensor}}_{\text{sf}} := [\varepsilon L_{\text{sf_ground}}_{\text{sf}} + (F \cdot L_{d\varepsilon} + (1 - F) \cdot L_{b\varepsilon}) \cdot r] \cdot \tau_2 + L_{\mu\varepsilon}$$

Write out the results of the sensitivity analysis to an output file

$$\begin{aligned} \text{sens}_0 &:= 0600 & \text{sens}_5 &:= \text{slope}(P_{\text{them}}, L_{\text{them_sensor}}) \\ \text{sens}_1 &:= \text{slope}(P_{\text{th}}, L_{\text{th_sensor}}) & \text{sens}_6 &:= \text{slope}(P_{\text{expp}}, L_{\text{expp_sensor}}) \\ \text{sens}_2 &:= \text{slope}(P_{\text{tc}}, L_{\text{tc_sensor}}) & \text{sens}_7 &:= \text{slope}(P_{\text{expn}}, L_{\text{expn_sensor}}) \\ \text{sens}_3 &:= \text{slope}(P_{\text{hc}}, L_{\text{hc_sensor}}) & \text{sens}_8 &:= \text{slope}(P_{\text{sgp}}, L_{\text{sgp_sensor}}) \\ \text{sens}_4 &:= \text{slope}(P_{\text{visem}}, L_{\text{visem_sensor}}) & \text{sens}_9 &:= \text{slope}(P_{\text{sf}}, L_{\text{sf_sensor}}) \end{aligned}$$

	TH	TC	HC	Visem	Them	Expp	Expn	SGP	SF
$\text{sens}^T =$	1	2	3	4	5	6	7	8	
	-0.006	0.016	0.218	0.033	-0.74	-2.831	3.066	0.396	

$$\text{temp_sens} := \frac{\text{sens}}{\Delta L_{\text{bb}}}$$

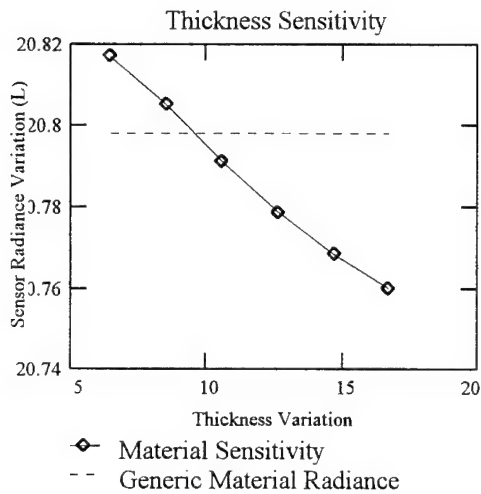
$$\text{temp_sens}_0 := 0600$$

	0	1	2	3	4	5	6	7
$\text{temp_sens}^T =$	600	-0.009	0.025	0.354	0.053	-1.203	-4.602	4.983

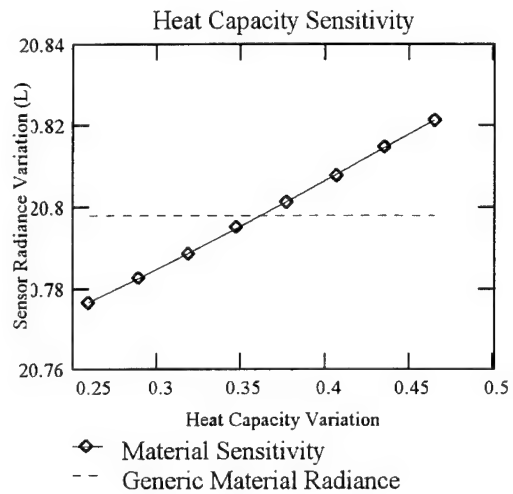
$$\text{WRITEPRN}(\text{time_analysis1}) := \text{temp_sens}^T$$

Time Dependent Sensitivity Analysis - Asphalt 0600

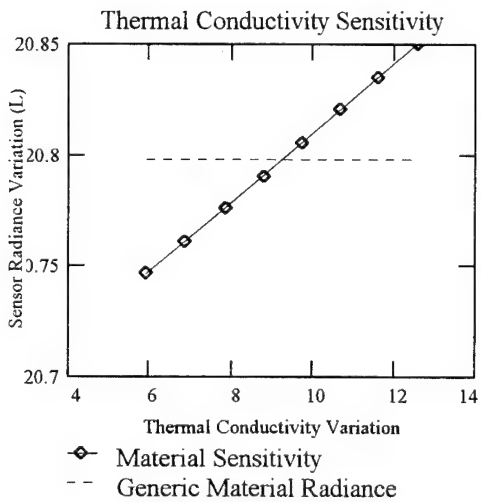
The following graphs show the change in radiance at the sensor as the material parameter of the object on the ground was varied. The resulting linear regression shows the final output sensitivity of the material parameter.



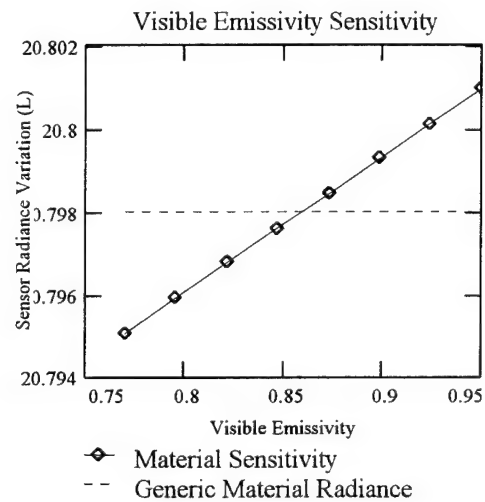
$$\text{sens}_1 = -0.006$$



$$\text{sens}_3 = 0.218$$

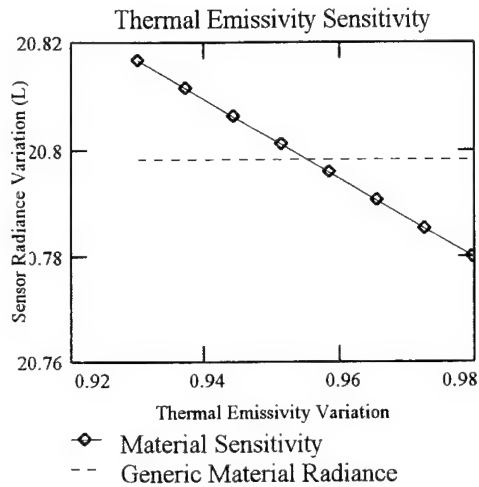


$$\text{sens}_2 = 0.016$$

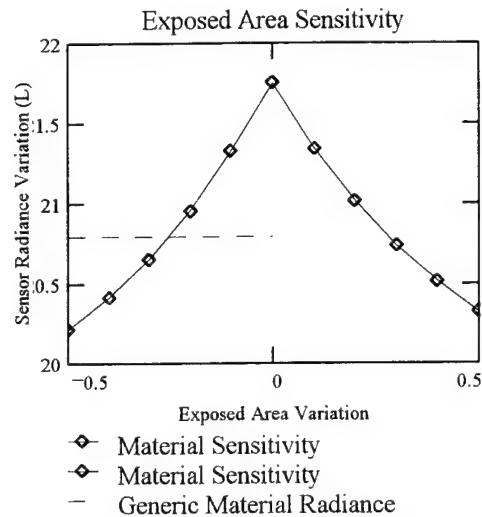


$$\text{sens}_4 = 0.033$$

Time Dependent Sensitivity Analysis - Asphalt 0600 Continued

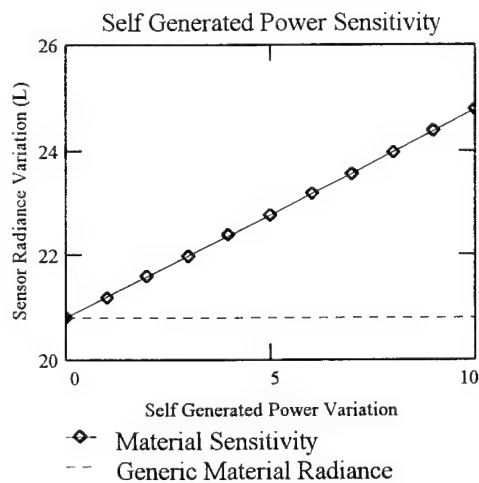


$$\text{sens}_5 = -0.74$$

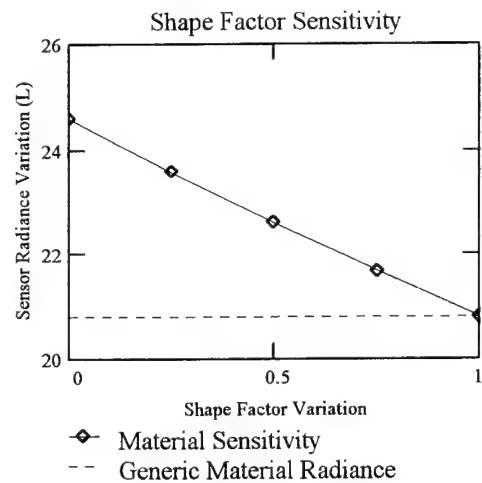


$$\text{sens}_6 = -2.831$$

$$\text{sens}_7 = 3.066$$



$$\text{sens}_8 = 0.396$$



$$\text{sens}_9 = -3.779$$

```

#!/bin/csh

set path=($path $(dirs $(pkg/bin))

set INPUT_FILE=input.tmp
set OUTPUT_FILE=output.tmp
set MAT_FILE=material.tmp
set READ_FILE=mats.dat
set FINAL_FILE=scene.prm
set MASTER=./r_master

# Input files that are needed for sensitivity analysis
#
set SND_FILE=${MASTER}/hawkeye.snd
set WITH_FILE=${MASTER}/hawkeye_opt.wh
set DIRSIG_MAT_FILE=${MASTER}/hodd_mat_opt.mat

#
# clear a new FINAL output file which contains the
# material parameter and the resulting temperature
echo -n "" > $FINAL_FILE

set MATIDS_ARRAY=cat $READ_FILE | cut -f1 | tr "012" " "
set ORIENT_ARRAY=cat $READ_FILE | cut -f2 | tr "012" " "
set STOP=${MATIDS_ARRAY}
set COUNTER=1

# while not at the end of the file
while ($COUNTER <= $STOP)

# Set the material ID, thickness, orientation for the sensitivity analysis
#
set MATID=${MATIDS_ARRAY[$COUNTER]}
set ORIENTATION=${ORIENT_ARRAY[$COUNTER]}

set ORIENTATION_FILE=${MASTER}/or_${ORIENTATION}.dat
set junk=cat $ORIENTATION_FILE | paste ...
set SHAPE_FACTOR=${junk[1]}
set ZENITH=${junk[2]}
set AZIMUTH=${junk[3]}

# Scene specific variables
#
set AVG_TEMP=0.00
set TIME_INCR=24.0
set SGP=0.0

# Read in the generic material parameters from the DIRSIG material file
# and set those values to variables in the shell program
#
nawk -f ${MASTER}/test.awk ID=${MATID} $DIRSIG_MAT_FILE > $MAT_FILE

```

```

set line=cat $MAT_FILE | paste
set SP_HEAT=$line[1]
set TCOND=$line[2]
set MASS_DENSITY=$line[3]
set E_VIS=$line[4]
set E_THERM=$line[5]
set EXP_AREA=$line[6]
set THICKNESS=$line[7]
set HCAP= echo $MASS_DENSITY * $SP_HEAT | bc -l

# create a temporary file with these parameters in it ...
echo $SND_FILE > $INPUT_FILE
echo $WITH_FILE > $INPUT_FILE
echo $OUTPUT_FILE > $INPUT_FILE
echo $AVG_TEMP > $INPUT_FILE
echo $SHAPE_FACTOR > $INPUT_FILE
echo $ZENITH > $INPUT_FILE
echo $AZIMUTH > $INPUT_FILE
echo $TIME_INCR > $INPUT_FILE
echo $HCAP > $INPUT_FILE
echo $TCOND > $INPUT_FILE
echo $THICKNESS > $INPUT_FILE
echo $E_VIS > $INPUT_FILE
echo $E_THERM > $INPUT_FILE
echo $EXP_AREA > $INPUT_FILE
echo $SGP > $INPUT_FILE

# call thermal_model(1)
thermal_model < $INPUT_FILE > /dev/null

# add the last run to the file for this material
echo -n $MATID >> $FINAL_FILE
echo -n " " >> $FINAL_FILE
echo -n $E_THERM >> $FINAL_FILE
echo -n " " >> $FINAL_FILE
echo -n $SHAPE_FACTOR >> $FINAL_FILE
echo -n " " >> $FINAL_FILE
awk '{ print( "%6.4f\n", $2 ) }' $OUTPUT_FILE >> $FINAL_FILE

set COUNTER= echo $COUNTER + 1 | bc -l

# iterate and go to the next material number

end

mm * .tmp

```

```

#!/bin/csh

set path=( $path /dirs/pkg/bin )

set INPUT_FILE= input.tmp
set OUTPUT_FILE=output.tmp
set MAT_FILE= material.tmp
set MASTER= ./2_master

# Read in the material ID and the thickness for the sensitivity analysis
#
set MATID=5
set ORIENTATION=1
set time=$1

# Input files that are needed for sensitivity analysis
#
set SND_FILE=${MASTER}/hawkeye_`${time}`.snd
set WITH_FILE=${MASTER}/hawkeye.with
set DIRSIG_MAT_FILE=${MASTER}/odd_mat_var.mat
set ORIENTATION_FILE=${MASTER}/or_`${ORIENTATION}`.dat

# Scene specific variables
#
set AVG_TEMP=0.00
set TIME_INCR=24.0
set SGP=0.0

set junk= cat $ORIENTATION_FILE | paste ...
set SHAPE_FACTOR=${junk[1]}
set ZENITH=${junk[2]}
set AZIMUTH=${junk[3]}

# Variation Parameters for Sensitivity Analysis of the Material Parameters
#
set NUM_INCREMENTS=7.0

# Read in the generic material parameters from the DIRSIG material file
# and set those values to variables in the shell program
#
nawk -f $(MASTER)/testvar.awk ID=${MATID} $DIRSIG_MAT_FILE > $MAT_FILE

set line1='head -6 $MAT_FILE | paste .....
set line2='tail -7 $MAT_FILE | head -6 | paste .....
set line3='tail +13 $MAT_FILE | paste .....
set line=( $line1 $line2 $line3 )

set SP_HEAT=${line[1]}
set TCOND=${line[2]}
set MASS_DENSITY=${line[3]}
set E_VIS=${line[4]}
set E_THERM=${line[5]}
set EXP_AREA=${line[6]}
set THICKNESS=${line[7]}

set HC_MIN=${line[8]}
set HC_MAX=${line[9]}
set TC_MIN=${line[10]}
set TC_MAX=${line[11]}
set VE_MIN=${line[12]}
set VE_MAX=${line[13]}
set TE_MIN=${line[14]}
set TE_MAX=${line[15]}
set TH_MIN=${line[16]}
set TH_MAX=${line[17]}
set IICAP= echo "$MASS DENSITY * SSP_HEAT" | bc -l

# -----
# # Material Parameter Variation: Thickness ...
# #
set VAR_INCR= echo "4k $THH_MAX $THH_MIN - $NUM_INCREMENTS / p" | dc

# set the initial thickness variation value
set THICKNESS_VAR=$THH_MIN

set FINAL_FILE=th_`${MATID}`_`${time}`.pm

# clear a new FINAL output file which contains the
# material parameter and the resulting temperature
echo -n "" > $FINAL_FILE

# loop around for while, varying one parameter
while (0 == `echo "${THICKNESS_VAR,$THH_MAX}" | bc -l ${MASTER}/test.bc`)

# create a temporary file with these parameters in it ...
echo $SND_FILE > $INPUT_FILE
echo $WITH_FILE > $INPUT_FILE
echo $OUTPUT_FILE > $INPUT_FILE
echo $AVG_TEMP > $INPUT_FILE
echo $SHAPE_FACTOR > $INPUT_FILE
echo $ZENITH > $INPUT_FILE
echo $AZIMUTH > $INPUT_FILE
echo $TIME_INCR > $INPUT_FILE
echo $IICAP > $INPUT_FILE
echo $TCOND > $INPUT_FILE
echo $THICKNESS_VAR > $INPUT_FILE
echo $E_VIS > $INPUT_FILE
echo $E_THERM > $INPUT_FILE
echo $EXP_AREA > $INPUT_FILE
echo $SGP > $INPUT_FILE

# call thermal_model(1)
thermal_model(1)

# add the last run to the file for this material
echo -n $THICKNESS_VAR > $FINAL_FILE
echo -n " " > $FINAL_FILE
awk '{ printf "%6.4f\n", $2 }' $OUTPUT_FILE >> $FINAL_FILE

# increment the thickness
set THICKNESS_VAR= echo $THICKNESS_VAR + $VAR_INCR | bc -l

end

```

```

# -----
# Material Parameter Variation: Thermal Conductivity ...
#
set VAR_INCR=echo "4k $TC_MAX $TC_MIN - $NUM_INCREMENTS / p" | dc
# set the initial thermal conductivity
set TCOND_VAR=$TC_MIN
set FINAL_FILE=tc_$(MATID)_$(time).pm

# clear a new FINAL output file which contains the
# material parameter and the resulting temperature
echo -n "" > $FINAL_FILE

# loop around for while, varying one parameter
while (0 == echo "t($HCAP_VAR,$HC_MAX)" | bc -l $(MASTER)/test.bc)

# create a temporary file with these parameters in it ...
echo $SSND_FILE > $INPUT_FILE
echo $SWTH_FILE > $INPUT_FILE
echo $SOUTH_FILE > $INPUT_FILE
echo $AVG_TEMP > $INPUT_FILE
echo $SHAPE_FACTOR > $INPUT_FILE
echo $ZENITH > $INPUT_FILE
echo $AZIMUTH > $INPUT_FILE
echo $TIME_INCR > $INPUT_FILE
echo $HCAP_VAR > $INPUT_FILE
echo $THICKNESS > $INPUT_FILE
echo $E_VIS > $INPUT_FILE
echo $E_THERM > $INPUT_FILE
echo $EXP_AREA > $INPUT_FILE
echo $SGP > $INPUT_FILE

# call thermal_model(1)
thermal_model < $INPUT_FILE > /dev/null

# add the last run to the file for this material
echo -n $HCAP_VAR >> $FINAL_FILE
echo -n " " >> $FINAL_FILE
awk '{ printf "%6.4f\n", $2 }' $OUTPUT_FILE >> $FINAL_FILE

# increment the heat capacity
set HCAP_VAR=echo $HCAP_VAR + $VAR_INCR | bc -l

end

# -----
# Material Parameter Variation: Visible Emissivity ...
#
set VAR_INCR=echo "4k $VE_MAX $VE_MIN - $NUM_INCREMENTS / p" | dc
# set the initial visible emissivity
set E_VIS_VAR=$VE_MIN
set FINAL_FILE=vem_$(MATID)_$(time).pm

# clear a new FINAL output file which contains the
# material parameter and the resulting temperature
echo -n "" > $FINAL_FILE

# loop around for while, varying one parameter
while (0 == echo "t($E_VIS_VAR,$VE_MAX)" | bc -l $(MASTER)/test.bc)

# create a temporary file with these parameters in it ...
echo $SSND_FILE > $INPUT_FILE
echo $SWTH_FILE > $INPUT_FILE
echo $SOUTH_FILE > $INPUT_FILE
echo $AVG_TEMP > $INPUT_FILE

```

```

echo $SHAPE_FACTOR >> $INPUT_FILE
echo $ZENITH >> $INPUT_FILE
echo $AZIMUTH >> $INPUT_FILE
echo $TIME_INCR >> $INPUT_FILE
echo $HCAP >> $INPUT_FILE
echo $COND >> $INPUT_FILE
echo $THICKNESS >> $INPUT_FILE
echo $E_VIS >> $INPUT_FILE
echo $THERM >> $INPUT_FILE
echo $EXP_AREA >> $INPUT_FILE
echo $SGP >> $INPUT_FILE

# call thermal_model(1)
thermal_model < $INPUT_FILE > /dev/null

# add the last run to the file for this material
echo -n $E_THERM_VAR >> $FINAL_FILE
awk '{ printf "%6.4f\n", $2 }' $OUTPUT_FILE >> $FINAL_FILE

# increment the thermal emissivity
set E_THERM_VAR=echo $E_THERM_VAR + $VAR_INCR | bc -l

end

# -----
# # Material Parameter Variation: Exposed Area (positive)...
# set MIN_VAR=0.0
# set MAX_VAR=0.5
# set VAR_INCR=0.1
# set the initial exposed area
set EXP_AREA_VAR=$MIN_VAR
set FINAL_FILE=xpp_$(MATID)_'$(time).pm

# clear a new FINAL output file which contains the
# material parameter and the resulting temperature
echo -n "" > $FINAL_FILE

# loop around for while, varying one parameter
while (0 == `echo "${EXP_AREA_VAR,$MAX_VAR}" | bc -l ${MASTER}/test.bc`)

# create a temporary file with these parameters in it ...
echo $SND_FILE >> $INPUT_FILE
echo $WTH_FILE >> $INPUT_FILE
echo $OUTPUT_FILE >> $INPUT_FILE
echo $AVG_TEMP >> $INPUT_FILE
echo $SHAPE_FACTOR >> $INPUT_FILE
echo $ZENITH >> $INPUT_FILE
echo $AZIMUTH >> $INPUT_FILE
echo $TIME_INCR >> $INPUT_FILE
echo $HCAP >> $INPUT_FILE
echo $COND >> $INPUT_FILE
echo $THICKNESS >> $INPUT_FILE
echo $E_VIS >> $INPUT_FILE
echo $THERM >> $INPUT_FILE
echo $EXP_AREA_VAR >> $INPUT_FILE
echo $SGP >> $INPUT_FILE

# call thermal_model(1)
thermal_model < $INPUT_FILE > /dev/null

# add the last run to the file for this material
echo -n $EXP_AREA_VAR >> $FINAL_FILE
awk '{ printf "%6.4f\n", $2 }' $OUTPUT_FILE >> $FINAL_FILE

# increment the exposed area
set EXP_AREA_VAR=echo $EXP_AREA_VAR + $VAR_INCR | bc -l

end

```

```

echo $SHAPE_FACTOR >> $INPUT_FILE
echo $ZENITH >> $INPUT_FILE
echo $AZIMUTH >> $INPUT_FILE
echo $TIME_INCR >> $INPUT_FILE
echo $HCAP >> $INPUT_FILE
echo $COND >> $INPUT_FILE
echo $THICKNESS >> $INPUT_FILE
echo $E_VIS >> $INPUT_FILE
echo $THERM >> $INPUT_FILE
echo $EXP_AREA >> $INPUT_FILE
echo $SGP >> $INPUT_FILE

# call thermal_model(1)
thermal_model < $INPUT_FILE > /dev/null

# add the last run to the file for this material
echo -n $E_VIS_VAR >> $FINAL_FILE
awk '{ printf "%6.4f\n", $2 }' $OUTPUT_FILE >> $FINAL_FILE

# increment the visible emissivity
set E_VIS_VAR=echo $E_VIS_VAR + $VAR_INCR | bc -l

end

# -----
# # Material Parameter Variation: Thermal Emissivity ...
# set VAR_INCR=echo "4k $TE_MAX $TE_MIN - $NUM_INCREMENTS / p" | dc

# set the initial thermal emissivity
set E_THERM_VAR=$TE_MIN
set FINAL_FILE=tem_$(MATID)_'$(time).pm

# clear a new FINAL output file which contains the
# material parameter and the resulting temperature
echo -n "" > $FINAL_FILE

# loop around for while, varying one parameter
while (0 == `echo "${E_THERM_VAR,$TE_MAX}" | bc -l ${MASTER}/test.bc`)

# create a temporary file with these parameters in it ...
echo $SND_FILE >> $INPUT_FILE
echo $WTH_FILE >> $INPUT_FILE
echo $OUTPUT_FILE >> $INPUT_FILE
echo $AVG_TEMP >> $INPUT_FILE
echo $SHAPE_FACTOR >> $INPUT_FILE
echo $ZENITH >> $INPUT_FILE
echo $AZIMUTH >> $INPUT_FILE
echo $TIME_INCR >> $INPUT_FILE
echo $HCAP >> $INPUT_FILE
echo $COND >> $INPUT_FILE
echo $THICKNESS >> $INPUT_FILE
echo $E_VIS >> $INPUT_FILE
echo $THERM_VAR >> $INPUT_FILE
echo $EXP_AREA >> $INPUT_FILE
echo $SGP >> $INPUT_FILE

# call thermal_model(1)

```

```

#-----
# # Material Parameter Variation: Exposed Area (negative)...
# #
set MIN_VAR=0.5
set MAX_VAR=0.0
set VAR_INCR=0.1
# set the initial exposed area
set EXP_AREA_VAR=$MIN_VAR

set FINAL_FILE=xpm_$(MATID)_$(time).pm

# clear a new FINAL output file which contains the
# material parameter and the resulting temperature
echo -n "" > $FINAL_FILE

# loop around for while, varying one parameter
while (0 == `echo "${SSGP_VAR,$MAX_VAR}" | bc -l ${MASTER}/test.bc`)
# create a temporary file with these parameters in it ...
echo $SSND_FILE > $INPUT_FILE
echo $SWTH_FILE > $INPUT_FILE
echo $SOUTH_FILE > $INPUT_FILE
echo $SAVG_TEMP > $INPUT_FILE
echo $SHAPE_FACTOR > $INPUT_FILE
echo $ZENITH > $INPUT_FILE
echo $AZIMUTH > $INPUT_FILE
echo $TIME_INCR > $INPUT_FILE
echo $HCAP > $INPUT_FILE
echo $TCOND > $INPUT_FILE
echo $THICKNESS > $INPUT_FILE
echo $E_VIS > $INPUT_FILE
echo $E_THERM > $INPUT_FILE
echo $EXP_AREA > $INPUT_FILE
echo $SGP_VAR > $INPUT_FILE

# call thermal_model(1)
thermal_model < $INPUT_FILE > /dev/null

# add the last run to the file for this material
echo -n $SGP_VAR > $FINAL_FILE
echo -n " " > $FINAL_FILE
awk '{ print( "%6.4f\n", $2 ) }' $OUTPUT_FILE > $FINAL_FILE

# increment the self generated power
set SGP_VAR= echo $SGP_VAR + $VAR_INCR | bc -l
end

#-----
# # Material Parameter Variation: Shape Factor ...
# #
set MIN_VAR=0.0
set MAX_VAR=1.0
set VAR_INCR=0.25

# set the initial shape factor
set SHAPE_FACTOR_VAR=$MIN_VAR

set FINAL_FILE=sf_$(MATID)_$(time).pm

# clear a new FINAL output file which contains the
# material parameter and the resulting temperature
echo -n "" > $FINAL_FILE

# loop around for while, varying one parameter
while (0 == `echo "${SSHAPE_FACTOR_VAR,$MAX_VAR}" | bc -l ${MASTER}/test.bc`)
# create a temporary file with these parameters in it ...
echo $SSND_FILE > $INPUT_FILE

```

```

echo $WITH_FILE >> $INPUT_FILE
echo $OUTPUT_FILE >> $INPUT_FILE
echo $AVG_TEMP >> $INPUT_FILE
echo $SHAPE_FACTOR_VAR >> $INPUT_FILE
echo $ZENITH >> $INPUT_FILE
echo $AZIMUTH >> $INPUT_FILE
echo $TIME_INCR >> $INPUT_FILE
echo $HCAP >> $INPUT_FILE
echo $TCOND >> $INPUT_FILE
echo $THICKNESS >> $INPUT_FILE
echo $E_VIS >> $INPUT_FILE
echo $E_THERM >> $INPUT_FILE
echo $EXP_AREA >> $INPUT_FILE
echo $SGP >> $INPUT_FILE

# call thermal_model(1)
thermal_model < $INPUT_FILE > /dev/null

# add the last run to the file for this material
echo -n "$SHAPE_FACTOR_VAR >> $FINAL_FILE
echo -n " " >> $FINAL_FILE
awk ' { printf "%6.4f\n", $2 } ' $OUTPUT_FILE >> $FINAL_FILE

# increment the shape factor
set SHAPE_FACTOR_VAR= echo $SHAPE_FACTOR_VAR + $VAR_INCR | bc -l

end

# -----
# # Material Parameter Variation: Generic Materials ...
# #

set FINAL_FILE=gen_$(MATID).pm

# clear a new FINAL output file which contains the
# material parameter and the resulting temperature
echo -n "" > $FINAL_FILE

# create a temporary file with these parameters in it ...
echo $SND_FILE > $INPUT_FILE
echo $WITH_FILE >> $INPUT_FILE
echo $OUTPUT_FILE >> $INPUT_FILE
echo $AVG_TEMP >> $INPUT_FILE
echo $SHAPE_FACTOR >> $INPUT_FILE
echo $ZENITH >> $INPUT_FILE
echo $AZIMUTH >> $INPUT_FILE
echo $TIME_INCR >> $INPUT_FILE
echo $HCAP >> $INPUT_FILE
echo $TCOND >> $INPUT_FILE
echo $THICKNESS >> $INPUT_FILE
echo $E_VIS >> $INPUT_FILE
echo $E_THERM >> $INPUT_FILE
echo $EXP_AREA >> $INPUT_FILE
echo $SGP >> $INPUT_FILE

# call thermal_model(1)
thermal_model < $INPUT_FILE > /dev/null

# add the last run to the file for this material

```

```

echo -n $MATID >> $FINAL_FILE
echo -n " " >> $FINAL_FILE
echo -n " " >> $FINAL_FILE
echo -n $E_THERM >> $FINAL_FILE
echo -n " " >> $FINAL_FILE
echo -n $SHAPE_FACTOR >> $FINAL_FILE
echo -n " " >> $FINAL_FILE
awk ' { printf "%6.4f\n", $2 } ' $OUTPUT_FILE >> $FINAL_FILE

m *.imp

```